การศึกษาการเผาไหม้ของระบบเชื้อเพลิงร่วมที่ใช้ ก๊าซหุงต้มในเครื่องยนต์ดีเซลชนิดห้องเผาไหม้ล่วงหน้า

นาย ดึค มิน ฟาน

A STUDY ON THE LPG DUAL FUEL COMBUSTION CHARACTERISTICS

OF AN INDIRECT INJECTION COMPRESSION IGNITION ENGINE

Mr. Phan Minh Duc

A Dissertation Submitted in Partial Fulfillment of the Requirements

for the Degree of Doctor of Philosophy Program in Mechanical Engineering

Department of Mechanical Engineering

Faculty of Engineering Chulalongkorn University

Academic year 2006

Thesis Title	A STUDY ON THE LPG DUAL FUEL COMBUSTION CHARACTERISTICS OF AN INDIRECT INJECTION COMPRESSION IGNITION ENGINE
By	Phan Minh Duc
Field of Study	Mechanical Engineering
Thesis Advisor	Assistant Professor KANIT WATTANAVICHIEN, Ph.D.

Accepted by the Faculty of Engineering, Chulalongkorn University in Partial Fulfillment of the Requirements for the Doctoral's Degree

.............................Dean of the Faculty of Engineering

(Professor Direk Lavansiri, Ph.D.)

THESIS COMMITTEE

.... Chairman

(Associate Professor Staporn Suprichakorn)

.... Thesis Advisor

(Assistant Professor Kanit Wattanavichien, Ph.D.)

.... Member

(Associate Professor Tharapong Vitidsant, Ph.D.)

.... Member

(Assistant Professor Chinda Charoenphonphanich, D. Eng.)

.... Member
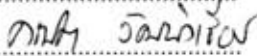
(Captain Samai Jai-In, Ph.D.)

Phan Minh Duc: การศึกษาการเผาไหม้ของระบบเชื้อเพลิงร่วมที่ใช้ ก๊าซหุงต้มในเครื่องยนต์ดีเซลชนิด ห้องเผาไหม้ล่วงหน้า. (A STUDY ON THE LPG DUAL FUEL COMBUSTION CHARACTERISTICS OF AN INDIRECT INJECTION COMPRESSION IGNITION ENGINE) อ. ที่ ปรึกษา: ผู้ช่วยศาสตราจารย์ ดร.คณิต วัฒนวิเชียร, 284 หน้า

งานวิจัยนี้มีวัตถุประสงค์ที่จะศึกษาผลของการใช้ไบโอดีเซลเป็นเชื้อเพลิงช่วยจุดระเบิดในเครื่องยนต์ระบบ เชื้อเพลิงร่วม โดยแบ่งการวิจัยออกเป็น 3 ส่วน ส่วนแรกเป็นการศึกษาการเผาไหม้ของระบบเชื้อเพลิงคู่ LPG-ดีเซล ตาม ด้วยการศึกษาการเผาไหม้ของระบบเชื้อเพลิงคู่ LPG-ปาล์มไบโอดีเซล(PME) และส่วนสุดท้ายจะเป็นการศึกษาผลจาก การปรับค่าองศาการฉีด ซึ่งงานวิจัยนี้จะใช้เครื่องยนต์ดีเซล 4 สูบ IDI โดยดำเนินการบนแท่นทดสอบที่สภาวะคงตัว ตาม จุดทดสอบที่เลือกจากวัฏจักร ECE15 + EUDC ในช่วง 10-70 N.m ความเร็วรอบเครื่องยนต์ 1250-2750 รอบต่อนาที โดยใช้วงจรควบคุมการจ่าย LPG อีเลคทรอนิค โดยจัดเก็บข้อมูลความดันในท่อจ่ายเชื้อเพลิง ความดันในห้องเผาไหม้ และภาพถ่ายละอองฝอยและการเผาไหม้ในห้องเผาไหม้ เพื่อนำมาวิเคราะห์เปรียบเทียบหาประสิทธิภาพการแปลง พลังงาน การสิ้นเปลืองเชื้อเพลิงรวม ปริมาณการทดแทนดีเซล การปลดปล่อยความร้อนสุทธิ รวมทั้งภาพปรากฏการณ์ ของละอองฝอยจากการฉีด การเผาไหม้ ความน่าจะเป็นของเปลวไฟ อุณหภูมิการเผาไหม้ ปริมาณ soot ในเปลวไฟ และ ได้นำเสนอแนวทางใหม่สำหรับพิจารณาจุดเริ่มต้นการฉีดของเชื้อเพลิงจากข้อมูลความดันในท่อจ่ายเชื้อเพลิง

การใช้ทั้งดีเซลและปาล์มไบโอดีเซล เครื่องยนต์เดินเรียบปราศจากการเขกทุกจุดที่ทำการทดสอบและทุกค่า ส่วนผสมของ LPG ที่ใช้ แม้ว่าจะมีประสิทธิภาพการแปลงพลังงานต่ำกว่า ซึ่งจะลดลงเมื่อความเร็วรอบหรือภาระต่ำลง และเมื่อสัดส่วนของ LPG เพิ่มขึ้น การใช้ LPG ร่วมดีเซลสามารถทดแทนดีเซลได้ราวร้อยละ 26-27 ที่ความเร็วรอบและ ภาระสูง และราวร้อยละ 60-65 ที่ภาระต่ำ (โดยการใช้ LPG-PME จะสามารถทดแทนได้น้อยกว่า) พบช่วงการติดไฟล่าช้า เพิ่มขึ้นราว 0.6°CA เมื่อใช้ LPG ร่วมดีเซล และเพิ่มมากขึ้นถึง 1.2°CA เมื่อใช้ LPG-PME โดยเฉพาะที่ความเร็วรอบต่ำ และเมื่อเพิ่มปริมาณ LPG พบว่าจุดเริ่มต้นการเผาไหม้ล่าช้าลงเมื่อใช้ LPG-ดีเซล ซึ่งส่วนใหญ่เนื่องมาจากการฉีดที่ล่าช้า จากการลดปริมาณการฉีด ขณะที่จุดเริ่มต้นการเผาไหม้ของ LPG-PME จะเร็วกว่าเนื่องมาจากผลของการฉีดที่เร็วขึ้นจาก ผลของ bulk modulus และความหนืดที่สูงกว่าของ PME ทั้ง LPG-ดีเซล และ LPG-PME มีช่วงเวลาการเผาไหม้ที่สั้นลง เมื่อเปรียบเทียบกับการเผาไหม้ของดีเซล เป็นผลให้อุณหภูมิไอเสียมีค่าต่ำลง และทำให้จุดกึ่งกลางของการปลดปล่อย ความร้อนเลื่อนเข้าหา TDC มากขึ้น แม้ว่าในกรณีของ LPG-PME จะให้ผลชัดกว่า(เลื่อนไปถึง 2.8°CA) แต่กลับพบว่า ช่วงเวลาการเผาไหม้มีระยะเวลายาวกว่าเมื่อเทียบกับ LPG-ดีเซล เนื่องจากอิทธิพลของค่าความร้อนและคุณสมบัติการ ระเหยที่ต่ำกว่าดีเซลของ PME แม้การเผาไหม้ทั้งสองจะให้ค่า IMEP ที่มีค่า COV ที่ไม่แตกต่างกัน แต่พบว่า LPG-PME มีความแปรปรวนของการเผาไหม้สูงกว่าเล็กน้อย มีเสถียรภาพต่ำกว่าและเปลวไฟที่มีอุณหภูมิสูงปรากฏในบริเวณที่แคบ กว่า ทั้งนี้เนื่องมาจากคุณสมบัติของ PME อาทิ ค่าความร้อนที่ต่ำกว่า ค่าอุณหภูมิอะเดียบาติกของเปลวไฟต่ำกว่า และ ความหนาแน่นที่สูงกว่า ความเข้มข้นของ soot ในเปลวไฟมีปริมาณลดลงเมื่อปริมาณสัดส่วนของ LPG มีค่าสูงขึ้น โดย สัดส่วนการลดเมื่อใช้ LPG-PME ให้ค่าการลดลงที่สูงกว่า ผลจากการฉีดล่วงหน้า 1.2°CA จะให้การเผาไหม้ใน LPG-ดีเซล ที่ดีกว่า ขณะที่องศาการฉีดที่แนะนำโดยผู้ผลิตเหมาะสมกับการเผาไหม้ของกรณี LPG-PME

ผลการวิจัยนี้สามารถสรุปได้ว่า การนำระบบเชื้อเพลิงร่วมมาใช้งานให้เกิดประโยชน์สูงสุดจะต้องคำนึงถึง ค่าใช้จ่ายที่ลดลงควบคู่ไปกับการพิจารณาประสิทธิภาพเชิงพลังงานที่ลดต่ำลง

ภาควิชา.......วิศวกรรมเครื่องกล............. ลายมือชื่อนิสิต..................................

สาขาวิชา.......วิศวกรรมเครื่องกล........... ลายมือชื่ออาจารย์ที่ปรึกษา.....คณิต วัฒนวิเชียร

ปีการศึกษา 2549

4671841821 ...... MAJOR MECHANICAL ENGINEERING

KEY WORD: DIESEL DUAL FUEL/ LPG / BIODIESEL / COMBUSTION / VISUALIZATION

PHAN MINH DUC: A STUDY ON THE LPG DUAL FUEL COMBUSTION CHARACTERISTICS OF AN INDIRECT INJECTION COMPRESSION IGNITION ENGINE. THESIS ADVISOR: ASST. PROF. KANIT WATTANAVICHIEN, Ph.D., 284 pp.

This investigation which aimed to identify the effect of biodiesel as the pilot injection in dual fuelled engine can be divided into 3 parts. Firstly, combustion characteristics of liquefied petroleum gas (LPG) premixed charge-diesel dual fuelled engine was studied. Next, the investigation continued with the pilot injection changed to palm biodiesel (PME). Lastly, it finished with varied injection timing for neat liquid as well as dual fuelling to fulfill a comparison. Test bench experiments (steady state) were conducted with a 4-cylinder IDI CI engine, at selected high probability operating points corresponding to the ECE15+EUDC cycle, covering the range [10-70] Nm @ [1250-2750] rev/min. The engine ran at overall lean mixture. The LPG-air premixed mixture was maintained at four fixed values by an electronic controlling system. The acquired data included basic parameters, pressure history of fuel line and combustion chambers, and accessed combustion chamber visualization. The comparative analysis deal with: energy conversion efficiencies, specific total energy consumption, liquid fuel substitution, net heat release, combustion chamber phenomena including spray, combustion, flame probability distribution, flame temperature, and soot concentration (two color method). A new approach to determine the start of injection (SOI) based on fuel line pressure data was also proposed.

Both diesel and PME provided smooth, knock-free dual fuel operation, at all planned test points and LPG-air premixed charge, with the energy conversion efficiency deterioration increased at lower speeds and higher LPG ratios. Achieved substitution was about 26%-27% at high speed, load and 60%-65% at low speed, load (lower with LPG-PME). Ignition delays which retarded within 0.6°CA in LPG-diesel might increase up to 1.2°CA with LPG-PME, especially at low speed, increased LPG. The start of combustion which retarded in LPG-diesel, mostly due to retarded start of injection brought by pump effect as diesel was reduced, was found to advance in LPG-PME due to their shorter ignition delays and advanced SOI caused by the higher bulk modulus and viscosity of the PME. Both LPG-diesel and LPG-PME produced faster combustion compared to the neat liquid fuel, leading to reduced exhaust gas temperatures and the centers of heat release area's moving of towards TDC. Though the moving was much more (up to 2.8°CA) in LPG-PME cases, their combustion duration was longer compared to LPG-diesel due to the lower heating value and volatility of the PME. While the coefficient of variation of IMEP was comparable, the combustion noise of LPG-PME was slightly higher. With LPG-PME, the flame probability distribution and the area of high flame temperature was smaller, due to the PME properties: lower heating value, lower adiabatic flame temperature, and heavier. This was also thought due to the limit of the two color method when applied for gaseous and oxygenated fuel combustion. Concentration of soot in flame was observed to be lower with higher LPG and was much lower in LPG-PME cases. The 1.2-degree-advanced injection timing gave better LPG-diesel combustion while the OEM setting was suitable for LPG-biodiesel combustion.

It can be concluded that the reasonable operational must rely on the compromise between LPG saving cost and the efficiency deterioration, for both LPG-diesel and LPG-PME cases.

Department.....Mechanical Engineering   Student's signature...

Field of study...Mechanical Engineering Advisor's signature ...Kanit Wattanavichien.........

Academic year 2006

Acknowledgements

Three years of my studying in Chulalongkorn University comes to an end and it remains to take the opportunity to acknowledge the people who made this time so enjoyable.

Firstly, I would like to specially thank my advisor, Prof. Kanit Wattanavichien for his guidance, support, and establishing the environment for any student who finds an interest in internal combustion engine.

My stay and study in Thailand would not have been possible without the funding of the "Project 322" of Vietnamese Government. I would also like to acknowledge all Vietnamese citizens for their contribution.

Thank is also to Takuni Co., who partially supported me fuel, equipment and my maintenance allowance during my time here in Bangkok.

Back home in Vietnam, I would like to thank all the friends in our laboratory, who have been always willing to help me, and hope that we will always find opportunities to get together independent of where in the world we will end up.

Finally, I would like to thank my family who have always stood behind me and given me the love and resources I need to succeed in life. Especially, my mom did not speak English, so "Mẹ ơi, con nhớ thương mẹ vô cùng và nguyện cố gắng hết mình để thỏa ước mong của ba mẹ".

Contents

List of tables

List of figures

Abbreviation and symbols

Abbreviation	Explanation	Units
CI	Compression Ignition	
CR	Compression Ratio	
DI, IDI	Direct Injection, Indirect Injection	
NG	Natural Gas	
CNG	Compressed Natural Gas	
LNG	Liquefied Natural Gas	
LPG	Liquefied Petroleum Gas	
PME	Palmitic Methyl Ester	
EGR	Exhaust Gas Recirculation	
DDF	Diesel dual fuel	
TDR	Turn-down ratio	
HMC	Homogeneous combustion	
HTC	Heterogeneous combustion	
HPDI	High Pressure Direct Injection	
TDC	Top Dead Center	
BDC	Bottom Dead Center	
bTDC	Before Top Dead Center	
aTDC	After Top Dead Center	
CA, $^{\circ}$CA	Crank angle, crank angle degree	
UHC	Unburnt Hydrocarbon	
NMHC	Non-Methane Hydrocarbon	
PM	Particulate Matter	
NO_x	Nitrogen Oxide	
PAH	Polycyclic Aromatic Hydrocarbons	
SOF	Soluble Organic Fraction	
HV	Low heating value	
HR, NHR	Heat Release, Net Heat Release	
HRR	Heat Release Rate	

Abbreviation	Explanation	Units
PRR	Pressure Rise Rate	
CN	Cetane number	
ASTM	American Society for Testing and Materials Standards	
STD	Standard deviation	
COV	Coefficient of variation	
ADC	Analog-to-digital converter	
CCD	Charge coupled device	
SOL	Start of luminescence	
EOL	End of luminescence	
AOS	Appearance of spray	
SDC	specific diesel consumption	g/kWh
STEC	specific total energy consumption	MJ/kWh
Sub	Liquid fuel substitution	%
A/V	Surface to volume ratio of the combustion chamber	m^{-1}
m	Mass delivered (of diesel, biodiesel, LPG, air)	kg, kg/cycle
$\overset{*}{m}$	Mass flow rate (of diesel, biodiesel, LPG, air)	kg/s
$(A/F)_{st}$	Stoichiometric fuel air ratio	
bmep	Brake mean effective pressure	$kPa, N/m^2$
IMEP	Indicated Mean Effective Pressure	$kPa, N/m^2$
P	Engine brake power output	W, kW
T	Engine brake torque	Nm
N	Engine rotational speed	rev/min
V	Combustion chamber volume	m^3
V_d	Swept volume	m^3
$W_{c,i}$	Indicated work per cylinder per cycle	J/cyc./cyl.
GEF	Gas energy fraction in dual fuel mode	%
η_f	Brake total energy conversion efficiency	-
STEC	Specific total energy consumption	MJ/kWh

Abbreviation	Explanation	Units
p	Pressure	bar, kPa
$\dfrac{dQ}{dt}$, $\dfrac{dQ}{d\theta}$	Heat release rate	J/s, J/^{O}CA
$\dfrac{dm}{dt}$	Mass flow rate	kg/s
$\dfrac{dU}{dt}$	Rate of change of internal energy	J/s
$\dfrac{dV}{dt}$	Rate of change of combustion chamber volume	m^3/s
T	Absolute temperature	K
h	Specific enthalpy	J/kg
n	Number of consecutive cycles used in heat release analysis, cyclic variation analysis	-
E	Radiation intensity	Wm^{-3}
C_1	1st constants of Plank equation, $C_1 = 3.7418 \times 10^{-16}$	Wm^2
C_2	2nd constants of Plank equation, $C_2 = 1.4388 \times 10^{-2}$	mK
I	Monochromatic emissive power	
K	Absorption coefficient	-
L	Geometric thickness of the flame along the optical axis of the detection system	m
C_V	Soot volumetric density	kg/m^3
m	Complex refractive index of the soot particle	-
T_{a1}, T_{a2}	Apparent temperatures	K
C_{DO}	Discharge coefficient of the orifice	-
A_O	Orifice area	m^2
D_O	Diameter of the orifice	m
Δh	The head at manometer	mm

Greek

γ	Polytropic index	-
Δp	Differential pressure between the chambers	bar, kPa
θ	The instant considered in heat release calculation	^{O}CA

Abbreviation	Explanation	Units
ρ	Density	kg/m^3
η_v	Volumetric efficiency	-
η_f	Brake total energy conversion efficiency	-
η_m	Mechanical efficiency	-
ϕ	Total fuel air equivalent ratio	-
ε	Monochromatic emissivity	-
λ	Wave length	μm
α	Constant for limited wave length range	μm

Subscripts

D	Diesel
B	Biodiesel
BL	Biodiesel-LPG dual fueling operation mode
DL	Diesel-LPG dual fueling operation mode
LPG	Liquefied petroleum gas
air	Air
1	Main chamber
2	Pre-chamber
21	Refer to the fluid transferring across the passage
f	Fuel
st	Stoichiometric
o	Standard condition

Superscripts

–	Mean value
*	Time derivative

CHAPTER 1

INTRODUCTION

1.1. Motivation for this investigation

The increasingly strict oil crisis and emissions legislations introduced put strong stress on engine researchers and manufacturers, forcing them to find realistic solutions within a time frame. Dual-fuelling is one among the feasible solutions since it permits to use gaseous fuels which are cheap fuels, in a diesel engine.

In homogeneous combustion diesel dual fuel (DDF) engines, good diesel substitution levels are only obtained at mid-load range; at low load the diesel injectors still require a substantial fuel delivery while at high load the prolonged ignition delay increases the tendency for diesel knock as well as end-gas knock of the mixture of gaseous fuel, residual, and air. While different gaseous fuels have been applied to dual fuel operation, less type of liquid fuels as the pilot has been investigated. A pilot-injection fuel which can offset, to some extent, the prolonged ignition delay is expected to offer an improvement at the low end as well as having improved potential at the high end. Oxygenated fuel is expected to be such fuel, in addition, to improve combustion process of dual fuel engine in mid-load range as well. The current work, therefore, aims to investigate dual fuel combustion characteristic with biodiesel as the pilot.

1.2. Benefits from diesel dual fuel operation

DDF operation represents advantages compared to diesel counterparts and spark ignition (SI) engines: theoretically higher thermal efficiency resulted from faster burning, less toxic emission, high power density, strong ignition sources providing more reliable, less sensitive with respect to changes in the second fuel composition, lower fuel cost, ability to operate with many types of alternative fuel; gaseous fuels or alcohols, and ability to switch back as necessary. Moreover, in contrast with diesel operation, DDF provides ability of reducing simultaneously both soot and NO_X emissions in certain conditions. Beside these advantages, DDF operation reveals some disadvantages. Among them, perhaps issues related to "homogeneous" type and the complexity

resulted from two-fuel system in relation to the target of achieving effective engine operation is the most prominent.

1.3. Target of the study

This investigation aims to identify the effect of biodiesel as the pilot injection in dual fuelling operation with LPG. Comparison is made with diesel operation (as the baseline) and diesel-LPG operation. The study is carried out on a test cell with a commercial 4-cylinder indirect injection (IDI) compression ignition (CI) engine at steady state at selected engine operating points determined from the ECE15+EUDC test cycle.

1.4. Thesis outline

After the brief above introduction the remainder of this dissertation is organized as follows:

Chapter 2 gives a brief description of diesel combustion process and its main emission source, in the first section, then continues with the definition, classification, and review on diesel dual fuel engine investigation.

Chapter 3 presents mentions possible fuels, gases and liquid, for diesel dual-fuelling that have been applied. Properties of the fuels used in this study are described. Their effect on injection and combustion are then addressed.

Chapter 4 describes the test system. The construction of the system and the specification of equipments/ instruments used are given.

Chapter 5 gives, firstly the definition of parameters related engine performance and energy consumption and the method to estimate uncertainty of their results, followed by a description of the combustion system of the test engine. Its features with respect to diesel combustion improvement are also addressed. The effects on dual-fuel operation are then forecasted. The chapter concludes with heat release model applied for the combustion system and some background of cycle-by-cycle variation.

Chapter 6 presents the requirement for recorded in-cylinder pressure data including crank angle resolution and the number of consecutive cycles recorded, the pressure referencing and phasing. The chapter continues with the techniques used in in-cylinder pressure data treatment to perform heat release prediction. It ends with the

brief description of the computational tool which is built to predict as well as manager predicted result of the net heat release and cycle-by-cycle variation.

Chapter 7 presents the results and the analysis, including:

- The effect of LPG energy fraction on the combustion characteristic of the test engine in LPG-diesel dual-fuelled operation;

- The effect of biodiesel used as the pilot injection on the combustion characteristic of the test engine in LPG-diesel dual-fuelled operation;

- The effect of injection timing on the combustion characteristic of the test engine in LPG-diesel as well as LPG-biodiesel dual-fuelled operation.

Chapter 8 presents conclusions and contributions of the presented work. Potential areas for future work are then highlighted.

CHAPTER 2

DUAL FUELLING FOR DIESEL ENGINES

Internal combustion engines are mainly of two types: the Otto (SI) engine and the Diesel (CI) engine. Ingenious ideas about alternative combustion systems have been around for a long time. Many books and papers can be found to give complete descriptions on them. In this section, only the major differences between diesel and diesel dual fuel engines are mentioned.

2.1. Diesel engines

Diesel engines in which varying the amount of the liquid fuel injected into the cylinder controls the load operate at higher compression ratios than SI engines. Instead of ignition by a spark plug, the air-fuel mixture self-ignites due to compression. The processes, from the time the liquid fuel leaves the injector nozzles until it starts to burn, are complicated. Droplet formation, collisions, break-up, evaporation and vapor diffusion are some of these processes. The rate of the combustion process is generally limited by these processes; a part of the air and fuel are premixed and burn fast, but for the larger fraction of the fuel the time scale of evaporation, diffusion, etc. is larger than the chemical time scale. Liquid fuel partially burning results in soot formation. Together with NO_X, the emissions of soot characterize the diesel combustion process. For present engines, a trade-off between these two emissions is observed, which poses a major challenge to reach future legislation for both emissions. The major advantages of the CI compared with the SI engine are the low pumping losses, due to the lack of a throttle, and a higher compression ratio, leading together to higher efficiency.

2.1.1. Diesel combustion

Diesel engines combust compression-ignition inhomogeneous charge. Our understanding of the diesel combustion process has evolved over the years and significant progress has been made with optical techniques such as laser imaging. Dec J.E. et al. [1] combined laser techniques with chemical kinetic models to postulate a new description of the combustion process in DI CI engines.
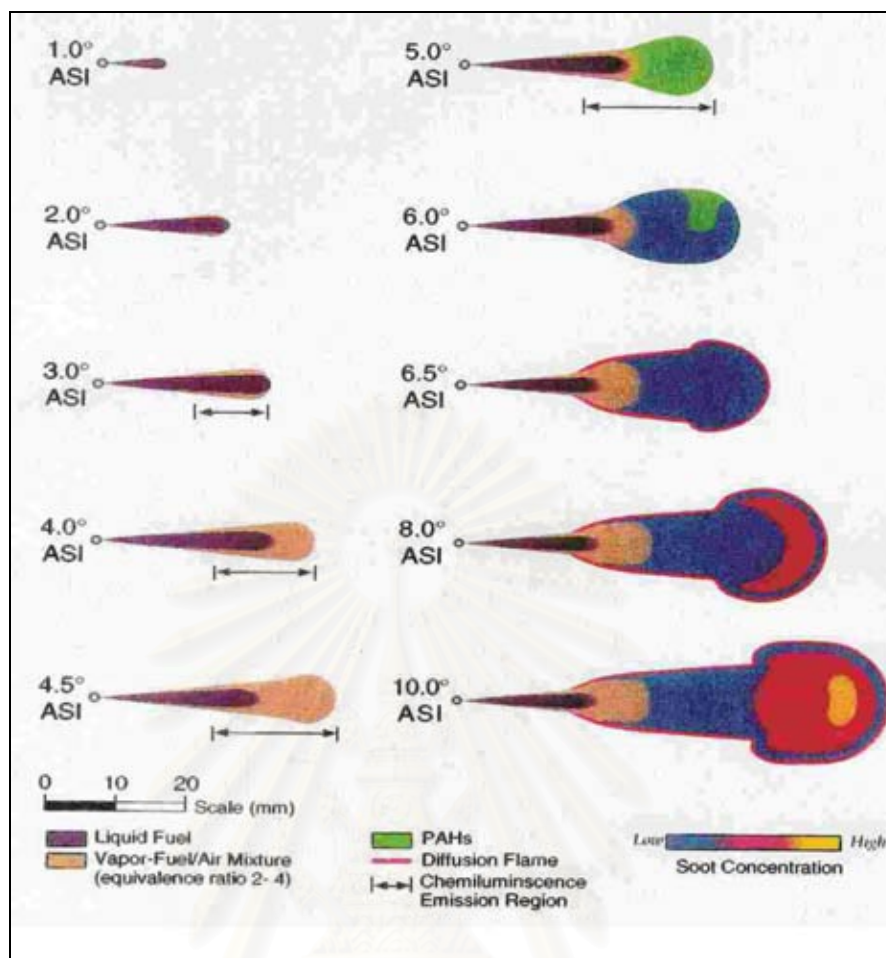
Figure 2–1   Diesel combustion process[1, 2]

Figure 2–1 shows a sequence of idealized schematics of the diesel combustion during injection for different crank angle degrees after the start of injection (ASI). The cold fuel jet penetrates the combustion chamber and entrains hot air in the cylinder, causing the liquid fuel to warm up and vaporize. A sheath of vaporized air/fuel mixture (with relative air/fuel ratio $\lambda = 0.25 - 0.5$, i.e. four to two times richer than stoichiometric) encloses the growing fuel jet until it reaches a temperature of around 750K at which point the fuel begins to react (~5°CA ASI). These reactions and the additional hot air entrained into the jet raise its temperature to approximately 825K increasing the rate of combustion. As these partial oxidations take place, reaction products are formed, pushed aside by and then re-entrained into the penetrating jet (heating it up to 1600-1700K). At around 6.5°CA ASI, a diffusion flame sheath forms around the cloud of partial oxidation products where temperatures reach 2700K. At 10°CA ASI, the process reaches a quasi-steady state as depicted in the last frame. Eventually, the air entrained

during the premixed burn is entirely consumed and the mixing-controlled combustion in a quasi-steady flame continues until the end of injection, and after.

Although the model assumes a continuous single input of fuel which is not valid for multiple injections with common rail injection systems it gives a good qualitative understanding of the diesel combustion process and the formation of pollutants, and the nature of the heat release.

2.1.2. Diesel emissions

The diesel engine's reputation with noise and smoke has changed due to modern diesel engine technology allowing combining the inherent low fuel consumption with excellent driving performance and low emission characteristics. After carbon dioxide (CO_2) was identified as a greenhouse gas contributing to global warming, diesel engines have emerged as an alternative to gasoline engines due to their low fuel consumption and hence low CO_2 emission. While carbon monoxide (CO) emissions are negligible in CI engines due to lean operation and emissions of unburnt hydrocarbons (UHC) can be handled with oxidation catalysts, the emissions of oxides of nitrogen (NO_X) and particulate matter (PM) are of particular concern.

The formation of NO_X and PM is closely linked to the combustion process which depends on engine design variables such as combustion chamber and fuel injector design, pressure and injection timing, rate and profile, swirl ratio, valve timing, compression ratio, etc. Generally, these parameters can only be optimized for the reduction of one of the two main pollutants due to the so-called NO_X-PM trade-off. Typically, the other pollutant is controlled by after-treatment. Alternatively, NO_X and PM after-treatment solutions can be integrated which allows the combustion system and engine calibration to be optimized with respect to performance/efficiency.

Formation of Nitrogen Oxides and Particulate Matter

Diesel engine combustion begins around 5^0CA ASI in a locally rich premixed zone, as described in Figure 2–1. The products from this early reaction are small, partially burnt fragments of hydrocarbons which are generally believed to lead to the formation of polycyclic aromatic hydrocarbons (PAH) that constitute the building blocks for particulates in flames[1]. When the air entrained during the premixed burn is entirely consumed, the temperature reached by this partial oxidation is about 1600K and the

reaction products will subsequently receive heat from the hot diffusion flame to form an environment favorable for the formation and agglomeration of soot particles. The fuel fragments and soot particles are subsequently transported through the interior of the plume toward the boundary of the diffusion flame sheath where they are oxidized in a thin reaction layer at temperatures around 2700K. Experiments show that these particulates are completely consumed by the hot diffusion flame sheath so that diesel soot emissions appear to be the result of quenching this final phase of oxidation. The temperature profile of the quasi-steady flame is shown in Figure 2–2.
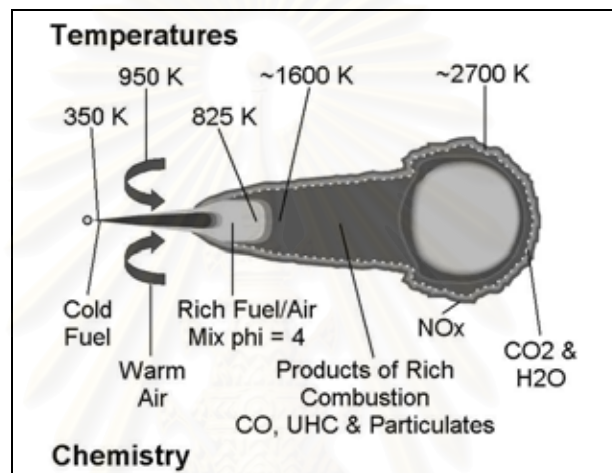
Figure 2–2   Quasi-steady flame [1, 2]

The major part of NO from the diesel combustion is formed by the oxidation of atmospheric nitrogen via the extended Zeldovich mechanism [3]:

$$O + N_2 \rightarrow NO + N \tag{2-1}$$

$$N + O_2 \rightarrow NO + O \tag{2-2}$$

$$N + OH \rightarrow NO + H \tag{2-3}$$
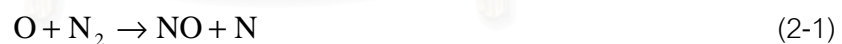
The formation of NO is highly temperature dependent due to large activation energies for the forward reaction, Eq. 2-1 and the reverse reactions in Eq. 2-2 and 2-3. It is initiated at temperatures greater than 1900K and the NO stays around during cooling since the reverse reaction is very slow. Fuel nitrogen is also a source of NO via a different and yet to be fully explained mechanism, however, its contribution is less significant in diesel engine combustion than the formation of NO via the Zeldovich mechanism. The produced NO can then be converted to NO_2 by reactions such as:

$$NO + HO_2 \rightarrow NO_2 + OH \tag{2-4}$$

However, this NO_2 is converted back to NO via:

$$NO_2 + O \rightarrow NO + O_2 \tag{2-5}$$

In the preceding discussion on diesel combustion process, high temperatures in a region where oxygen is available along with nitrogen characterize the diffusion flame sheath rendering this area the ideal region for the formation of NO_X. According to[1], two-thirds of the total NO_X emissions are formed in the diffusion flame while one-third is formed in the hot post-combustion gas regions. Chemical equilibrium considerations indicate that at typical flame temperatures, the NO_2/NO ratio should be negligibly small which is true for SI engines. However, in CI engines, NO_2 can contribute 10 to 30% of the total NO_X emissions because the back reaction from NO_2 formed in the flame to NO (Eq. 2-5) is quenched by mixing with cooler regions especially at light load[3].

Particulate Matter

Most of the particle *number* emitted by engines is in the nano-particle range, D<50nm, while most of the *mass* is in the accumulation mode, 50nm<D<1000nm [4].

Nanoparticles: Typical type is UHC/sulphate, but may also contain solid carbon and metal compounds; they form by nucleation during dilution and cooling; they also appear in SI engines; there may actually be more in some state-of-the-art diesel engines (the better combustion produces less accumulation mode particles on which small particles can adsorb; this was observed on an engine with high values of the soluble organic fraction SOF).

Accumulation mode particles: Mainly carbonaceous soot agglomerates directly from the combustion; 10 to 100 times more than in SI engines.

Typical particle composition (mass basis) for a heavy duty diesel engine on a transient cycle:

- 41% Carbon (Soot);
- 14% Sulphate and water;
- 13% Ash (from metal compounds in fuel and lube) and other;
- 32% Soluble Organic Fraction (SOF), consisting of 25% unburnt oil and 7% unburnt fuel with high boiling point; the low boiling point unburnt components become UHC emissions. SOF values can range between 10% and 90% and are highest at light engine loads when exhaust temperatures are low. The sulphuric acid/sulphate

concentration is roughly proportional to the fuel sulphur content. As the exhaust gas is cooled and diluted, nucleation, condensation, and adsorption transform volatile materials to solid and liquid particulate matter.

A review of particulate research is given in [5]. Following remarks can be drawn. The particle size distribution of solid soot particles generated in the cylinder varies little with fuel. Soot mass is generated about 10 to 20^0CA aTDC, with sizes up to 110 nm; as the piston drops, these particles oxidize and decrease in number about two orders of magnitude and in size to about 70 nm.

NO_X-PM trade-off

Soot particles, which heavily contribute to the total mass of particulate matter emitted by the engine, are formed in the cylinder in the locally rich regions of the inhomogeneous combustion. The subsequent soot burn-up at the boundary of the diffusion flame sheath is favored by high temperatures. However, high temperatures also favor the generation of NO_X. Thus, to decrease combustion temperature for lower NO_X emissions results in increase of PM. This dilemma is known as the NO_X-PM trade-off.

2.2. Dual-fuelled engines

2.2.1. Definition and classification of diesel dual fuel engines

Diesel dual fuel engine is an engine in which energy release in its operating cycle comes from two fuels. The first fuel, called the pilot and having high cetane number, produces a certain amount of heat release after its injection, auto-ignition and acts as an innumerable ignition sources to burn the mixture of air, residual gas, and a second fuel having relatively high octane number. The mixture may be formed homogeneously in intake process, being compressed prior to the pilot injection or heterogeneously sooner-or-later with it. The former can be classified as "homogeneous combustion" (HMC) or "conventional" while "heterogeneous combustion" (HTC) or "high pressure direct injection" (HPDI) is for the latter.

The main target of DDF is operational cost; the replacement by cheaper fuel tends to be maximized throughout the whole load range. This is accomplished usually without undermining the operation and performance of the diesel engine with sophisticate solutions.

2.2.2. History of Diesel dual fuel engines

Due to their advantages, DDF engines have attracted engine researchers for a long time. The earliest dual fuel systems, by Cave in 1929, Helmore and Sokes in 1930, were performed with hydrogen as a second fuel; resulting in 20% saving in diesel fuel[6]. The first commercial dual fuel engine, fuelled by town gas fuel, was produced in 1939 by the National Gas and Oil Engine Co., England. The engine was relatively simple in operation and employed in areas where cheap stationary power production was required. During the Second World War, due to the shortage of liquid fuels DDF engines got more attention in Europe. Some vehicles with diesel engines were converted and fuelled with many kinds of gaseous fuels: coal gas, sewage gas or methane. After the war, dual fuel engines have been further developed and employed in wide range of applications: stationary power production, haul trucks and buses, and marine transport. Several conversions were made by manufacturers with the usage of double plunger systems or two pumps to handle pilot quantity. From the mid 1980s, several projects were launched in the United States and Canada to assess the viability of NG fuelled locomotives[7]. A research project was attempted by Bombardier to review the use of NG as an alternative fuel for locomotives. Southwest Research Institute (SwRI) conducted similar project on a two-cylinder EMD engine. Concurrently, Burlington Northern Railroad began their own experiments with dual-fuelled locomotives, using CNG and LNG in combination with diesel fuel. These locomotives powered by up to 2237 kW two-stroke dual fuel engines could be able to run 2700 km round trip with single fuelling stop. Since then, other research projects on NG fuelled locomotives were completed in the United States, Russia, Germany, Japan, Finland, and the Czech Republic. In 1984, Russia started a program to develop NG fuelled locomotives. In 1993, four types of NG fuelled locomotives, which consisted of CNG/diesel switching locomotives and LNG freight trains, were commissioned in the Russian railway industry. Germany has successfully developed 165 kW CNG locomotives and tested them in rail yard switching operation. Japan, Finland, and the Czech Republic are also designing locomotives that operate on NG. In the United States, ongoing experiments on LNG/diesel dual-fuelled locomotives were conducted by BN until the mid 1990s. Morrison Knudsen Corporation introduced a MK1200G LNG-burning locomotive in 1994.

At this time, General Motors had developed an NG fuelled engine as a part of a cooperative industry research program with SwRI, to furnish new technologies for LNG fuelled freight and passenger locomotives.

Currently, DDF engines with power level up to approximate 1MW/cylinder have been commercially produced by companies, such as MAN B&W[8], Wartsila[9]. In addition, HPDI DDF engines for road vehicles, mainly medium and heavy duty trucks, has been investigated widely and applied in several countries such as the United States, several European countries, and China. Dedicated dual fuel vehicles are commercially available from the "Clean Air Partners" in the United States. Westport Innovations Inc. cooperates with Cummins Inc., developing and marketing their high performance engines and fuel systems [10, 11]. Their HPDI engines, 400 and 450HP, have been used to power heavy duty tractors, mine hauls, and waste-hauls in the United State. Although DDF engines have been practically used, further investigation is still needed.

2.2.3.   Diesel dual fuel homogeneous combustion engine

In these engines, homogeneous mixture of the second fuel with air and residual gas is compressed as the piston moves towards TDC in compression stroke. Close to TDC, the pilot fuel is injected in the same manner as in diesel engine, auto-ignites and burn the second fuel in the pilot spray. The combustion continues with the remaining pilot fuel (mixing control) and remaining homogeneous mixture distributed through out the combustion chamber. Under knock-free condition, combustion of the remaining homogeneous mixture is flame propagation. The engine operates at higher total fuel-air equivalent ratio since inducted air is partially replaced by the second fuel.

Combustion characteristics

Ignition delay

Ignition delay plays an important role and affects the whole combustion process of conventional diesel as well as DDF engines. Physical/chemical properties of the charge in this engine type, characterized by the presence of the second fuel accompanied with air and residual gas during compression process, at the time of pilot injection differ from that in a conventional diesel engine. This definitely results in change in ignition delay of the pilot by several factors.

First, generally the second fuel which can often be gaseous or liquid and has relatively lower polytropic index compared with air, causes decrease in maximum charge temperature.

Second, volumetric efficiency reduction caused by the replacement of a fraction of air by gaseous/vapor fuel leads to relatively lower oxygen concentration of the charge. In addition, the reduction is also caused by a gas mixer which is often installed into the intake manifold to introduce the gaseous fuel and form homogeneous charge.

Third, some fuels having high heat of vaporization and initially introduced to the engine at liquid form cause a decrease in the charge temperature.

And last but the dominant factor, gaseous/vapor fuels occupying long time period in compression process undergo chemical pre-ignition reactions prior to pilot injection, even the mixture strength is lean. Species produced from that reactions will actively participate to the pre-ignition chemical processes of the pilot. Naturally, this process is thus affected by the nature of the gaseous/vapor fuel, its mixture strength, and prevailing conditions inside the cylinder. Pre-ignition reaction of the premixed charge would cause its temperature to increase, especially at richer mixture. Figure 2–3 gives an example of this. As seen in the figure, an increase of approximate 20K in the maximum temperature may be found in a DDF engine with volumetric CR of 14.2, CH_4-air premixed mixture with equivalent ratio of 0.5 at initial temperature of 323K.

The prolonged DDF ignition delay, that often reaches a peak at certain mixture strength depending on the gaseous/vapor fuel, is the net effect of above factors. The prolonged delay would lead to the shift of DDF combustion process some CA degrees towards BDC. A comparison in the ignition delay of a DDF engine operating with different gaseous fuels and straight diesel is represented in Figure 2–4. Among considered gases, hydrogen produced least prolonged ignition delay, followed by methane, ethylene and propane.

A correlation to predict ignition delay for premixed charge CI DDF engine had been proposed by Prakash G. et al [12] based on the modification of Hardenberg and Hase correlation for the delay in diesel engine.
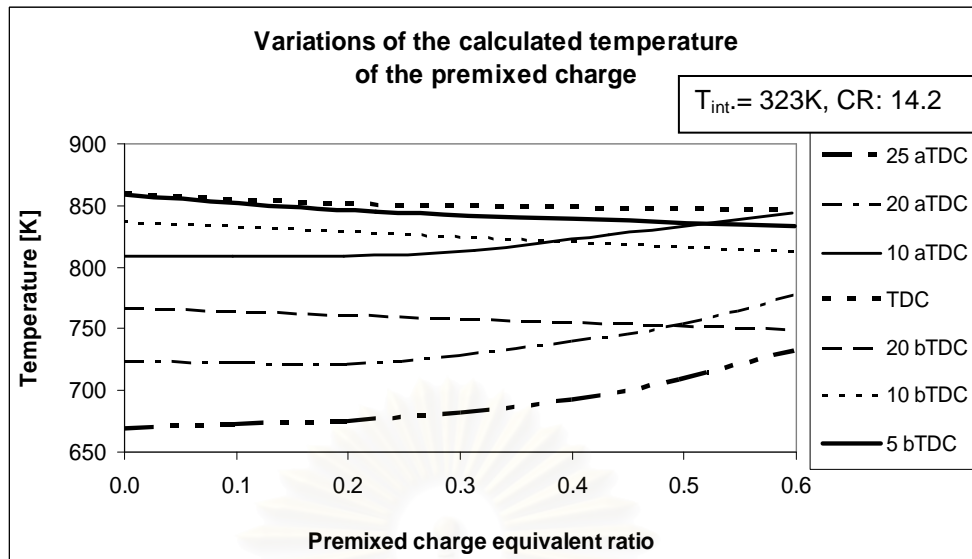
Figure 2–3 - Variations of calculated CH$_4$-air charge temperature in compression and expansion strokes of a motored engine without pilot injection, *(reproduced from [13])*
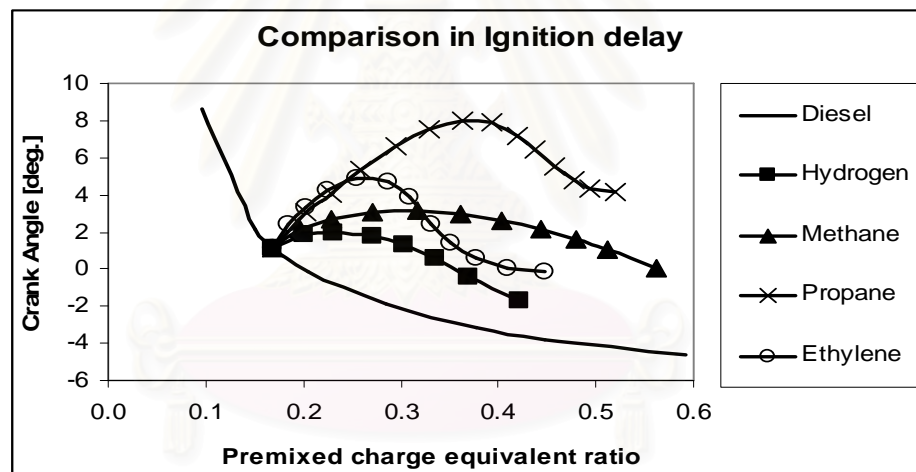
Intake charge temperature: $T_{int} = 0\,^{\circ}C$; Pilot injection: 4kg/h; Injection timing $\theta = -20\,^{\circ}CA$

Figure 2–4 - Ignition delay of a diesel-gaseous DF engine, (reproduced from [14])

In-cylinder pressure, heat release, engine performance, and energy consumption

The pilot fuel after its auto-ignition acts as innumerable ignition sources for the premixed mixture inside the combustion chamber. The presence of premixed charge contributes to changes in heat release characteristic of DDF engines; making it different from that of the diesel counterparts. DDF heat release under knock-free conditions can be considered as a summation of three components which last three stages: ①the heat release from premixed burning phase of part or whole the pilot injection and that from a

fraction of premixed mixture entraining in the pilot spray, ②that from rapid combustion of the premixed mixture in immediate vicinity of the pilot spray, and diffusive combustion of the remain pilot fuel, and ③that from consequent turbulent flame propagation in the remain premixed mixture, as seen in Figure 2–5. The interrelation among these 3 components may change; depending on overall fuel-air ratio, the premixed mixture strength, diluents, charge temperature, as well as engine geometry. As the overall equivalent ratio and premixed mixture strength decrease to certain value, especially at low intake air temperature, the first and second components may merge together as seen in Figure 2–6.
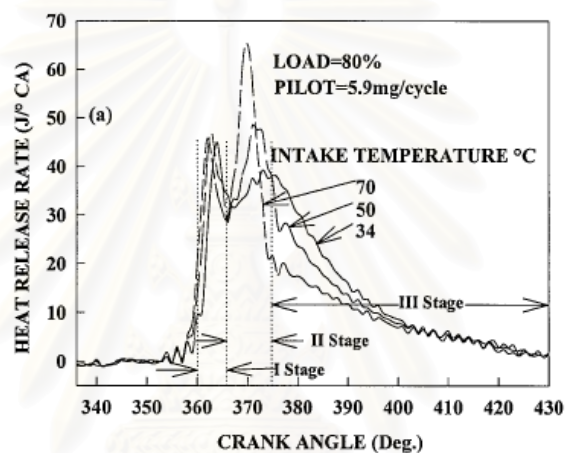
Figure 2–5 - Three-component HRR of a DI LPG-DDF engine with CR=15 at 1500 rpm, 80% load, different intake air temperatures: 34, 50, and 70^{0}C [15].
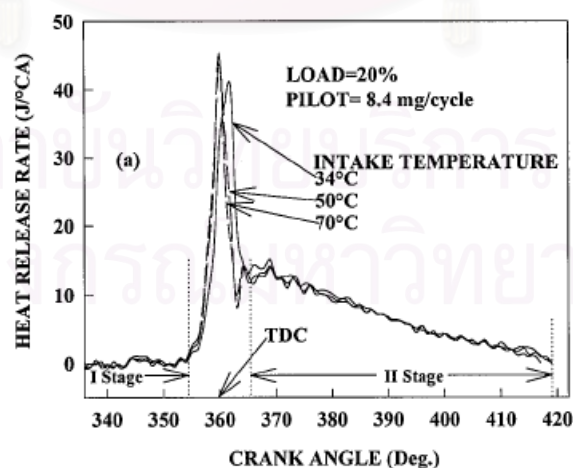
Figure 2–6 – Two-component HRR of a DI LPG-DDF engine with CR=15 at 1500 rpm, 20% load, different intake air temperatures: 34, 50, and 70^{0}C [15].

Peaks of pressure and PRR in DDF engines depend on combustion chamber (type and compression ratio), diesel injection system, nature and amount of gaseous fuel used, intake and pressure charge temperature, injection timing as well as EGR. The peaks of pressure and PRR in diesel engines are prescribed by the premixed combustion phase of diesel. They are higher in DI engines since large fraction of diesel burns in premixed combustion phase whilst they are limited in IDI due to high turbulent mixing of fuel and air in the pre-chamber. With the application of multi-stage injection or depressed injection rate at initial period, the peaks of pressure and PRR are reduced for both DI and IDI types[16-20]. With EGR applied, diesel ignition delay is prolonged and oxygen concentration is reduced, leading to lower peaks of pressure and PRR for both DI and IDI engines[21, 22]. Consequently, heat release characteristics in dual fuel operation may reveal different trends with different engines.

For DI engines with conventional injection system, operating in DDF mode at medium/high loads and sufficient high diesel substitution ratio, while the peak of pressure may be lower because less fuel burns in premixed phase, in the next combustion stages in-cylinder pressure may be higher than in diesel engine since the second fuel being mixed well with air burns faster than the diffusive combustion of diesel[23, 24]. Too high diesel substitution by gaseous fuels at high load may result in high pressure and PRR in the second combustion stage, even higher than that in the diesel counterpart[25]. The increase is caused by faster burning of the premixed charge since its burning velocity increases with mixture strength. This trend is enhanced with increased intake air temperature[15, 26, 27]. Diesel substitution ratios, at which the peaks of pressure and PRR in DDF exceed that in straight diesel, for DI engines with multi-stage injection or depressed injection rate at initial period are thought to be significantly lower than that with single stage injection. Considering different gaseous fuels with the same engine and operational conditions, LPG produced highest peak of pressure and PRR, followed by NG and then CH_4[28]. The use of fuels having high vaporization heat and supplied in liquid form (alcohols or LPG, LNG) as the second fuel with high substitution might cause high decrease in peak of pressure and PRR since they have high heat of vaporization compared to diesel, leading to the reduction of cycle

temperature and pressure[29]. However, too high substitution may lead to end gas knock[30].

For IDI engine, except low loads DDF operation generally produces higher peak of pressure and PRR than diesel operation due to the contribution of premixed fuel-air mixture, at relatively low diesel substitution compared to DI engine[28, 31]. This is thought easier to be observed with IDI engine having multi-stage injection. While ignition delay is less sensitive with respect to changed operational conditions in diesel operation, it is more sensitive in DDF operation. Due to this, the peak of PRR in DDF might move to after TDC whilst it is at before TDC in IDI diesel engine[31]. Due to high heat loss resulted from high A/V ratio, especially with the main combustion chamber, and the specific geometry of piston crown (For example, the double leaf, trench, and divider areas with Ricardo combustion system) designed satisfactorily for diesel combustion, a certain fraction of the premixed fuel-air mixture far from the double leaf area may not burn if the mixture strength is low. However, for combustion of the mixture in the main chamber there is no heat loss due to the throat as in diesel operation. Resulted from this, deterioration in indicated pressure of DDF IDI engines compared to that in DI engines may be lower.

Generally, compared to their counterparts DDF engines operating with commercial NG or LPG produce almost no significant deterioration in engine performance, even increase trends might be occurred in some studies[32, 33]. This is clear to understand since they operate at higher total fuel-air equivalent ratio. In contrast, alcohols and low BTU gases DDF may result in lower maximum engine output.

Exhaust gas emission characteristics

Exhaust gas emission of DDF combustion reveals differences from that of conventional diesel combustion in which diffusion combustion dominates, due to the replacement of a fraction diesel by the second fuel burning in homogeneous form. Obviously, trends and levels in emission depend on the nature of fuels used, diesel substitution ratio, engine type: DI or IDI, fuel injection system (injection timing and profile), and operational conditions.

Although the pilot fuel injected provides strong ignition sources the premixed mixture can not burn completely, leading to UHC and CO in exhaust gas. The flame front

propagation which depends on the second fuel properties, fuel-air equivalent ratio of premixed mixture and prevailing conditions in combustion chamber takes place in certain period of time corresponding to combustion process. While the lower limit of premixed mixture strength in DDF engines appears to be in reasonable agreement with extrapolated values of the flammability limits of the fuel-air mixtures up to engine conditions, the rich limit is much lower than the accepted higher flammability limit which is thought due to pilot ignition failure[14]. However, normally knock limit of the premixed mixture is much lower than the rich limit.

As the premixed mixture is very lean, flame front propagation can not spread the whole combustion chamber, leaving a large amount of UHC and CO which will exit to the exhaust manifold. This is more severe with IDI engine in which quenching is naturally high due to high A/V ratio especially for the main chamber. While UHC and CO concentration in exhaust gas decrease with increased loads in diesel operation[3], these emissions may increase [24, 29, 34-37] with increased loads in DDF with a fixed diesel pilot injection until a certain premixed mixture strength with which the total equivalent ratio is in the range (0.45-0.55) [14, 34-36]. Accompanied with this, the UHC may escape to exhaust manifold in overlap or scavenging period. As the premixed mixture strength exceeds some certain limits the flame front spread faster and throughout the combustion chamber, producing higher PRR and HRR, the UHC and CO emissions then decrease with increased mixture strength.

While diesel operation produces higher smoke level at increased loads, DDF operation for DI engine leads to drastic decrease in soot emission[26, 37, 38] since diesel diffusion combustion is reduced. The decrease level in DDF IDI engines is less than that in DI engines. It seemed that peaks of smoke emission and CO emissions are at the same total fuel-air equivalent ratio of about 0.45 [14]. However, the emission was also reported to decrease proportional with increased diesel substitution ratio[39]. Typical trends in emissions of a CH_4-DDF DI engine, with fixed pilot injection and 1000 rpm are represented in Figure 2–7.

Generally, NO_X emission reveals increase trends with IDI DDF engines [35, 39] whereas decrease trends with DI DDF engines at low-to-medium loads [27, 32, 40, 41] and, may be increase trends at high/full loads compared to straight diesel[32, 41]. In

diesel engine, critical equivalent ratio for NO_X formation in high-temperature high-pressure burnt gases is close to stoichiometric and critical time period is when burnt gas temperatures are at a maximum: between start of combustion and shortly after the occurrence of the peak of pressure[3]. After the time of peak pressure, decreased temperature due to expansion and mixing of high-temperature gas with air and/or cooler burnt gas freezes the NO_X chemistry, leading to much less decomposition of the NO_X. Thus, in DI engines the emission is roughly proportional to the mass of diesel injected. In contrast, with IDI engines the mixture in the pre-chamber rapidly becomes stoichiometric or fuel-rich and composition across the chamber is essentially non-uniform. After the time of peak pressure, due to fuel-rich mixture substantial NO_X decomposition in pre-chamber can occur while the NO_X formation ceases with about one-half of fuel being forced and burn in the main chamber, leading to the level-off of NO_X emission as load increases. Multi-stage injection and depressed initial injection pressure result in decreased amount of diesel burning in premixed-combustion phase, hence reduce soot and NO_X emission for DI engines but soot emission for IDI engines[19].
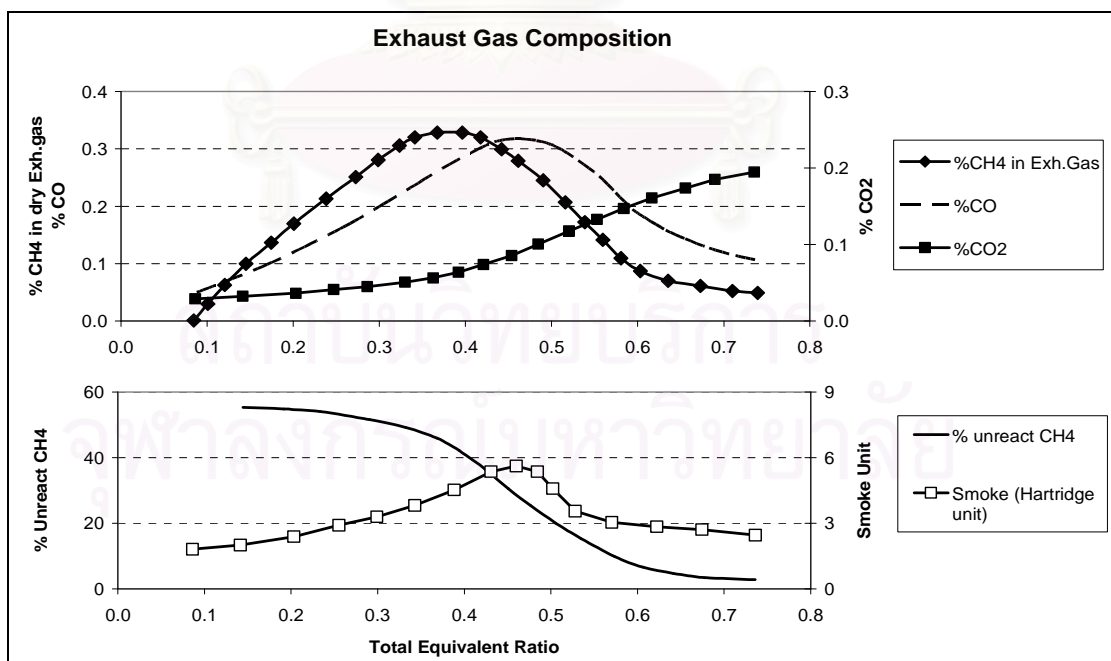
Figure 2–7 - Variation of exhaust gas composition of a CH_4-diesel DF DI engine at 1000 rev/min, pilot injection 0.227kg/hr and injection timing 18°bTDC, *(reproduced from [14]).*

Consequently, an IDI DDF engine normally produces higher NO_X level at medium-to-high loads since its combustion is faster at these conditions, and comparable levels [39] at low loads compared to diesel counterpart. For DI DDF engines, since diesel diffusion combustion is partly replaced NO_X level is reduced. However, as engine load increases, with higher fuel-air equivalent ratio brought by diesel substitution and increased amount of fuels, faster combustion will result in higher temperature and pressure, causing higher NO_X.

There are several factors that contribute to DDF soot emission characteristics as a fraction of diesel is replaced by gaseous fuels: ①The gas is more readily to burn; ②the faster burning of premixed mixture provides longer time of high-temperature, high-pressure for the unburnt fuel; ③the wall-impingement of liquid fuel is reduced; ④higher fuel-air equivalent ratio of DDF results in higher flame temperature; ⑤the second fuels used (often gaseous fuels) have lower carbon content. As a result, reduction in soot emission of DDF engines is obvious and the decrease level depends on the second fuel used, diesel substitution ratio, combustion chamber type, diesel injection system, as well as operational conditions. A drastic reduction in soot emission may be achieved, especially at high/full loads for both single-stage injection DI and IDI engines [14, 24, 39, 42]. Less decrease will be with multi-stage injection DDF engines since these engines inherently have low soot emission. However, for IDI engines, at low loads DDF soot emission may be at comparable levels with that in diesel operation due to dominant effect of heat transfer to combustion chamber wall.

Liquid fuels having high heat of vaporization such as alcohols, when used as the second fuel may produce higher level of soot and lower level of NO_X emissions with a certain range of diesel substitution compared to gaseous fuels.

Boundaries of the premixed mixture in DDF HMC engines

Obviously, the premixed mixture combusts only as its strength is within a certain range between lean and rich limits at prevailing conditions in combustion chamber. These conditions are functions of engine operating variables: intake charge temperature and pressure, compression ratio, pilot injection quantity and timing, heat transfer, and the physical properties of the premixed charge. Elliot and Davis reported such apparent

limits in a DDF engine operating with different gaseous fuels[43]. As the strength is under lean limit, although starting from multitudinous ignition sources the flame front can not propagate fast and far enough to consume the whole mixture in the chamber in available period of time; misfire may occur if the mixture is too lean.

Based on their experimental data, Badr O., Karim G.A. et al established a correlation between flame spread limits in combustion chamber of DDF engine with quiescent flammability limit[44]. The flame spread limits are corresponding to quiescent flammability limit at temperature of ($T_{TDC} + \alpha\Delta T$) where T_{TDC} is the temperature of the premixed charge at TDC with assumption that pilot ignition does not contribute to the change of premixed mixture charge until TDC is reached, ΔT is charge temperature increase due to pilot fuel heat release contributed uniformly in combustion chamber, α is a factor (<1) accounted for the non-uniform temperature distribution, heat loss and unburnt pilot fuel at the start of flame propagation within unburnt premixed mixture zone.

The flame spread speed increases with the increased mixture strength, leading to higher PRR and HRR. Knock-limit of the strength is then one with which end-gas knock in unburnt premixed mixture occurs. Past researches revealed that it is much lower than the apparent rich limit for ignition failure[14]. Therefore, normally DDF engines operate safely only with premixed mixture strength under knock limits.

End-gas knock limit in DDF engines is well defined and consistent, with abrupt change in cylinder pressure and HRR [14]. It also essentially depends on the nature of the second fuel used and its mixture strength as well as prevailing combustion chamber conditions at time of flame propagation [45]. It is thought that diesel knock causes the end-gas easier to knock, especially with increased intake temperature and/or high diesel substitution. However, Karim G.A. reported that the pilot ignition has relatively little effect on the onset of end-gas knock compared to that of ignition characteristics of the gaseous fuel[14] and proposed a correlation as shown in Figure 2–8 and below

$$\log[\text{power}]_{\text{knock}} = A + B / T_0 \qquad\qquad (2\text{-}6)$$

Where A is the characteristics power output at a reference condition, B is the function of operational conditions and the effective overall activation energy of the pre-ignition reactions of the system used, and T_0 is the initial temperature of premixed mixture just prior to compression. Elements A and B depend on auto-ignition

characteristics of the premixed charge. Hence, it is clear that the above correlation has not accounted the effect of liquid pilot fuel.
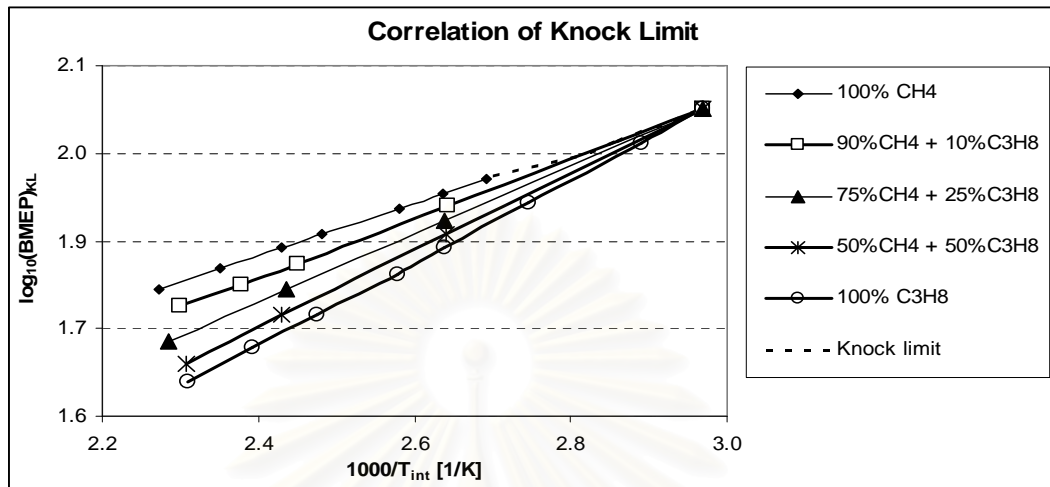
Figure 2–8 - Correlation between knock-limit output with intake charge temperature under the same operating conditions with fixed pilot quantity and intake pressure of methane, propane, and their mixtures, *(reproduced from [14])*
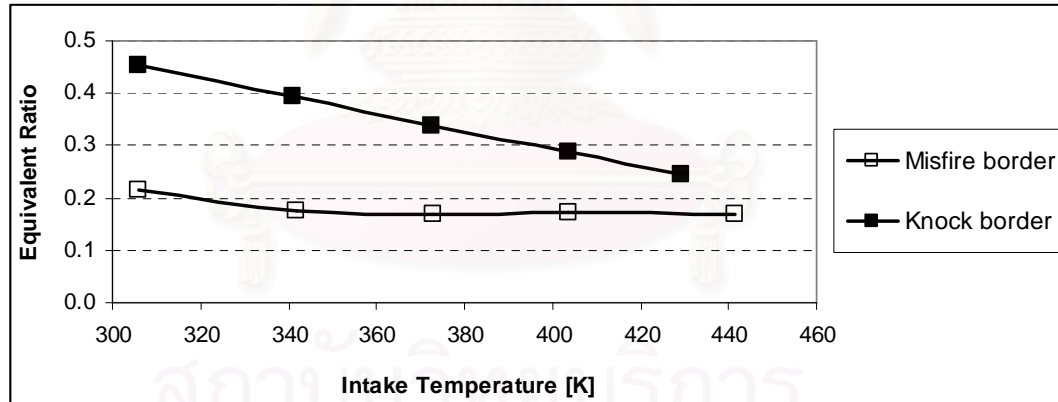
Figure 2–9 - Misfire and end-gas knock limits of premixed hydrogen-air mixture with constant pilot injection, *(reproduced from [14])*

As mentioned early, DDF emission characteristics also depends on the premixed mixture strength; the higher the mixture strength the shorter the combustion duration, and then higher combustion temperature and NO_X emission. Therefore, the "rich limit" (which is improbably rich) of the mixture may also be determined based on emission criterion, and it is naturally under knock limits.

Solutions to improve diesel dual fuel homogeneous combustion

One of high concerns on DDF operation is its poor fuel utilization efficiencies and high UHC and CO exhaust concentrations at light engine loads. As mentioned early, these are mainly resulted from un-complete burning of the premixed mixture as it is too lean and/or the flame front does not propagate through out the combustion chamber. A number of feasible solutions that can improve DDF light-load operation have been identified and analyzed by G.A. Karim[46] and others [24, 27, 34, 36, 40, 42]. These include factors that ①contribute to the lowering of effective lean limit of the premixed mixture which is the problem's origin, ②intensify the ignition sources, ③provide longer time for its combustion, ④contribute to the fuel-air charge formation, or ⑤increase premixed fuel-air ratio. Furthermore, DDF light load can also be improved by reducing engine operational speed (hence higher torque to achieve needed power output) or switching back to straight diesel operation at idle/light loads.

Effective lean limit of the charge is lowered by increasing temperature of the charge at the time of start combustion. This can be performed with increased intake air temperature increased temperature of cooling water jacket, solutions to reduce heat transfer across combustion chamber wall, and hot EGR. Another solution for this is the use of hydrogen or additives blended with the second fuel so as to reduce the low flammability limit of the mixture.

Ignition sources from pilot fuel combustion is intensified by increasing its quantity or any solutions to enlarge its distribution in the combustion chamber (such as reduced opening pressure of nozzle) but still in accordance with diesel operation. Higher energy release, bigger ignition source zone from increased pilot quantity obviously enhances combustion of the premixed mixture, since prevailing temperature and pressure increase. In addition, higher pilot quantity also causes ignition delay to decrease and provides diesel vapor in a bigger space in the vicinity of the liquid spray, thus, boost up the initial stage of premixed mixture combustion. Wider spray from reduced nozzle opening pressure, higher pilot quantity could shorten the needed paths of flame front propagation.

Advancing the pilot injection timing at light loads provides longer period for the premixed mixture to burn completely, and more activities corresponding with chemical

component of the pilot ignition delay. Nevertheless, this also causes longer ignition delay. This solution seems to be limited in case of conventional injection systems since it is out of their possibility.

Stratifying the premixed mixture by gas port-injection in combination with number, relative position of liquid pilot spray, combustion chamber size and shape for two-stroke engines with meticulous organization could, although difficult, achieve local richer mixture.

Bulk fuel-air ratio of the charge can be increased at unchanged fuel quantity by throttling the intake air or reducing air boost pressure.

Currently, combined with EGR and CDPF after-treatment technology DDF HMC could achieve emission level: 0.54g/bhp-hr of NO_X and 0.004g/bhp-hr of PM (Engine: 12.0L Caterpillar C-12, 410 hp/1,250 ft-lb with ESC13).

It is promised that fully electronically control for both fuels (port injection for the alternative fuel) is satisfactory means to improve DDF homogeneous combustion. With this means, the amount of pilot injection and alternative fuel as well as injection timing for them are monitored precisely; emission due to overlap time is completely eliminated; light load issue may be solved by by-pass turbocharged technology; engine operation can also be switched back to straight diesel or skip-fire strategy can be applied. However, this involves more complex fuel system. In addition, diesel substitution is also limited (not exceed 90%) since ①diesel operation is still involved and ②TDR of conventional diesel injection system does not exceed 10.

In addition, it is thought that DDF homogeneous combustion can be improved if the pilot ignition delay is reduced, at least to the level of diesel operation. However, it seems that the use of other fuels as pilot injection or/and the modification to improve diesel fuel property with respect to DDF operation have not been investigated satisfactorily.

2.2.4. Diesel dual fuel heterogeneous combustion engine

HPDI for the alternative fuels has been applied with big, low speed engines for relatively long time, since 1980s. Einang P.M. et al [47], Miyake M. et al [48], and Wakenell J.F. et al [49] had shown that direct injection of high pressure NG into these

diesel engines can provide high efficiency over a wide load range with diesel substitution as high as 95%.
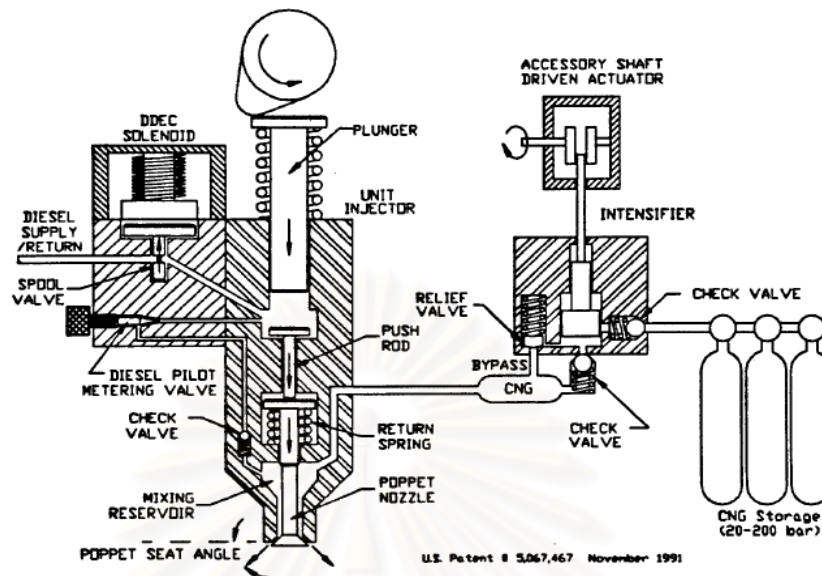
Figure 2–10 - Intensifier-injector schematic in Hodgins K. B.'s study in 1992 [50]

However, its application for engines in road transport has only been started in early 1990s since it is more difficult to adapt HPDI system in limit space of these engines. The gaseous fuel and diesel DI system, schematically shown in Figure 2–10, applied for relatively small engines proposed by Hodgins K. B. et al in 1992 [50] (US. Patent 5067 467) was impressive. This injector was based on a EUI. Diesel pilot and NG mix together in mixing reservoir before they enter the combustion chamber of a two-stroke DI Detroit 1.71 engine having CR of 16, bore of 108mm, and stroke of 127mm. The DDF engine achieved full load performance and efficiency as in diesel operation. At part loads, the pilot ignition delay was prolonged, revealing the effect of NG. Meanwhile, the flow visual investigation of Ouelette P. and Hill P.G. [51, 52] with a high speed valve ServoJet 3000 marked the long-term cooperation between Westport Innovations Inc. and the University of British Columbia, US. Since 1998, from the time Westport announced an alliance with Cummins Inc., achievement in HPDI technology has been increased [10, 53]. With their current DDF HPDI engines, diesel-like power and efficiency can be achieved whereas average diesel substitution is 95% and emissions are reduced drastically: by 40-50% for NO_X, 70-80% for PM, and 20-25% for CO_2. The Executive

Order from California Air Resources Board (CARB) certifies the Cummins-Westport HPDI system to 1.2g/bhp-hr [NO_X + NMHC], 0.1 g/bhp-hr CO and 0.02g/bhp-hr PM [11].
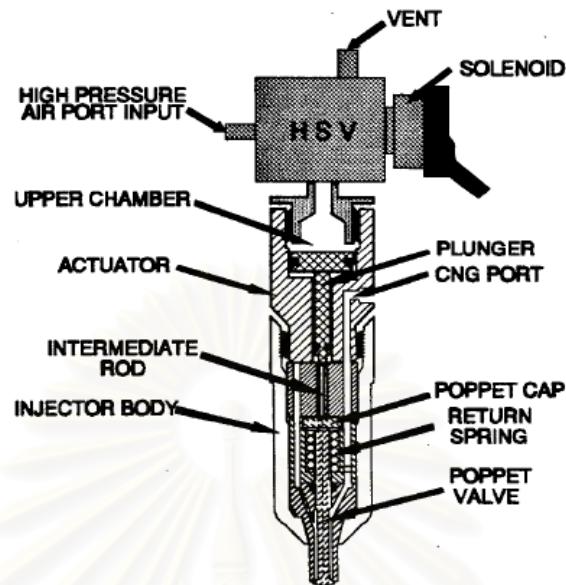
Figure 2–11 - High speed valve ServoJet 3000 schematic in Ouelette P. and Hill P.G.'s study [51, 52]

Fully electronically controlled DI for both the pilot and alternative fuel provides a prospect of maintaining high efficiency and power capacity of diesel engines while reducing emission to achieve near-term emission legislation. All the issues related to DDF "homogeneous combustion" is thought to be strictly solved. *First*, it permits the stratified distribution of this fuel in the chamber in desired relative position with the pilot spray. This leads to local relatively richer mixture and shorter paths of flame propagation, hence solving light load issue of HMC type (high UHC and CO emission, low efficiency). *Second*, it enhances the mixing among the pilot, gaseous fuel, and air. This leads to NO_X decrease since fraction of gaseous fuel after its burning is moved to the relatively cooler spaces in the chamber. This effect is available for both single- and multi-stage injection systems. The NO_X decrease is also resulted from combustion of leaner gaseous fuel air mixture whereas that of close stoichiometric mixture in diesel operation. *Third*, pilot ignition delay is no longer affected by the gaseous fuel if the pilot is injected prior to gaseous fuel. This factor also contributes to reduced peaks of pressure and PPR, less combustion noise, and NO_X emission. *Forth*, because the gaseous occupies in cylinder only around the time of pilot injection the end-gas knock is

no longer serious. *Fifth*, theoretically pilot fuel can be reduced to the amount required to ignite the gaseous fuel at prevailing condition. This leads to ①the reduction of diesel knock, combustion noise as the amount of diesel burns in premixed combustion phase is reduced drastically, ②the reduction of NO_X emission as high- temperature high-pressure condition may be eliminated, ③less PM emission since higher amount of gaseous fuel which has lower carbon content and negligible sulphur can be used.
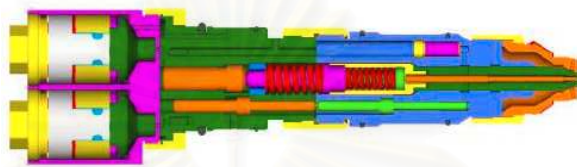
Figure 2–12 - Combined Injection Valve for HPDI of NG with pilot injection, Westport Innovations Inc. [53]

2.2.5. Recent studies on DDF engines at Chulalongkorn University

Several investigations have been conducted as the co-operation between Internal Combustion Engine Research laboratory and Siam Kubota Co., PTT Co., TAKUNI Co. A study on the premixed charge biogas diesel CI engine had been finished last year. From this research, the following results were obtained and concluded[54].

− Biogas premixed charge-diesel dual fuelling for the engine produced almost no performance deterioration at all test speeds.

− The DDF produced lower energy conversion efficiency which was offset by large replacement of diesel by biogas which has relatively low cost and is being a renewable energy source. The efficiency deterioration reduced when engine load increased. At full load, the efficiency was comparable with that in diesel fuelling. It is then inferred that at low/medium loads the DDF engine produced higher UHC and less soot.

− The DDF high efficiency island moved to higher engine speeds and loads, revealing effect of fraction of gaseous fuel occupying in the main combustion chamber.

- The DDF resulted in lower exhaust gas temperature regardless of engine load and speed, higher cooling water and lube oil temperatures at high loads, high engine speeds. These changes are thought due to the shorter combustion period brought about by DDF. A critical area was observed with very relatively high temperatures of lubricant oil and cooling water.

- The endurance test revealed that lube oil consumption was high at unacceptable levels due to the increased oil and cooling water temperatures and its suction to cylinder as a gas mixer was installed. The engine could not withstand higher thermal load brought by faster DDF burning at engine speed and load proposed for diesel fuel.

- The DDF engine with high diesel substitution should be avoided to operate at the critical area for keeping engine longevity.

CHAPTER 3

FUELS USED IN DIESEL DUAL FUEL ENGINES

3.1. The fuels used to form homogeneous mixture

The alternative fuels may either be gases or liquids. The gases are often relatively high octane number fuels such as biogas[55-58], producer gas[59-64], LNG, CNG[39, 40, 42], [26, 46, 65-69], and LPG[14, 15, 28, 32, 70, 71] or hydrogen[13, 74, 75] whereas the liquids are often alcohols[30, 72] may be used. Due to their lower cost, these fuels contribute to reduced operational cost which is the main purpose of DDF operation. Regarding to this, substitution of diesel fuel by the alternative tends to be maximized so as to achieve maximum saving in total fuel cost. However, it is noticed that this is definitely different from best energy conversion efficiency point of view; meaning that lowest fuel cost does not mean maximum total energy conversion efficiency. Among these alternatives, NG is frequently considered as the most promising near-term alternative because of its long-term availability, well-balanced geographic distribution, and clear ecologic benefits.

The properties of the alternative fuels such as low heating value, slow flame spread speed, low octane number, and low auto-ignition temperature contribute to DDF engine performance. Hence, NG- or LPG-DDF generally causes almost no significant deterioration in engine performance since their main constituents have high octane number, high auto-ignition temperature, comparable energy content compared to diesel and fuel-air equivalent ratio is higher in DDF HMC operation. NG contents mainly methane (88-96%) with LHV of 50 MJ/kg. LPG contents mainly propane (60-85%) with LHV of 46.3 MJ/kg, as seen in Table 3-1. However, the reduction may occur with biogas, producer gas, or alcohols due to their much lower energy content and/or high inert gas.

Octane number, auto-ignition temperature, and flammability limit attribute to diesel substitution ratio. Thus, in LPG-DDF diesel substitution is lower, the engine tends to knock easier than that in NG-DDF HMC.

Table 3-1   Properties of fuels

Properties	Unit	CH_4	C_3H_8	C_4H_{10}	Diesel $C_{14.4}H_{24.9}$	Methanol	Ethanol
Molecular mass		16.04	44.09	58.12	198.04	32.04	46.07
Carbon content	% mass	74.8	81.8		87.36	37.45	69.46
Oxygen content	% mass	0	0	0	0	49.9	34.73
Polytropic index	-	1.299	1.126	1.091		1.227	1.145
Density	kg/m^3	0.648	1.808	2.407	0.85	1.31	1.883
Boiling point	^{0}C,1 at		-42.07	-11.73	210÷235	65	78
Auto ignition Temp.	^{0}C,1 at	537	470	365	254	385	365
Flash point	^{0}C,1 at	-188	-104	-60	52	11	12
Flammability limit	% vol.	5÷15	2.1÷9.5	1.8÷8.4	0.6÷7.5	6.7÷36 (60^{0}C)	3.3÷19 (60^{0}C)
Laminar flame velocity	cm/s	43.4	45.6	44.8		48	
Flame Temperature	^{0}C	2250	2270	1900	2300	1975	2155
Octane No.	RON	130	112	94		89	90
Cetane No.	-				40÷56	<15	<15
Low heating value	MJ/kg	50.01	46.36	44.65	42.94	20.1	27
Heat of vaporization	kJ/kg				375	1185	920
(A/F)s. mass / vol. basis	-	17.23/31.13	15.67/10.31	15.5/7.73	14.3/-	6.47/-	9.00/-

Flame temperature: at stoichiometric combustion, with air at 1 at, reactants initially at 298K.

Laminar flame velocity: at 25^{0}C, 1 at, stoichiometric combustion.

Flammability limit: in standard air, 25^{0}C, 1at   Density: at 25^{0}C, 1at

Lower carbon content accompanied with gaseous form of the gaseous fuels used (zero with hydrogen) result in extremely lower soot and CO_2 emission. Higher NO_x emissions may be resulted from their faster burning and higher flame temperature due to higher fuel-air equivalent ratio. Higher UHC and CO are resulted from incomplete combustion, especially with HMC type at light loads. Fuel having lower flammability limit would burn better at lean condition than one having higher limit. In addition, other toxic emissions such as sulphur, benzene and 1,3 butadiene are drastically reduced as diesel is replaced.

High heat of vaporization of alcohols causes decrease in temperature of the charge, leading to prolonged ignition delay of the pilot in DDF HMC and increased tendency of diesel knock and emissions at light-medium load.

3.2. The pilot injection fuel

Diesel or other liquid fuels such as heavy oil can be the pilot injection which is injected into the combustion chamber as normal manner in diesel engines. Diesel often used contributes to the ability of switching back to straight diesel operation as necessary. Substitution ratio, engine performance, energy conversion efficiency, combustion and emission characteristics will be affected as another fuel is used.

3.3. The fuels used in this study

3.3.1. Gaseous fuel

The gaseous fuel used is commercial LPG distributed by PTT Co., Thailand. Its properties are given in Table 3-2. The LPG is used due to the following reason. The test engine has high compression ratio (21.6). It is prone easily to knock with relatively lower octane-number fuel as LPG. Thus, the effect of liquid fuel with respect to knock improvement is thought easier to be recognized.

Table 3-2   Properties of LPG used

Test item	Test method	Limit	Result
Vapor pressure (37.8 ^{0}C), kPa	ASTM D 1267-02	max 1380	785
Evaporated temp. (95% vol.), ^{0}C	ASTM D 1837-02a	max 2.2	-0.8
Specific gravity (15.6/15.6 ^{0}C)	ASTM D 1657-89	report	0.539
Residue after evaporation, ml/100ml	ASTM D 2158-97	max 0.05	< 0.05

Table 3-2 Properties of LPG used (Contd.)

Test item		Test method	Limit	Result
Copper strip corrosion, No		ASTM D 1838-05	max 1	1
Sulphur content, % wt		ASTM D 2784-98	max 0.014	0.0071
Free water content		Visual	Nil	Nil
Odor		Visual	Easily detectable	Easily detectable
Composition	C_5 & heavier, % vol.	ASTM D 2163-91	max 2	1.03
	Methane, % vol.	ASTM D 2163-91	---	0.00
	Ethane, % vol.	ASTM D 2163-91	---	0.17
	Propane, % vol.	ASTM D 2163-91	---	50.89
	Propylene, % vol.	ASTM D 2163-91	---	0.00
	i-Butane, % vol.	ASTM D 2163-91	---	23.20
	n-Butane, % vol.	ASTM D 2163-91	---	24.53
	Butene, % vol.	ASTM D 2163-91	---	0.18
	Average molecular weight	Calculation	---	50.51
	Heating value, MJ/kg	Calculation	---	49.9234

3.3.2. Liquid fuels

Oxygenated fuels may lead to shorter ignition delay due to their oxygen content. They are expected to improve DDF HMC and have not been considered in past studies. In this study, palmitic methyl ester (PME), one type of biodiesel produced by the Chemical Department - Faculty of Science - Chulalongkorn University is used in dual fuel investigation in comparison with commercial diesel produced by PTT Co. Henceforth, the biodiesel or PME is designated to this liquid fuel. Properties of the commercial diesel fuel and the PME are given in Table 3-3 and Table 3-4, respectively. The heating value ratio and volume ratio (based on the same energy) of the PME and the diesel are 87.565% and 107.2%, respectively. All the PME properties which were available until the time of this study match the biodiesel-fuel requirement given in Table 3-5.

Figure 3–1   The diesel (left) and biodiesel (right) used in the study.

Table 3-3   Properties of the commercial diesel

Properties	Unit	Test method (ASTM)	Value
Specific gravity	-	D 1298	0.826
Cetane number	-	D 613	47 min.
Cetane index	-	D 976	47 min.
Viscosity at 40°C	cSt	D 445	1.8 - 4.1
Pour point	$^{\circ}$C	D 97	10 max.
Cloud point	$^{\circ}$C	D 2599	16 max.
Carbon residue	%wt.	D 4530	0.05 max.
Water and sediment	%vol.	D 2709	0.05 max.
Ash	%wt.	D 482	0.01 max.
Flash point	$^{\circ}$C	D 93	52 min.
Lubricity by HFRR	μm	CEC F-06-A-96	460 max.
LHV	kJ/kg		42,500 min.
(A/F)s	-		14.5

Table 3-4   Properties of the PME

Properties	Unit	Test method (ASTM)	Value
Methyl Ester content	% mass		99.85
Flash point	^{0}C	D 92	166
Viscosity at 40^{0}C	mm^2/s	D 277	4.63
Specific gravity	kg/m^3	D 1298	880
Heating value	MJ/kg	D 611	37.215

Table 3-5   Requirement for biodiesel fuel

Properties	BS EN 14214:2003		ASTM D 6751	
	Unit	Limits	Unit	Limits
Ester content	%	96.5	-	-
Density (15^{0}C)	kg/m^3	860-900	-	-
Viscosity (15^{0}C)	mm^2/s	3.50-5.00	mm^2/s	1.9-6.0
Flash point	^{0}C	120 min	^{0}C	130 min
Sulfur content	mg/kg	10 max	% mass	0.05 max
Carbon residue	% (m/m)	0.3 max	% mass	0.05 max
Cetane number		51 min		47 min
Sulfated ash	% (m/m)	0.02 max	% mass	0.02 max
Water content	mg/kg	500 max	% volume	0.05 max
Total contamination	mg/kg	24 max	-	-
Copper strip corrosion	rating	class 1		No.3 max
Cloud point	-	-	^{0}C	report
Oxidation stability	hour	6.0 min	-	report
Acid value	mgKOH/g	0.5 max	mgKOH/g	0.8 max
Iodine value	g/100g	120 max	-	-
Linolenic acid ME	% (m/m)	12 max	-	-
Polyunsat ME	% (m/m)	1 max	-	-
Methanol content	% (m/m)	0.20 max	-	-

Table 3-5 Requirement for biodiesel fuel (Contd.)

Properties	BS EN 14214:2003		ASTM D 6751	
	Unit	Limits	Unit	Limits
Monoglyceride	% (m/m)	0.80 max	-	-
Diglyceride	% (m/m)	0.20 max	-	-
Triglyceride	% (m/m)	0.20 max	-	-
Free glycerol	% (m/m)	0.20 max	% mass	0.02
Total glycerol	% (m/m)	0.25 max	% mass	0.24
Group I metals	mg/kg	5.0 max	-	-
Group II metals	mg/kg	5.0 max	-	-
Phosphorus content	mg/kg	10.0 max	% mass	0.001 max
Distillation T90	-	-	^{0}C	360 max

Biodiesel is identified as diesel replacement in future. Information of this fuel type can be found in many documents such as [73, 74]. Its advantages and disadvantages are addressed as bellows.

Benefits of biodiesel use

- Biodiesel is renewable energy resource, biodegradable and non-toxic.

- Biodiesel displaces imported petroleum. Energy required to produce biodiesel is much less than its energy. For example, the fossil fuel energy required to produce biodiesel from soybean oil is only 31% of the energy contained in soybean methyl ester. Because biodiesel is an energy-efficient fuel, it can extend petroleum supplies and makes sound for energy policy.

- Biodiesel reduces emissions. As it displaces petroleum, it reduces global warming gas emissions such as CO_2. The recycling of CO_2 with biodiesel is not 100%, but substituting biodiesel for petroleum diesel reduces life-cycle CO_2 emissions by 78%. B20 reduces CO_2 by 15.66%. Biodiesel reduces tailpipe PM, UHC, and CO emissions from most modern four-stroke CI engines. These benefits result from oxygen content in the fuel, for example 11% oxygen by weight with PME. Oxygen content allows the fuel to burn more completely, so fewer unburned fuel emissions result. This same phenomenon

reduces air toxics, because the air toxics are associated with the unburned or partially burned HC and PM emissions. Using biodiesel can make diesel exhaust smell better; more like cooking odors.

- Biodiesel and human health. Some PM and HC emissions from diesel fuel combustion are toxic or are suspected of causing cancer and other life threatening illnesses. Using B100 can eliminate as much as 90% of these "air toxics." B20 reduces air toxics by 20% to 40%. The effects of biodiesel on air toxics are supported by numerous studies, starting with the former Bureau of Mines Center for Diesel Research at the University of Minnesota. The Department of Energy (DOE, US.) conducted similar research through the University of Idaho, Southwest Research Institute, and the Montana Department of Environmental Quality. The National Biodiesel Board conducted Tier I and Tier II Health Effects Studies that also support these claims.

- Biodiesel improves lubricity. Low-level blends of biodiesel such as 1% or 2% can improve lubricity of diesel fuels and this may be particularly important for ultra low sulfur diesel (ULSD) as these fuels can have poor lubricating properties. Engine manufacturers depend on lubricity to keep moving parts, especially fuel pumps, from wearing prematurely. Even 2% biodiesel can restore adequate lubricity to dry fuels such as kerosene or Fischer-Tropsch diesel.

- Biodiesel is easy to use. In blends of B20 or less, it is literally a "drop in" technology. B20 can be stored in diesel fuel tanks and pumped with diesel equipment.

Drawbacks of biodiesel use

- *Biodiesel contains less energy than diesel.* Compare to typical No.2 diesel in the United States, biodiesel has 12.5% less energy on mass basis. The difference between these two measurements is caused by the fact that it is slightly denser than diesel fuel. All biodiesel, regardless of its feedstock, provides about the same amount of energy.

- *Its cold flow properties.* The cold flow properties of biodiesel and conventional diesel are extremely important. As diesel, biodiesel can start to freeze or gel as the temperature gets colder. If the fuel begins to gel, it can clog filters or eventually it can become thick enough that it cannot even be pumped from the fuel tank to the engine.

- NO_x *emission.* Biodiesel has been shown to increase NO_x emissions in many engines on engine stand tests. The NO_x increase observed for B20 is believed to occur primarily at low engine speed but high torque conditions. Testing of entire vehicles may be a better predictor of real-world emission impacts than engine stand tests. Ongoing testing of B20 in heavy-duty vehicles at the National Renewable Energy laboratory is showing that NO_x emissions do not always increase for B20 and in some cases actually decrease. Because of the conflicting results of engine stand and vehicle tests, the impact of B20 on NO_x must be regarded as unknown at this time.

CHAPTER 4

TEST SYSTEM CONSTRUCTION, SETUP AND COMMISSIONING

4.1. Laboratory rig construction

4.1.1. Scope of the work

With the objective addressed earlier, the scope of this investigation includes following tasks:

- To identify the effect of diesel substitution (LPG energy fraction) on the combustion characteristic of LPG-diesel dual fuel engine.

- To identify the effect of biodiesel as pilot fuel injection on the combustion characteristic of LPG-biodiesel dual fuel engine.

- To identify the effect of injection timing on the combustion characteristic of LPG-diesel and LPG-biodiesel dual-fuelled engine.

Test points which are the selected high probability operating points corresponding to the ECE15 + EUDC test cycle (Appendix A), are list in Table 4-1.

Table 4-1   Selected test points

Brake torque [Nm] / Speed [rev/min]	10	20	30	40	70
1250	X	X	X	X	
2000	X	X	X	X	X
2750	X	X	X	X	X

A comparison in energy consumption, conversion efficiency among these operations with different LPG energy fraction, different liquid fuel, different injection timing will be performed. The combustion characteristics are studied by analyzing the cylinder pressure data (indirect analysis: heat release prediction; direct analysis: statistical analysis). Combustion phenomena are studied by visualization technique (two color method).

To perform these tasks, the following instruments which are available at the Internal Combustion Engine Research Laboratory, are used in this investigation.

4.1.2. Main instruments used and their construction

4.1.2.1. Test engine

The test engine is a 4-cylinder high speed IDI engine (FORD model WL 2.5L). Its combustion chamber system is of Ricardo Comet MK Vb type, with a downstream glow-plug. Its specification is given in Appendix C. The engine (with clutch and gear box) has been coupled with an AVL Dynamometer Alpha 40.

4.1.2.2. Dynamometer and control unit

The dynamometer and control unit of the test cell were produced by AVL List GmbH, Austria. Detail information of the system can be found in [75, 76]. A brief description is given in Appendix C and only difference made for this study is presented in this section.

Throttle Position Control: Originally, a pneumatic actuator SMC-SPCP-004 is used to monitor throttle position. A mechanical throttle control had been made for easier manipulation and finer setting as the engine runs in DDF mode since the steps of this actuator may not match the required position of the fuel pump lever. The arrangement is shown in Figure 4–1.

Figure 4–1   Pneumatic actuator SMC-SPCP-004 and mechanical throttling controller

4.1.2.3. Indicating system

Pressure history in pre-chamber, main chamber and liquid fuel line has been recorded by a high speed data acquisition system. The system includes:

- A DEWETRON acquisition system model 5000-CA-SE. This system functions with a software named Combustion Analyzer version 6. Specification of the DEWETRON system is given in Appendix C.

- Two AVL transducers model AVL GU12P, produced by AVL List GmbH. are used for combustion chamber pressure measurement. The first transducer is installed into an AGO3 glow plug adapter to collect pre-chamber pressure and the second is installed into an adapter designed and machined suitable for the cylinder head of the test engine, to collect main chamber pressure.

- A Kistler high pressure transducer, model 607C1 is installed to an adapter welded to the fuel injection line and located 15 mm upstream the fuel injector. Pressure history from this transducer is then used to predict the start of injection (SOI). Transducers' specification is given in Appendix C.

All these pressure measurement mentioned above are performed for the forth cylinder. Arrangement for these transducers is shown in Figure 4–2. An adapter has been designed and machined for Kistler transducer 607C1 to measure fuel line pressure, followed general requirement for setting fuel line pressure transducer as well as that of Kistler, as below:

- It must be small, so that it does not introduce significant cavities in the fuel line, which may interfere with the pressure dynamics.

- It must not alter the stiffness of the fuel line, which may interfere with the fuel pressure dynamics.

- It must have sufficiently high frequency response so that it can respond adequately to the rapid fuel pressure pulsation during injection process; at the same time, it must also be capable of recording the steady residual pressure between injections.

- It must have high natural frequency so as to avoid resonant output oscillation. The geometry of this adapter is shown in Figure 4–3. It is welded onto the fuel steel pipe by brass without cutting the pipe. A small communicating-hole (ϕ2.5) is drilled to the fuel pipe.

The DEWETRON software provides ability to estimate "Cylinder pressure offset", based on the second method. In this software, the predefined setting for CI engine is:

- Considered points: 100°CA bTDC and 65°CA bTDC
- Polytropic index: 1.37
- Number of cycles considered: 20 to 200

Injector

Glow-plug with
Transducer 2

Sleeve for
Light Guide

Exhaust Valve

Sleeve for
Endoscope

Sleeve +
Transducer 1

Intake Valve

Piston

Heat
regenerator
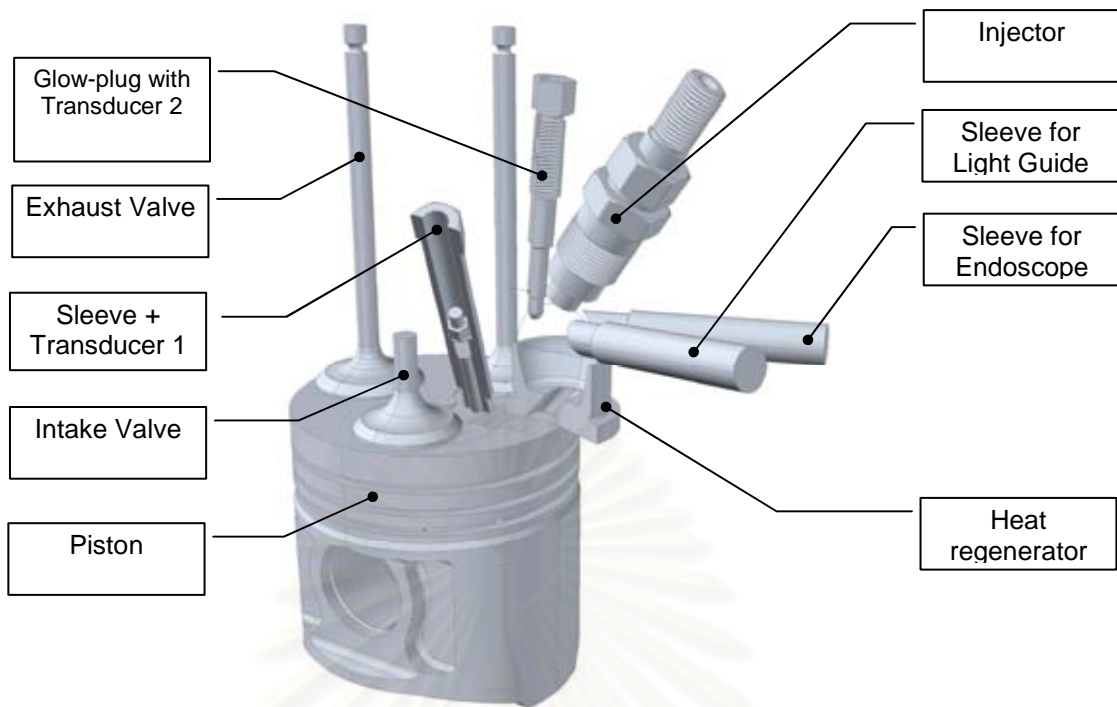
Figure 4–2   Setup of transducers for cylinder pressure measurement

3/8-24 UNF
2A THD

9.2

11.05

22.5

8.66

10

2.3−0.05

6.15−0.05

150°

R3

R10

16

Ø2.5−0.1

Ø6.35−0.05
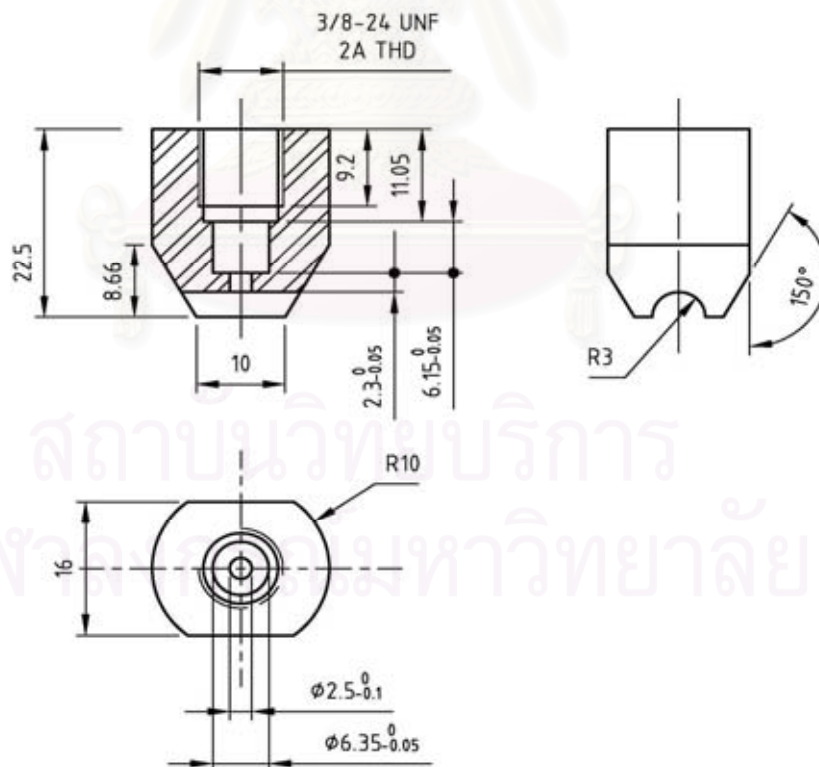
Figure 4–3   Adapter for Kistler transducer 607C1
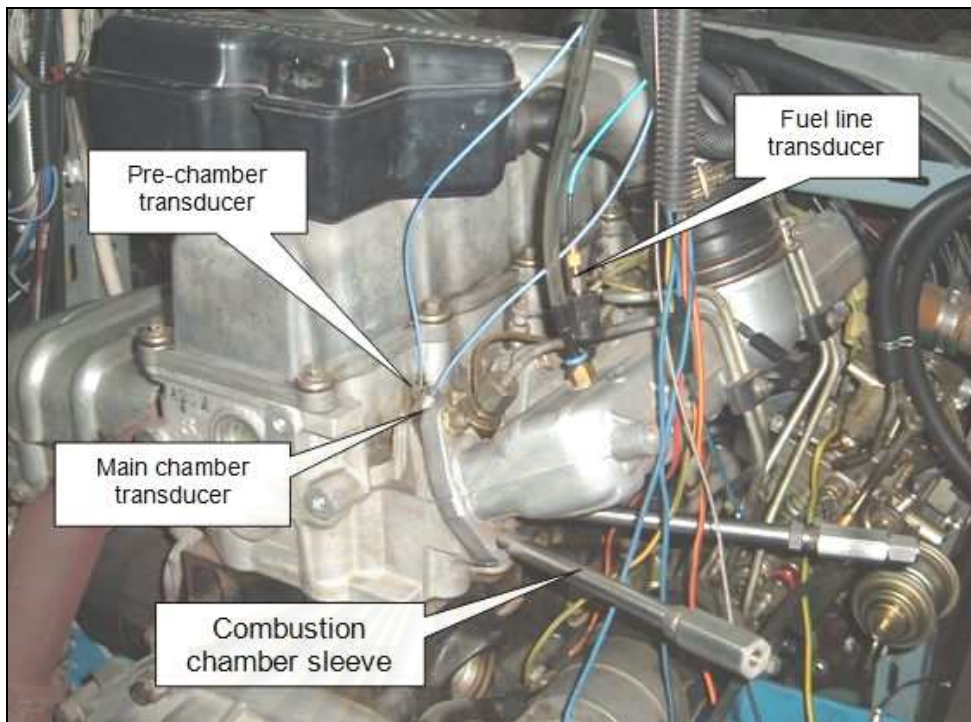
Figure 4–4   Setup for fuel line and combustion chamber pressure measurement, combustion chamber visualization.

4.1.2.4. Optical diagnostic system

The AVL VisioScope system has been used for combustion chamber visualization. Description of the system is given in the Appendix.

4.1.2.5. LPG injection system

LPG, in gaseous form, is injected to a mixer installed upstream the manifold to ensure it mixes well with air before coming to the cylinder. Configuration of the gas mixer is shown in Figure 4-5. The injectors, reducer used in this study are commercial product, from a conversion kit for SI engine of Zavoli Co., Italia.

The injector's duty cycle (LPG flow rate) is controlled by a controlling board which had been designed and made as the result of the Project "Development of a Natural Gas Engine Controller", Department of Computer Engineering, Faculty of Engineering, 2003. The voltage supplied to the injectors is kept as it will be from the alternator on the engine ($14.3^{\pm0.1}$ V) during calibration. Simulated cycle is achieved by a multi-function generator GW INSTEK model GFG-8015G. Square wave with frequency of

20Hz from this generator is sent to the controlling board. The injector's duty cycle can be set manually from 7% to 62% (step 1%) and observed on the display of an oscilloscope (Tektronik TDS 210). This control system is shown in Figure 4–6.
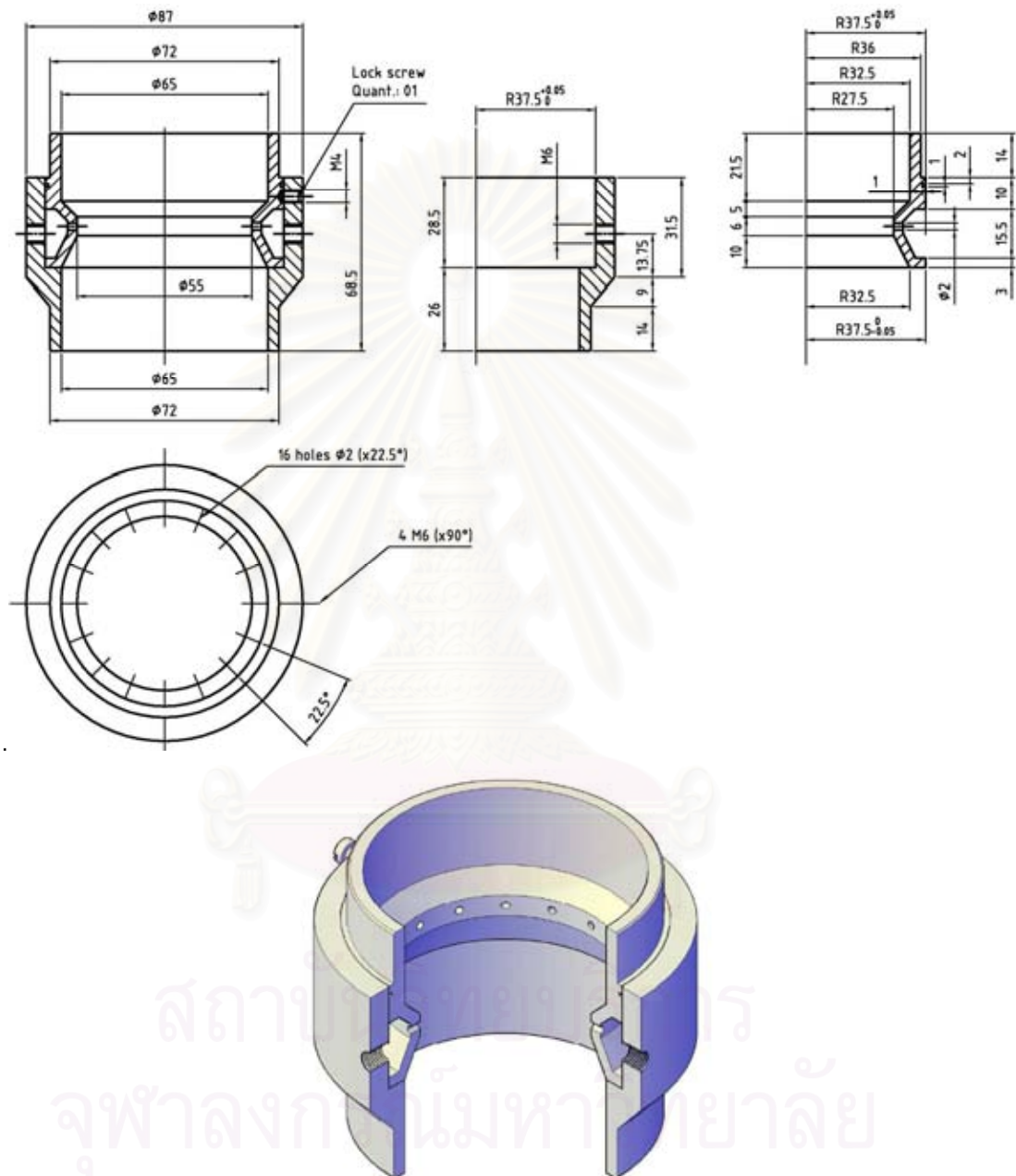
Figure 4–5   Gas-mixer
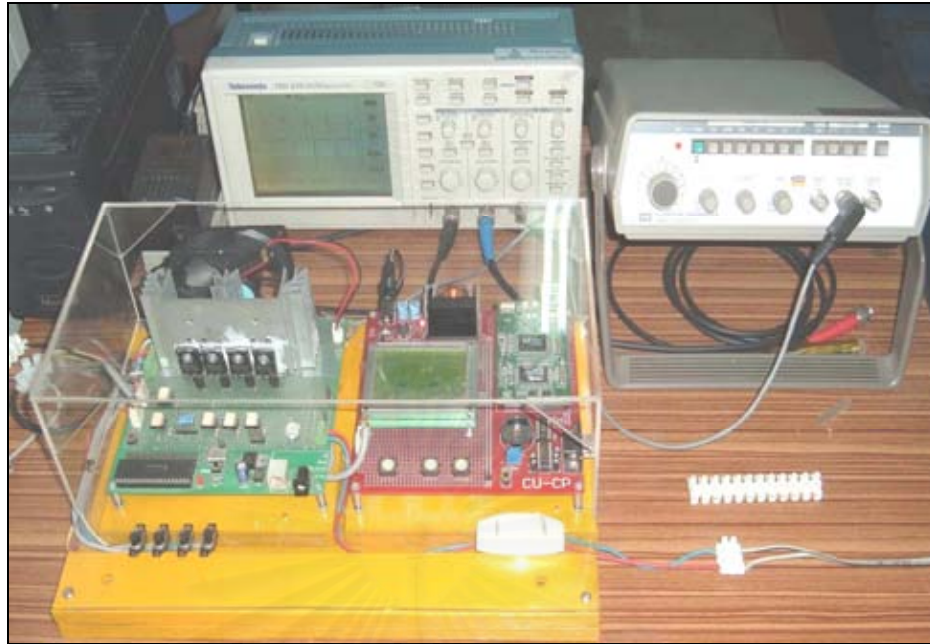
Figure 4–6   LPG injection control system

For more convenience, the LPG injection system had been calibrated before the main tests. The relation between the LPG flow rate and the duty cycle is then determined. Moreover, during the main tests the LPG flow rate will also be measured directly by a high precision balance (ZENTECH model JWA-60K) to make a comparison.

The injection system was calibrated with regulated compressed air at the same condition as that with the test engine. Diagram for the calibration is shown in Figure 4–7. A hot water flow from a boiler with fixed temperature is maintained during calibration. This temperature is $84.5^{\pm 1.5}$ ^{0}C, same as that of cooling water temperature which is monitored by the AVL control unit when the test engine runs. Regulated compressed air at 6 bar from a compressed air tank flows to the reducer after passing a solenoid valve. The air leaves the reducer with pressure approximate 1.7 bar and passes the calibrated injector as it is powered by the controlling board PC1. It then flows to a damper before passing a Parkinson Cowan flow-meter. Air temperature, pressure at the flow-meter's outlet and the time corresponding to its flow of 10 dm^{3} at the flow-meter (4 revolutions, at steady state) are recorded at each injector duty cycle. The air volumetric flow rate is then determined. Neglect the difference in viscosity of air and LPG at this condition, the LPG volumetric flow rate should be equal to that of air. The LPG mass flow rate is then

predicted. The relation between injector's duty cycles, air mass flow rate and equivalent LPG flow rate is shown in Table 4-3 and Figure 4-8.
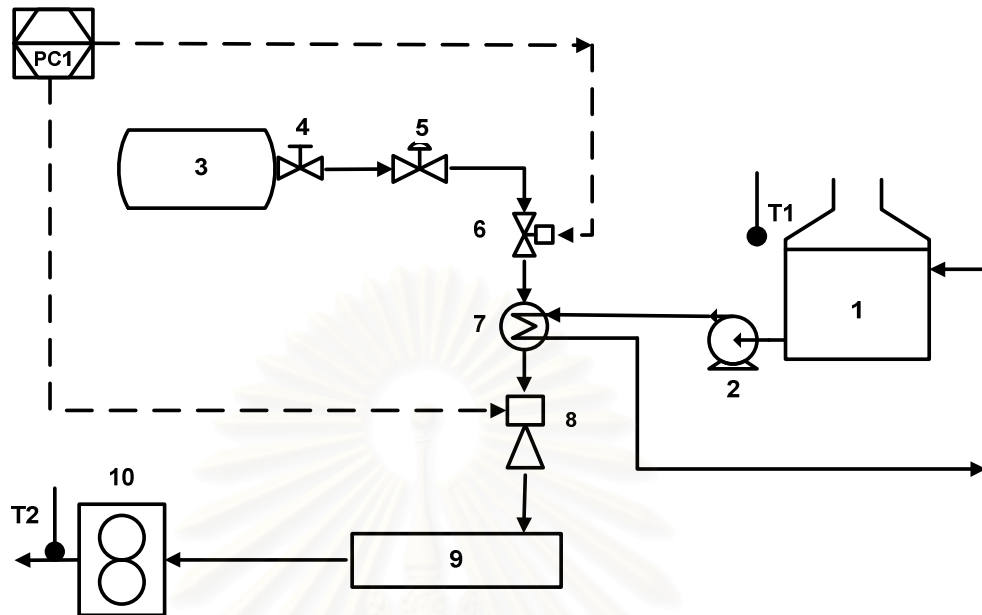
Figure 4–7   Diagram of LPG injection system calibration

1- Electrical boiler   2 - Centrifugal pump   3 - Compressed air tank

4 - Valve   5 - Regulator   6 - Solenoid valve

7 - LPG vaporizer   8 - Injector   9 - Damper

10- Flow meter   T1, T2 - Thermometer

Table 4-2   Result of LPG Injection system calibration

Duty cycle	LPG Flow Rate (1 injector)	Duty cycle	LPG Flow Rate (1 injector)
%	g/s	%	g/s
0	0.000000	31	0.397902
7	0.108568	32	0.408073
8	0.118826	33	0.422460
9	0.128752	34	0.436564
10	0.139773	35	0.449640
11	0.151518	36	0.459512
12	0.164563	37	0.470392
13	0.177428	38	0.481863
14	0.189597	39	0.493568
15	0.203202	40	0.505307

Table 4-2 Result of LPG Injection system calibration (Contd.)

Duty	LPG Flow Rate (1 injector)	Duty	LPG Flow Rate (1 injector)
16	0.216007	41	0.511261
17	0.230780	42	0.527064
18	0.242736	43	0.533608
19	0.255608	44	0.543296
20	0.268501	45	0.556981
21	0.282664	46	0.570403
22	0.291440	47	0.579695
23	0.301438	48	0.591399
24	0.314497	49	0.602991
25	0.327038	50	0.613160
26	0.339208	51	0.621400
27	0.349435	52	0.632374
28	0.362473	53	0.641956
29	0.373465	54	0.652396
30	0.377771	55	0.667155

The input signal of the controlling board had a frequency of 20Hz and this frequency was kept unchanged throughout the calibration as well as the main test period.
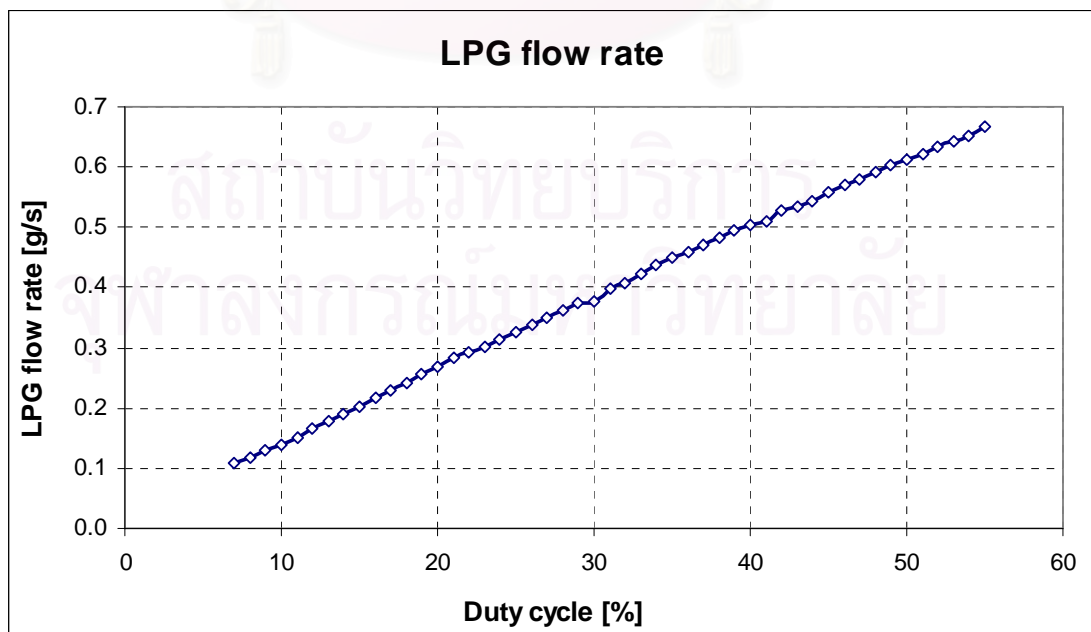
Figure 4–8   LPG injection system characteristic

4.1.2.6. Instrument for measurement of liquid fuel consumed

The mass of liquid fuel consumed, M_f is measured directly by an electrical high precision balance, produced by ACUWEIGH Co. A plastic box was made to segregate this balance and liquid fuel tank from air motion and vibration to achieve high accuracy during the tests. The time duration, Δt corresponding to the mass of liquid fuel consumed is measured by an ALBA stop-watch with division of 1/100 second.
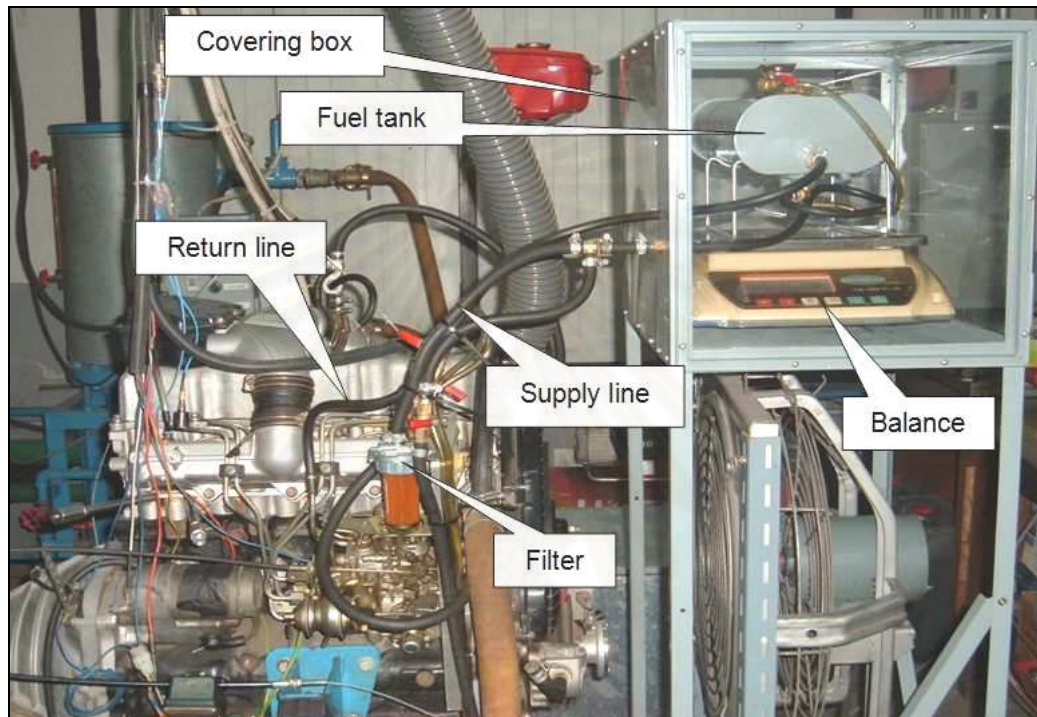
Figure 4–9   Setting for liquid fuel consumption measurement

4.1.2.7. Instrument for measurement of air consumption

Air consumed by the engine is measured by "air box" method. The air passes an orifice (designed and machined according to the British standard BS 1042) which is mounted to a surge tank before flowing into the intake manifold. Differential pressure across the orifice is measured by an inclined manometer (with slope 20%, division 1 mm, and water as working fluid). Temperature of the air inside the tank is measured by thermocouple type K. The air mass flow rate is then determined by following equation:

$$\overset{*}{m}_a = C_{DO} A_O \sqrt{2\rho_{air}\rho_{H_2O}g\ \Delta h} = \pi C_{DO}\frac{D_0^2}{4}\sqrt{2\rho_{air}\rho_{H_2O}g\ \Delta h} \qquad 4\text{-}1$$

where $C_{DO} \approx 0.6$ - discharge coefficient of the orifice

$D_O = 0.05\,(m)$ - diameter of the orifice

$\rho_{H_2O} = 997\,kg/m^3$ - density of water

Δh - the head difference of water in the inclined manometer (m).

ρ_{air} - density of air in the air box, is calculated via ideal gas equation with measured air box temperature and atmospheric pressure.

$$\rho_{air} = \rho_{o,air} \cdot \frac{To}{T_{air}} \cdot \frac{p_{air}}{p_o} = \rho_{o,air} \cdot \frac{To}{T_{air}} \cdot \frac{p_{amb} + \rho_{H_2O}\Delta h}{p_o}$$

$\rho_{o,air} = 1.169$ kg/m^3 - density of air at standard condition T_o, p_o

$T_0 = 298.15K$ and $p_0 = 750.06$ mmHg

4.1.2.8. Instrument for exhaust gas and lube oil temperature measurement

Exhaust gas, lube oil, intake air, and ambient temperatures are measured by thermocouples connected to a display unit. These values are recorded manually.

4.2. Test system setup and commissioning

Arrangement for the whole test system is shown in Figure 4–10 to Figure 4–14.
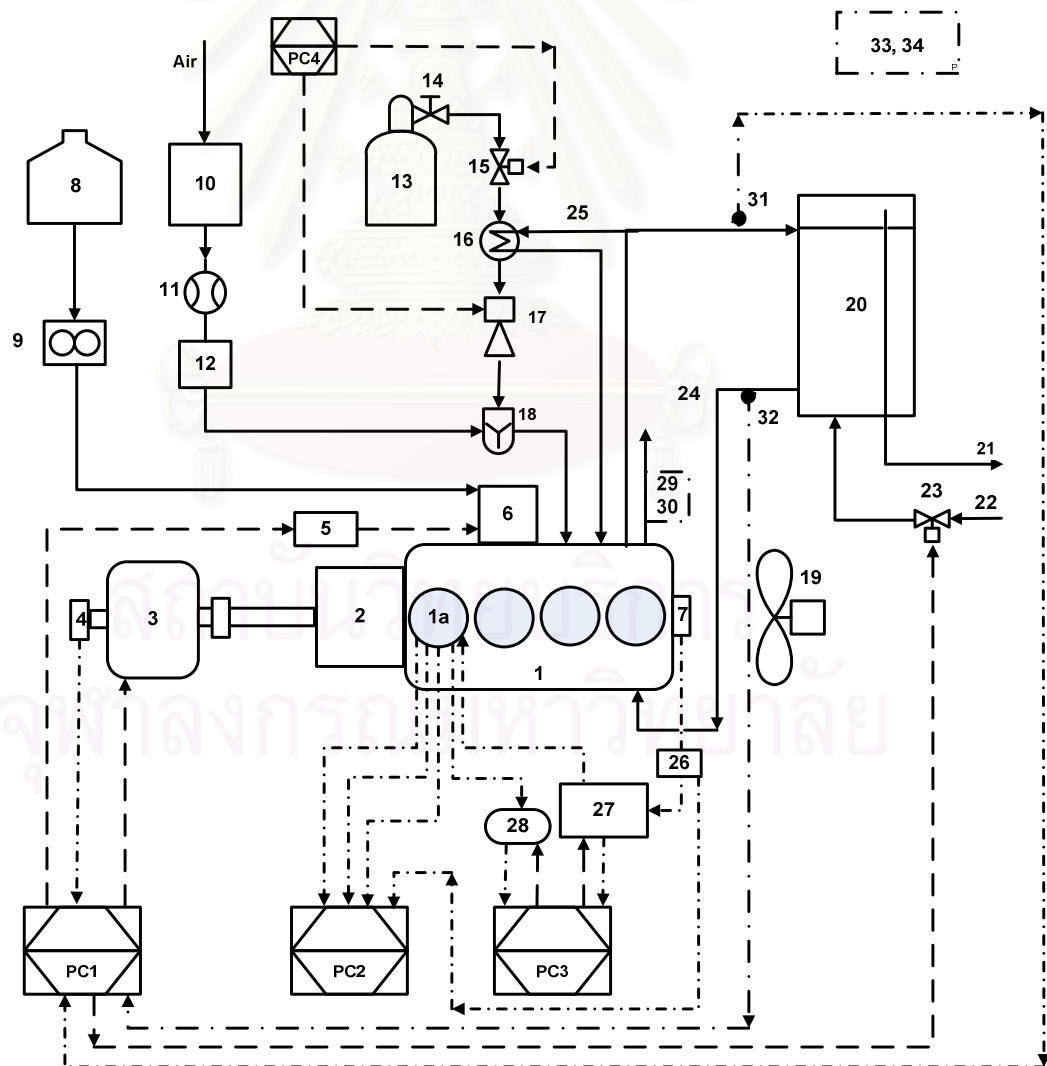
Figure 4–10   Diagram of the test system

1 - Engine

1a - Measured cylinder

2 - Gear box

3 - Dynamometer

4 - Speed sensor

5 - Pneumatic actuator

6 - Fuel pump

7 - Encoder

8 - Liquid fuel tank

9 - Fuel flow meter

10 - Surge tank with temperature measurement

11 - Orifice

12 - Air filter

13 - LPG tank, balance and box

14 - Valve

15 - Solenoid valve

16 - LPG vaporizer

17 - LPG injector

18 - Mixer

19 - Cooling fan

20 - Cooling water tank

21 - Drain-water pipe

22 - Inlet water, to water tank

23 - Solenoid valve

24 - Inlet water, to engine

25 - Inlet water, to LPG vaporizer

26 - AVL Pulse converter

27 - AVL Light unit

28 - CCD Camera

29 - Exhaust gas temperature measurement

30 - Exhaust gas pressure measurement

31 - Water-out temperature measurement

32 - Water-in temperature measurement

33 - Ambient temperature measurement

34 - Ambient pressure measurement

PC1 - AVL Control unit

PC2 - DEWE-5000-CA-SE Indicating system

PC3 - AVL Visual TM Visualization system

PC4 - LPG injection Control unit
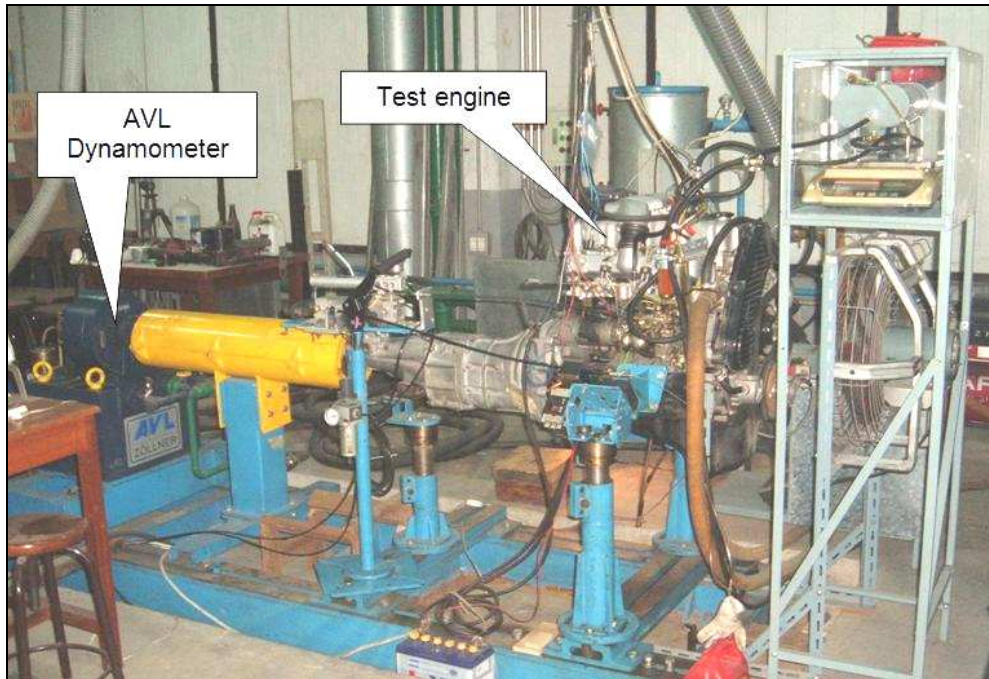
Figure 4–11   Arrangement of the test engine and dynamometer
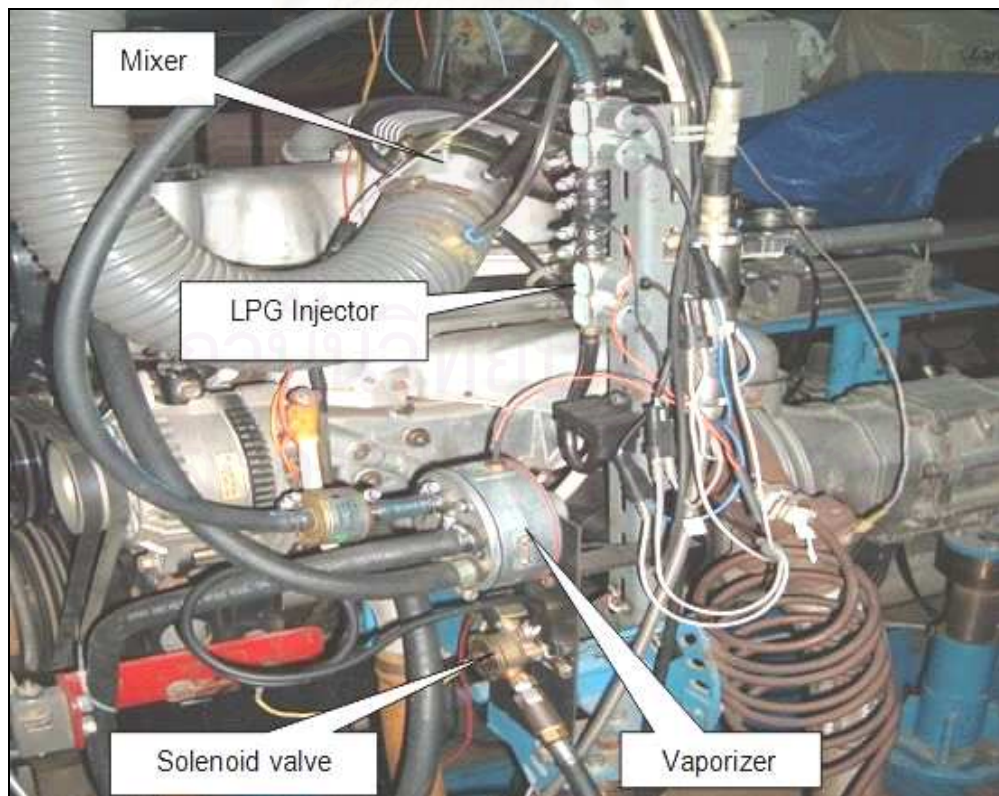
Figure 4–12   Arrangement of LPG injection system
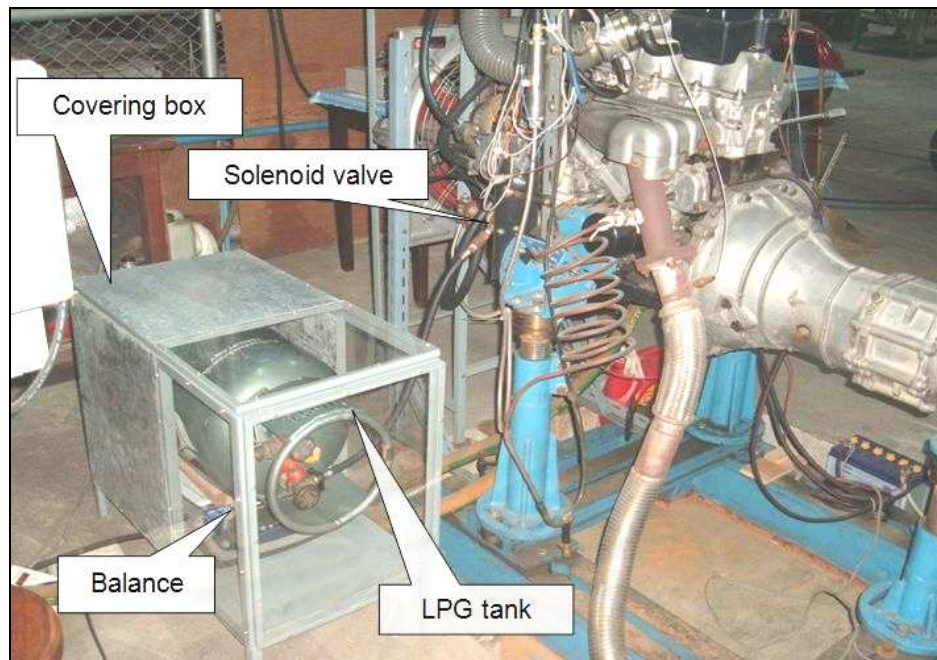
Figure 4–13   LPG measurement setup

Figure 4–14   Arrangement of air consumption measurement

4.3. Test procedure

Firstly, the engine is test with diesel fuel as the baseline. Air consumption, fuel consumption, specific diesel consumption, specific energy consumption, fuel-air equivalent ratio, net heat release rate and accumulative net heat release rate are then evaluated. Second, these steps are repeated with neat biodiesel. Next, the dual-fuel operation (LPG- diesel and LPG- biodiesel) is performed.

In dual fuel modes four different values of the premixed mixture strength (fuel-air equivalent ratio) are selected. Thus, the LPG flow rate obviously depends on engine speed. The LPG flow is controlled by the injection system via adjusting the duty cycle of the LPG injector. The values are selected to achieve as closed as possible of the mixture strength among the considered speeds. Detail information is given in Table 4-3. The fuel-air equivalent-ratio of homogeneous premixed mixture and the total fuel-air equivalent ratio are shown in Table 4-4 and Figures 4-15 to 4-24. Similar experiments in case of adjusted injection timing of liquid fuel will be continued. The visualization is conducted at interesting points.

Engine performance, fuel consumption, cylinder pressure trace, and combustion chamber phenomena have been conducted (steady state) at the test points as mentioned earlier. Steady state is considered as the instant at which fuel consumption, exhaust gas temperature, lube oil temperature, engine brake torque, and engine speed are stable. The valve on the water pipe is adjusted in each test point, to achieve the variation range from 83 to 86 ^{0}C of cooling water temperature. As the engine reaches steady state, a set of following parameters is collected, 5 times per each test point:

- Operation type (neat diesel or biodiesel, or LPG-diesel, or LPG-biodiesel);
- The injection timing setting for liquid fuel (OEM / adjusted setting);
- Engine speed and brake torque;
- Temperature of lube oil, exhaust gas, air in the air box, and ambient air;
- Differential pressure between ambient air and the air box;
- Absolute ambient pressure;
- Mass of liquid fuel consumed and the corresponding time;
- The LPG injection system setting as the engine is dual-fuelled. Mass of LPG consumed and the corresponding time;

Combustion chamber and fuel line pressure for each test point are recorded 2 times (one for reserve). The measurement is performed as follows:

- The system setting, including engine geometry, CA resolution, CA measurement range, pressure referencing, TDC determination, number of consecutive cycles recorded, is determined prior to the main tests and saved to hard disk and loaded as necessary.

- The DEWETRON Combustion Analyzer system runs at real-time mode with proper setting and it is thermally stable.
- As the engine reaches steady state, the record is performed and the result will be saved to the hard disk.

Table 4-3   Operation modes, LPG injection system setting and the LPG flow rate

LPG mode	Speed [rev/min]	Duty cycle [%]	LPG rate [g/s]	LPG rate [kg/h]
L1	1250	7	0.108568	0.390844
	2000	13	0.177428	0.638742
	2750	17	0.230780	0.830808
L2	1250	12	0.164563	0.592427
	2000	19	0.255608	0.920188
	2750	27	0.349435	1.257967
L3	1250	14	0.189597	0.682549
	2000	23	0.301438	1.085177
	2750	31	0.397902	1.432446
L4	1250	17	0.230780	0.830808
	2000	28	0.362473	1.304904
	2750	38	0.481863	1.734705

Table 4-4   Total fuel-air equivalent ratio at test points

Speed	Diesel & LPG-Diesel				Biodiesel & LPG-Biodiesel			
	Mode	Torque	ϕ_g	ϕ_t	Mode	Torque	ϕ_g	ϕ_t
1250	1250-D	9.91	0.00000	0.17106	1250-B	9.75	0.00000	0.17493
	1250-DL1	9.65	0.06541	0.16483	1250-BL1	9.62	0.06360	0.18949
	1250-DL2	9.67	0.09972	0.17821	1250-BL2	9.69	0.09678	0.20039
	1250-DL3	9.69	0.11556	0.18692	1250-BL3	9.72	0.11344	0.20919
	1250-DL4	9.70	0.14219	0.20169	1250-BL4	9.67	0.13694	0.20762

Table 4-4 Total fuel-air equivalent ratio at test points (Contd.)

Speed	Diesel & LPG-Diesel				Biodiesel & LPG-Biodiesel			
	Mode	Torque	ϕ_g	ϕ_t	Mode	Torque	ϕ_g	ϕ_t
1250	1250-D	19.85	0.00000	0.21320	1250-B	19.64	0.00000	0.21765
	1250-DL1	19.16	0.06519	0.21252	1250-BL1	19.24	0.06361	0.22548
	1250-DL2	19.35	0.09975	0.22107	1250-BL2	19.35	0.09688	0.23656
	1250-DL3	19.38	0.11558	0.22976	1250-BL3	19.36	0.11325	0.24573
	1250-DL4	19.48	0.14243	0.23419	1250-BL4	19.42	0.13738	0.24857
1250	1250-D	29.77	0.00000	0.25764	1250-B	29.52	0.00000	0.25710
	1250-DL1	28.85	0.06530	0.25761	1250-BL1	28.99	0.06388	0.25917
	1250-DL2	29.04	0.09976	0.26299	1250-BL2	29.11	0.09746	0.27243
	1250-DL3	28.99	0.11544	0.27634	1250-BL3	29.04	0.11325	0.27699
	1250-DL4	29.11	0.14256	0.27694	1250-BL4	29.05	0.13721	0.28472
1250	1250-D	39.85	0.00000	0.30150	1250-B	39.37	0.00000	0.28782
	1250-DL1	38.48	0.06532	0.29262	1250-BL1	39.33	0.06482	0.30342
	1250-DL2	38.73	0.09978	0.30364	1250-BL2	39.38	0.09878	0.31010
	1250-DL3	38.66	0.11544	0.31127	1250-BL3	39.39	0.11464	0.32287
	1250-DL4	38.90	0.14233	0.30609	1250-BL4	39.38	0.13920	0.31806
2000	2000-D	9.65	0.00000	0.19496	2000-B	9.68	0.00000	0.20980
	2000-DL1	9.73	0.06938	0.23258	2000-BL1	9.67	0.06953	0.24294
	2000-DL2	9.46	0.09894	0.23432	2000-BL2	9.73	0.10047	0.25464
	2000-DL3	9.67	0.11816	0.24595	2000-BL3	9.55	0.11717	0.25618
	2000-DL4	9.67	0.14207	0.24793	2000-BL4	9.63	0.14091	0.25700
2000	2000-D	19.30	0.00000	0.22515	2000-B	19.37	0.00000	0.24844
	2000-DL1	19.46	0.06937	0.26068	2000-BL1	19.33	0.06953	0.27263
	2000-DL2	18.92	0.09904	0.26602	2000-BL2	19.55	0.10048	0.28601
	2000-DL3	19.34	0.11816	0.27643	2000-BL3	19.16	0.11730	0.28951
	2000-DL4	19.32	0.14217	0.27998	2000-BL4	19.32	0.14119	0.29372

Table 4-4 Total fuel-air equivalent ratio at test points (Contd.)

| Speed | Diesel & LPG-Diesel | | | | Biodiesel & LPG-Biodiesel | | | |
	Mode	Torque	ϕ_g	ϕ_t	Mode	Torque	ϕ_g	ϕ_t
2000	2000-D	28.96	0.00000	0.26314	2000-B	29.12	0.00000	0.28134
	2000-DL1	29.19	0.06937	0.29463	2000-BL1	29.12	0.06988	0.30325
	2000-DL2	28.46	0.09927	0.30537	2000-BL2	29.33	0.10055	0.31533
	2000-DL3	29.01	0.11815	0.30908	2000-BL3	28.81	0.11735	0.31636
	2000-DL4	28.98	0.14231	0.31653	2000-BL4	29.11	0.14149	0.32574
2000	2000-D	38.68	0.00000	0.30231	2000-B	38.90	0.00000	0.31935
	2000-DL1	38.91	0.06936	0.33091	2000-BL1	38.79	0.06963	0.33901
	2000-DL2	38.84	0.10068	0.34355	2000-BL2	39.11	0.10066	0.35206
	2000-DL3	38.67	0.11815	0.34401	2000-BL3	38.46	0.11738	0.35106
	2000-DL4	38.49	0.14207	0.35294	2000-BL4	38.82	0.14156	0.35655
2000	2000-D	67.72	0.00000	0.42253	2000-B	68.10	0.00000	0.42813
	2000-DL1	67.78	0.06894	0.43720	2000-BL1	67.73	0.06956	0.44709
	2000-DL2	67.70	0.10041	0.44766	2000-BL2	68.44	0.10024	0.45405
	2000-DL3	67.68	0.11815	0.45101	2000-BL3	67.49	0.11751	0.45369
	2000-DL4	67.33	0.14220	0.45481	2000-BL4	67.97	0.14159	0.45769
2750	2750-D	9.72	0.00000	0.22583	2750-B	9.77	0.00000	0.23751
	2750-DL1	9.53	0.06520	0.24746	2750-BL1	9.75	0.06649	0.27140
	2750-DL2	9.58	0.09919	0.26392	2750-BL2	9.70	0.10067	0.28002
	2750-DL3	9.70	0.11392	0.27130	2750-BL3	9.62	0.11345	0.27888
	2750-DL4	9.73	0.13862	0.27907	2750-BL4	9.82	0.14009	0.29099
2750	2750-D	19.48	0.00000	0.25949	2750-B	19.56	0.00000	0.26778
	2750-DL1	19.12	0.06524	0.27742	2750-BL1	19.51	0.06635	0.30018
	2750-DL2	19.21	0.09898	0.28850	2750-BL2	19.42	0.10062	0.31063
	2750-DL3	19.37	0.11361	0.29298	2750-BL3	19.28	0.11358	0.30811
	2750-DL4	19.43	0.13824	0.30300	2750-BL4	19.63	0.14001	0.32106

Table 4-4 Total fuel-air equivalent ratio at test points (Contd.)

Speed	Diesel & LPG-Diesel				Biodiesel & LPG-Biodiesel			
	Mode	Torque	ϕ_g	ϕ_t	Mode	Torque	ϕ_g	ϕ_t
2750	2750-D	29.24	0.00000	0.29386	2750-B	29.34	0.00000	0.30570
	2750-DL1	28.68	0.06512	0.30739	2750-BL1	29.33	0.06632	0.33071
	2750-DL2	29.08	0.09992	0.32910	2750-BL2	29.10	0.10034	0.33714
	2750-DL3	29.14	0.11350	0.32533	2750-BL3	28.92	0.11358	0.33625
	2750-DL4	29.19	0.13801	0.33638	2750-BL4	29.45	0.13977	0.34599
2750	2750-D	38.99	0.00000	0.32555	2750-B	39.08	0.00000	0.34309
	2750-DL1	38.15	0.06488	0.34180	2750-BL1	39.04	0.06626	0.36356
	2750-DL2	38.67	0.09936	0.35285	2750-BL2	38.81	0.10013	0.37009
	2750-DL3	38.85	0.11325	0.35841	2750-BL3	38.57	0.11359	0.37107
	2750-DL4	38.92	0.13755	0.36970	2750-BL4	39.26	0.13954	0.38021
2750	2750-D	68.27	0.00000	0.44278	2750-B	68.41	0.00000	0.45287
	2750-DL1	66.94	0.06482	0.44408	2750-BL1	68.60	0.06612	0.47173
	2750-DL2	67.88	0.09917	0.45263	2750-BL2	68.13	0.09982	0.47242
	2750-DL3	68.17	0.11321	0.46243	2750-BL3	67.60	0.11309	0.46692
	2750-DL4	68.03	0.13688	0.46356	2750-BL4	68.71	0.13907	0.47590
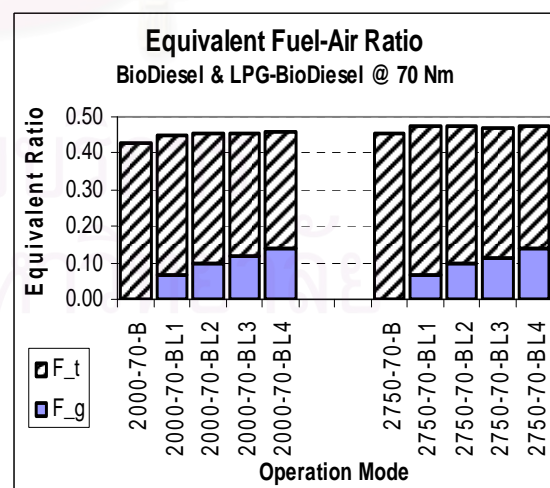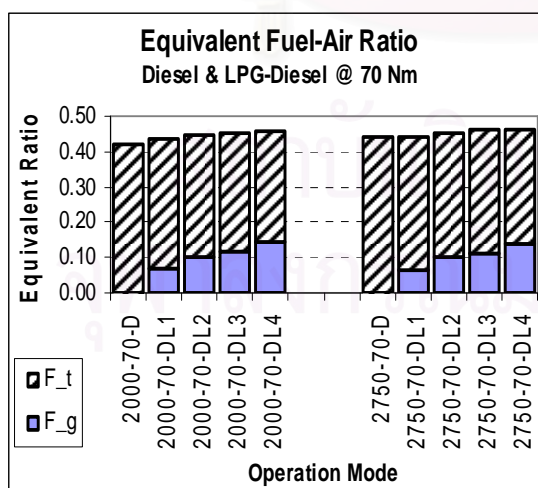
Figure 4–15 ϕ of the premixed charge and total (70 Nm)
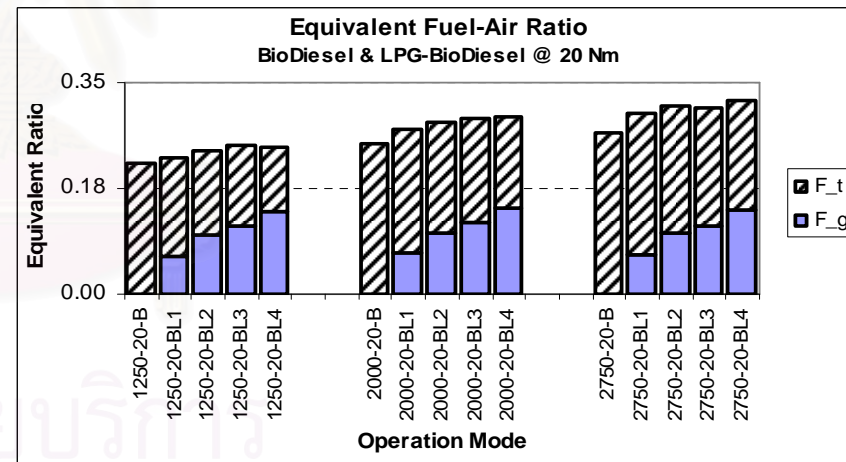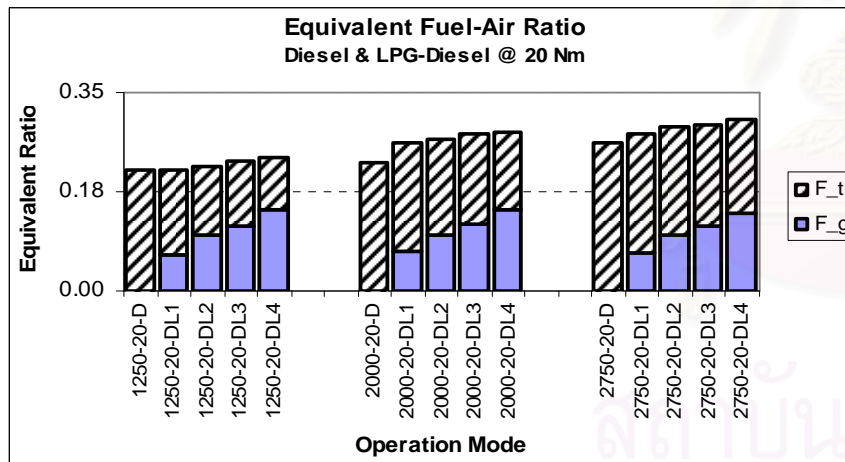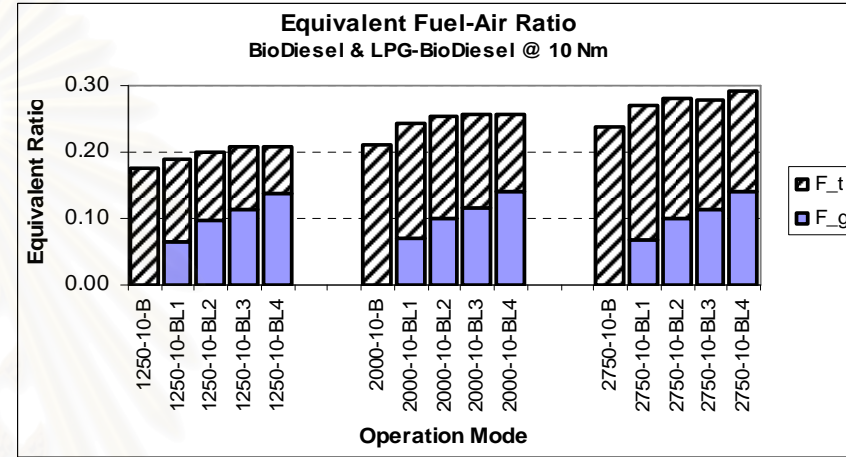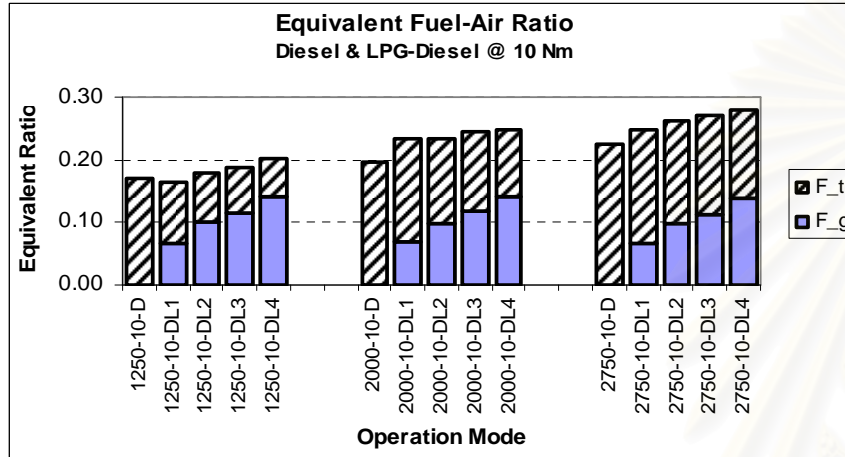
Figure 4–16 ϕ of the premixed charge and total (10 and 20 Nm)
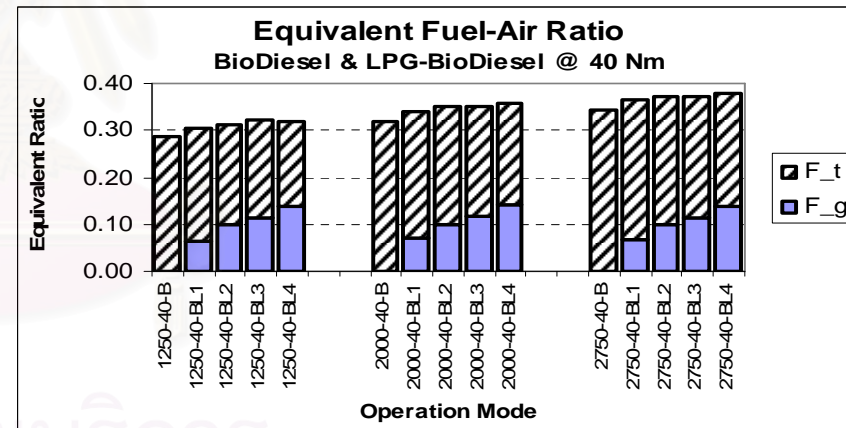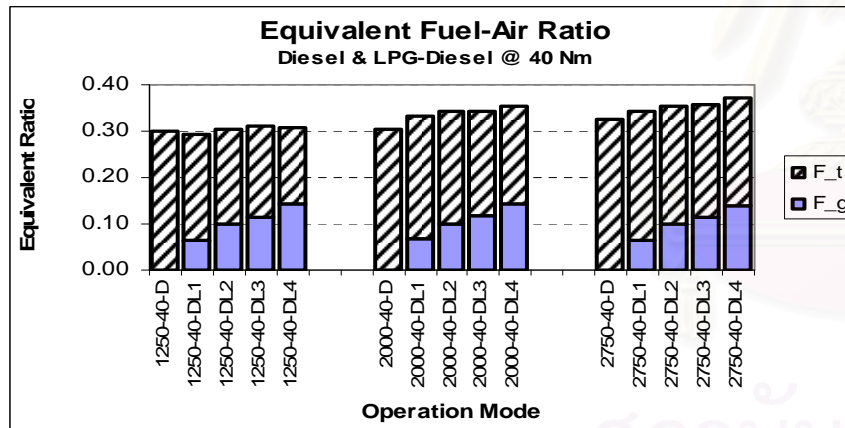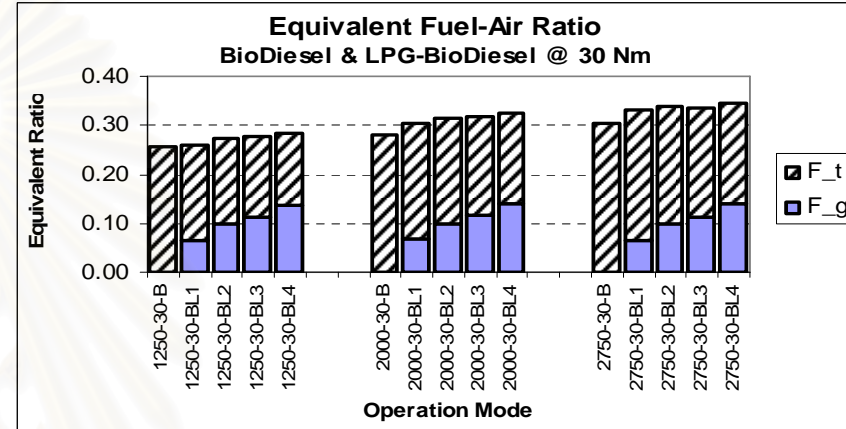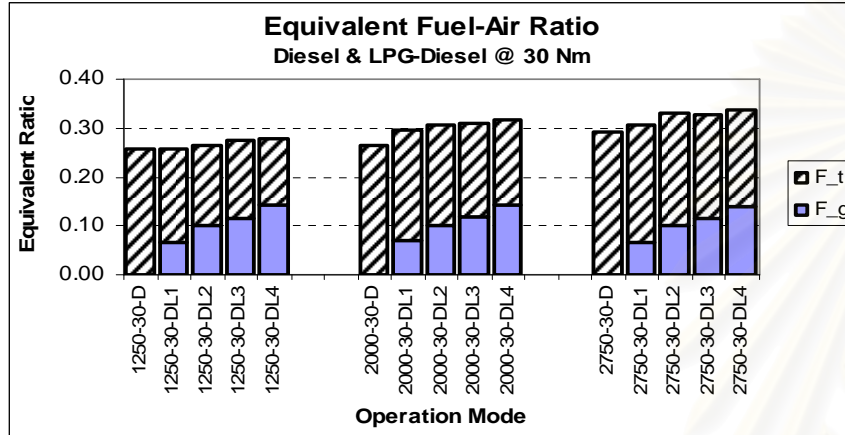
Figure 4–17 ϕ of the premixed charge and total (30 and 40 Nm)

CHAPTER 5

THEORETICAL BACKGROUND

5.1. Definition of parameters relating to engine performance and energy consumption

5.1.1. The definition

The measured values at steady state of engine brake torques, power outputs are corrected to the standard condition according to the standard ISO 3046 before other calculation are performed. The brake torque and power output henceforth refer to their corrected values. The definition of considered parameters is described as following:

Engine brake power output, P, is determined from its rotational speed, N [rev/min], and brake torque, T [Nm], as follows:

$$P = \pi.T.\frac{N}{30}$$ (5-1)

Indicated work per cylinder per cycle, $W_{c,i}$, is determined based on main chamber pressure, p_1 [N/m^2], via:

$$W_{c,i} = \oint p_1 dV$$ (5-2)

Mechanical efficiency, η_m, is determined as the ratio between brake power output, P [W], and indicated work per cycle, $W_{c,i}$ [W]:

$$\eta_m = \frac{P}{W_{c,i}}$$ (5-3)

It is noticed that, for this investigation, the mechanical efficiency defined above includes the efficiency of the clutch and gear box which are mounted with the test engine. The gear box is set at 4th gear during the experiments.

Substitution is defined as the ratio between equivalent liquid fuel mass flow rate replaced by LPG in dual fuel operation and that in diesel operation, or biodiesel operation to achieve the same engine speed and torque, as below

- For diesel-LPG operation:

$$Sub_D = (1 - \overset{*}{m}_{D,DL} / \overset{*}{m}_{D,D}).100 \, (\%)$$ (5-4)

- For biodiesel-LPG operation:

$$Sub_B = (1 - \overset{*}{m}_{B,BL} / \overset{*}{m}_{B,B}).100 \, (\%)$$ (5-5)

LPG energy fraction, GEF, is defined as the ratio between energy of the LPG and the total energy of LPG and liquid fuel, as follows.

- For diesel-LPG operation:

$$GEF_{DL} = \frac{\overset{*}{m}_{LPG} HV_{LPG}}{\overset{*}{m}_D HV_d + \overset{*}{m}_{LPG} HV_{LPG}} \qquad (5\text{-}6)$$

- For biodiesel-LPG operation:

$$GEF_{BL} = \frac{\overset{*}{m}_{LPG} HV_{LPG}}{\overset{*}{m}_B HV_B + \overset{*}{m}_{LPG} HV_{LPG}} \qquad (5\text{-}7)$$

Brake total energy conversion efficiency is defined as the ratio between engine brake power output and rate of total fuel energy supplied to the engine:

- For diesel-LPG operation:

$$\eta_{f,DL} = \frac{P}{\overset{*}{m}_D HV_d + \overset{*}{m}_{LPG} HV_{LPG}}.100\,(\%) \qquad (5\text{-}8)$$

- For biodiesel-LPG operation:

$$\eta_{f,BL} = \frac{P}{\overset{*}{m}_B HV_B + \overset{*}{m}_{LPG} HV_{LPG}}.100\,(\%) \qquad (5\text{-}9)$$

Specific total energy consumption, STEC, is defined as the energy of fuel (liquid and LPG) needed to produce 1 kWh of brake work, as follows

- For diesel-LPG operation:

$$STEC_{DL} = SEC_{D,DL} + SEC_{LPG,DL} = \frac{3600}{P}\left(\overset{*}{m}_D.HV_D + \overset{*}{m}_{LPG}.HV_{LPG}\right) \qquad (5\text{-}10)$$

- For biodiesel-LPG operation:

$$STEC_{BL} = SEC_{B,BL} + SEC_{LPG,BL} = \frac{3600}{P}\left(\overset{*}{m}_B.HV_B + \overset{*}{m}_{LPG}.HV_{LPG}\right) \qquad (5\text{-}11)$$

Total fuel air equivalent ratio is defined as the ratio between actual fuel air ratio and stoichiometric fuel air ratio. Hence, it is the ratio between the stoichiometric mass of air required to burn completely the diesel (or biodiesel) and LPG inside the cylinder and the actual air introduced to the cylinder, as below.

- For diesel-LPG operation:

$$\Phi_{DL} = \frac{m_D (A/F)_{st,D} + m_{LPG} (A/F)_{st,LPG}}{m_{air}} \qquad (5\text{-}12)$$

- For biodiesel-LPG operation:

$$\Phi_{BL} = \frac{m_B (A/F)_{st,B} + m_{LPG} (A/F)_{st,LPG}}{m_{air}} \qquad (5\text{-}13)$$

The above equations are also adequate with diesel (or biodiesel) fuelling ($m_{LPG}=0$), corresponding with subscript "D" (or "B") of parameters Φ and η_f.

Volumetric efficiency is defined as below:

$$\eta_v = \frac{m_{air}}{\rho_{air,i} . V_d} \qquad (5\text{-}14)$$

Where m_a [kg] - mass of air trapped per cycle

$\rho_{air,i}$ [kg/m^3]- density of air at working condition

V_d [m^3] - swept volume of the engine

5.1.2. Uncertainty estimation for the measured and calculated parameters

Combined standard uncertainty u_r in the result of calculated parameter r, which involves J measurands can be estimated as follows[77],

$$u_r^2 \approx \sum_{i=1}^{J} (\theta_i)^2 u_{xi}^2 + 2\sum_{i=1}^{J-1} \sum_{j=i+1}^{J} (\theta_i)(\theta_j) u_{xi,xj} \qquad (5\text{-}15)$$

where $\theta_i = \dfrac{\partial r}{\partial x_i}$, the absolute sensitivity coefficient

$u_{xi,xj} = \sum_{k=1}^{L} (u_i)_k (u_j)_k$ and L is the number of elemental error sources common to measurands x_i and x_j

As covariances are neglected, the above equation becomes

$$u_r^2 \approx \sum_{i=1}^{J} (\theta_i u_{xi})^2 \qquad (5\text{-}16)$$

The value of result's uncertainty of parameter r follows Student's t distribution, based on the number of effective degrees of freedom, ν_{eff}

$$\nu_{eff} = \frac{\left(\sum_{i=1}^{J} (\theta_i u_{xi})^2 \right)^2}{\sum_{i=1}^{J} (\theta_i u_{xi})^4 / \nu_i} \qquad (5\text{-}17)$$

With $\nu_i = Ni - 1$, is the number of degrees of freedom for u_{xi}, and N_i is the sample size.

The true value, r_{true} of parameter r, with C% confidence is then represented as

$$r_{true} = \bar{r} \pm U_r = \bar{r} \pm t_{veff,C} . u_r \qquad (5\text{-}18)$$

where $t_{\nu_{eff},C}$ is the Student's t variable evaluated with C% confidence.

Relative uncertainty is presented as ratio of absolute uncertainty, U_r and mean value, $\bar{r}$.

Uncertainty of brake torque, brake power, specific diesel consumption, specific total energy consumption, brake total energy conversion efficiency, diesel substitution, total fuel-air equivalent ratio, and volumetric efficiency was estimated with C95% confidence. Following assumption was made:

- Heating value and stoichiometric air-fuel ratio of diesel, biodiesel, and LPG, diesel density, swept volume, discharge coefficient of the orifices are considered constants.

- Neglect the uncertainty generated as above parameters are corrected to the standard condition.

5.2. Combustion system of the test engine and heat release analysis

5.2.1. Combustion system of the test engine

Combustion system of the test engine is a variant of Ricardo Comet MK Vb combustion chamber system with one-nozzle injector. Figure 5–1 shows the conventional Ricardo Comet MK Vb combustion chamber system. Description of combustion process in this chamber type can be seen in documents, such as [3, 78, 79]. As follows are some its features. Initially, the process takes place in a swirl chamber housed in the cylinder head and then the second half of the process is completed in the twin disc shaped recesses (swirl pockets or double-leaf area) in the piston crown.

The spherical swirl chamber is located at one side and above the cylinder wall in the cylinder head. The upper half of the sphere is cast directly in the cylinder head and the lower half is a separate heat resisting alloy member flanged and cylindrical in shape with an upward facing semi-hemispherical chamber; it fits in a machined recess so that its under-side is flush with the flat face of the cylinder head. It is located and secured by a pin and flange while the outer cylindrical vertical wall stands away from the machined cylinder head recess to create an isolating air gap. This part is a heat regenerative member since it absorbs heat from combustion and dissipates it during the compression stroke. An inclined passage through the base of the lower regenerative member forms a

throat between the spherical swirl chamber and twin adjacent circular cavities cast in the piston crown. An injector is positioned over the chamber at an acute angle to the swirl chamber.
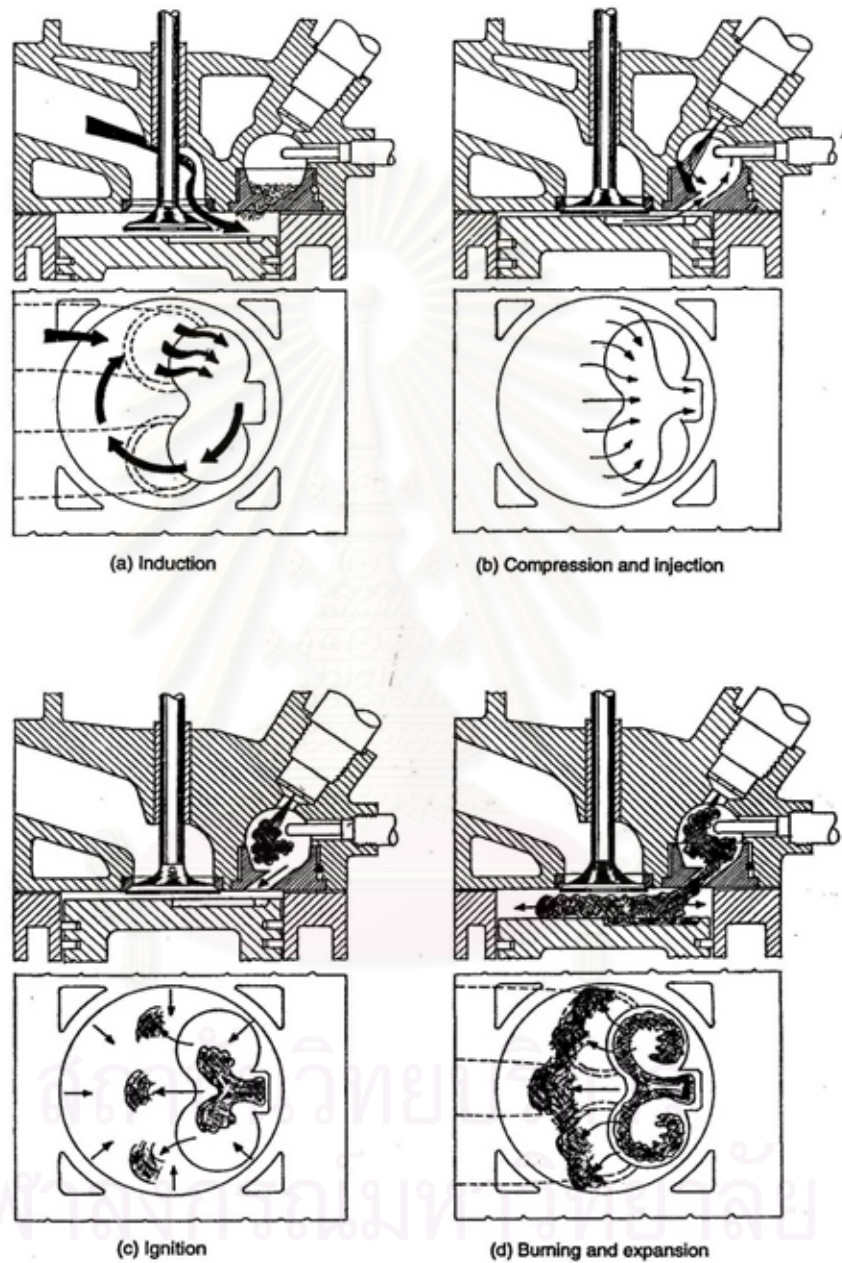
Figure 5–1   Ricardo Comet MK Vb swirl chamber combustion system [79]

Air is drawn tangentially into the cylinder (a) via the twin induction port where it then moves in a circular downward path around the cylinder wall as the piston moves away from TDC. In the return stroke (b) the air charge is compressed causing a part of

the trapped air to be transferred through the throat into the swirl chamber. The throat angle guides the air stream so that it is forced to follow the contour of the chamber wall in a vertical circular swirl many times during the compression stroke. As air passes the throat it absorbs heat from the hot alloy mass and from the chamber walls as it circulates around the chamber, attaining a temperature well above the auto-ignition temperature of the liquid fuel.

As fuel is injected at a downstream direction to the air swirl to one side of the chamber, the spray penetrates the dense air charge and impinges onto the spherical surface of the regenerative member. Instantly, the liquid fuel spreads out to form a thin film, which then vaporizes and is immediately swept around with the air stream. The fuel vapor, oxygen and heat then combine to cause the oxidation reaction which is essential for ignition at random nuclei sites surrounding the vapor clouds within the swirl chamber. Rapid flame spread follows as unburnt vapor seeks out the oxygen in the dense but rapidly rotating air charge. The high burning rate produces a corresponding rapid pressure rise in the swirl chamber. The burning charge will blow down the throat (c) and divide into two separate flame fronts as it enters the twin, shallow disc-shaped recesses formed in the piston crown. The tangential entry compels the flame fronts to swirl clockwise and anticlockwise around their respective cavity walls, which gives the burning and unburnt vapor the maximum opportunity to search out the oxygen simultaneously, to displace the burnt products of combustion whereas to limit the heat transfer from the flame to the cool cylinder chamber. With further crank-angle movement (d), the flame-fronts now spread beyond the piston cavities into the main cylinder until all or almost all of the injected charge of liquid fuel has been consumed.

Combustion system of the test engine is a modified version with downstream glow plug, as depicted in Figure 4–2. With this modification the swirl intensity is higher and the nozzle coking problem is eliminated.

5.2.2. Heat release model

The use of heat release rate analysis techniques for investigation of combustion in diesel engines is well researched and documented. Krieger and Borman proposed a method for calculating the heat release rate curves including the effects of dissociation

of the combustion products and modeling the rate of heat transfer [80]. Gatowski, et al., also developed a heat release method that maintains simplicity while including the effects of heat transfer, crevice flows, and fuel injection [81]. Rakopoulos and Hountalas estimated the gross rate of heat release using experimentally determined corresponding net rates of heat release and several different heat transfer models [82]. The net apparent rate of heat release can be determined from the cylinder pressure time history. The heat transfer rate to the walls has historically been determined through the use of models and correlations. Krieger and Borman used the Annand correlation [80]. Gatowski, et. al. used the Woschni correlation [81], Rakopoulos and Hountalas used the $k-\varepsilon$ turbulent kinetic energy model and Annand, Woschni and Eichelberg correlations [83]. The gross rate of heat release has been determined by summing the two former rates. The gross rate of heat release and the rate of heat transfer to the walls have to be determined experimentally.

In this study, the apparent net heat release of the test engine is concerned. The heat release model adapted from [3] is used to analyze the combustion process. Figure 5–2 shows schematically combustion system of the test engine. It includes two open systems linked by a connecting passage.
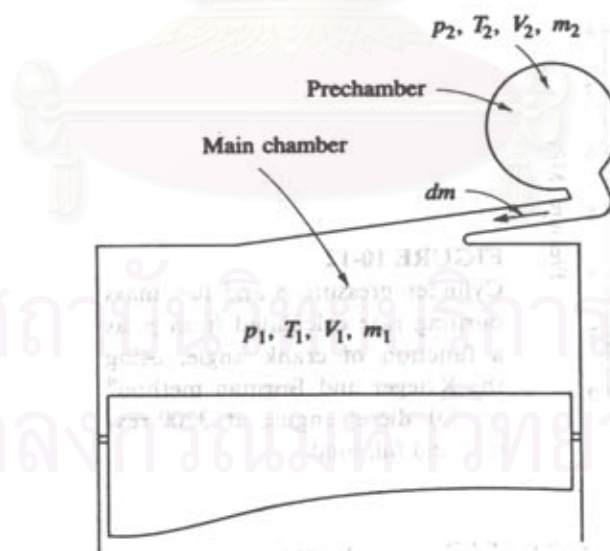
Figure 5–2   Schematic of heat release model for IDI combustion system[3]

Assume that:

- Uniform properties of the fluid in each combustion chamber;

- There is no crevice flow (the valves close properly, no blow by);

and applying the first law to these systems yields:

- For the first – main chamber:

$$\frac{dQ_1}{dt} - p_1 \frac{dV_1}{dt} + h_{21} \frac{dm_{21}}{dt} = \frac{dU_1}{dt}$$ (5-19)

- For the second – prechamber:

$$\frac{dQ_2}{dt} + h_f \frac{dm_f}{dt} - h_{21} \frac{dm_{21}}{dt} = \frac{dU_2}{dt}$$ (5-20)

The mass flow rate between the two chambers, $dm_{2,1}/dt$, is considered positive as the flow is from the pre-chamber to the main chamber.

if $\frac{dm_{21}}{dt} > 0$ then $h_{21} = h_2$

if $\frac{dm_{21}}{dt} < 0$ then $h_{21} = h_1$

If U_1 and U_2 are defined as sensible internal energies and h_f as the sensible enthalpy of the fuel, dQ_1/dt and dQ_2/dt represent the net heat release rates; the difference between the combustion energy release rates (gross) and the rates of heat transferred (loss) to the chamber walls.

As working fluid in the two chambers is considered ideal gas, with c_p, c_v, and M constant, the relation:

$$p_1 V_1 = m_1 R T_1$$ (5-21)

$$p_2 V_2 = m_2 R T_2$$ (5-22)

can be used to eliminate m and T from the dU/dt terms. Then the above equation can be written as

$$\frac{dQ_1}{dt} = \frac{\gamma}{\gamma-1} p_1 \frac{dV_1}{dt} + \frac{1}{\gamma-1} V_1 \frac{dp_1}{dt} - c_p T_{21} \frac{dm_{21}}{dt}$$ (5-23)

$$\frac{dQ_2}{dt} = \frac{1}{\gamma-1} V_2 \frac{dp_2}{dt} + c_p T_{21} \frac{dm_{21}}{dt}$$ (5-24)

The term representing the enthalpy flux between the two chambers is canceled out as the two above equations are added together, yielding following equation for the total net heat release from the two chambers:

$$\frac{dQ}{dt} = \frac{dQ_1}{dt} + \frac{dQ_2}{dt} = \frac{\gamma}{\gamma-1} p_1 \frac{dV_1}{dt} + \frac{1}{\gamma-1}\left(V_1 \frac{dp_1}{dt} + V_2 \frac{dp_2}{dt} \right)$$ (5-25)

If the pressure in the pre-chamber is described as, $p_2 = p_1 + \Delta p$, the net heat release equation becomes

$$\frac{dQ}{dt} = \frac{\gamma}{\gamma-1}p_1\frac{dV_1}{dt} + \frac{V_1+V_2}{\gamma-1}\frac{dp_1}{dt} + \frac{V_2}{\gamma-1}\frac{d(\Delta p)}{dt} \tag{5-26}$$

The cumulative net heat release from SOI until the instant considered, t corresponding with θ of crank angle is then determined by

$$Q_{net} = \int_{SOI}^{\theta} dQ \tag{5-27}$$

The net heat release rate and the cumulative net heat release of an IDI CI engine is shown in Figure 5–3 and Figure 5–4.
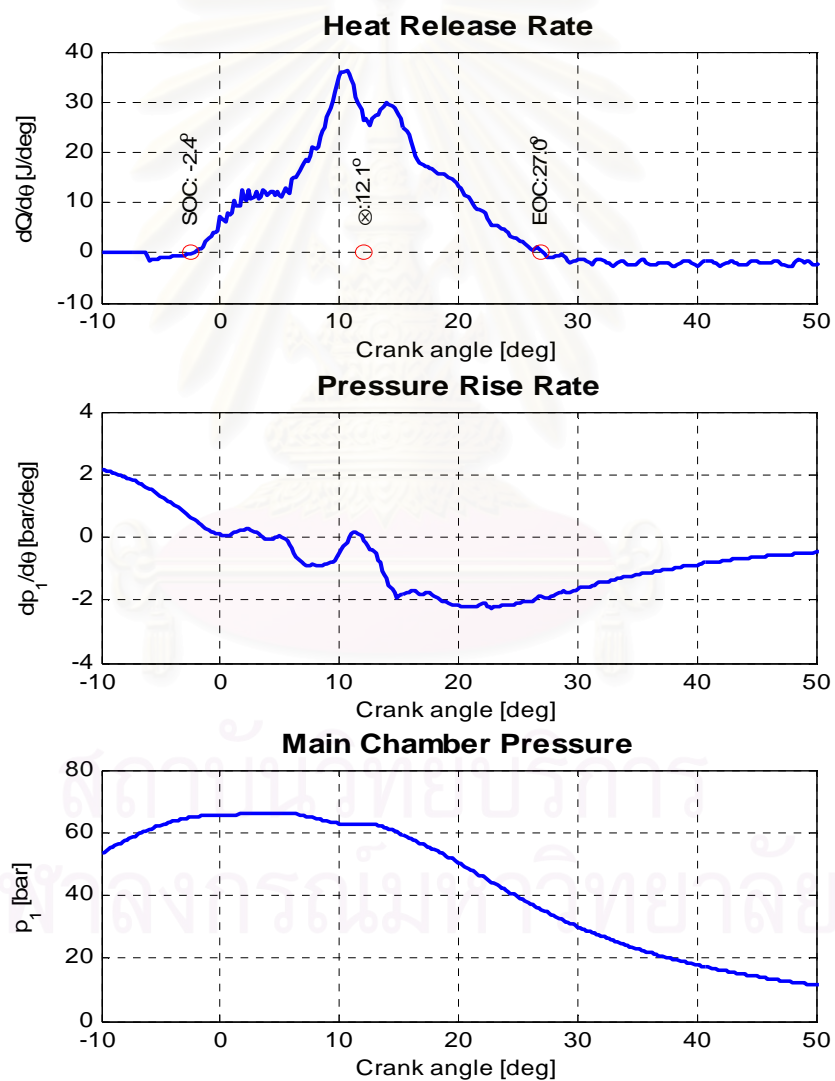
Figure 5–3   Typical predicted net HRR, main chamber pressure and PRR
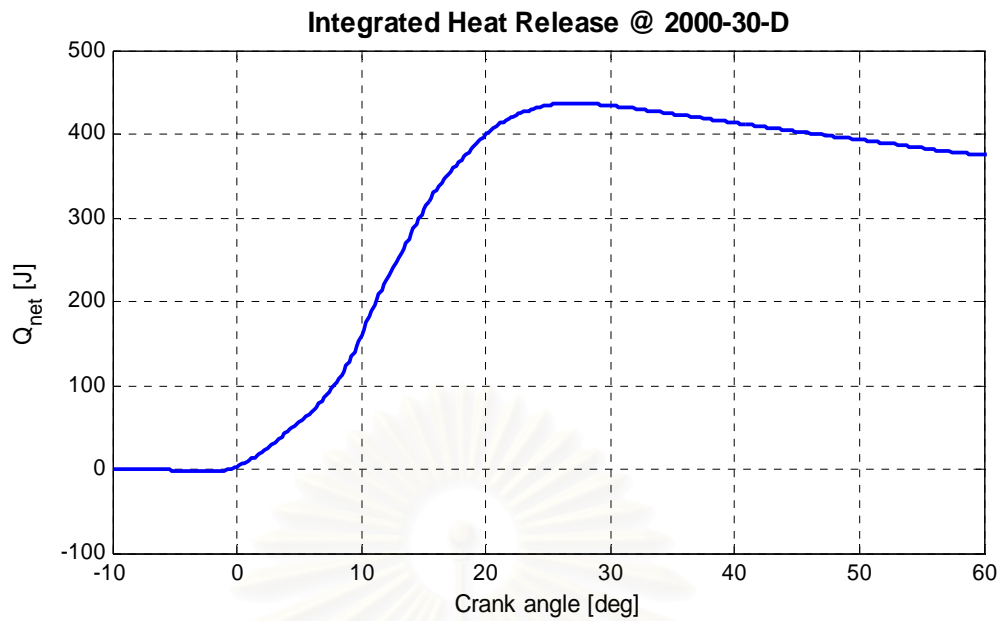
Figure 5–4   Typical predicted cumulative net HR of the test engine

5.2.3. Determination of SOI, ignition delay, SOC, combustion duration

5.2.3.1. Determination of liquid injection events
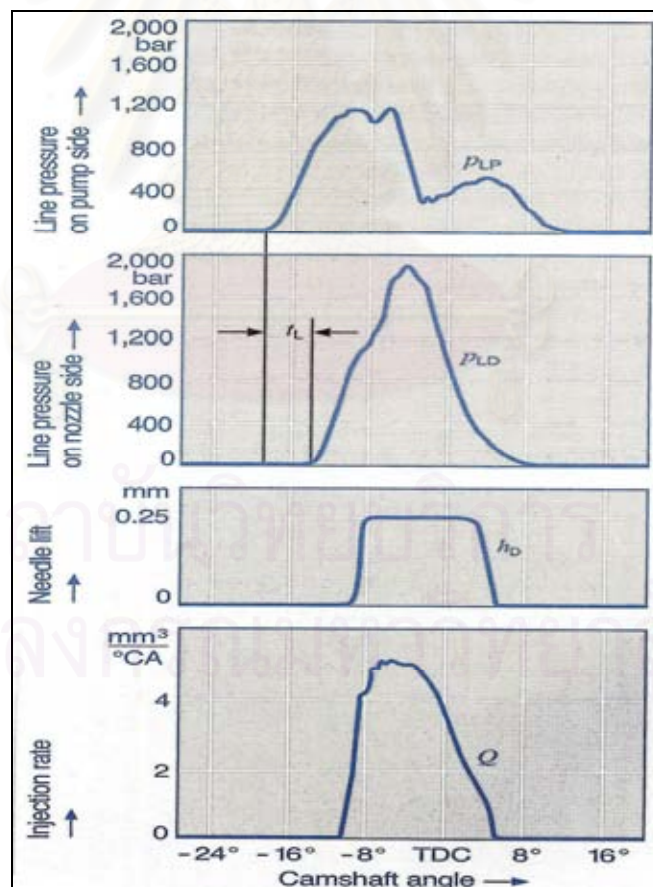
Figure 5–5   Pressure in fuel injection system, needle lift, and injection rate of a fuel

system with distributor pump, adapted from [84]
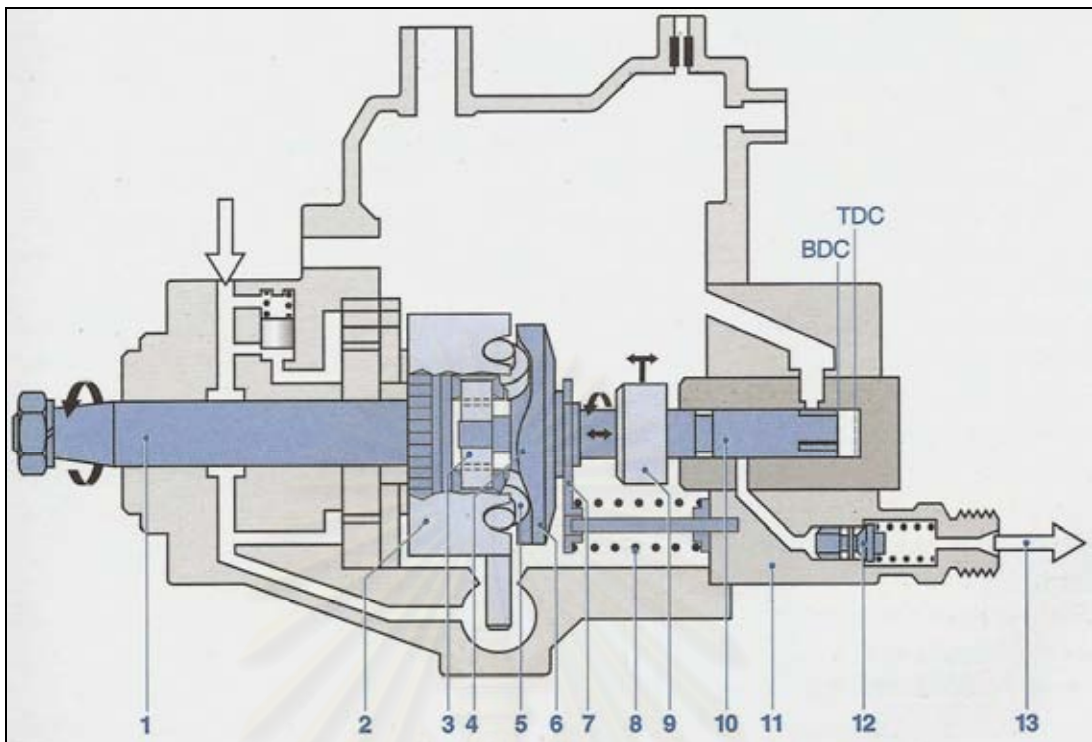
Figure 5–6   High pressure circuit in inner chamber of a helix-port controlled

distributor injection pump, adapted from [84]

1 – Input shaft	8 – Plunger return spring
2 – Rolling ring	9 – Control collar
3 – Yoke	10 – Distributor plunger
4 – Cams	11 – Distributor head
5 – Roller	12 – Delivery valve
6 – Cam plate	13 – Discharge to high pressure line
7 – Spring-loaded cross brace	TDC – Top dead center of the plunger
	BDC – Bottom dead center of the plunger
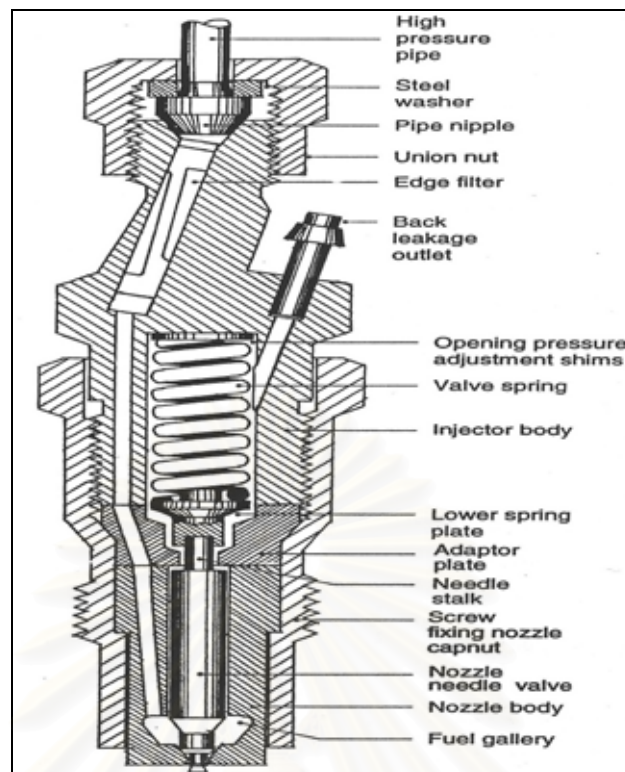
Figure 5–7   Geometry of the Pintle-nozzle injector, adapted from [79]

The start of injection (SOI) of liquid fuel into the combustion chamber is the instant at which the needle starts to lift its seat. The end of injection (EOI) is the instant at which it moves back and locates properly in the seat. Injection duration is the period between these two instants. Normally, these parameters are determined by the signal from needle lift sensor. The injection rate can then be determined by orifice flow model if the discharge coefficient of the nozzle and the mass of fuel injected per cycle are known. Figure 5–5, adapted from [84] presents pressure in fuel pump, pressure in fuel line, needle lift, injection lag, and injection rate of a fuel system with distributor pump.

Whereas there is not difficult to determine the parameters related to liquid fuel injection using needle lift signal, the reverse is true as using fuel line pressure. There is no reported information about the determination of EOI based on fuel line pressure. Szybist J.P. and Boehman A.L. [85] conducted an experimental investigation on the behavior of diesel fuel injection system with diesel, biodiesel by combination three technique: digital imaging, laser attenuation, and fuel line pressure. In their study, the probe for fuel line measurement was installed between the pump and the nozzle and forty consecutive cycles were considered. They found good agreement in the SOI determination with all the three methods; it is the crank angle of the appearance of the

first local maximum fuel line pressure (before TDC, in the pumping stroke). This also agreed with the result from Reitz R.D. and Choi C.Y.[86].

However, there may be no such local fuel line pressure maximum in certain condition. In this study, this occurs with the test engine at speed of 2750 rev/min. Therefore, attempt has been made to find another SOI-token which satisfies simultaneously two following terms:

- It gives the same result when the local maximum exists;
- It is reasonable in case of lacking the local maximum of fuel line pressure.

Observing the data of the fuel line pressure, the local maxima (if existing), the coefficient of variation (COV) of the fuel line pressure at different engine speeds and torques (mass of liquid fuel injected per cycle), as seen in Figure 5–8 to Figure 5–11, it is revealed that the first local minimum of the COV of fuel line pressure occur at the same abscissa (crank angle) with the local maxima (if existing) of fuel line pressure. In case no such local maximum of fuel line pressure, the crank angle corresponding to the local minimum of the COV gives reasonable token of SOI. Thus, the minima of COV of fuel line pressure are considered to be the token of SOI. This can be explained as follows.

The delivery valve, shown in Figure 5–6, shuts off the high pressure line from the pump, between injection cycles. The residual pressure retained in the fuel line ensures rapid and precise opening of the nozzle for the next injection cycle. The fuel line pressure is resulted from the pump effect and the wave transferred from the distributor plunger. Obviously, this pressure is also affected by the engine vibration; it causes variation in the pressure magnitude. During compression stroke of the plunger until SOI:

- The magnitude of the fuel line pressure increases increasingly.
- The opening pressure is constant since the spring steepness and the moving mass (mass of spring, lower spring plate, and needle as shown in Figure 5–7) are constant.
- The geometry of the space (in the fuel line, nozzle holder) which filled by the fuel is almost constant.

Thus, when the engine is at steady state, during compression stroke of the pump until SOI, the effect of vibration on the fuel line pressure as well as the coefficient of variation of the fuel line pressure becomes increasingly smaller.
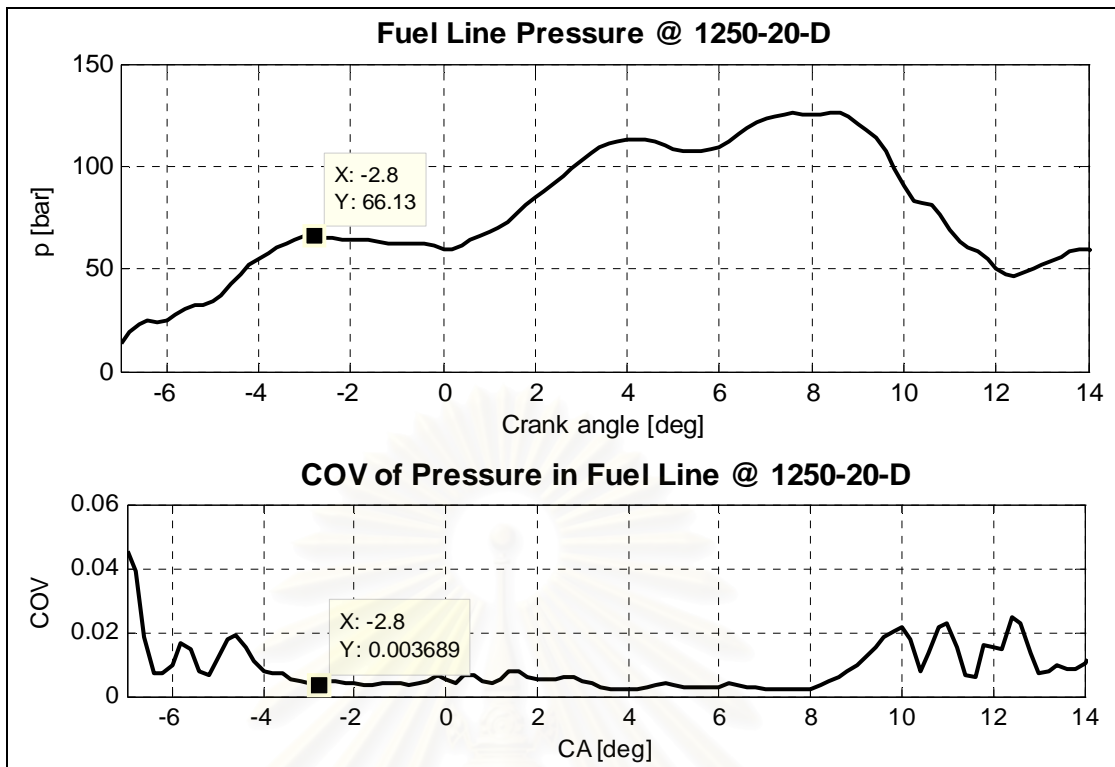
Figure 5–8   Average fuel line pressure and COV of fuel line pressure of 120

consecutive cycles, at engine speed of 1250 rev/min, 20 Nm, diesel fuel
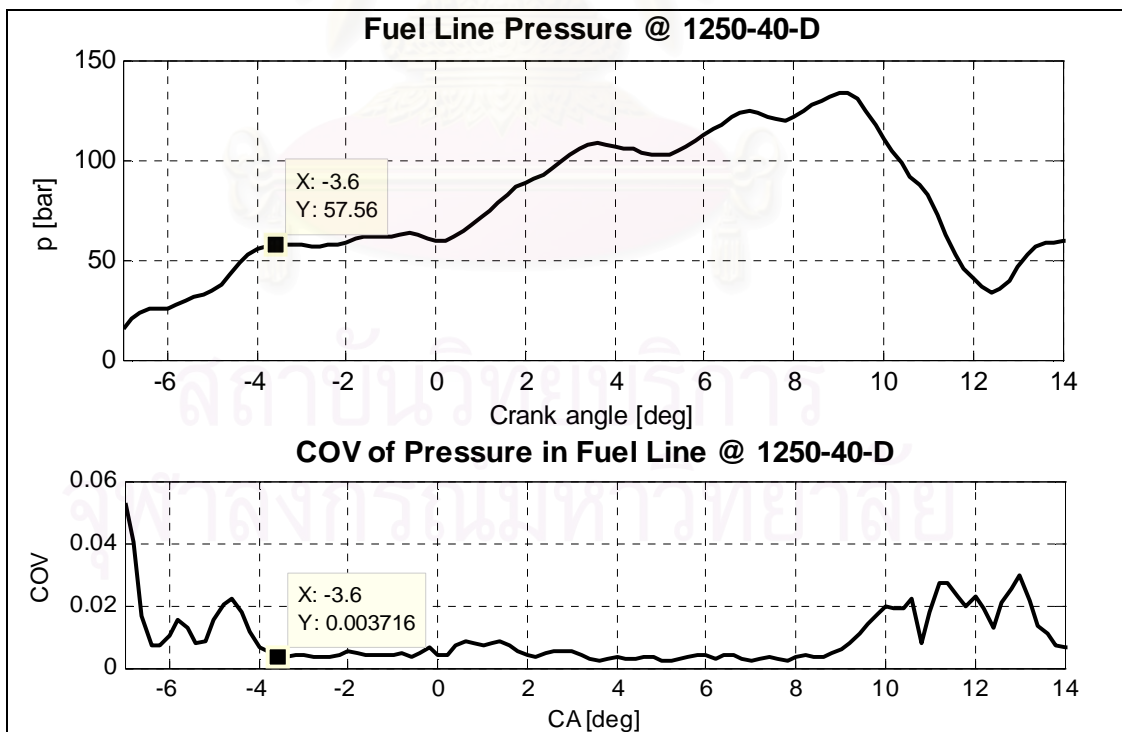
Figure 5–9   Average fuel line pressure and COV of fuel line pressure of 120

consecutive cycles, at engine speed of 1250 rev/min, 40 Nm, diesel fuel
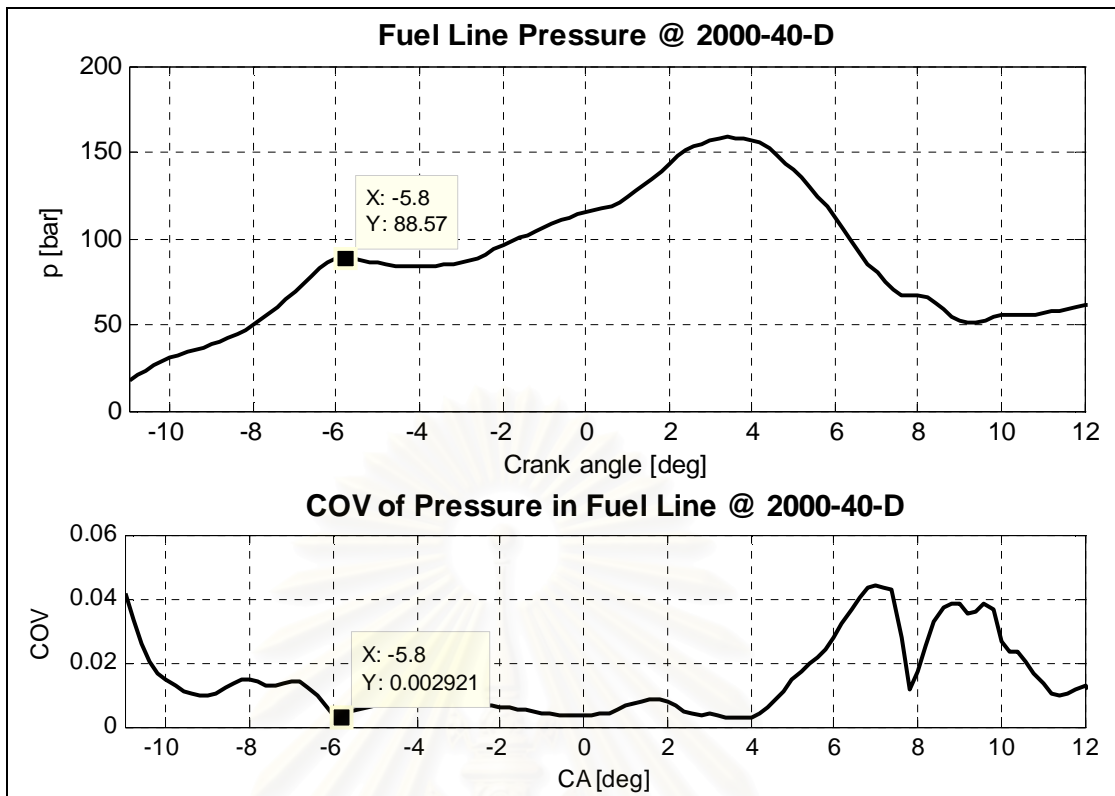
Figure 5–10   Average fuel line pressure and COV of fuel line pressure of 120

consecutive cycles, at engine speed of 2000 rev/min, 40 Nm, diesel fuel
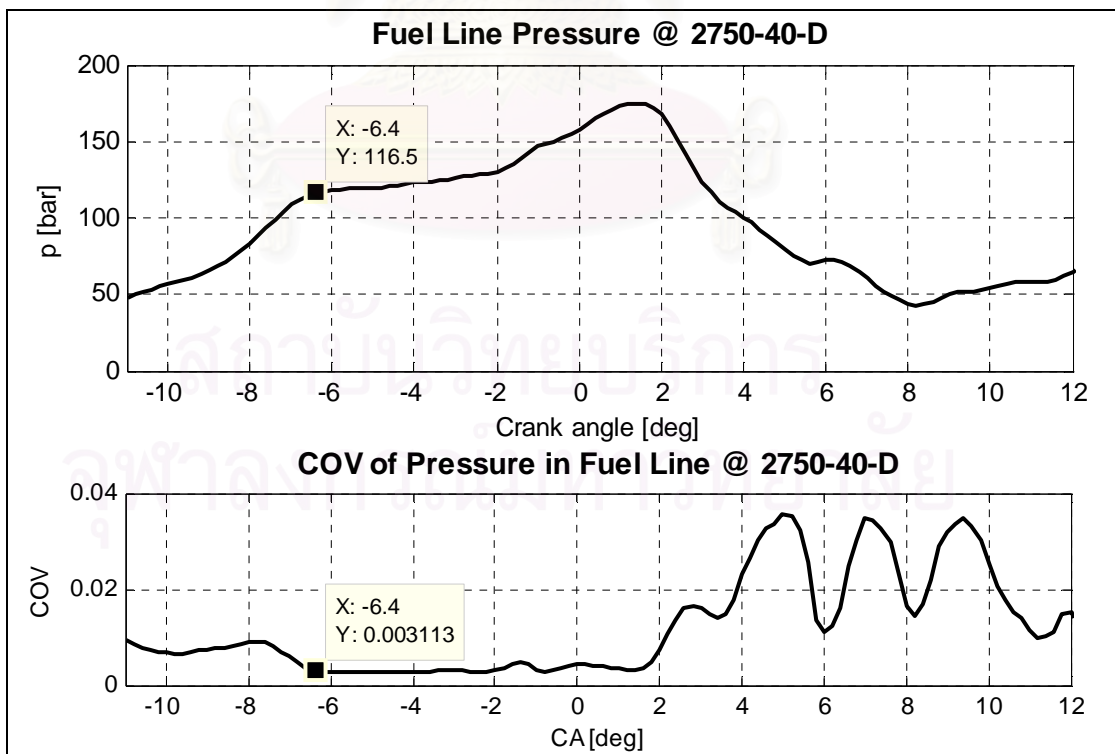
Figure 5–11   Average fuel line pressure and COV of fuel line pressure of 120

consecutive cycles, at engine speed of 2750 rev/min, 40 Nm, diesel fuel

5.2.3.2. Determination of start of combustion, end of combustion, and combustion duration

There are some definition of the start of combustion (SOC) and end of combustion (EOC), such as that based on the cylinder pressure, or based on heat release rate, or on luminescence in the cylinder. Combustion duration is defined as the time period between these two instants in one engine cycle.

In this investigation, for convenience the instant (after SOI) at which the net heat release rate reaches zero, as seen in Figure 5–3 is considered as SOC. Similarly, the instant (after SOC) at which the net heat release decreases to zero is considered as EOC. Obviously, at these instants the rate of gross heat release is equal to the rate of heat transfer to the wall chamber. The center of the area enveloped by the net heat release curve and abscissa from SOC to EOC is considered corresponding to 50% of apparent net heat release.

5.3. Cycle-by-cycle variation

A comparison among engine cycles reveals random variations in the cylinder peak and IMEP. This phenomenon is particularly noticeable in lean and highly diluted mixture and at low loads and engine speeds where the irregularities are usually audible. It is known that the cycle-by-cycle variations (henceforth called CCV) are the result of variations in the combustion process and can be characterized by a number of parameters, such as the rate of the heat release due to combustion or the crank angle corresponding to a given fraction of the burnt mass.

CCV leads to a situation in which combustion in some cycles is faster, while in others is slower. This variation is associated with losses of power and thermodynamic efficiency and fluctuation in the amount of work done. Consequently, fluctuation in the engine speed and torque which affect also the overall engine performance characteristics, such as the engine brake power and its specific fuel consumption, may be observed. Elimination of CCV could have improved the engine brake power for the same fuel consumption in lean mixtures. For some kinds of transmissions, such as lock-up torque converters and manual transmissions, torque fluctuations result in poor drive-ability of the vehicle (Young, 1981). In the fast combustion cycles, both the in-cylinder

peak pressures and the knock tendency are high, and therefore these cycles impose the lower limit for the allowed fuel octane number and the upper limit for the engine compression ratio. In the slow combustion cycles, the combustion may not be completed before EVO, and high UHC emission as well as high fuel consumption is expected. Previous studies have shown that part of the engine noise is attributed to CCV in the cylinder pressure (Young, 1981). Therefore, reducing the CCV may contribute also to suppress engine noise.

5.3.1. Indicators of cycle-by-cycle variations

One of resultant effects of the CCV in the combustion process, that is the most important with regard to the engine performance characteristics, is the CCV in IMEP. The IMEP is a parameter related to the cylinder pressure history, which, in turn, is determined by various factors such as the rate of heat release due to combustion process, heat losses to the cylinder walls, and the cylinder volume change due to the piston motion. The CCV can be characterized by the variations in different type of parameters which may be grouped into four main following categories:

Pressure-related parameters:

- Cylinder peak pressure, p_{max} and crank angle at which the cylinder peak pressure occurs, $\theta_{p_{max}}$,
- Maximum rate of pressure rise, $(dp/d\theta)_{max}$, and the crank angle at which maximum pressure rise rate occurs, $\theta_{dp_{max}}$
- IMEP of individual cycles.

The use of pressure-related parameters is a natural choice since these parameters can be measured through a pressure transducer. From the practical point of view, the impact of the CCV in the combustion process on the vehicle drive-ability, its fuel consumption and its pollution is of most interest. A measure of the cyclic variability, which may be obtained from pressure data, is the coefficient of variance in indicated mean effective pressure, which is usually expressed in percent. It has been found that vehicle drive-ability problems usually result when COV_{IMEP} exceeds about 10 percent [3].

$$COV_{IMEP} = \frac{STD_{IMEP}}{\overline{IMEP}} \qquad (5\text{-}28)$$

Where, the standard deviation in IMEP can be determined via

$$\text{STD}_{\text{IMEP}} = \sqrt{\left(\frac{1}{n-1} \sum_{i=1}^{n} (\text{IMEP}_i - \overline{\text{IMEP}})^2 \right)} \qquad (5\text{-}29)$$

$\overline{\text{IMEP}}$ is the average of IMEP calculated from n consecutive engine cycles, base on the main chamber pressure.

Combustion-related parameters:

- Ignition delay, $\Delta\theta_d$
- Combustion duration, $\Delta\theta_b$
- Maximum rate of heat release, $(dQ/d\theta)_{max}$
- Duration (crank angle degree) elapses from ignition to an instant at which a certain mass fraction is burnt, $\Delta\theta_{Xb}$

Practically, the combustion-related parameters are derived from the pressure data by means of thermodynamic heat release models. Therefore, they interpret the cylinder pressure history. The application of the maximum rate of heat release, $(dQ/d\theta)_{max}$ and the maximum rate of change of burnt mass fraction, $(dX_b/d\theta)_{max}$, can hardly be found in the literature as CCV indicators. Combustion-related parameters, such as the ignition delay, $\Delta\theta_d$, the combustion duration, $\Delta\theta_b$, and the crank-angle elapses from ignition to a moment at which a certain mass fraction is burnt $\Delta\theta_{Xb}$, are in frequent use. It should be noticed that as the combustion duration is used, $\Delta\theta_b$ variability seems to provide direct information about variations in the burning rate. It is also affected by the ignition delay $\Delta\theta_d$. As concern to the ignition delay, it is commonly accepted that both its mean value and its variance to a great extent determine the CCV. In general, the delay correlates well with the engine operation mode. A smaller delay is usually associated with a smoother engine operation, and therefore the delay seems to be a good parameter to indicate the extent of CCV in initial stages of combustion. However, ignition delay is not a very informative parameter since it does not provide any information about the reasons for early combustion cyclic variation. Since the delay is derived from the pressure measurements at the earliest stage of combustion it is highly sensitive to the accuracy of the pressure recording system. Thus, modest errors in the pressure recording may lead to significantly misleading results.

Flame front-related parameters:

- Flame front position, smoothed flame front area, or flame entrained volume at a specific crank angle,

- Crank angle lapse between flame front arrival to pre-specified different locations in the cylinder,

Flame front-related parameters are usually obtained by means of either visual techniques (fiber-optics, schlieren or shadow photography, LDV, etc.), or ionization gap techniques. These means make it possible to detect minor changes in the flame kernel development and also to distinguish between different factors, such as the flame kernel convection velocity and direction, the rate and the extent of the flame front wrinkling, the rate of the flame kernel radius growth. Thus the flame front-related parameters provide valuable information for the assessment of contributing factors. One disadvantage of applying some of the above techniques is the necessity in specially designed research engine allowing for optical access into its cylinder.

Exhaust gas-related parameters:

The parameters of this group are related to the cyclic fluctuations in concentration of the exhaust products. Although these parameters are not widely used to characterize, or to indicate, the cycle variability, one can use the data to gain important information about several CCV related phenomena, such as the in-cylinder non-homogeneity of the A/F (Pundir,1981), cyclic variability in the maximum temperature of the products of combustion, etc.

As it follows from the above discussion, a limited number of parameters are preferred as CCV indicators, such as: p_{max}, $\theta_{p_{max}}$, and IMEP - from the pressure-related parameters, and r_f and d_f - from the flame front related parameters. The CCV in IMEP is most useful for indicating the engine response to CCV in the combustion process. The two flame front-related parameters seem to provide valuable information for a deeper understanding of the in-cylinder combustion and the fundamental reasons for the CCV.

5.3.2. Factors that influence CCV

It is proposed to relate each of the CCV factors to one of the four following sources:

a. Mixture composition, which is directly related to the laminar burning velocity

The following factors were placed into this group:

- Type of fuel;
- The overall equivalence ratio of the mixture and its CCV;
- The overall fraction of diluents and its CCV;
- Mixture equivalence ratio and spatial heterogeneity.

b. Cyclic cylinder charging

This group includes factors which result in variations in the mass of mixture trapped in the cylinder. Unlike other factors, variations in cyclic cylinder charging mostly influence pressure-related parameters, and not combustion-related ones.

c. Ignition sources

d. In-cylinder mixture motion

The flow in the cylinder is essentially turbulent. The probabilistic nature of turbulence forces investigators to consider mixture-motion-related factors as the most influential with respect to CCV in engine performance (Namazian et al., 1980; Young, 1981; Johansson, 1993). CCV in engine performance cannot be eliminated completely since turbulence is an inevitable feature of the in-cylinder motion. The turbulence nature of the flow has a double effect. On the one hand, it accelerates the combustion by enhancing heat and mass transport between the burned and unburned parts of the charge, tending to decrease CCV. On the other hand, random flow pattern around the ignition source causes fluctuation in the magnitude and direction of the development of combustion flame. Both effects are related with other factors, such as combustion chamber geometry. Therefore, relative contribution of each of the two effects might differ from engine to engine, and the problem of the optimal in-cylinder flow pattern seems to be engine-dependent. The following factors are related to the mixture motion:

- Mean flow velocity vector, and its CCV;
- The orientation of fuel injection with respect to the mean flow velocity vector;
- Turbulence intensity and scales;
- Overall in-cylinder flow pattern.

5.3.3. Indicators of CCV used in this investigation

- The mean value, standard deviation, and coefficient of variation of IMEP.

5.4. Flame temperature and soot concentration prediction

The two color method has been used to predict flame temperature and soot concentration in the flame. Detail description for this method can be found in some documents such as[87, 88]. A brief description about the method is also given in Appendix B. The procedure related with the measurement and analysis with the AVL VisioScope system is described here.

5.4.1. Specification of the AVL two color system

- Two-color: Red and green.

- Model of analysis: Locally homogeneous thermal distribution and soot density along the optical penetration depth is assumed.

- Measurement range: 1200 K from 1800 to 3000 K.

- Resolution: Approximate 5 K.

5.4.2. Measurement setting

Based on the objective observation and capacity of the system, crank angle duration from 10 degree bTDC to 40 degree aTDC with an increment of 0.5 degree and a repetition of 7 have been set in the software for this investigation. The measurement result for one test point is an image record organized as follows:

- *A matrix of images consists of 7 rows corresponding to 7 repetitions and 101 columns corresponding to 101 instants in the period [-10, 40] ^{O}CA. The images in one repetition are from different cycles. Each image is an intensified image which has a size of 307200 (640x480) RGB pixels. Among these pixels are only valuable 105208 pixels which carry the information of the combustion chamber. The rest is the background and is not used.*

- *Additional information required for the analysis process such as reference image of the chamber. This image must be captured while the engine and the AVL system have already been warmed up, the engine stands, and there is no light inside the chamber. In this situation, the combustion chamber is considered as a black body.*

5.4.3. Analysis procedure

Flame temperature and soot concentration, as well as other function such as probability, spray-related parameters are predicted with the aid of the AVL software. Procedure for this prediction is explained as below.

- *Flame temperature and soot concentration,* is done step-by-step as following:

- Average the raw records to achieve an averaged record with one repetition.

- Calibrate the averaged record.

- Predict the flame temperature from calibrated record to achieve a flame temperature record.

- Predict the soot concentration from calibrated record to achieve a soot concentration record.

The intensity of each pixel in each image in the derived flame temperature record represents the temperature (of that point, at corresponding crank angle). Similarly, the intensity of each pixel in each image in the derived soot concentration record represents the soot concentration. A color scale (purple-blue-green-yellow-red-white) is used to present the flame temperature range from 1800 to 3000K and soot concentration levels from 1 to 15.

- *Flame area*, is defined by ① the number of pixels among the total of 105208 pixels of the images or ② the percentage of pixels at which the temperature is not less than a given value (for example 2400 K).

- *Probability*, is expressed in term of the intensity of pixels in the probability record which is produced by superimposing the corresponding images of all the repetitions to achieve one-repetition record. The probability record provides information of the development, distribution of the flame in the chamber.

- *Histogram*, is expressed in term of the number of pixels whose intensity are related to the color scale and are in the given segment.

CHAPTER 6

REQUIREMENT FOR THE RECORDED PRESSURE
AND THEIR TREATMENT

6.1. Requirement on recorded cylinder pressure

6.1.1. Crank angle resolution

Crank angle (CA) resolution, the CA interval at which the pressure data are measured, is one of the most important variables to be considered in measuring and analyzing engine cylinder pressure data. Increased CA resolution (short interval) leads to three main advantages. Firstly, the bandwidth is increased allowing higher cylinder pressure variations to be detected and analyzed. In CI engines, relatively high pressure rise and heat release rates can be experienced and high frequency post-combustion pressure oscillations may also be encountered, making a high bandwidth desirable. Secondly, it increases the accuracy of identifying the CA position at which an even, such as SOI, SOC occurs. Thirdly, the accuracy of the CA phasing may be improved, depending on the type of data acquisition and analysis system being used. With some proprietary systems, the position of TDC must be aligned with one of the shaft encoder marker pulses, thus potentially giving an error up to half the CA resolution. On the other hand, increasing the resolution has a number of disadvantages, including:

- Reducing the upper limit of the maximum engine speed and/or number of data channels which can be monitored due to data logger sampling rate limitations;

- Reducing the number of consecutive engine cycles that can be acquired due to data logger memory capacity limitations;

- Reducing the speed of data handling and processing due to the increased volume of data;

- Increasing the data storage requirements;

- Increasing the sensitivity to noise in some of the derived variable data.

The derived parameter noise increases with higher CA resolution due to two reasons. First, the increased bandwidth means that high frequency fluctuations due to

both unwanted noise and actual pressure oscillations can be detected. Second, noise is introduced in ADC digitization process due to the ADC resolution, which is typically 12 bit, imposing steps on the pressure signal. When combined with high CA resolution, the ADC resolution error can produce very large noise spikes in derived parameters which are functions of the cylinder pressure derivative.

The effect of CA resolution has been investigated since many years. Lancaster et al [89] briefly discussed CA resolution and suggested values of 0.5º and 1.0º for CI and SI engine work, respectively. Chen et al [90] suggested that 0.1 to 0.2º should be used for heat release and pressure rise rate determination. Chun and Heywood [91] in their knock study used 1º resolution over most of the engine cycle but increased this to about 0.1° during the knock window. The 100 kHz sampling rate employed allowed the knock signal to be isolated using 5 to 10 kHz digital band-pass filtering. Majority of others have used CA resolutions of either 0.5 or 1.0 degree, partly because commercial data loggers and analysis packages restrict the lowest resolution to 1.0 degree typically. Based on reviewing the past and their studies, Michael F.J.B and Gordon Lucas G. [92] gave conclusion that:

- IMEP calculation is not very sensitive to CA resolution. At very coarse CA resolution, noise and pressure fluctuations can however produce small errors in the calculated IMEP.

- For CI engine heat release analysis, a CA resolution of between 0.5 and 1.0^{O} should be most appropriate whilst the equivalent range for SI engine analysis would be 1.0 to 2.0^{O}.

- For knock studies, perhaps a CA resolution of 0.2^{O} would be required at low engine speeds.

With regard to noise sensitivity and bandwidth, it is important to distinguish between the CA resolution and the calculation CA resolution. The latter is the CA interval over which the calculation of the derived parameter is made. Hence, the calculation CA resolution can be either equal to or greater than the CA resolution. In the latter case, the bandwidth will be lower than that for the measured pressure data but the noise sensitivity will also be reduced.

6.1.2. The number of consecutive cycles recorded

The minimum number of consecutive cycles recorded depends on engine type and type of analysis. The maximum is limited by instrument capacity and time available. For SI and dual fuel engine analysis, a large number of engine cycles should be acquired if meaningful results are to be obtained due to the effects of cyclic dispersion. Zhong L., Henein N.A. and Bryzik W. [55] used 35 cycles. Michael F.J. Brunt [93] suggested 1000 cycles for calculation of knock intensity. Lancaster et al [89] suggested 300 cycles but most workers typically use 100 cycles, mainly due to the limitations imposed by (a) to (d) above. In CI engines, maximum engine speeds are lower and cyclic dispersion is much less significant and (a) to (d) impose less severe problems.

6.2. Pressure data referencing and phasing
6.2.1. The need of accurate absolute pressure referencing

Piezoelectric transducers are normally used for cylinder pressure measurement because of their best technical specification regarding accuracy, bandwidth, thermal characteristics, durability and size. However, they measure dynamic pressure rather than absolute pressure and since absolute pressure data are required for most applications some means of referencing (pegging) the measured pressure is required. Absolute pressure referencing may also be needed to compensate for inter-cycle and intra-cycle drift (long term and short term drift respectively) which necessitates individual cycle referencing. There are many potential sources of engine cylinder pressure measurement errors and they have been widely discussed and analyzed. Typical sources of error include:

- Absolute pressure offset;
- Incorrect crank angle phasing;
- Effects due to transducer mounting;
- Coarse ADC and crank angle resolutions;
- Inaccurate measurement system calibration;
- Sensitivity changes due to temperature variation;
- Thermal shock distortion / short term drift / long term drift;
- Mechanical vibration noise / Electrical noise.

The significance of each of these sources of errors will be dependent on the analysis being performed. For example, IMEP is slightly sensitive to crank angle phasing errors and thermal shock, virtually insensitive to random noise and totally unaffected by absolute pressure referencing errors. On the other hand, heat release analysis is sensitive to all errors list above.

6.2.2. Cylinder pressure referencing methods

Methods of estimating the transducer offset in cylinder pressure measurements can be divided into two groups: methods which require an additional absolute pressure reference and those which utilize the polytropic compression curve.

6.2.2.1. Additional absolute pressure reference methods

The idea behind these methods is that during some part of the cycle, the pressure in the intake manifold and the pressure in the cylinder are equal. The method is to take average of a number of consecutive pressure measurements near this point in the cycle, and compare them with an averaged pressure measurement in the intake manifold at the same time. As the pressures should be equal, the sensor offset can be determined.

One problem associated with this method is how to determine at which point in the cycle the pressures are equal. This will most likely have to be done experimentally over the whole load/speed range of the engine, which would be most time consuming. Another drawback with the approach, if cost is an issue, is that it requires another sensor. The sensor has to be reasonably high bandwidth also, since it has to resolve the relevant part of the cycle.

6.2.2.2. Polytropic compression methods

The idea is that a part of the compression stroke of a four-stroke engine after the intake valve has closed, and before the combustion has started, is accurately represented by a polytropic compression curve.

There are two existing methods: one involves a fixed polytropic exponent, and one involves varying polytropic exponent. Both methods use two pairs of matching values of cylinder pressure and combustion chamber volume, and fit a polytropic compression curve to these values. Polytropic compression can be defined by

$$pV^k = p_o V_0^k = C \tag{6-1}$$

where k is the polytropic exponent and C is a constant during the compression process.

If the sensor measurement is denoted *pm*, and the offset is denoted Δp, the cylinder pressure can be expressed as

$$p = p_m - \Delta p \tag{6-2}$$

Combining the two above equation yields

$$\left(p_m - \Delta p\right)V^k = C \tag{6-3}$$

Assuming k is known, there are two unknowns, Δp and C. These unknowns can be precisely determined using two matching pairs of pressure/volume measurements. When using time-varying polytropic exponents, the value of k is usually assumed to be a function of charge composition and temperature.

A drawback of this method is that it relies on only two pressure measurements, and fits an exponential curve to them. Hence, the noise existing in the measurements will contribute in the estimates of *C* and Δp. A solution to reduce this effect is to consider a number of cycles. Firstly, low-pass filter is applied to measured pressure window enveloping two considered points and then pressures of the two considered points are averaged from the cycle set.

6.2.3. Data phasing

The correct TDC in cylinder pressure trace is one of crucial factors in pressure-based engine combustion analysis. The effect of TDC error on heat release analysis has been investigated by many researchers. An error of 1 degree yields a significant error (up to 10%) in estimating net heat released as documented in Rocco V. [94] study on combustion characteristics of a DI CI engine with TDC error.

6.2.4. The referencing and phasing of the pressure data with system used, the selected CA resolution and number of consecutive cycles recorded

The DEWETRON Combustion Analyzer software provides ability to estimate the offset and determine TDC, based on the second method. In this software, the predefined setting for CI engine is:

- Considered points:	-100 and -65 (deg. bTDC)
- Polytropic index:	1.37
- Number of cycles considered:	20 to 200
- Thermodynamic loss:	0.7 deg.

Additional information of engine geometry is also needed. This function must be done as the test engine reaches its working temperature (about 75 ^{0}C) prior to the main test. The setting can be saved to hard disk and re-called for later use.

TDC determination function is also available with the AVL visualization system. This system can be integrated with DEWETRON system and the TDC synchronization between them can be established.

The measurement CA resolution is chosen as 0.2 degree and the number of recorded consecutive cycles is chosen as 230. For heat release and CCV analysis, a set of 120 consecutive cycles and 0.2 degree of crank angle step are used.

6.3. Smoothing the pressure data

Pressure waves, generated by fuel injection and/or the rapid rate of premixed combustion and measured by transducers, can cause errors in the heat release rate prediction. Pressure waves are highly strong in IDI engines. In this engine type, with ignition starts in the prechamber, if the prechamber pressure increases significantly over a time short in comparison to the acoustic time of the main chamber, a significant pressure difference between the two chambers results and finite-amplitude compression and expansion waves are generated from the throat region. These waves propagate back and forth in the two chambers and are detected as pressure oscillations. The amplitude of the oscillations, and the rate at which they decay, depend not only on the maximum value of the pressure difference between the two chambers, but also on the strength and extent of the first pressure wave formed by the throat in the main chamber. The greater the pressure and the larger the extent, the higher the amplitude of oscillations and the longer they will persist.

The use of data averaged from large number of cycles, and/or using coarse crank angle degree could help to reduce errors caused by pressure oscillation. The

cycle-averaged records are digitally used to remove the random noise and the high frequency components associated with acoustic oscillations in the cylinder. However, the pressure trace still need to be filtered/ smoothed after the premixed burn spike and the early pressure rise because of the effect of pressure waves initiated by combustion flame. The use of coarse crank angle degree is simple but it is not appropriate in cases of diesel combustion.

Many smoothing methods have been used. Andrew L.R. [95], Gatowski J.A. and Heywood J.B. [81] applied the 3-point, 5-point and 7-point polynomial least-square smoothing algorithms to smooth cylinder pressure traces. In order to get further reduction in noise, Rohrer R. and Chehroudi B. [96] used overlapped-smoothing routine by combining 7-point third-order polynomial least- square algorithm. Harndorf [97] adopted "weighted smoothing" method to smooth pressure trace to low systematic error. Miles applied digital filter to smooth pressure trace. Lurun Zhong, N.A. Henein and W. Bryzik [98] applied Spline method.

In this study, "moving average filtering" method is used to smooth the pressure trace of the average cycle. 'Moving average filter" smoothes data by replacing each data point with the average of the neighboring data points defined within the span. This process is equivalent to low-pass filtering with the response of the smoothing given by the difference equation

$$y_s(i) = \frac{1}{2N+1}\big(y(i+N) + y(i+N-1) + ... + y(i-N)\big) \qquad (6\text{-}4)$$

where, $y_s(i)$ is the smoothed value for the ith data point,

N is the number of neighboring data points on either side of $y_s(i)$, and

2N+1 is the span.

The moving average smoothing method used follows these rules:

- The span must be odd.
- The data point to be smoothed must be at the center of the span.
- The span is adjusted for data points that cannot accommodate the specified number of neighbors on either side.
- The end points are not smoothed because a span cannot be defined.

The higher the span the smoother the pressure data, leading to decrease in its first derivative, and hence the peaks of the calculated heat release rate.

Figure 6–1, Figure 6–2, and Figure 6–3 present the calculated heat release rates and pressure rise rate for averaged cycle from 120 consecutive cycles of the test engine fuelled with diesel at 40 Nm of brake torque and 1250, 2000, and 2750 rev/min of speed, corresponding with different spans. Three values of 5, 7, and 9 are chosen when smoothing measured pressure data, corresponding to engine speeds of 1250, 2000, 2750 rev/min, respectively.
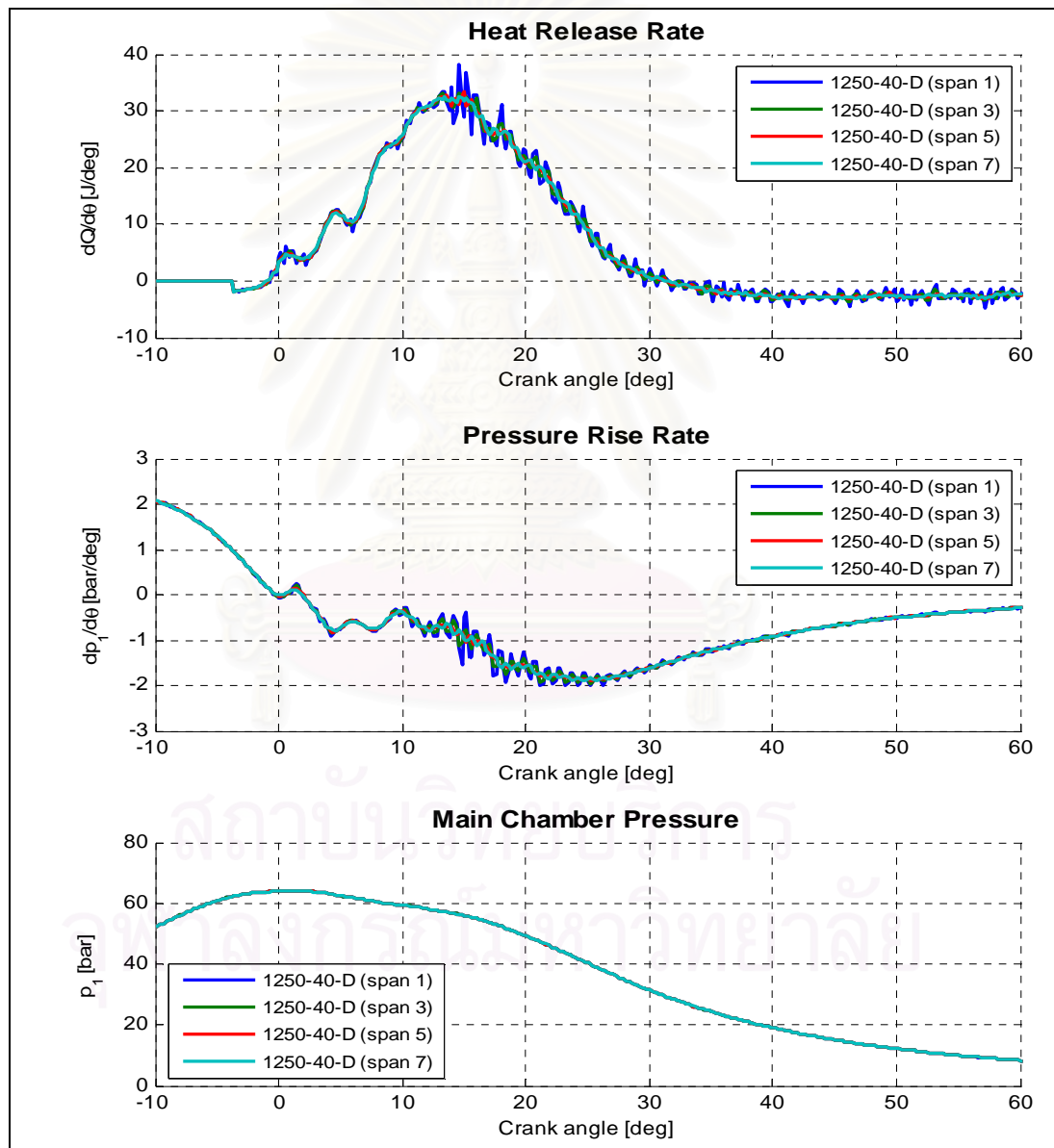

Figure 6–1   Predicted net HRR and smoothed measured pressure data with different spans, diesel operation at 1250 rev/min, 40 Nm.
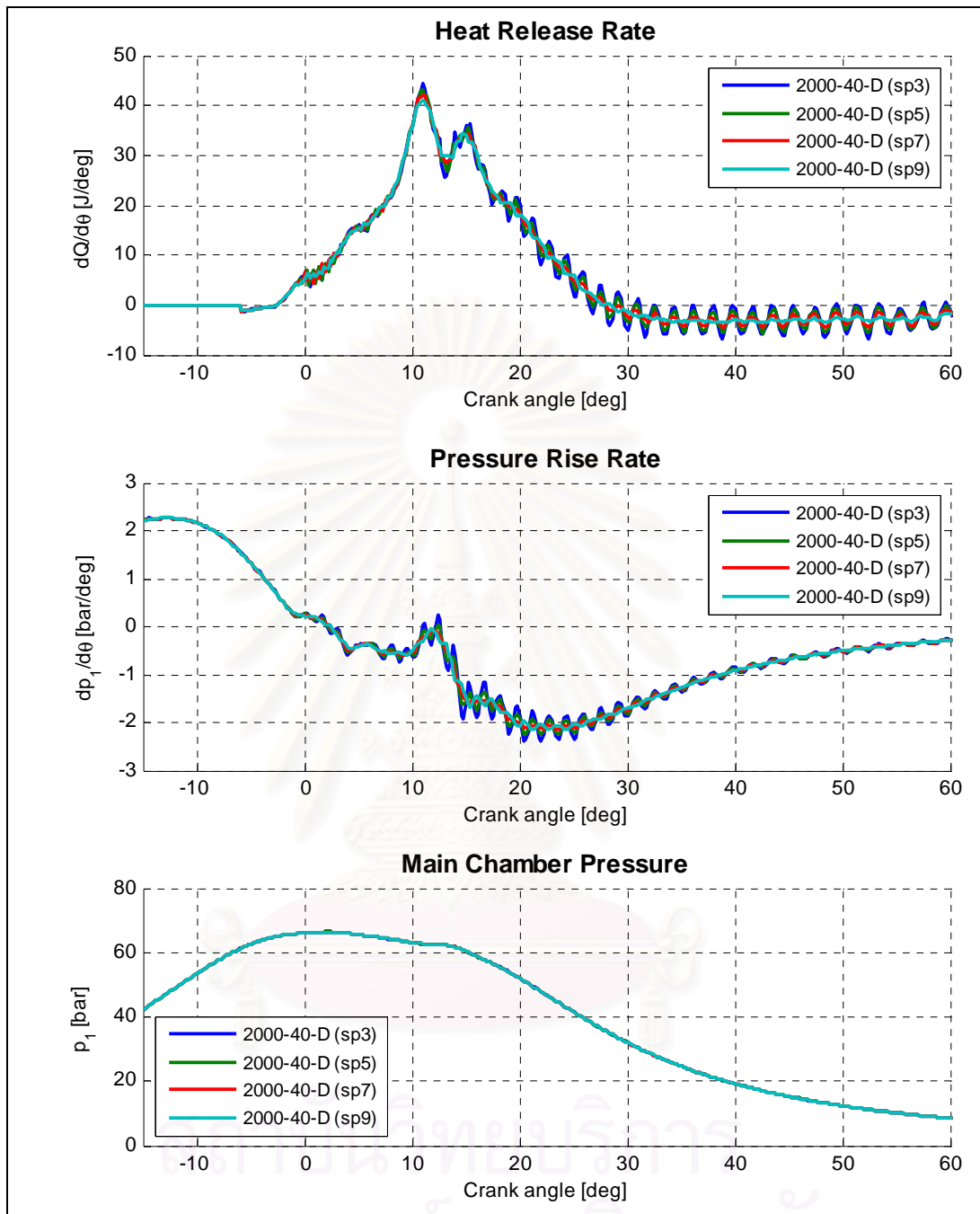
Figure 6–2   Predicted net HRR and smoothed measured pressure data with different

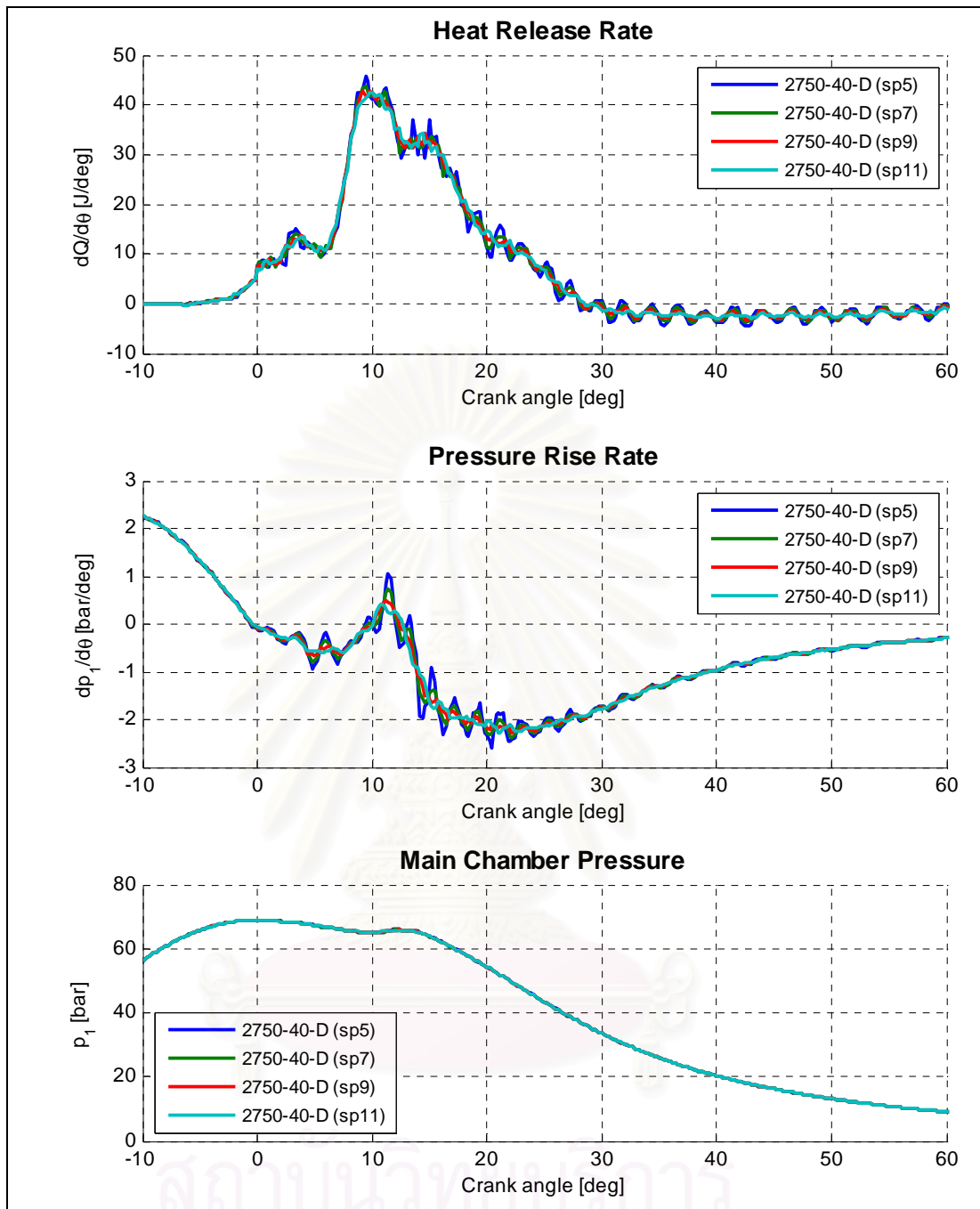spans, diesel operation at 2000 rev/min, 40 Nm.

Figure 6–3   Predicted net HRR and smoothed measured pressure data with different spans, diesel operation at 2750 rev/min, 40 Nm.

6.4. Computational tool

A computational tool named "Combustion Analyzer" has been developed for the prediction and analysis of the net heat release based on the model as explained in section 5.2.1, and the CCV as discussed in section 5.3. The tool has been programmed in Matlab language and compiled to become a stand-alone program in Windows

environment. Flow chart of the program is shown in Figure 6–4 and its main graphic user interface (GUI) is shown in Figure 6–5. The tool has following main functions:

- Input and hold information of fuels, engines;

- Predict the net heat release in both cases of operation: neat liquid fuel or dual fuel, for IDI engines as well as DI engine;

- Predict parameter relating to cycle-by-cycle variation;

- Manager and export the predicted result of heat release and CCV to XLS (Excel), different formats of image files, or MAT and FIG (Matlab) files, including comparison among cases of engine operation.

The input information for the program includes:

- Engine geometry;

- Fuel consumption (liquid fuel for neat liquid fuel operation; liquid and gas fuel for dual fuel operation);

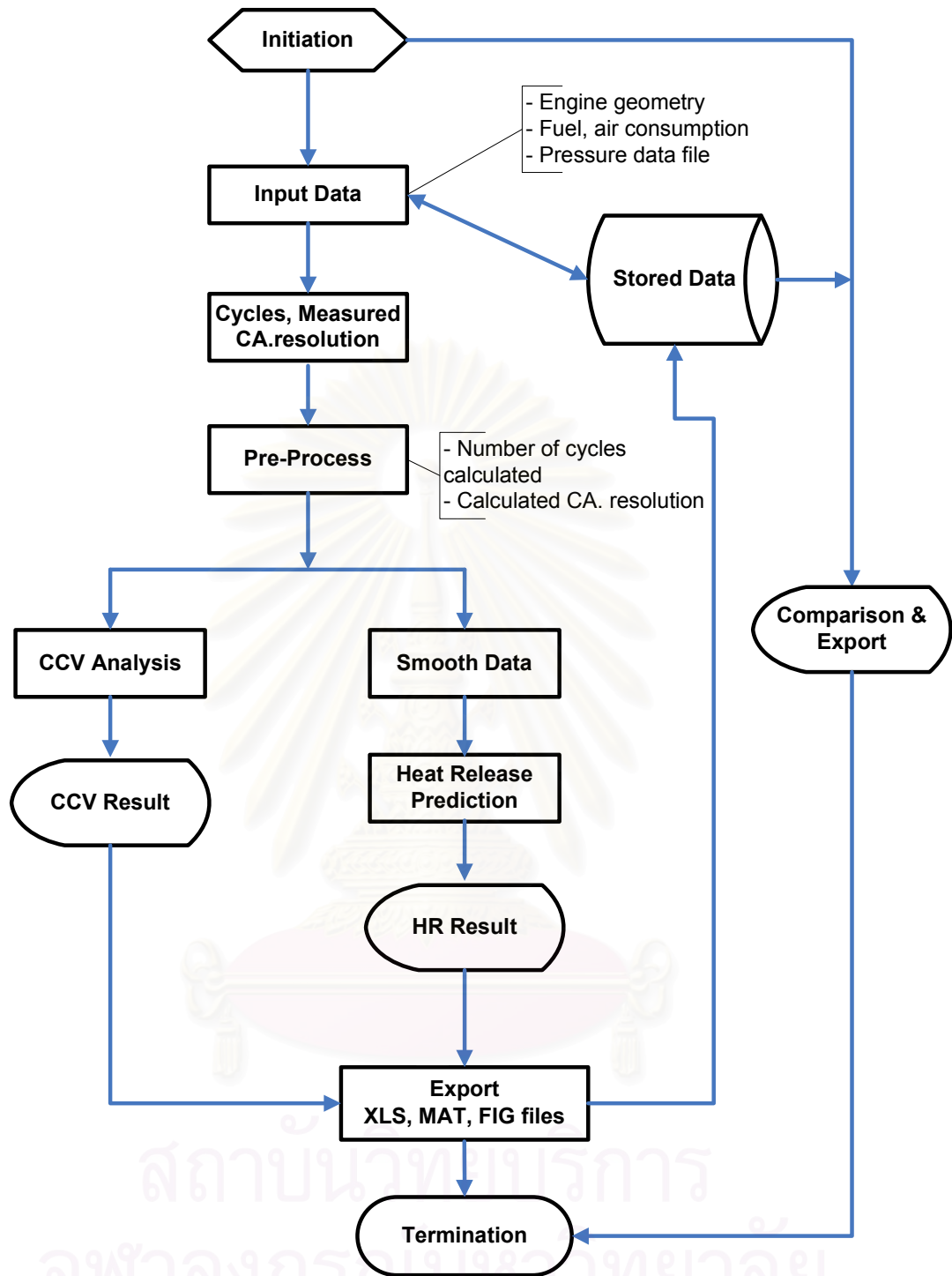- Pressure data of main chamber, pre chamber, and liquid fuel line.

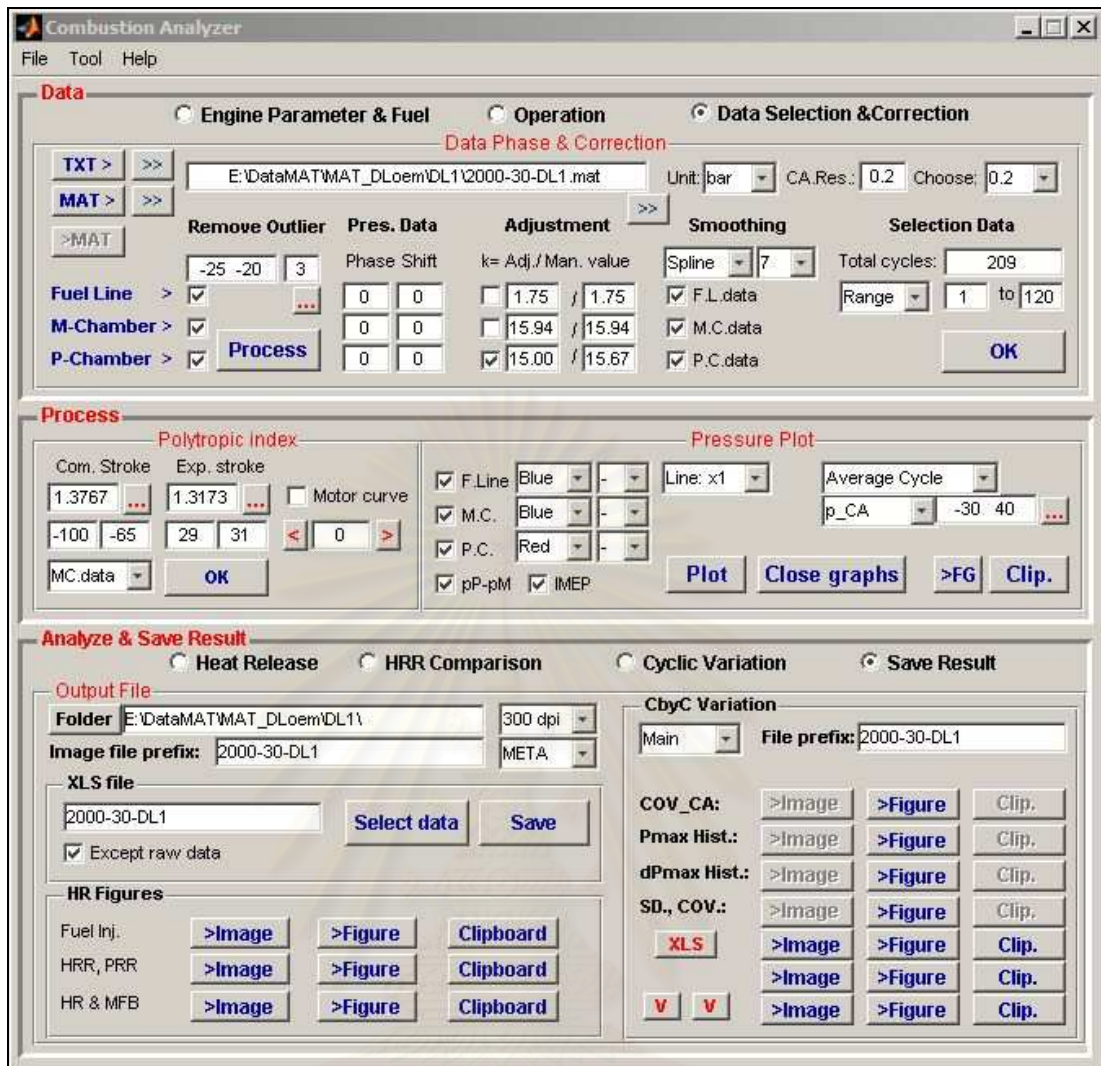Figure 6–4   Flow chart of the computational tool "Combustion Analyzer"

Figure 6–5   Main GUI of the computational tool "Combustion Analyzer"

CHAPTER 7

RESULTS AND DISCUSSION

The basic parameters including engine brake torque, brake power, specific liquid fuel consumption, specific total energy consumption, energy conversion efficiency, liquid fuel substitution, premixed LPG-air charge equivalent ratio, total fuel-air equivalent ratio have been calculated and their uncertainties have been estimated according to the method described in Section 5.1.2, with C95% confidence. The relative uncertainties of all mentioned parameters are in acceptable range, giving confidence to this investigation.

Table 7-1   Highest relative uncertainties of measured and calculated parameters

	Parameters										
	Speed	bmep	Torque	Power	ECE	STEC	ϕ	Toil	Tex	Tair	Sub
One fuel	0.3%	1.5%	2.1%	1.1%	1.6%	1.8%	1.6%	1.0%	0.8%	1.2%	
Dual fuel	0.3%	1.4%	2.0%	1.1%	1.8%	2.1%	1.7%	1.1%	1.0%	0.8%	2.8%

7.1. The effect of LPG energy fraction on LPG-diesel dual fuel operation

Engine operation with four fixed values of the mixture strength of the LPG-air premixed intake charge at different engine loads and speeds (as described in Section 4.3) has been established and studied.

7.1.1. Engine performance and energy consumption

The engine was able to operate at all planned test points and all planned LPG flow rates without end-gas knocking, even at high LPG fraction, namely 70.54% on energy basis at mode 1250-10-DL4 (Figure 7–1), 57.35% at mode 2000-10-DL4 (Figure 7–3), and approximate 50% at mode 2750-10-DL4 (Figure 7–5). The highest diesel substitutions were about 65%, 47%, and 38% (Figure 7–2, Figure 7–4, and Figure 7–6), respectively. The engine ran with lean mixtures: the highest strength of the premixed mixture was approximate 0.142 and that of total fuel was 0.476 at 2750 rev/min as seen in Table 4-4, Figure 4-15, 4-16, and 4-17.

Each line in Figure 7–1, Figure 7–3, and Figure 7–5 presents the LPG fraction and each line in Figure 7–2, Figure 7–4, and Figure 7–6 presents the diesel substitution corresponding to one mode of LPG supply (L1, L2, L3, and L4). In each mode of LPG supply, the increase in engine torque is corresponding to the increase of the mount of diesel injection and the decrease in LPG energy fraction since the LPG is fixed. The following general trends can be seen.

The energy conversion efficiency in LPG-diesel modes is always lower than that in diesel mode at all the test points. Figure 7–7, Figure 7–8, and Figure 7–9 represent comparison in energy conversion efficiency with diesel and different dual fuelling modes. Energy conversion efficiency fraction is the ratio between the energy conversion efficiencies in dual fuel and diesel modes. The deterioration in the efficiency with dual fuelling tended to increase with increased LPG energy fraction, except the two cases 1250-30-DL4 and 1250-40-DL4 as shown in Figure 7–7. At fixed engine speed, the highest deterioration appeared at lowest engine torque and highest LPG rate. As observed the reduction was about 17% from the value of 10.1% at 1250 rev/min (Figure 7–7), about 20% from the value of 8.6% at 2000 rev/min (Figure 7–8), and about 18% from the value of 7.7% at 2750 rev/min (Figure 7–9) in diesel cases.

As the load increased the efficiencies increased; this trend is similar to that in diesel fuelling. The efficiencies tended to converge to the values in corresponding diesel operation. In mode L4, the deterioration in the efficiencies was in the range of 4-5% at the highest torque; 39.8Nm @ 1250rev/min, 67.7Nm @ 2000rev/min, and 68.3Nm @ 2750rev/min.

The specific total energy consumption in LPG-diesel modes is always higher than that in diesel mode at all the test points. Figure 7–10 to Figure 7–12 represent comparison in the specific total energy consumption with diesel and different dual fuelling modes. The specific total energy consumption with dual fuelling increased with increased LPG energy fraction, except the two cases 1250-30-DL4 and 1250-40-DL4 as shown in Figure 7–10. For instance, the corresponding increases in specific total energy consumption from neat diesel mode to LPG-diesel mode with mode L4 (the highest LPG rate) at 10 Nm were: 35.5 to 42.66, 41.64 to 51.69, and 46.77 to 57.28 MJ/kWh at 1250, 2000, and 2750 rev/min, respectively.

Exhaust gas temperature revealed significant decreases but the lube oil temperature remained almost unchanged. The decreases in exhaust gas temperature were in the range of [1.0÷4.7], [0÷6.7], and [0÷10.3] degree at 1250, 2000, and 2750 rev/min, respectively. The highest decrease appeared at highest torque and mode L1 of LPG supply. It seems that there was no clear trend for the change of the temperature in relation with LPG energy fraction and engine load.

The change in lube oil temperature was within $1^{O}C$. It is thought that lubricant oil temperatures increase in DF operation since the combustion is shorter, giving longer period of time for heat transfer from the product occupying in the cylinder to the cylinder wall. However, due to the setting of the cooling water system of the test bench; the cooling water temperature was kept in the range of [83÷86] ^{O}C, the increase in lubricant oil temperature was difficult to observe.
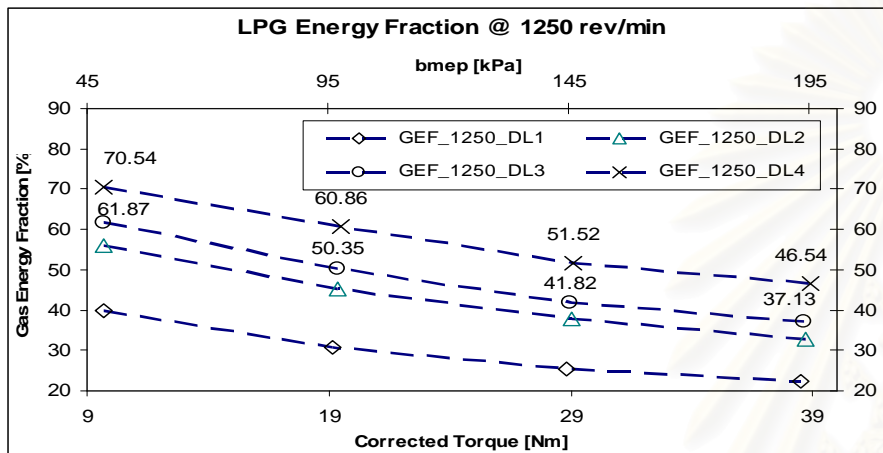
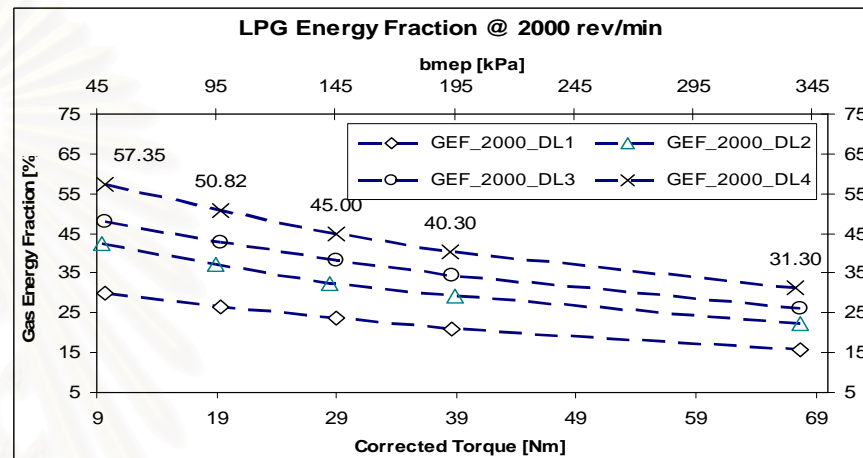Figure 7–1   LPG energy fraction # 1250 rev/min, LPG-diesel modes

Figure 7–3   LPG energy fraction # 2000 rev/min, LPG-diesel modes
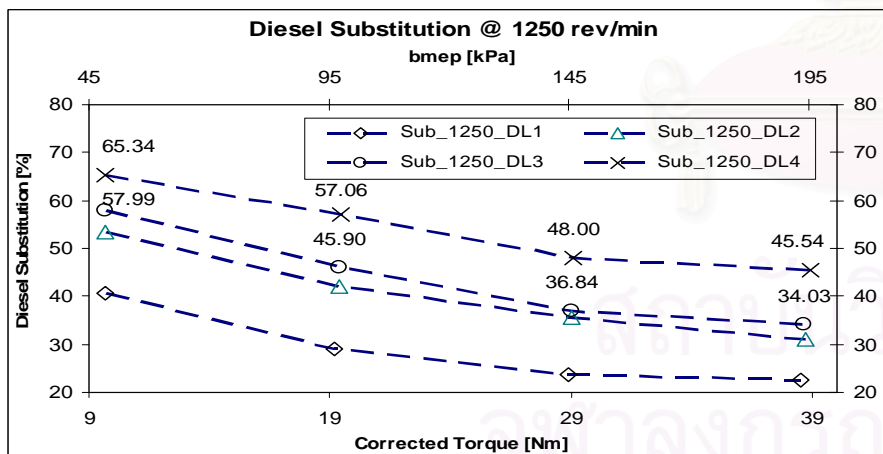

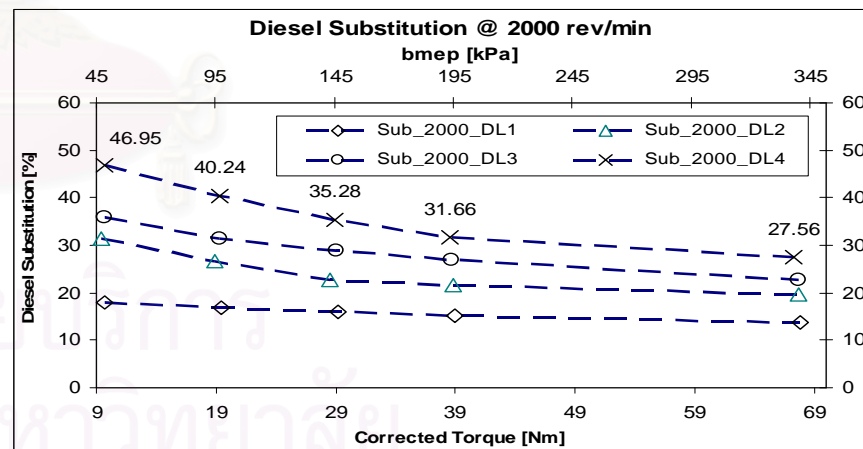Figure 7–2   Diesel substitution # 1250 rev/min, LPG-diesel modes

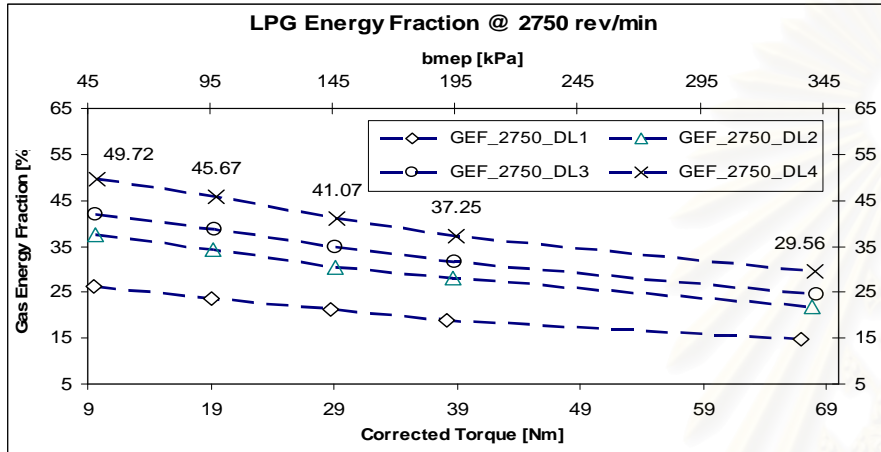Figure 7–4   Diesel substitution # 2000 rev/min, LPG-diesel modes

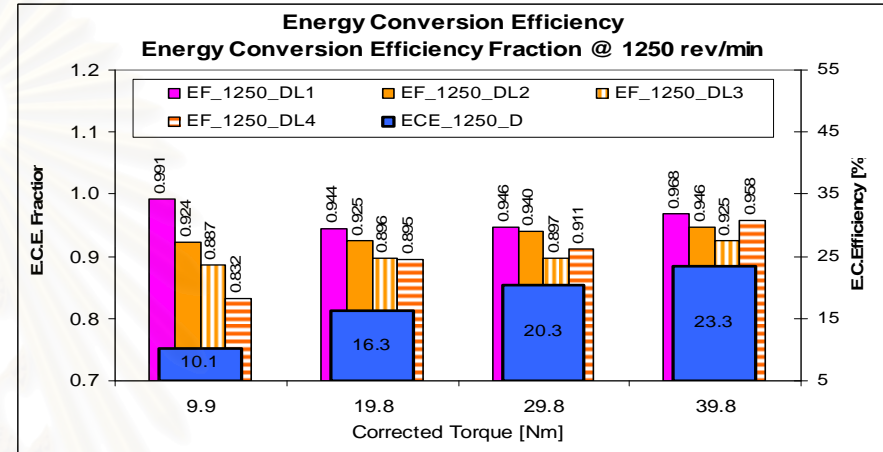Figure 7–5   LPG energy fraction # 2750 rev/min, LPG-diesel modes

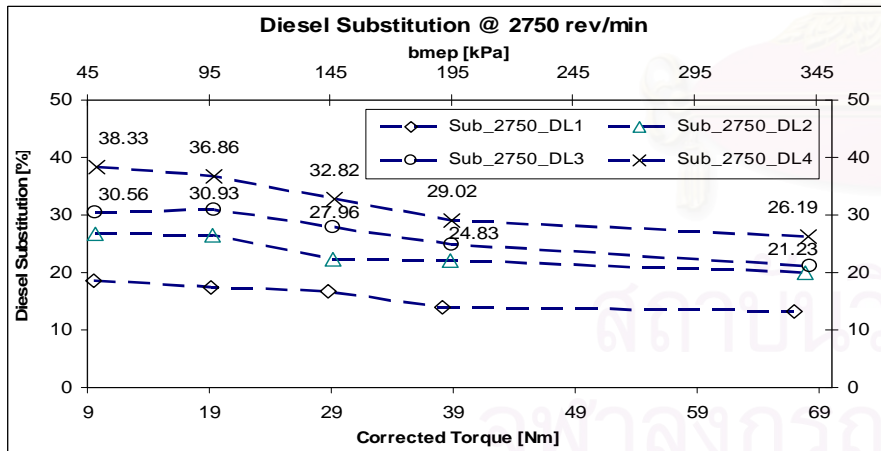Figure 7–7   ECE # 1250 rev/min, diesel and LPG-diesel modes

Figure 7–6   Diesel substitution # 2750 rev/min, LPG-diesel modes
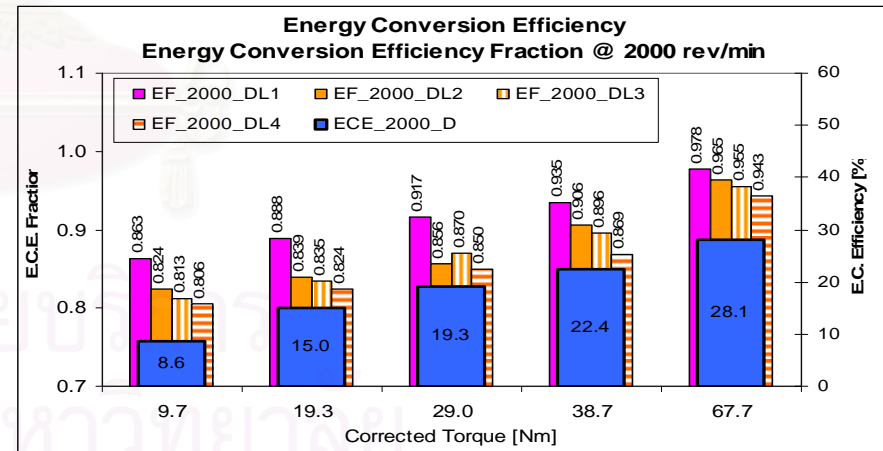

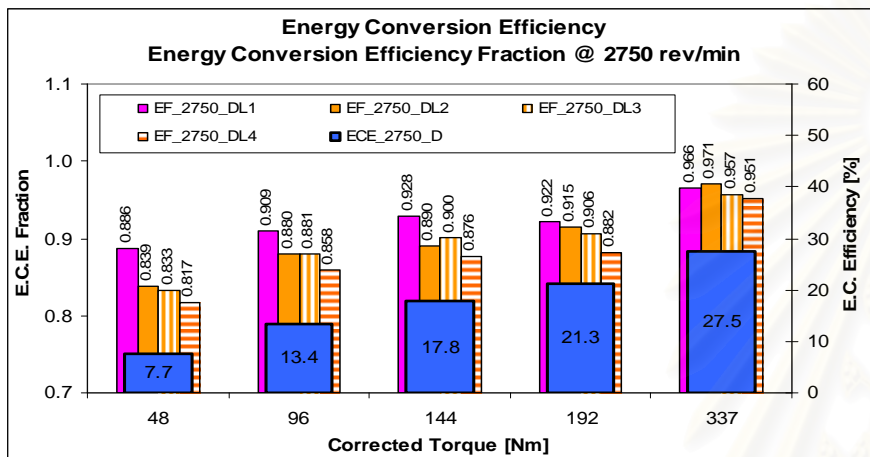Figure 7–8   ECE # 2000 rev/min, diesel and LPG-diesel modes

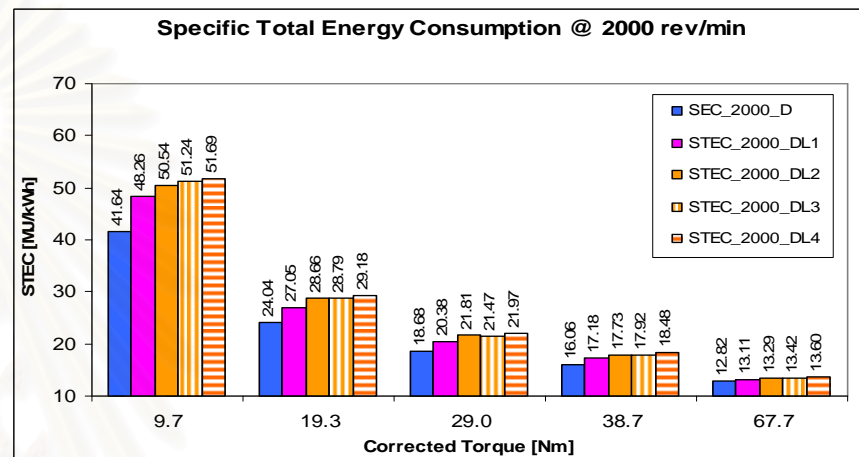Figure 7–9 ECE # 2750 rev/min, diesel and LPG-diesel modes

Figure 7–11 STEC # 2000 rev/min, diesel and LPG-diesel modes
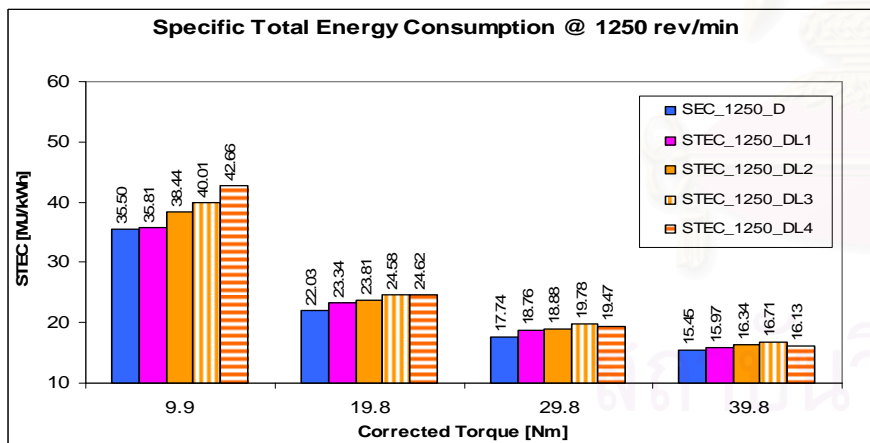

Figure 7–10 STEC # 1250 rev/min, diesel and LPG-diesel modes

Figure 7–12 STEC # 2750 rev/min, diesel and LPG-diesel modes

Figure 7–13   Exhaust gas temperature # 1250 rev/min, diesel and LPG-diesel

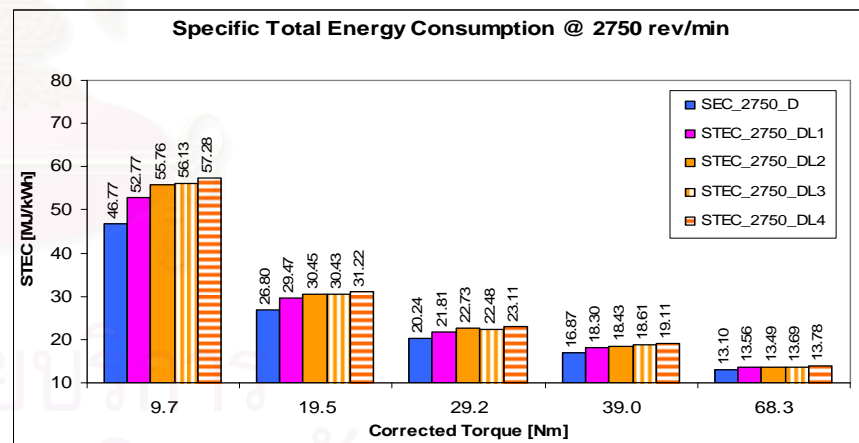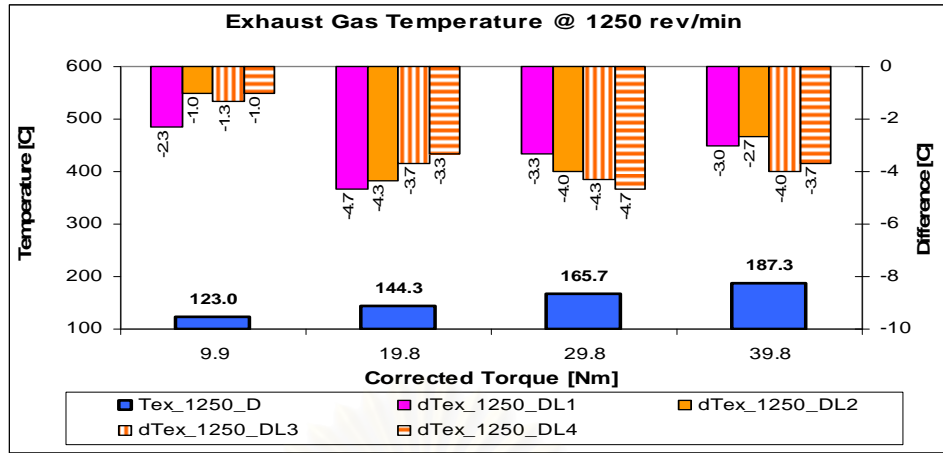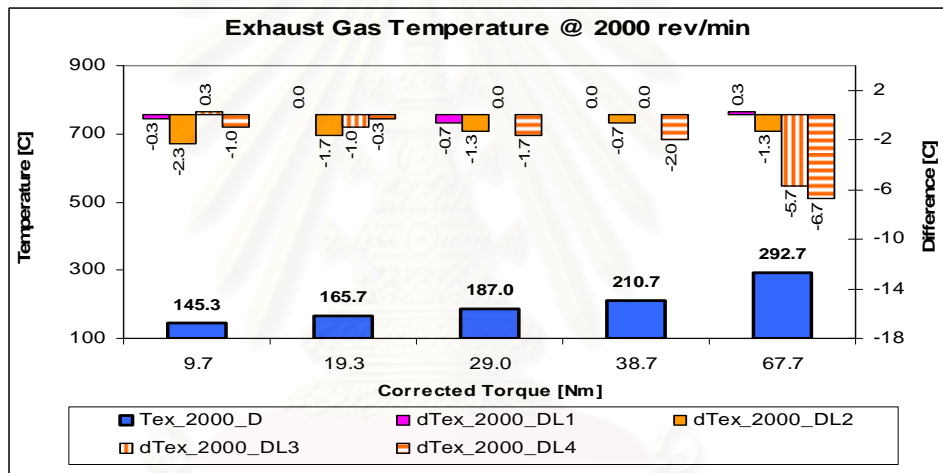Figure 7–14   Exhaust gas temperature # 2000 rev/min, diesel and LPG-diesel
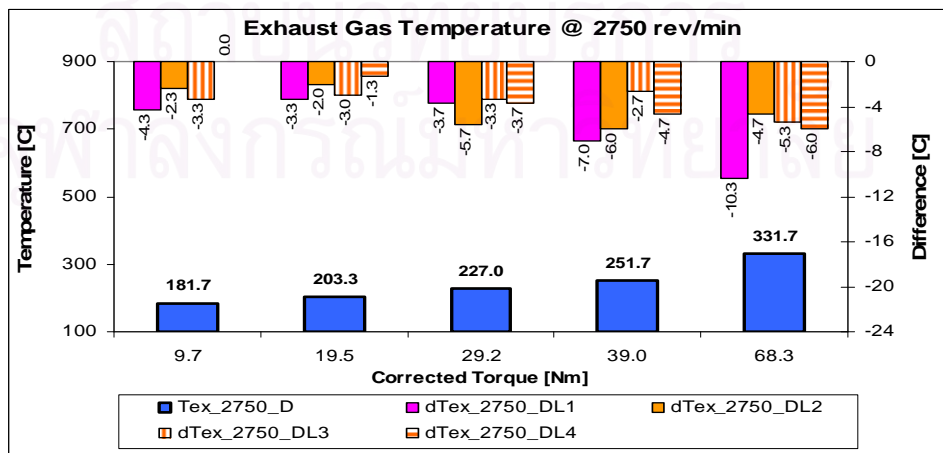

Figure 7–15   Exhaust gas temperature # 2750 rev/min, diesel and LPG-diesel
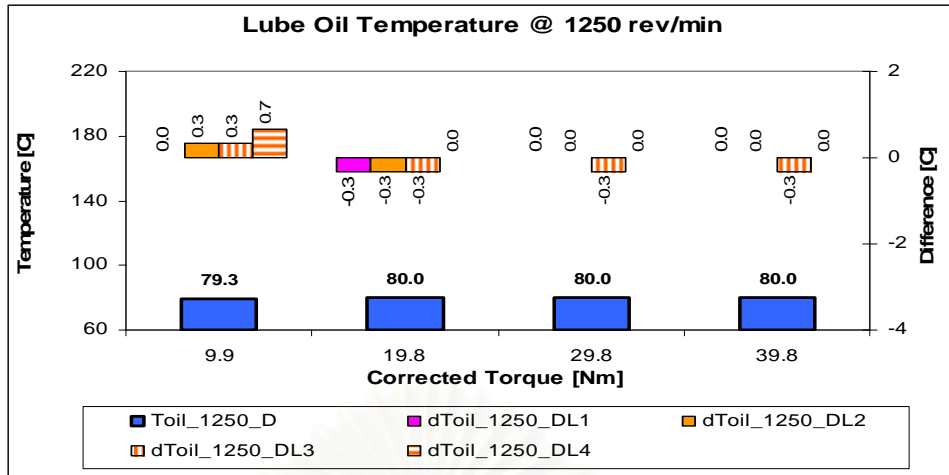
Figure 7–16   Lube oil temperature #1250 rev/min, diesel and LPG-diesel
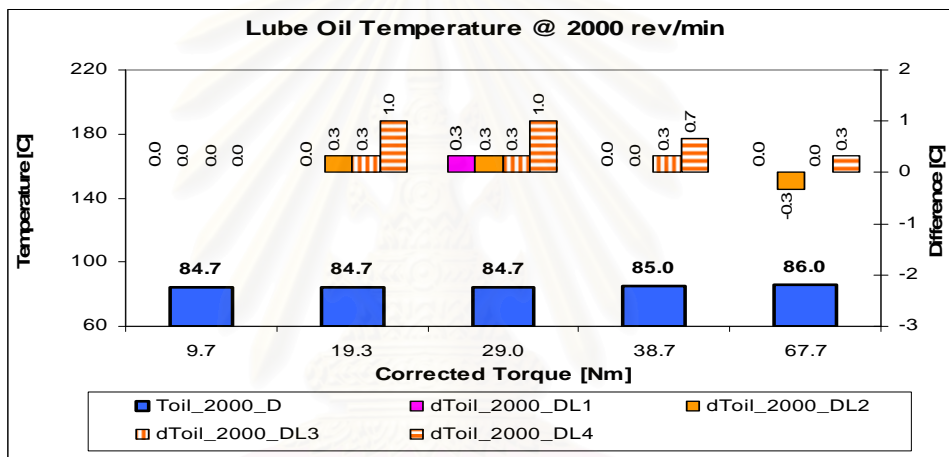

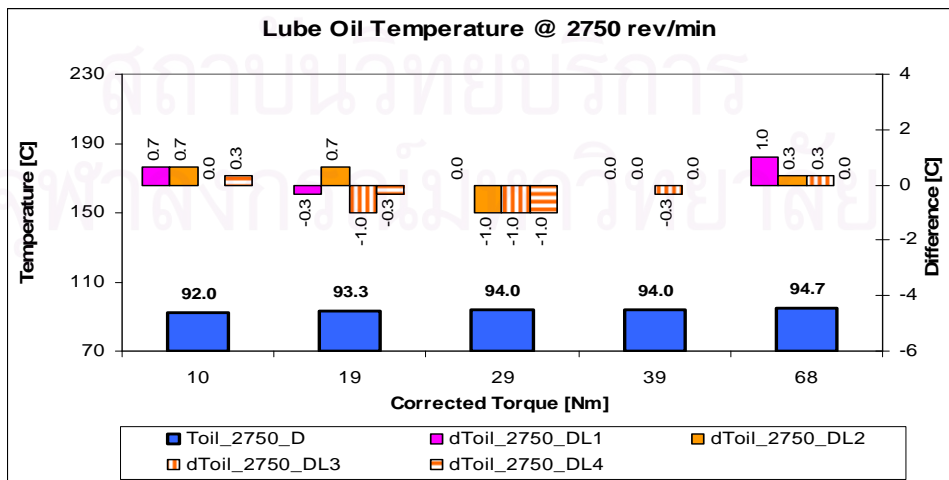Figure 7–17   Lube oil temperature # 2000 rev/min, diesel and LPG-diesel

Figure 7–18   Lube oil temperature # 2750 rev/min, diesel and LPG-diesel

7.1.2. Behavior of the fuel injection system with reduced injection mass

Fuel line pressure trace is the result from the wave and mass transfer in the fuel system. The pressure wave in the fuel line moves with the velocity of sound which is a function of the adiabatic bulk modulus and density of the fuel and remains almost unchanged in normal working condition. The mass transfer as well as the loss in the fuel line depends on the position of the collar in the fuel pump, speed and fuel viscosity.

Change in the fuel line pressure is presented in Figure 7–19 to Figure 7–22, corresponding to the operation with neat diesel and LPG-diesel at 1250 rev/min @ 10 and 20 Nm; 2000 rev/min @ 20 and 40 Nm. Figure 7–39 to Figure 7–41 give the whole scene of the change in the injection timing. The injection timing was detected to retard within the range [0.8-1.2] $^{\circ}$CA at 1250 rev/min, [0.6-0.8] $^{\circ}$CA at 2000 rev/min, whereas almost unchanged at 2750 rev/min. At fixed speed and engine torque, the increased LPG flow rates were corresponding to the decreased diesel flow rates. Thus, as the LPG increased, the maximum pressure in the fuel line tended to decrease. Although the stop of injection could not be detected, from the relation seen on the fuel line pressure it can be inferred that the injection duration was shorter. The injection timing detected tended to retard. This may be due to the increased loss in the fuel system with the decreased amount of fuel injection. At higher engine speed, since the time available for leakage is reduced, the effect of loss becomes lesser and the retardation in injection timing is more difficult to recognize.
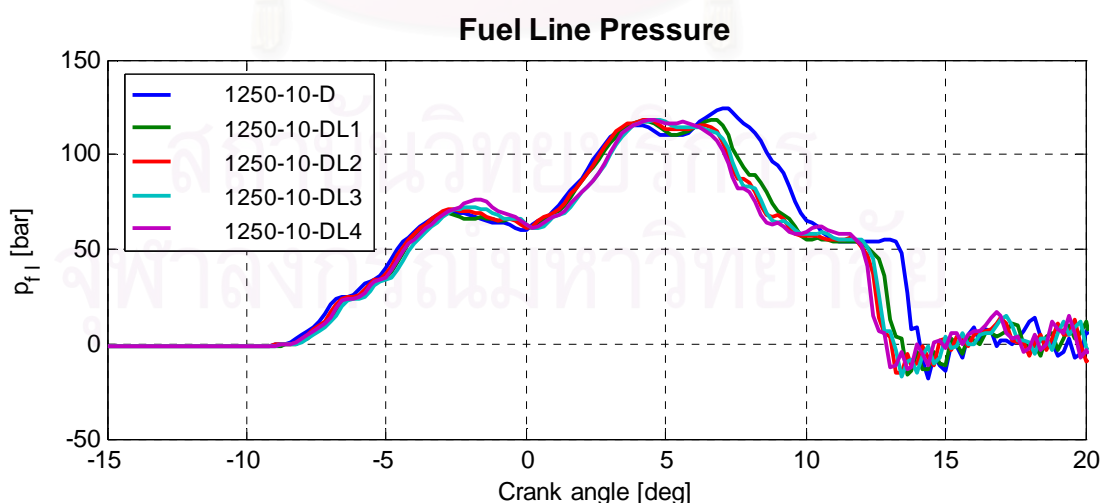

Figure 7–19   Fuel line pressure at 1250rev/min, 10 Nm (diesel and LPG-diesel)
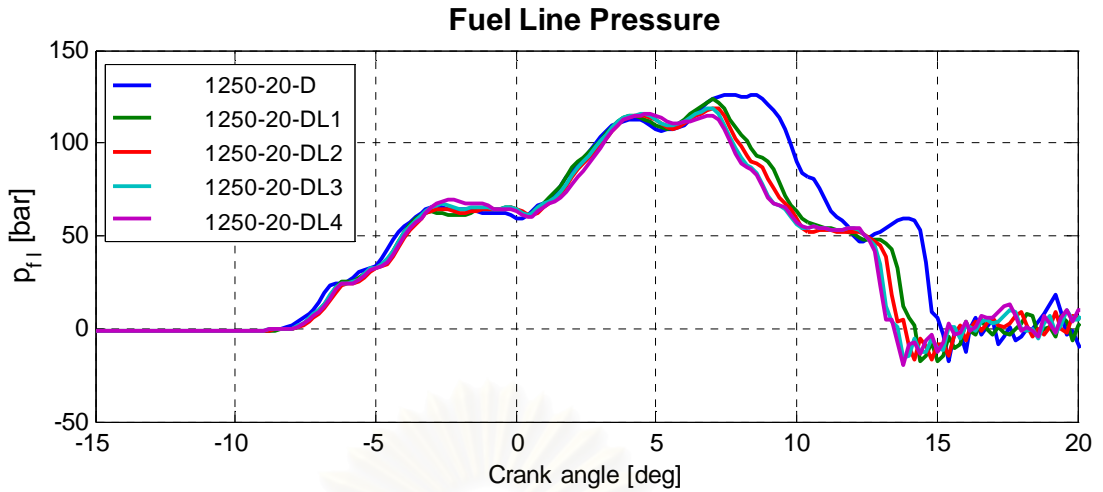
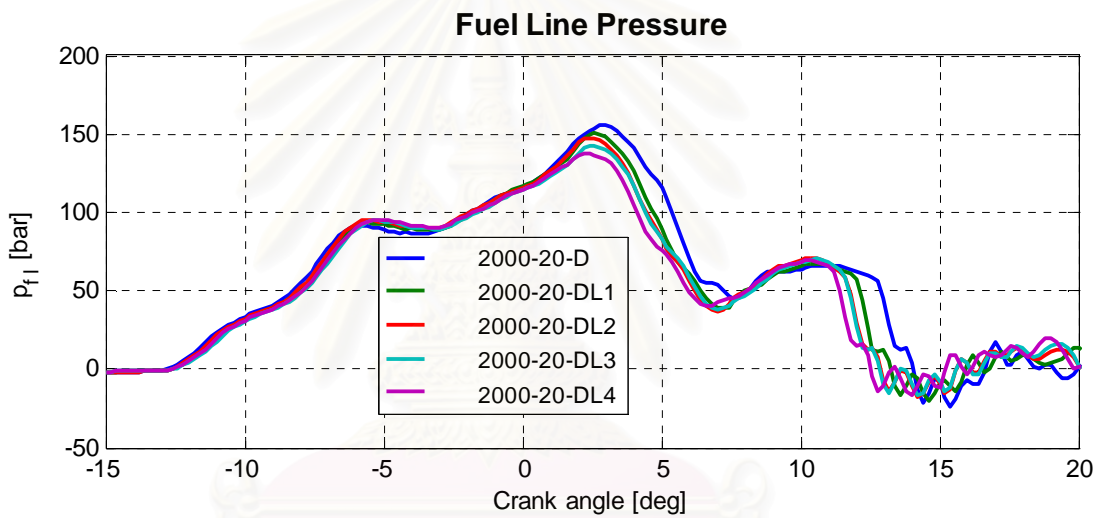Figure 7–20   Fuel line pressure at 1250rev/min, 20 Nm (diesel and LPG-diesel)

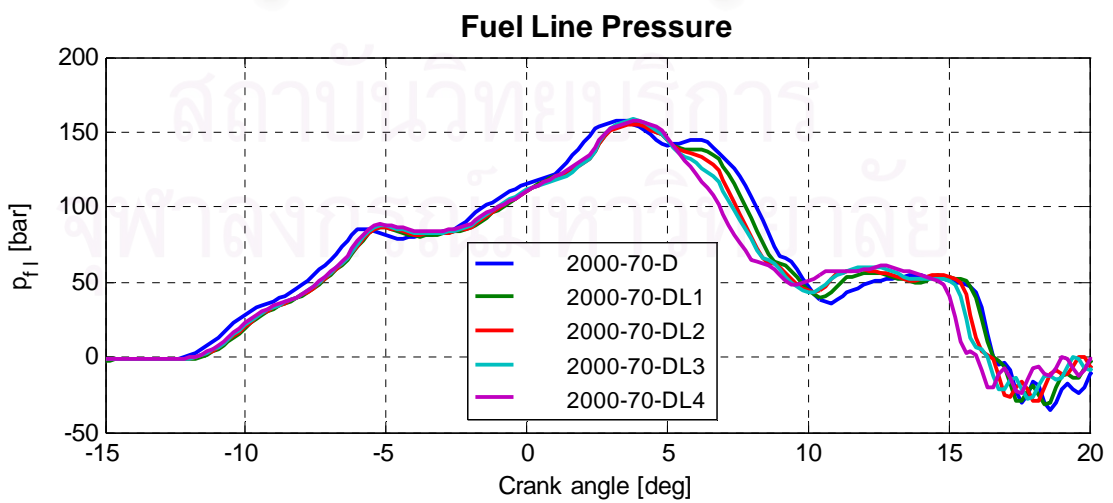Figure 7–21   Fuel line pressure at 2000rev/min, 20 Nm (diesel and LPG-diesel)

Figure 7–22   Fuel line pressure at 2000rev/min, 70 Nm (diesel and LPG-diesel)

7.1.3. Combustion characteristics

7.1.3.1. Spray combustion visualization

A comparison among six modes of operation: 1250-20-D, 1250-20-DL1, 1250-20-DL4, 2000-20-D, 2000-20-DL1, and 2000-20-DL4 is made as followings.

The combustion process in the prechamber in these six modes is presented in Figure 7–23 to Figure 7–27. Figure 7–23 presents sequential direct images captured by the visualization system with flash whereas Figure 7–24 presents those without flash. The predicted flame probability distribution, flame temperature distribution, and soot concentration are depicted in Figure 7–25, Figure 7–26, and Figure 7–27, respectively.

The spray revealed white color (Figure 7–23) as illuminated by the cool light from the AVL Light Unit. The SOI detected by the computational tool for these six modes were -2.8, -3.0, -2.4 ^{O}CA (Figure 7–39), -5.8, -5.6, and -5.2^{O}CA (Figure 7–40). Since the tip of the nozzle was not in the view-field of the camera, the first appearances of the spray (AOS) observed in the images with flash were some degrees later than these SOI, namely -2.5, -2.5, -2.0^{O}CA (Figure 7–23), -3.5, -4.0, and -4.0^{O}CA (Figure 7–24).

The combustion process with diesel fuel can be seen as following. The spray entered the pre-chamber at the top of it and continues a tangential motion, observed with clockwise direction in the images, with the chamber wall. Consider the case 1250-20-D in Figure 7–23, it is seen that the start of luminescence (SOL) appeared at -1.0^{O}CA (1.5^{O}CA after the first AOS) without aid of the glow-plug. The corresponding ignition delay detected from the heat release analysis was 2.8^{O}CA (Figure 7–39). The ignition started at a small space around the tip of the spray and then was expelled far from that due to the high swirl intensity in the chamber. While the injection was continued the spray quickly became a torch curved with the swirl. The spray core developed and became dazzling under the flash. At 4°CA, the torch enveloped approximate half of the viewed area and then almost all the area at 10°CA, in Figure 7–25. From this Figure, it can also be recognized that during the whole process the forth quadrant of the area, which is the downstream of the nozzle, was the lowest probability of flame distribution whereas the second was the highest. Toward border of the area, this probability reduced due to the effect of heat transfer to the wall. At 10°CA, the spray core still existed and started to dissipate from about 12°CA. During the combustion process, the

spray core always located in the first quadrant of the area. The combustion continued but the temperature in the chamber was difficult to increase since the total chamber volume increased increasingly as the piston moved down. The net HRR increased and reached a peak at a position about 14°CA whereas the luminosity of the direct images tended to reduce. Observing Figure 7–26, it can be recognized that high flame temperature appeared at the top of the torch during the first-three stages of combustion whereas at area around the connecting passage in the last stage. This can be understood since the top of the torch was the area corresponding with the premixed combustion in the first stage, and it was then expelled by the swirl whereas the spray continued to penetrate with increasing air utilization. The flame temperature was lower at upstream of the nozzle as well as in the spray core area due to the cooling effect of fuel heating and vaporization. In the late stage, from 18°CA the high flame temperature appeared at the connecting area due to the heat regenerative effect of the passage and the contribution of the flame in the main chamber. The high soot concentration area appeared at the spray core area at which was the high local fuel-air equivalent ratio.

The development of the combustion process with neat diesel at the same brake torque (20 Nm) at 2000 rev/min was similar to that at 1250 rev/min. Since the differential pressure between the two chambers is higher at 2000 rev/min, the swirl intensity is higher. This, accompanied with larger amount of diesel injection resulted in much more luminous of the direct images (10°CA in Figure 7–23 and Figure 7–24), larger maximum area of the high flame probability distribution (10°CA in Figure 7–25), higher flame temperature distribution (6°CA to 10°CA in Figure 7–26). However, the larger amount of diesel injected caused longer injection period and longer spray penetration, leading to larger area of the "dense-soot-cloud", as revealed in Figure 7–27.

The development of the process with LPG-diesel fuelling

The increase of LPG ratio in dual fuel modes leads to following effects. On one hand, due to the richer LPG-air premixed mixture the speed of flame propagation increases and the mixing-controlled combustion of the liquid reduces. On the other hand, the reduced amount of pilot injection leads to smaller size of the ignition sources, therefore increase the path that the flame needs to propagate to consume all the premixed mixture in the chamber.

Firstly, consider the three modes: 1250-20-D, 1250-20DL1, and 1250-20-DL4. Observing the sequential images in Figure 7–24, Figure 7–25, and Figure 7–26, it can be recognized that the flame, in mode 1250-20-DL1, was even initially weaker than that in mode 1250-20-D (before -2^{O}CA), it spread faster and enveloped almost all the area, at 10°CA. However, in mode 1250-20-DL4, the sequential images appeared with lesser luminous and the flame temperature seemed lower than that in the two modes 1250-20-D and 1250-20-DL1. Additionally, the flame area in this mode seemed smaller. The predicted results of the flame probability distribution and flame temperature provide clear information. The percentage of area at which 100% of the flame probability distribution for the three modes 1250-20-D, 1250-20-DL1, and 1250-20-DL4 is given in Figure 7–28. The net HRR and the percentage area of flame temperature above 2300K and 2600K for these three modes are shown in Figure 7–29. In the mode 1250-20-DL1 although the combustion started later, it was enhanced by the premixed mixture and became faster just after auto-ignition of the pilot injection. In this mode, the percentage of 100% probability area was slightly higher than that in diesel mode, until about 8°CA. Accompanied with wider flame, the flame temperature was also higher compared to that in neat diesel mode. Before about 4°CA, the area of flame temperature (above 2300 and 2600K) was wider. During the period from 5 to 8°CA, the area of flame temperature was slightly smaller than that in diesel mode. The fluctuation in the area with temperature above 2300K was high because the diesel was still injected into combustion chamber. There was a spike in the area with flame temperature above 2600K in neat diesel mode at about 6°CA; this might be resulted from the premixed combustion phase. Conversely, in mode 150-20-DL4 although the premixed mixture was richer the combustion started later and its development was weaker compared to 1250-20-D as well as 1250-20-DL1 mode. This is due to the reduced diesel injection, leading to less strong ignition source. During the period from 11 to 15°CA, the area of flame temperature above 2600K in the three modes was quite stable, perhaps due to the stability of mixing controlled combustion of the diesel. The area of flame temperature above 2300K in dual fuel modes was comparable, but slightly higher than that in diesel mode; this might be attributed by the flame propagation in the premixed mixture. Beyond 15°CA the area of flame temperature in the two dual fuel modes decreased and became significantly lower

than that in diesel mode. This means the dual-fuel combustion process was shorter; it ended earlier. The amount of diesel injection in mode 1250-20-DL1 seemed more reasonable than that in mode 1250-20-DL4, providing earlier SOC (-0.2^{O}CA compared to 0.2^{O}CA in diesel mode) and faster combustion in the second stage of combustion, hence leading to higher HRR and temperature than that in diesel mode. The amount of diesel injection in mode 1250-20-DL4 might be too little to produce ignition source large and strong enough to consume the whole premixed mixture in limit duration of time. The history of the soot concentration in the flame with the three modes is presented in Figure 7–30, Figure 7–31, and Figure 7–32. Since the combustion with dual fuel modes took place earlier, it caused slightly higher soot concentration until 2.5^{O}CA. The "thin-cloud-soot" area in mode 1250-20-DL1 was highest and accounted about 10% of the total area. Beyond 5°CA, the soot concentration with diesel mode was comparable or higher than that in dual fuel modes, except the "dense-soot-cloud". It became higher from 17.5^{O}CA and beyond 27.5^{O}CA the soot concentration with all modes was almost zero.

The development of the combustion process at the same engine torque, 20Nm but higher speed, 2000 rev/min can be seen as follows. The percentage of area at which 100% of the flame probability distribution for the three modes 2000-20-D, 2000-20-DL1, and 2000-20-DL4 is given in Figure 7–33. The net HRR and the percentage area of flame temperature above 2300K and 2600K for these three modes are shown in Figure 7–34. In both modes 2000-20-DL1 2000-20-DL4 although the combustion started later, it was enhanced by the premixed mixture and became faster just after auto-ignition of the pilot injection. In these modes, the percentage of 100% probability area was only slightly lower than that in diesel mode before about 3.5^{O}CA. The dual fuel combustion was then enhanced and its flame became wider than the diesel after about 4°CA until about 12°CA and 16°CA in mode 2000-20-DL1 and 2000-20-DL4, respectively. Since the dual duel combustion was shorter, after these instants the area of the flame probability dropped sharply. There was similarity in the area of flame temperature of dual fuel modes at 2000rev/min, 20Nm and 1250rev/min, 20Nm. However, since the mass of liquid fuel per cycle at 2000rev/min was higher than that at 1250 rev/min, the change in area of flame temperature seemed not much as that at 1250rev/min. When the LPG increased (mode L4 compared to mode L1), the area of flame temperature decreased

significantly (for the both ranges above 2300 and 2600K). This might be resulted from the reduced size of the ignition sources as the diesel auto-ignited and the lower adiabatic flame temperature of the LPG compared to that of diesel. The LPG consisted of, mainly propane (50.89% by volume) and butane (47.73% by volume), as shown in Table 3-2. The adiabatic flame temperature of propane, butane, and diesel are 2270, 1900, and about 2300K, respectively (Table 3-1). Thus, obviously the LPG had lower adiabatic flame temperature than the diesel. The history of the soot concentration in the flame with the three modes is presented in Figure 7–35, Figure 7–36, and Figure 7–37. The dual fuel soot concentration was comparable until $2.5^{O}CA$, slightly lower until $7.5^{O}CA$ compared to that in neat diesel mode. From $10^{O}CA$ until $12.5^{O}CA$ the area of "dense-soot" in mode DL1 was the largest, followed by that in neat diesel D and dual fuel DL1 mode. Later on, the "dense-soot-cloud" area in neat diesel mode then became the largest from $15^{O}CA$. This is thought due to the faster evolution of the combustion in mode 2000-20-DL1. Beyond $22.5^{O}CA$, the soot concentration with diesel mode was higher than that in dual fuel modes beyond $25^{O}CA$ the soot concentration with all modes was almost zero. Compared with the corresponding modes at 1250rev/min, it is revealed that the "thin-soot-cloud" area was smaller and the "dense-soot-cloud" area was slightly larger at 2000rev/min. The smaller "thin-soot-cloud" area might be resulted from the enhanced turbulent intensity whereas the larger "dense-soot-cloud" area might be resulted from larger amount of liquid fuel injection. With further increase of LPG (mode 2000-20-DL4) the reduced liquid lead to significant decrease of the "dense-soot-cloud" area.

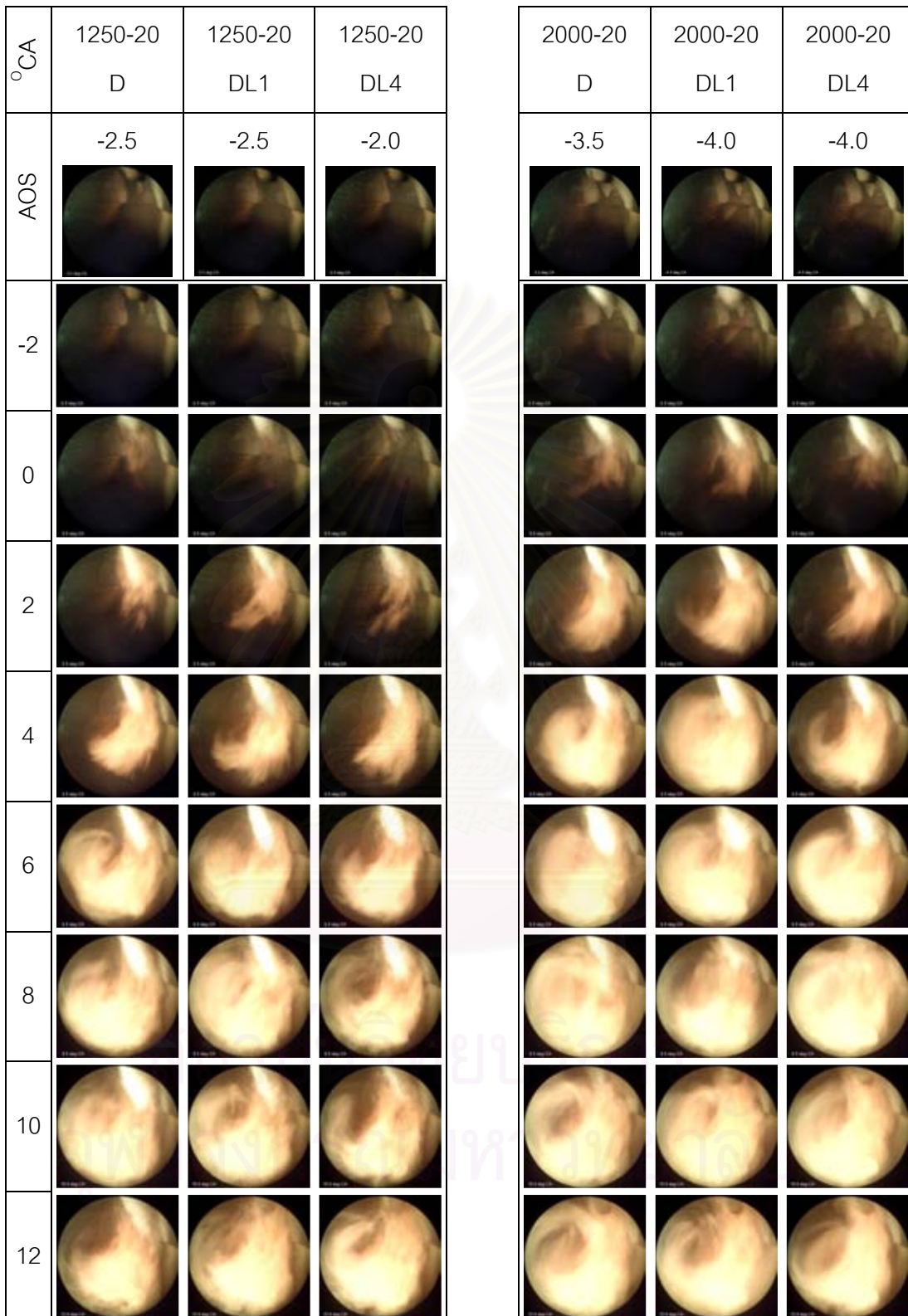| °CA	1250-20 D	1250-20 DL1	1250-20 DL4	2000-20 D	2000-20 DL1	2000-20 DL4
AOS	-2.5	-2.5	-2.0	-3.5	-4.0	-4.0
-2						
0						
2						
4						
6						
8						
10						
12						

Figure 7–23   Sequential images of combustion process with cool light (modes: 1250-20-D, 1250-20-DL1, 1250-20-DL4, 2000-20-D, 2000-20-DL1, and 2000-20-DL4)
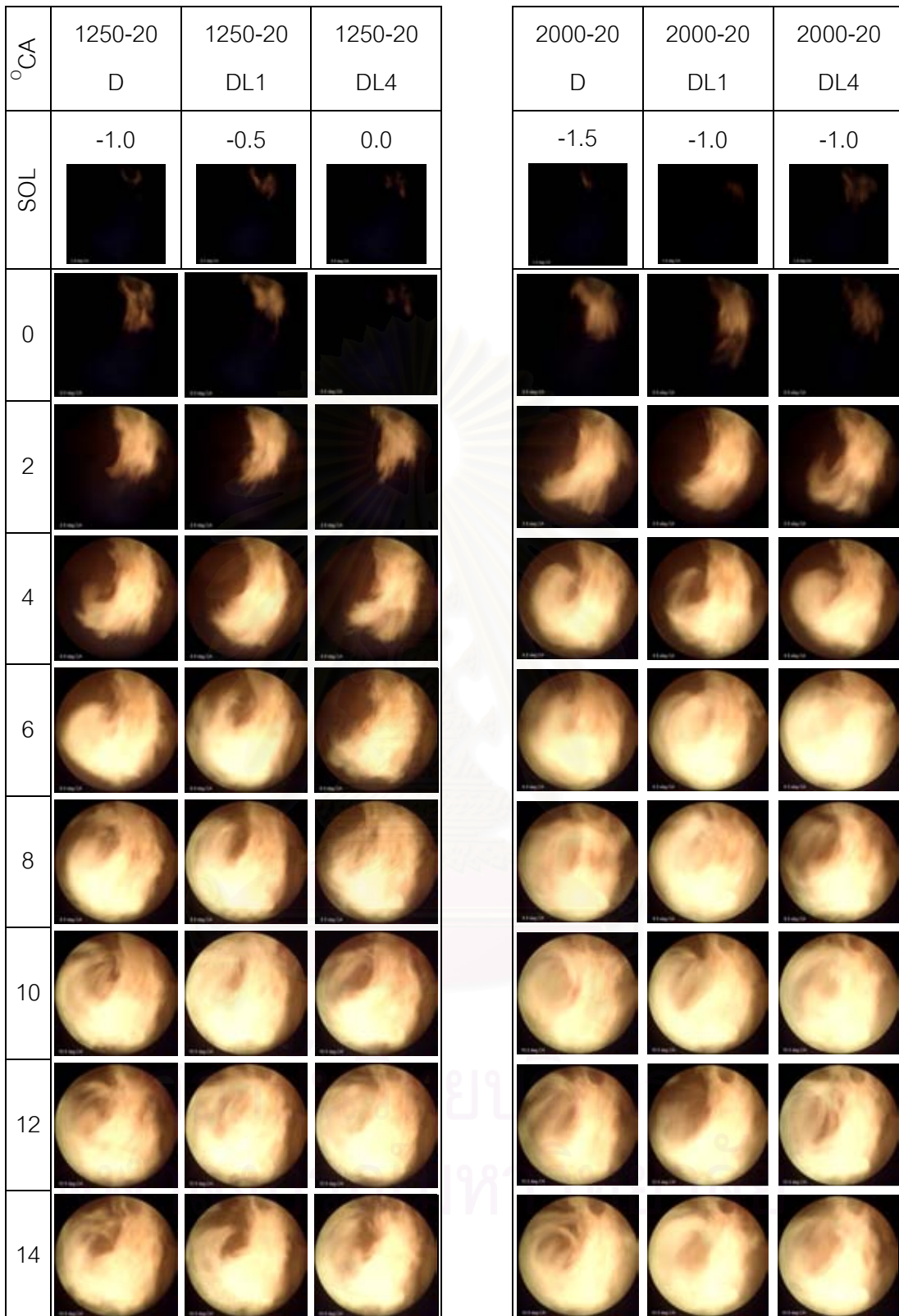
°CA	1250-20 D	1250-20 DL1	1250-20 DL4		2000-20 D	2000-20 DL1	2000-20 DL4
SOL	-1.0	-0.5	0.0		-1.5	-1.0	-1.0
0							
2							
4							
6							
8							
10							
12							
14							

Figure 7–24   Sequential images of combustion process (modes: 1250-20-D, 1250-20-DL1, 1250-20-DL4, 2000-20-D, 2000-20-DL1, and 2000-20-DL4)
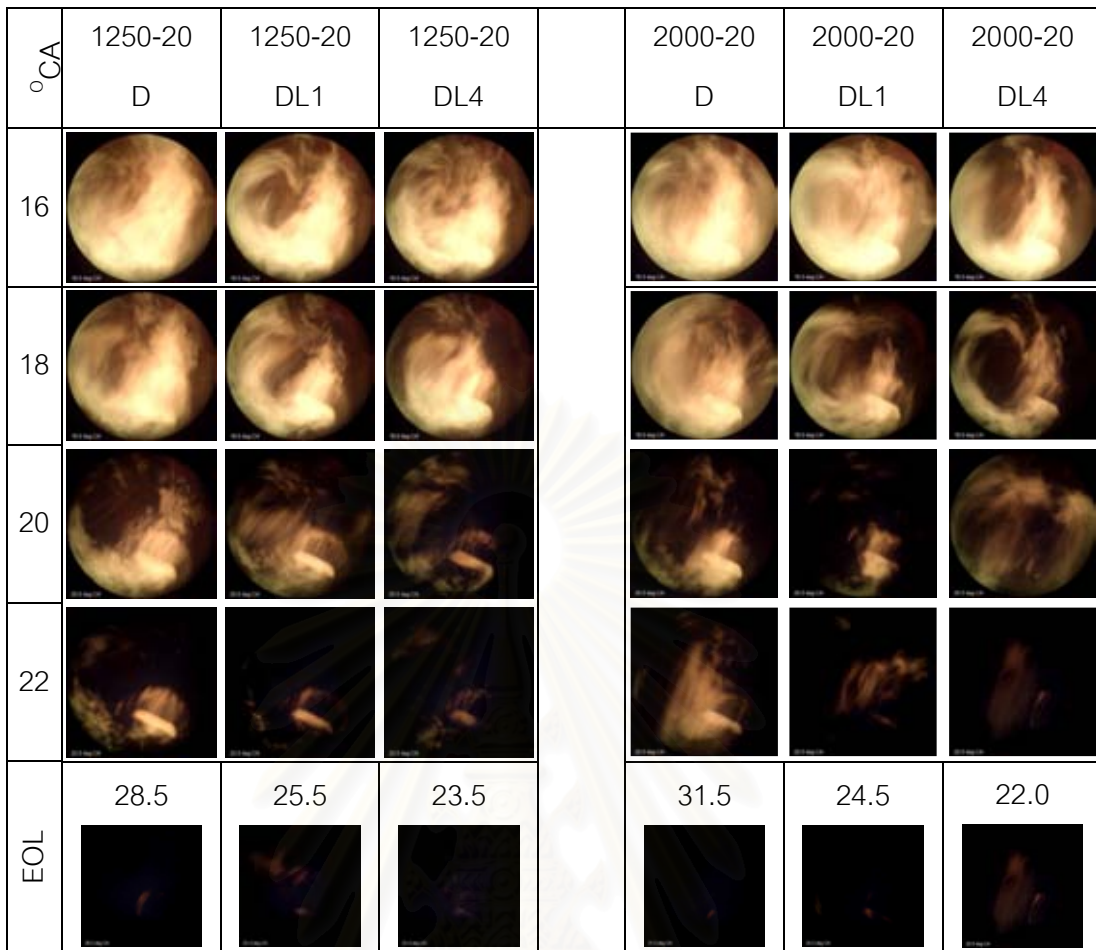
°CA	1250-20 D	1250-20 DL1	1250-20 DL4		2000-20 D	2000-20 DL1	2000-20 DL4
16							
18							
20							
22							
EOL	28.5	25.5	23.5		31.5	24.5	22.0

Figure 7-24   Sequential images of combustion process (modes: 1250-20-D, 1250-20-DL1, 1250-20-DL4, 2000-20-D, 2000-20-DL1, and 2000-20-DL4)

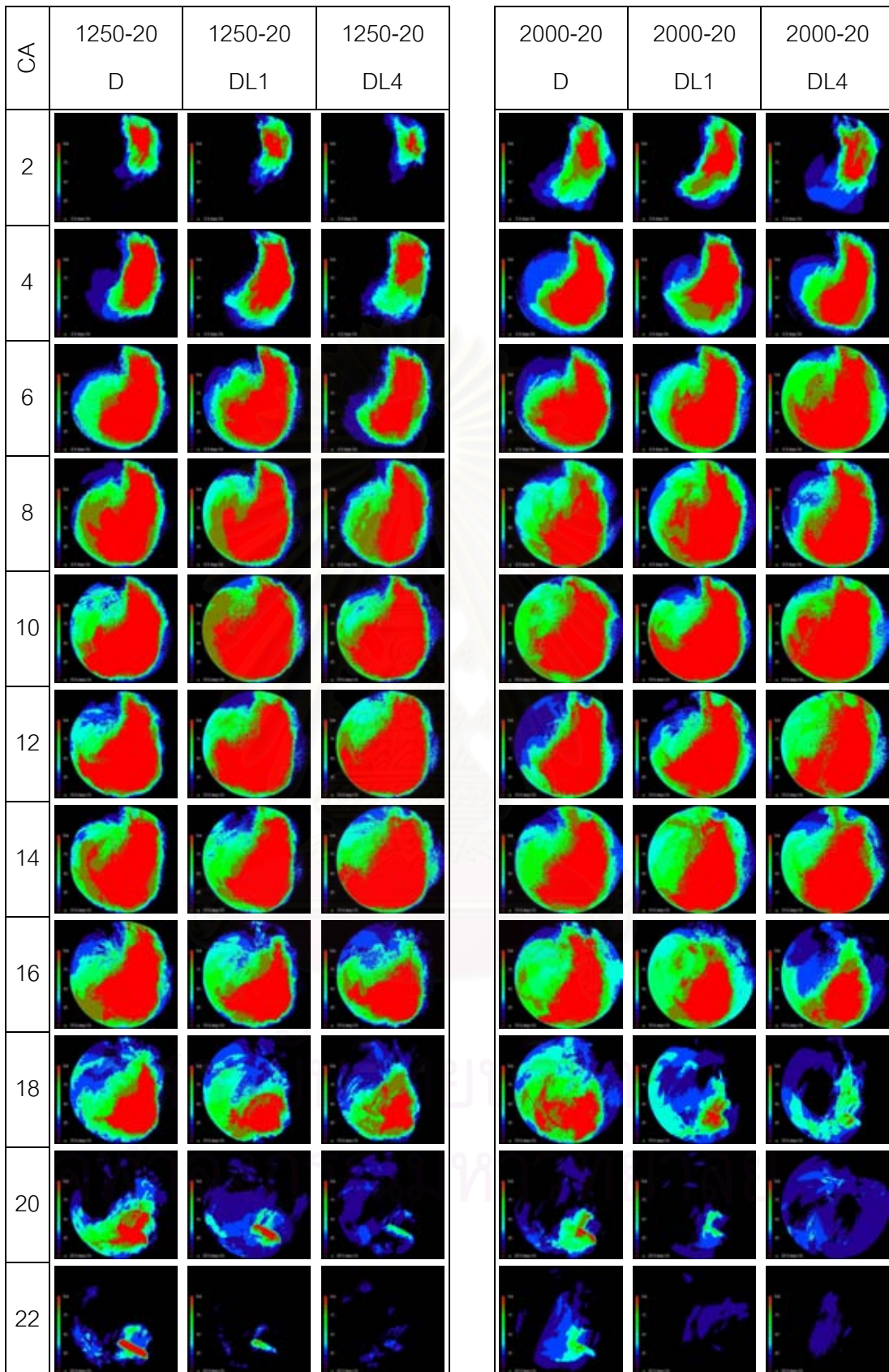| CA	1250-20 D	1250-20 DL1	1250-20 DL4	2000-20 D	2000-20 DL1	2000-20 DL4
2						
4						
6						
8						
10						
12						
14						
16						
18						
20						
22						

Figure 7–25   Images of flame probability distribution (Modes: 1250-20-D, 1250-20-DL1, 1250-20-DL4, 2000-20-D, 2000-20-DL1, and 2000-20-DL4)

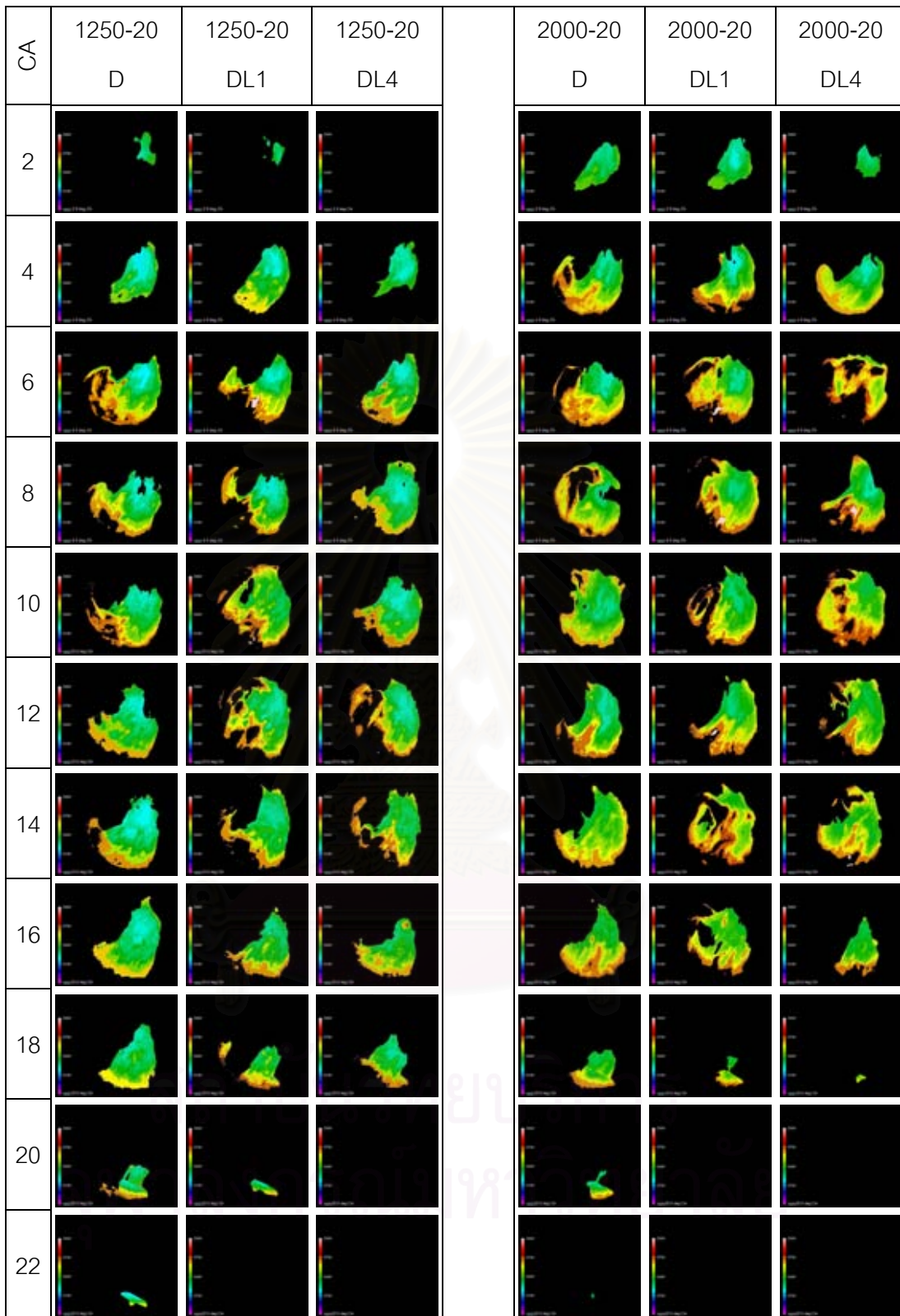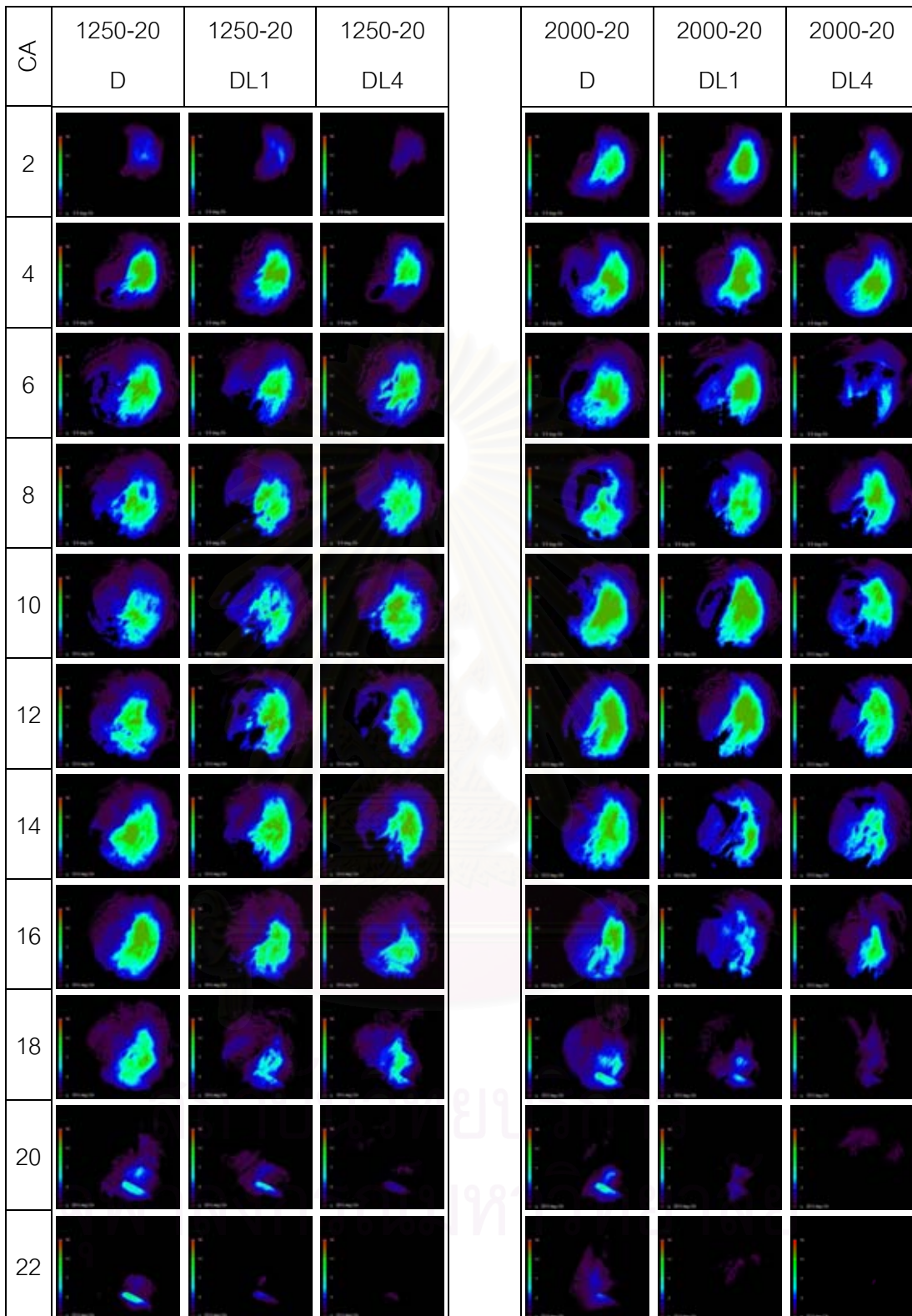| CA	1250-20 D	1250-20 DL1	1250-20 DL4		2000-20 D	2000-20 DL1	2000-20 DL4
2							
4							
6							
8							
10							
12							
14							
16							
18							
20							
22							

Figure 7–26   Sequential images of flame temperature distribution (modes: 1250-20-D, 1250-20-DL1, 1250-20-DL4, 2000-20-D, 2000-20-DL1, and 2000-20-DL4)

CA	1250-20 D	1250-20 DL1	1250-20 DL4		2000-20 D	2000-20 DL1	2000-20 DL4
2							
4							
6							
8							
10							
12							
14							
16							
18							
20							
22							

Figure 7–27   Sequential images of soot concentration (modes: 1250-20-D, 1250-20-DL1, 1250-20-DL4, 2000-20-D, 2000-20-DL1, and 2000-20-DL4)
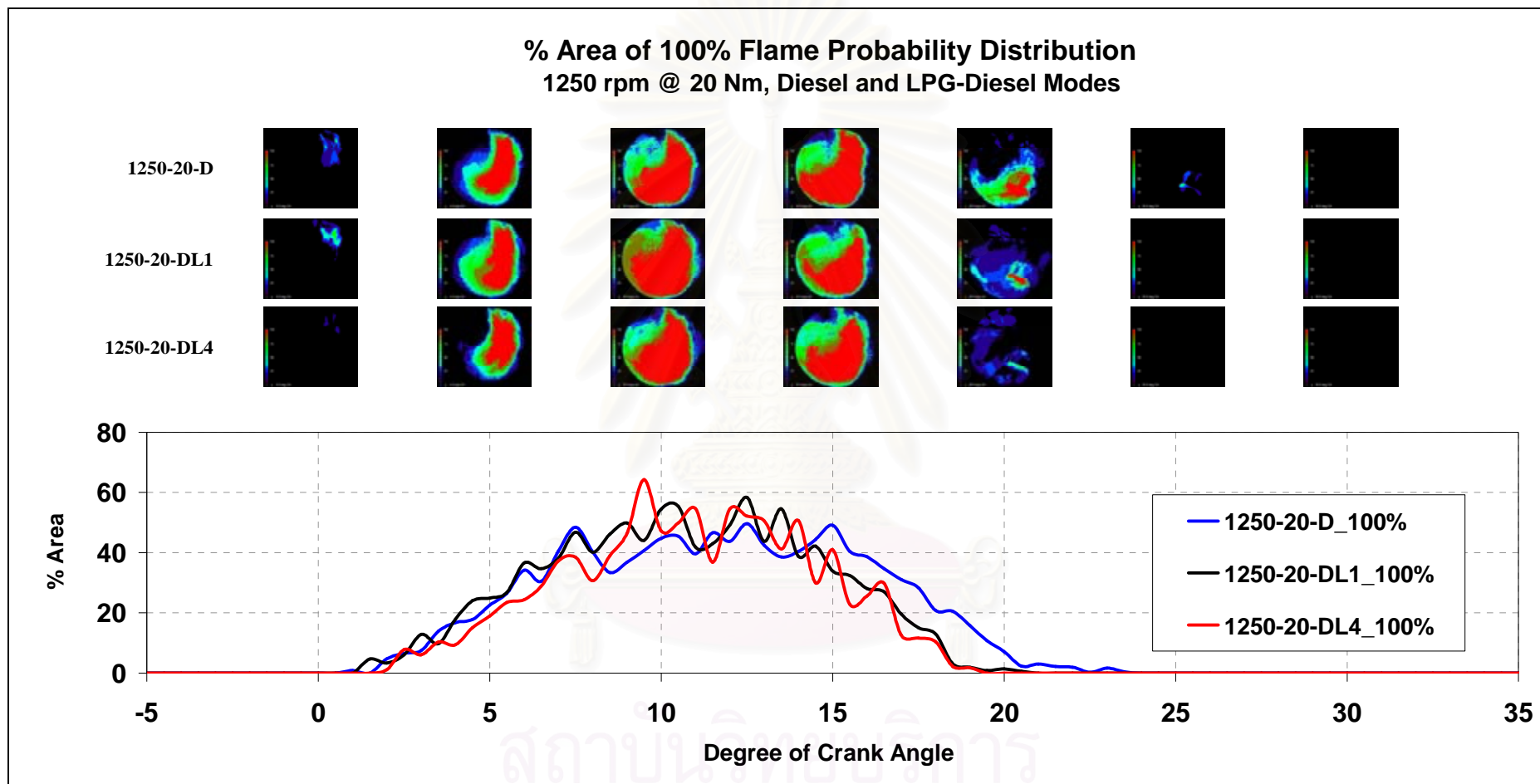
Figure 7–28   Flame probability distribution @ 1250 rev/min, 20 Nm (neat diesel and LPG-Diesel)
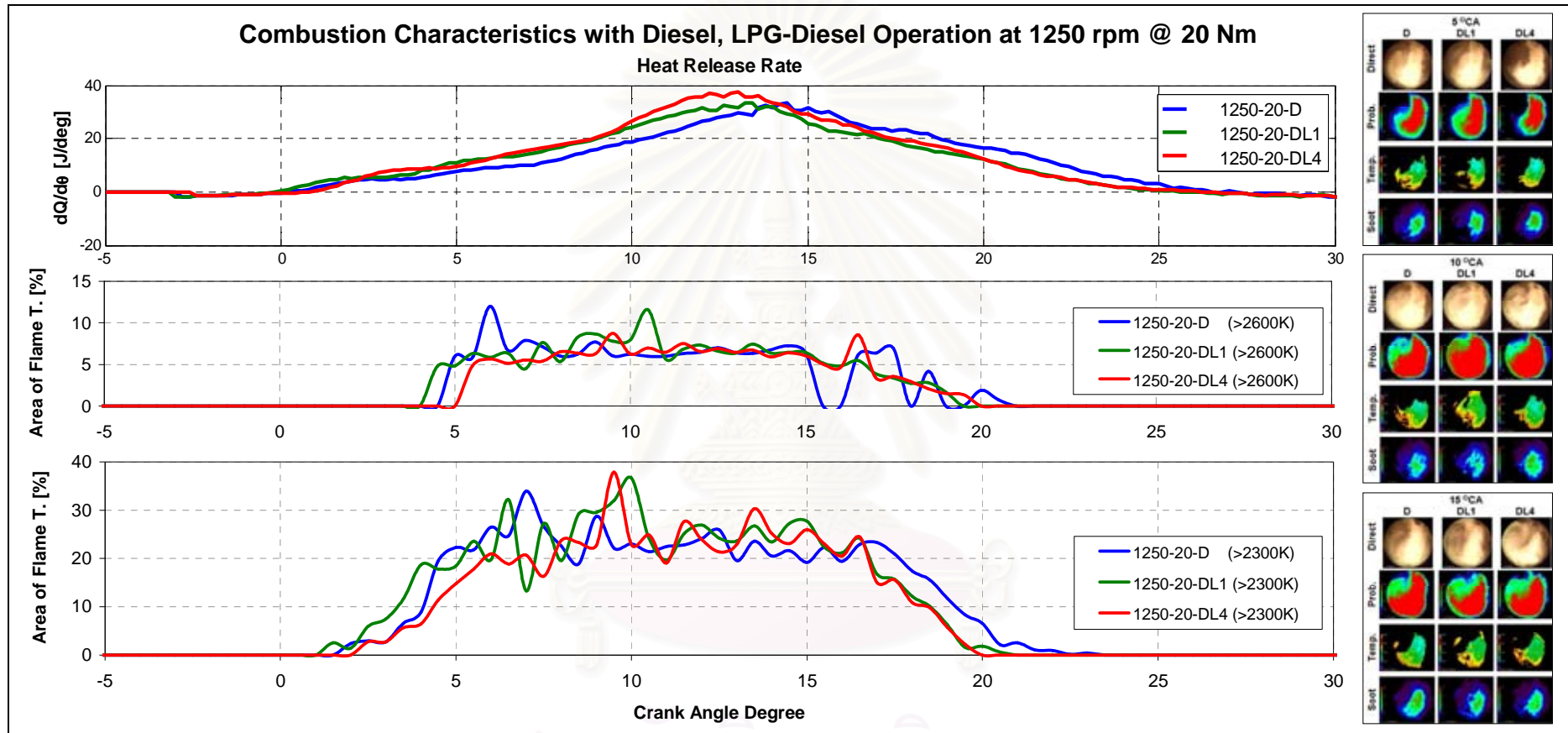
Figure 7–29   HRR and area of flame temperature above 2300 and 2600K @ 1250rev/min, 20Nm (Diesel and LPG-Diesel modes)

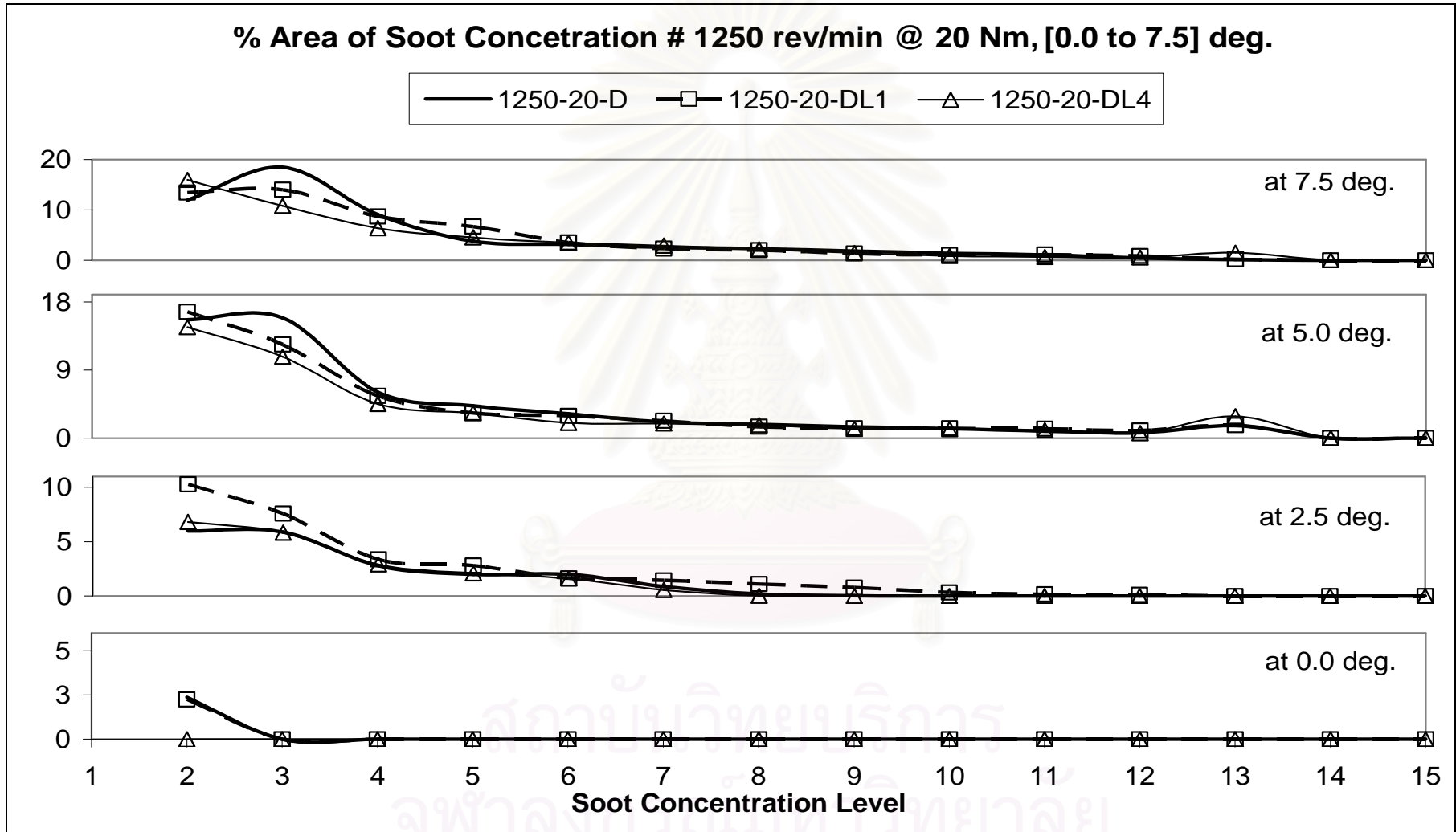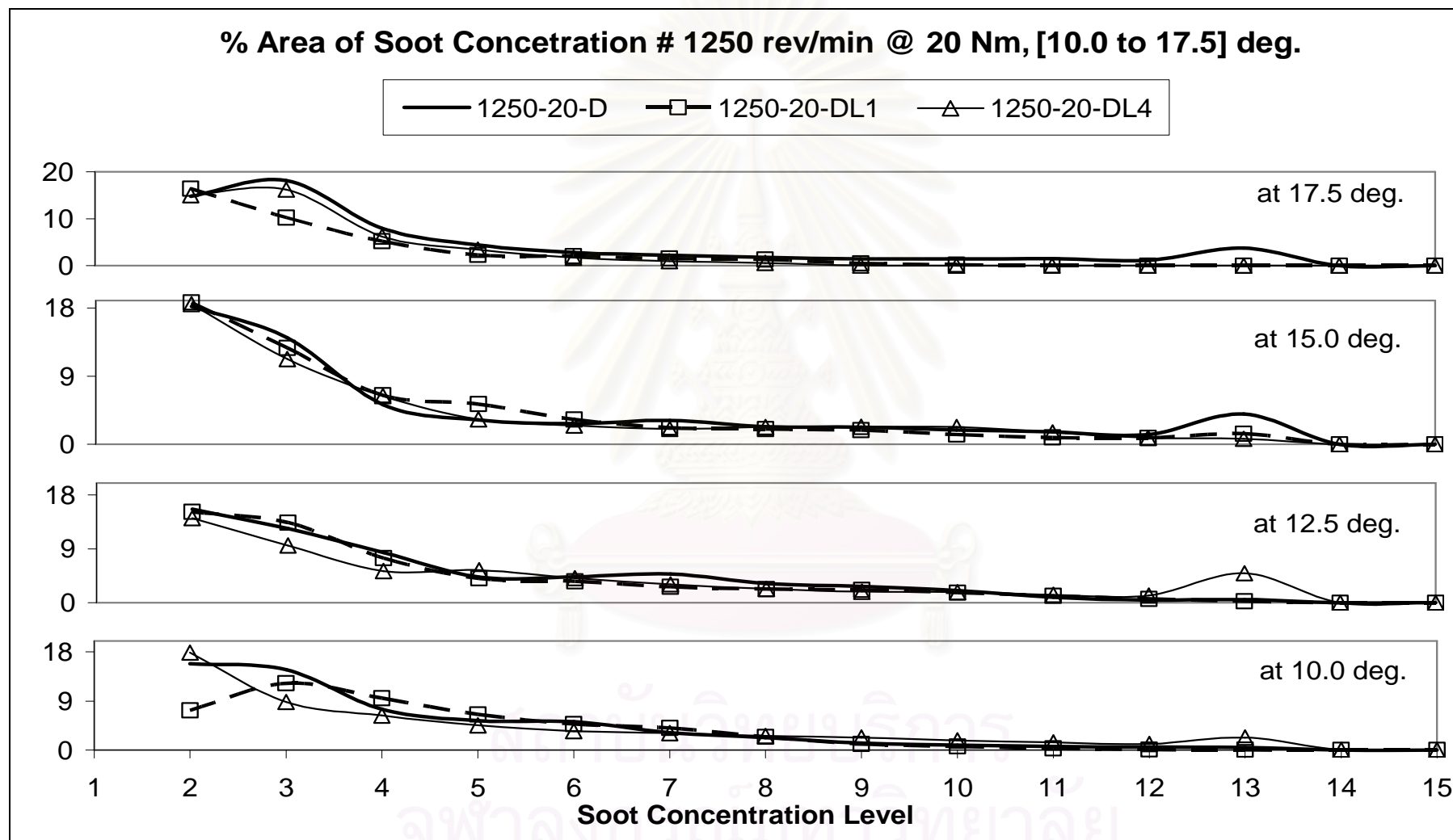*# Image groups are at 5, 10, and 15 ^{O}CA)*

Figure 7–30   Soot concentration trace, from 0 to 7.5 degree aTDC @ 1250rev/min, 20Nm, (Diesel and LPG-Diesel modes)

Figure 7–31   Soot concentration trace, from 10 to 17.5 degree aTDC @ 1250rev/min, 20Nm, (Diesel and LPG-Diesel modes)
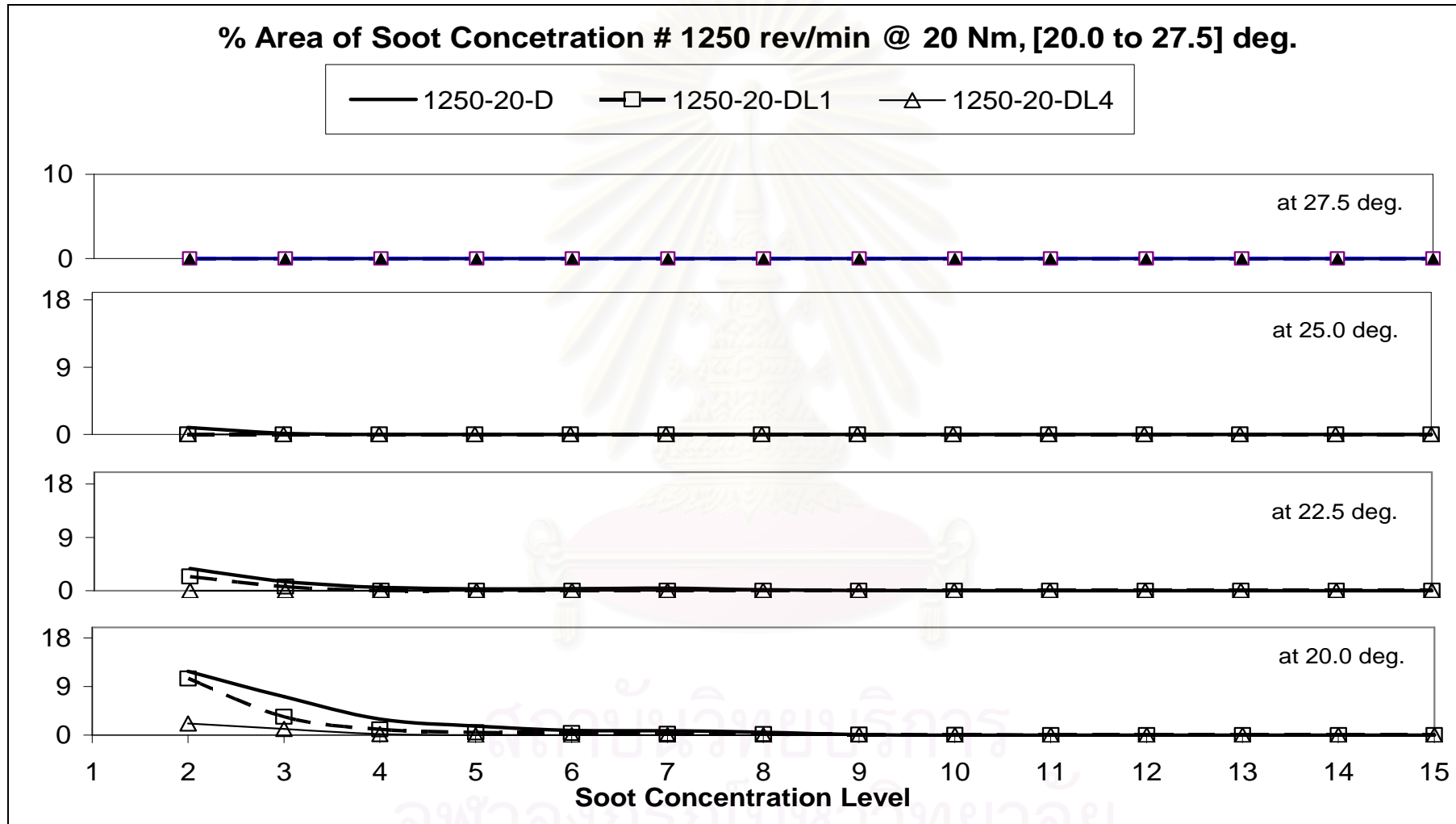
Figure 7–32   Soot concentration trace, from 20 to 27.5 degree aTDC @ 1250rev/min, 20Nm, (Diesel and LPG-Diesel modes)
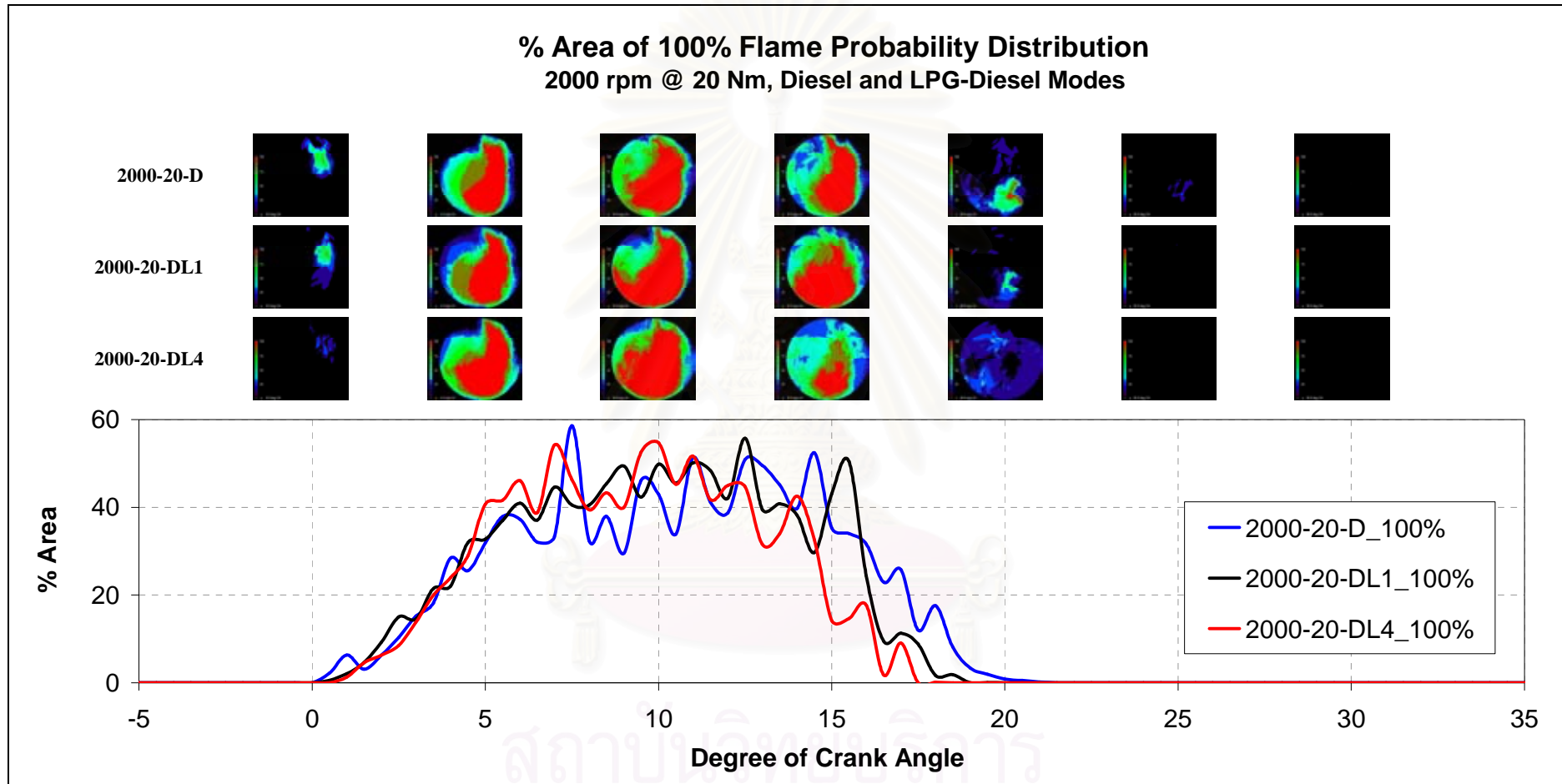
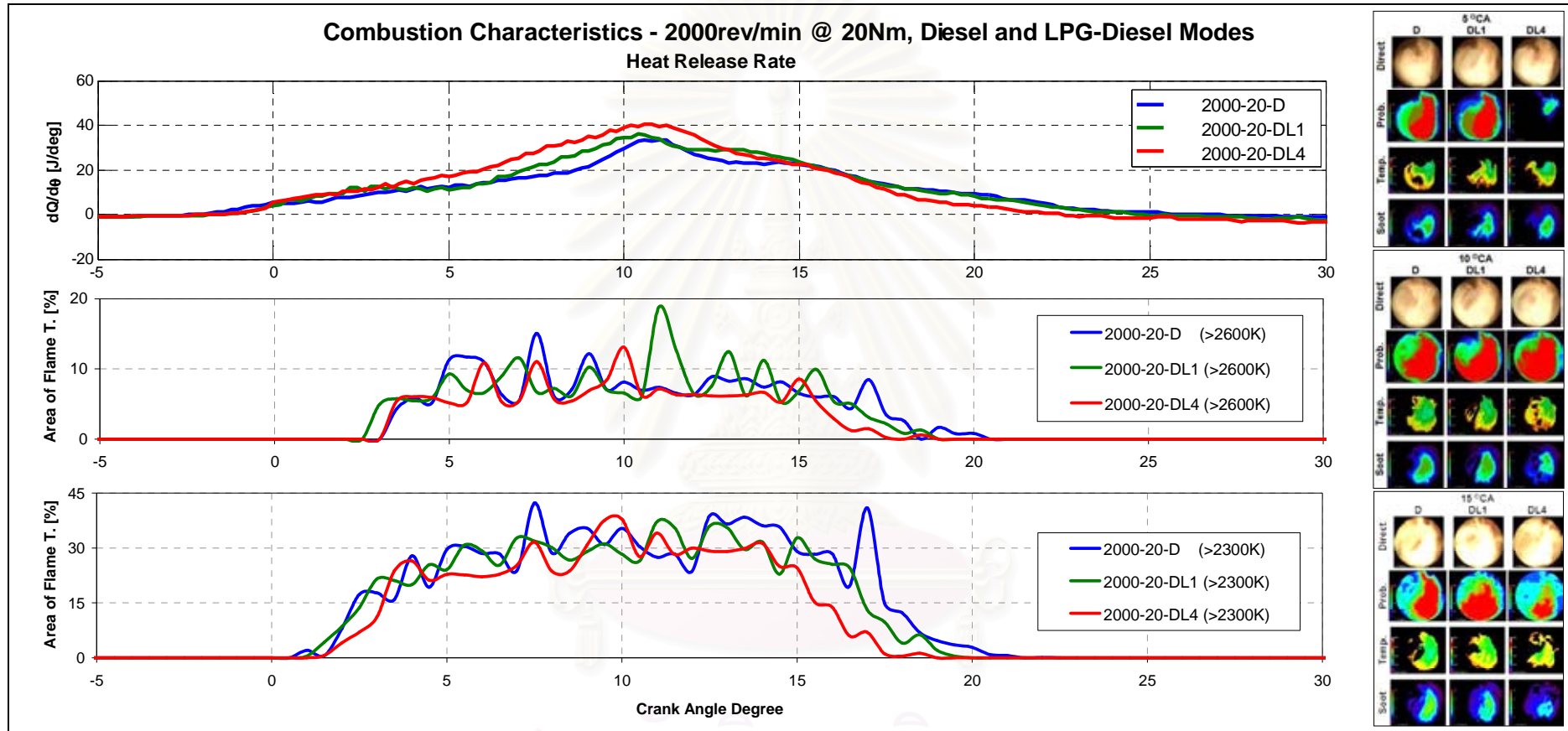Figure 7–33   Flame probability distribution @ 2000 rev/min, 20 Nm (neat diesel and LPG-Diesel modes)

Figure 7–34   HRR and area of flame temperature @ 2000rev/min, 20Nm (Diesel and LPG-Diesel modes)

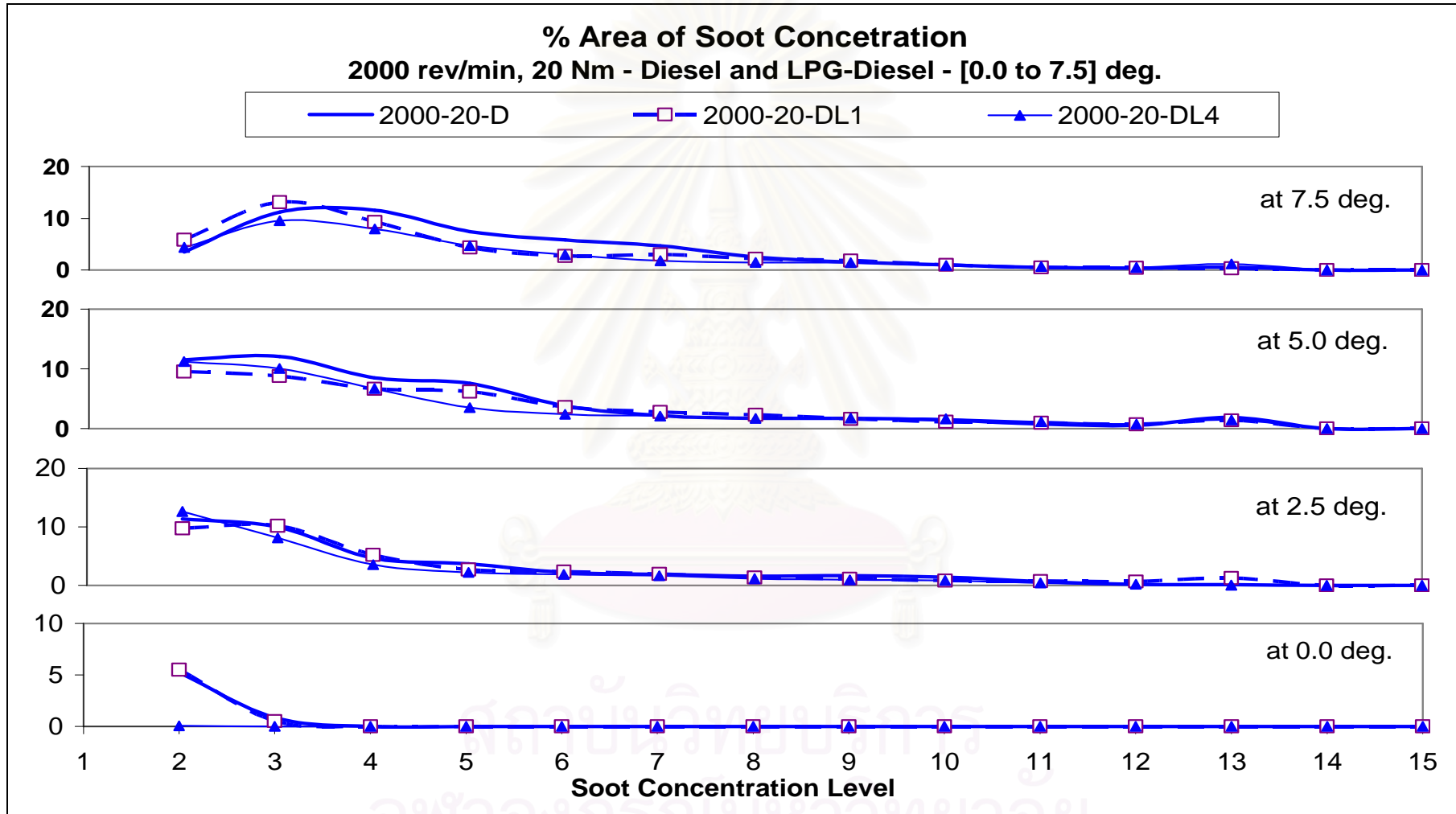*# Image groups are at 5, 10, and 15 ^{O}CA)*

Figure 7–35   Soot concentration trace, from 0 to 7.5 degree aTDC @ 2000rev/min, 20Nm (Diesel and LPG-Diesel modes)
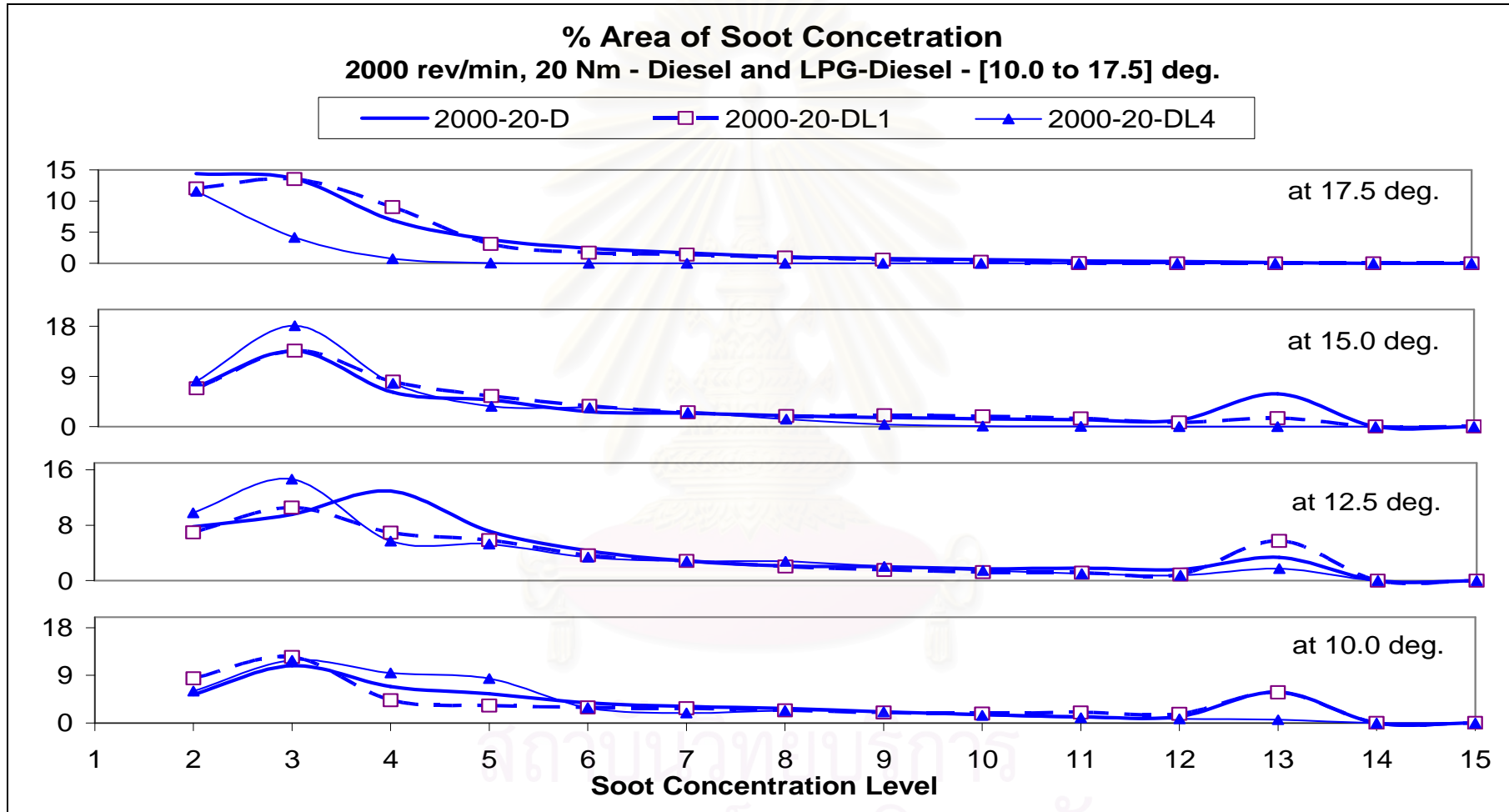
Figure 7–36   Soot concentration trace, from 10 to 17.5 degree aTDC @ 2000rev/min, 20Nm (Diesel and LPG-Diesel modes)
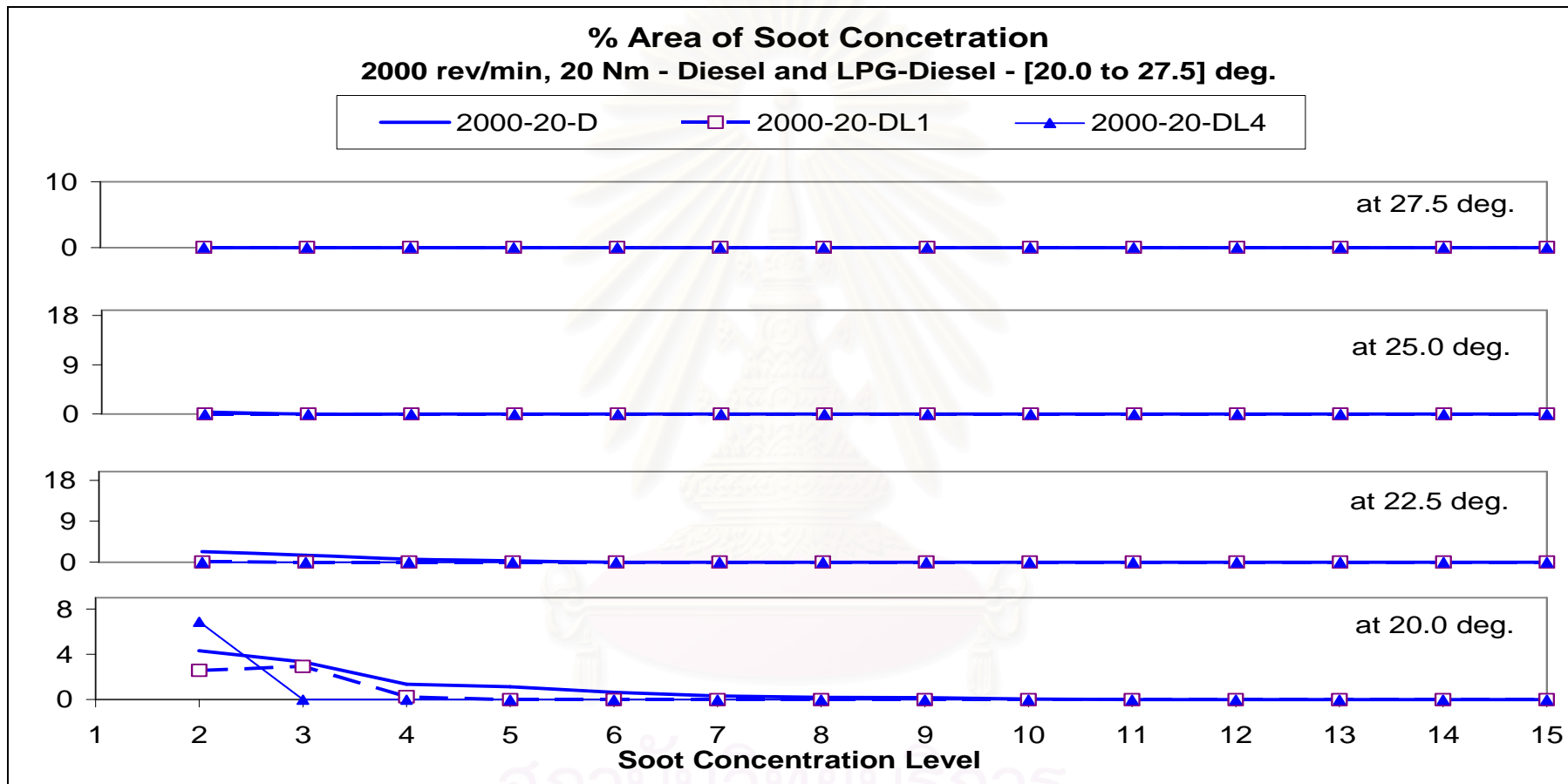
Figure 7–37   Soot concentration trace, from 20 to 27.5 degree aTDC @ 2000rev/min, 20Nm (Diesel and LPG-Diesel modes)

7.1.3.2. Ignition delay and start of combustion

The resultant ignition delay with different LPG ratio is contributed by the four factors, as analyzed earlier in Section 2.2.3.1.1. In addition, as can be seen later, since dual fuel resulted in higher engine temperature which leads to the increase in the temperature charge, the ignition delay tends to decrease. The decrease of the prevailing in-cylinder pressure is described typically in Figure 7–38 and the values detected for these cases are given in Table 7-2.
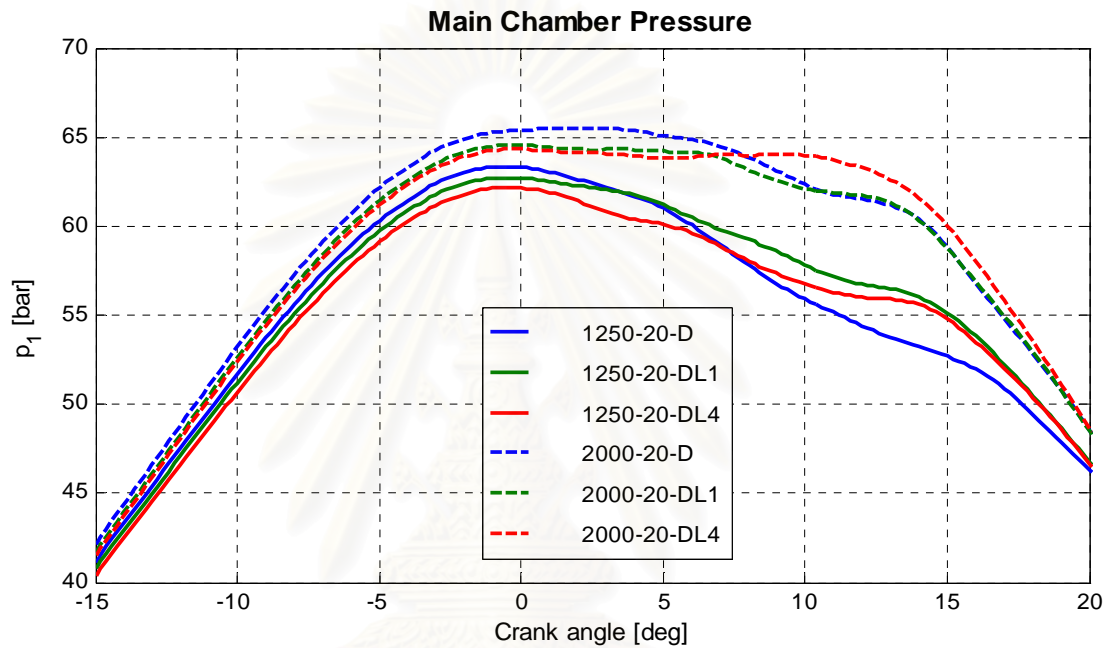

Figure 7–38   Pressure history in the main chamber (modes: 1250-20-D, 1250-20-DL1, 1250-20-DL4, 2000-20-D, 2000-20-DL1, and 2000-20-DL4)

Table 7-2   Prevailing pressure in the main chamber at injection timing instant

Mode	Injection timing [^{O}CA]	Chamber pressure [bar]	Ignition delay [^{O}CA]	SOC [^{O}CA]
1250-20-D	-2.8	62.53	3.0	0.2
1250-20-DL1	-3.0	62.38	2.8	-0.2
1250-20-DL4	-2.4	61.57	3.2	0.8
2000-20-D	-5.8	61.06	3.6	-2.2
2000-20-DL1	-5.6	60.64	4.0	-1.6
2000-20-DL4	-5.2	60.93	3.4	-1.8

The whole results of detected ignition delays at different engine speeds, loads, and gas energy fractions are given in Figure 7–39 to Figure 7–41. There was not significant difference in the ignition delay in LPG-diesel and diesel modes. Although the delay has been thought to increase, it even decreased. At 1250 rev/min, the delay was the same at 30 and 40 Nm, and the highest difference was 0.4 degree at 20 Nm. At 2000 rev/min the highest prolonged delay was 0.6 degree at 40Nm (in mode 2000-40-DL1) but also appeared to be advanced 0.6 degree at 70Nm (in mode 2000-70-DL4). At 2750rev/min, the delay appeared to be prolonged at 30, 40, and 70 Nm but advanced at 10Nm, at all modes of LPG supply. The reason for the observed feature in the change of ignition delay might be resulted from the high turbulent intensity in the pre chamber at the time of injection.

- The SOC detected by the tool "Combustion Analyzer" is also shown in Figure 7–39 to Figure 7–41. The change in SOC is resulted from the change in the SOI and the delay. At low and medium speeds, the SOC in dual fuel mode was later than that in neat diesel mode. At 1250 rev/min and constant engine torque, the retardation was longer with increased LPG and in a range of [0.6-1.0] ^{0}CA. At 2000 rev/min, the SOC was later than that with neat diesel and in a range of [0.4-0.8] ^{0}CA. However, at higher load at this speed, the retardation became lesser when the LPG ratio increased, especially at the same instant at 2000-70-DL4 mode.
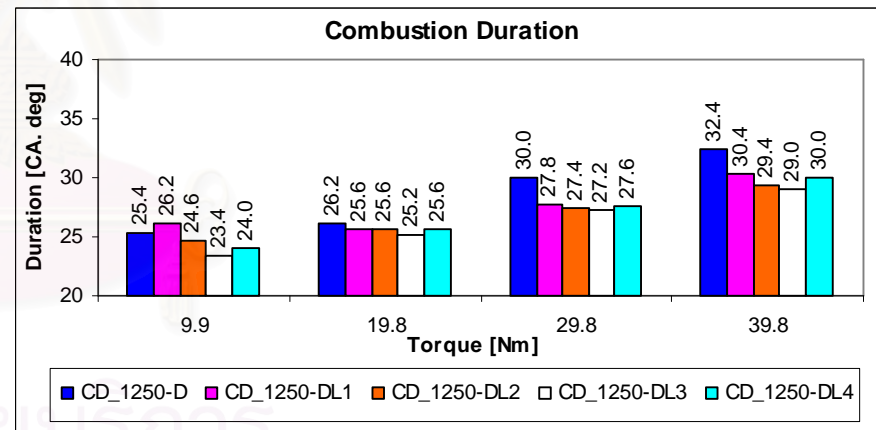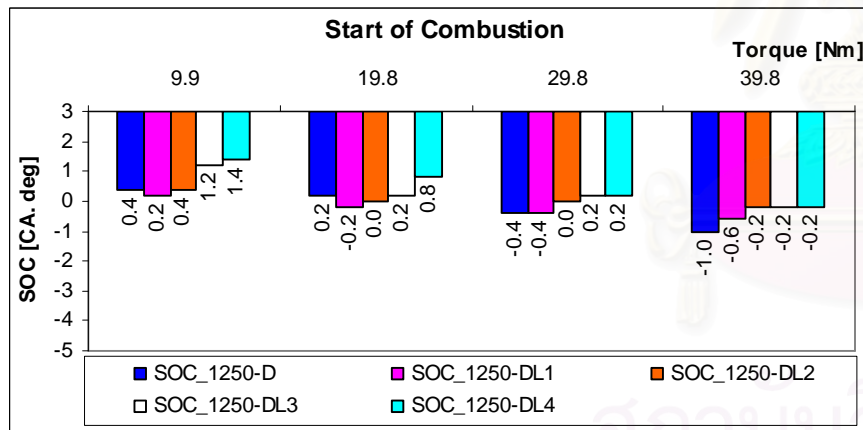
Figure 7–39   SOI, SOC, ignition delay and combustion duration # 1250 rev/min, diesel and LPG-diesel

Figure 7–40   SOI, SOC, ignition delay and combustion duration # 2000 rev/min, diesel and LPG-diesel
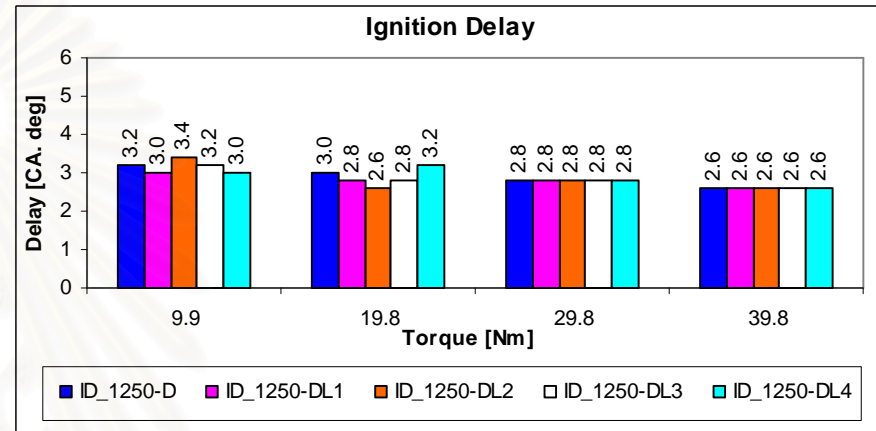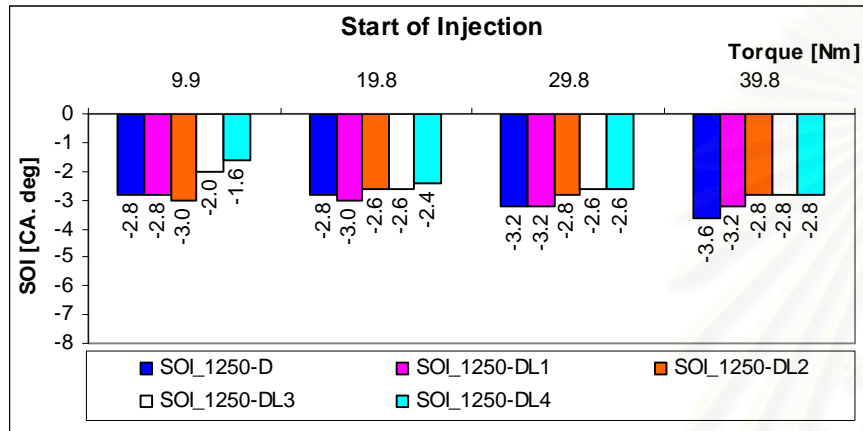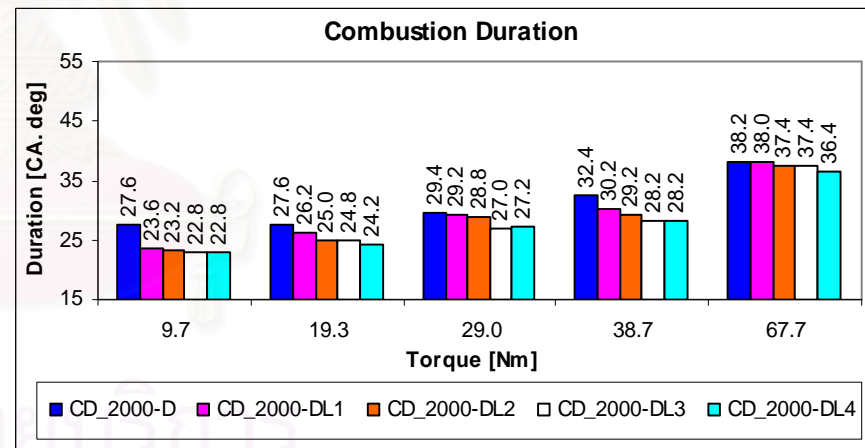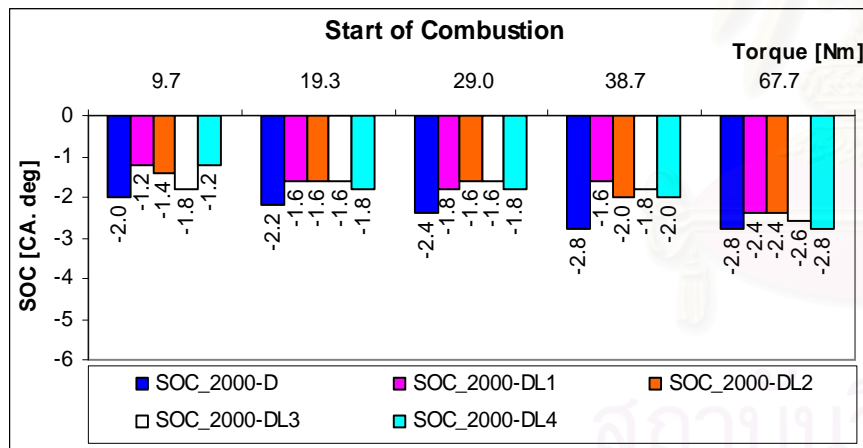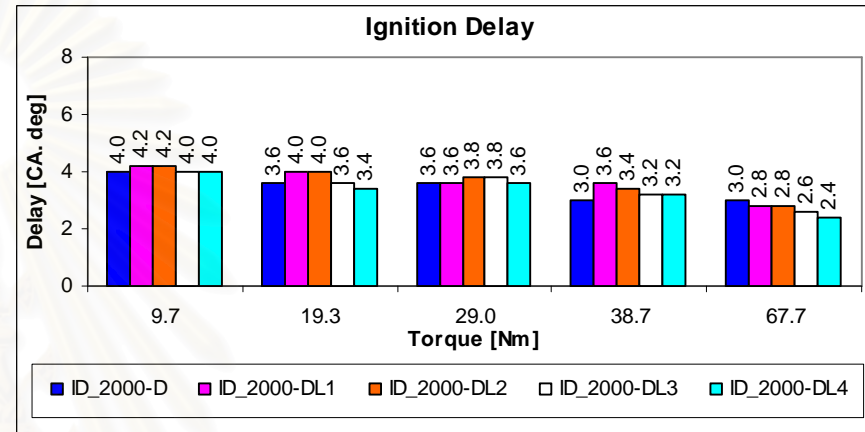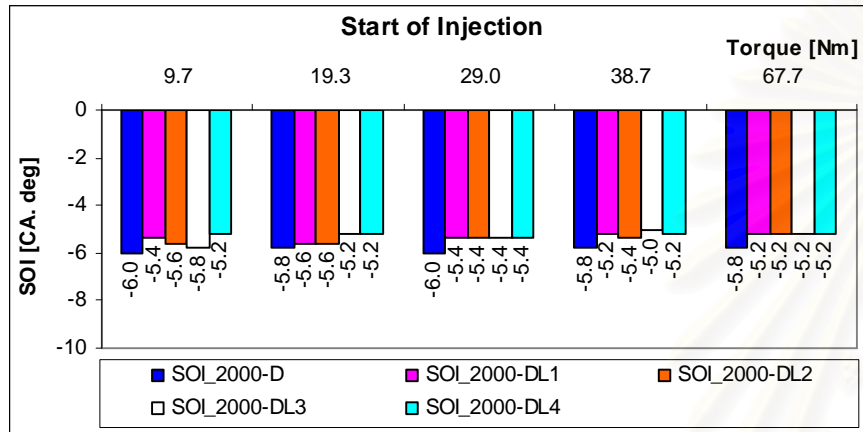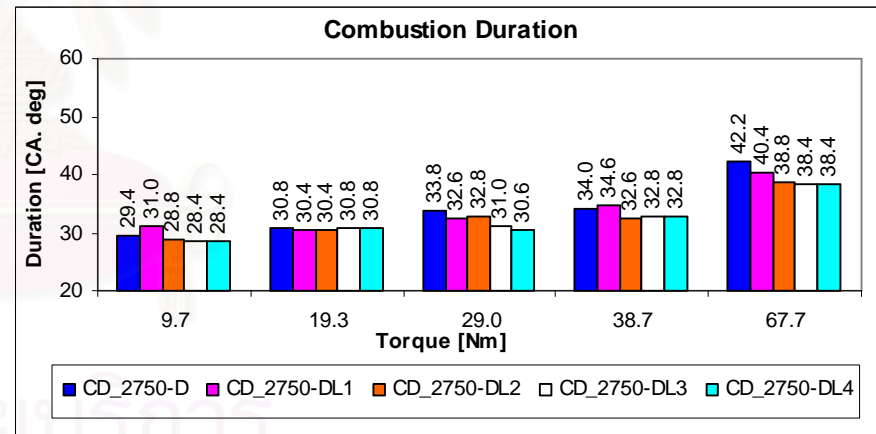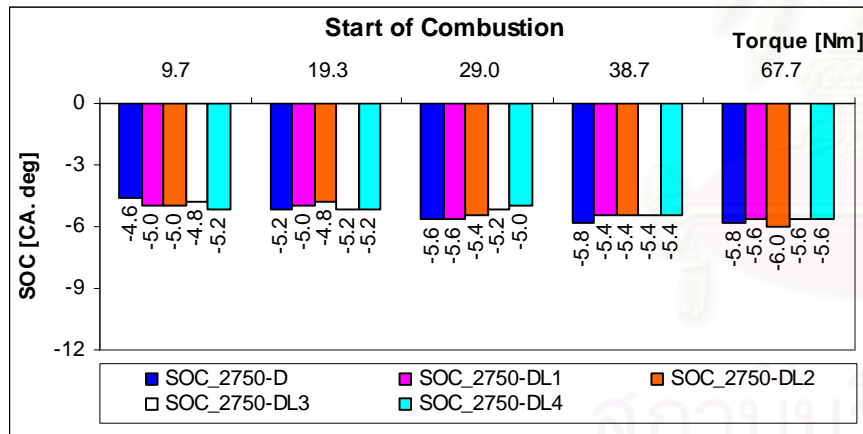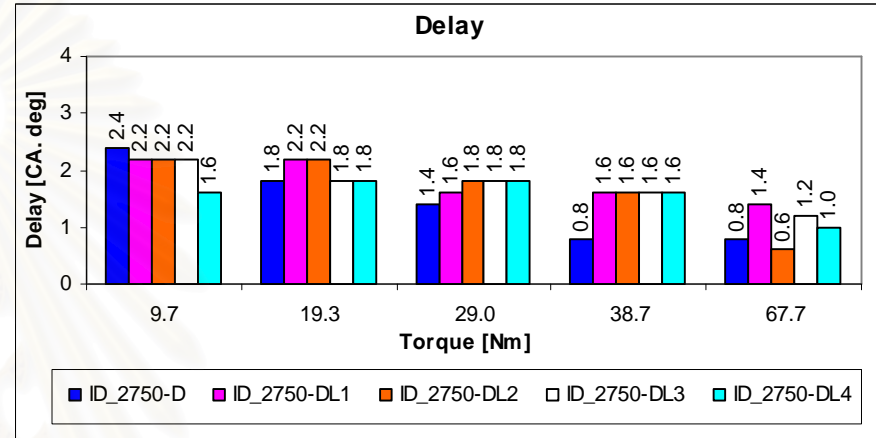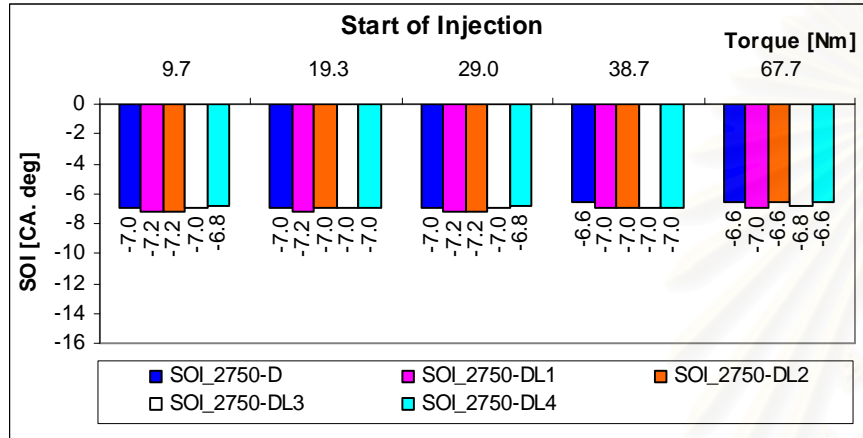
Figure 7–41   SOI, SOC, ignition delay and combustion duration # 2750 rev/min, diesel and LPG-diesel

7.1.3.3. The heat release rate, peak of pressure, pressure rise rate, and cyclic variation

The net HRR, PRR, and main chamber pressure (with neat diesel and LPG-diesel modes) are presented in Figure 7–44 to Figure 7–52. From these figures, these following general features are revealed:

@ The HRR profiles in LPG-diesel modes were almost similar to that in neat diesel modes. At all engine speeds, the peaks of HRR in dual fuel modes were higher than that in neat diesel modes.

@ Before reaching their peaks, the dual-fuel HRR became higher than the diesel after short duration (about 2.5^{O}CA) after SOC even with the retarded SOC. The combustion of the LPG premixed mixture in the vicinity of the ignition sources from diesel fuel contributes to the heat release in this period. The difference is more significant at 1250 rev/min. Differential pressure between the two combustion chambers drives the turbulent intensity inside the swirl chamber. In compression stroke this difference measured is in the range of about [0.7-3.0] bar, as shown in Figure 7–42. The higher the engine speed the higher the difference. In neat diesel operation, due to the cooling effect of the liquid fuel being injected in the chamber in the second and third stage of combustion, there is a fluctuation in the net HRR which can be recognized by the zigzag at few CA degrees after TDC. At low speed, the cooling effect of heated and vaporized fuel is higher since the turbulent intensity is lower and the engine temperature is lower. Conversely, in dual fuel modes there is less liquid fuel injected to the swirl chamber and the LPG, homogeneously distributed in the whole chamber, is readily to burn. As the diesel fuel auto-ignites, the LPG in the vicinity of these ignition sources immediately burns, followed by its flame propagation outwards the ignition sources and also enhance the combustion of the liquid fuel. The combustion of LPG in the vicinity of the ignition sources leads to rapidly increase in dual fuel HRR, aiding the vaporization of liquid fuel as well as the flame propagation of the gaseous fuel. As a result, the dual fuel net HRR becomes higher than that in neat diesel operation.

@ At low and medium speeds, the net HRR in the late-stage of combustion with dual fuelling was lower than that with neat diesel. This is shown by the steeper part of HRR curve before its intersection with the abscissa: from about 17-18°CA as shown in Figure 7–44 for 1250rev/min, after about 17°CA as shown in Figure 7–47 for 2000

rev/min. Two factors may contribute to lower HRR in this stage. Firstly, since the gaseous fuel is more readily to burn than the liquid fuel, it burn mostly in the previous stages. Second, at low engine speed, the liquid fuel is more difficult to vaporize than at high speeds. This emphasizes the role of gaseous fuel.
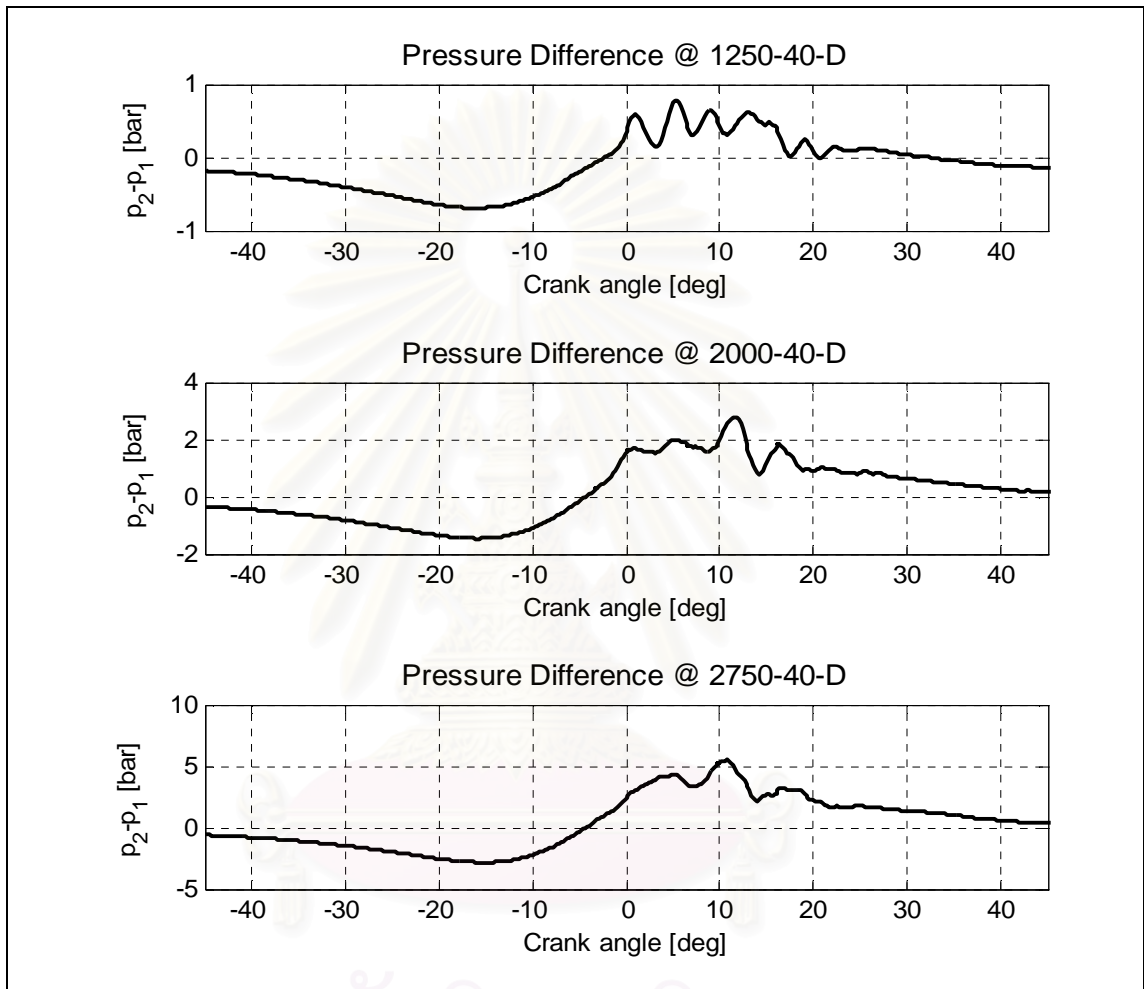
Figure 7–42   Typical differential pressure between the two combustion chambers

@ The faster burning of dual fuel resulted in the higher integrated net heat release, as shown in Figure 7–45 and Figure 7–46, Figure 7–48 and Figure 7–49, Figure 7–51 and Figure 7–52, corresponding to engine speed of 1250, 2000, and 2750 rev/min. Consequently, the center of the area enveloped by the HRR curve and the abscissa (henceforth called HRR area) tends to move towards TDC. As observed, the movement is about [0.6-1.3] $^{\circ}$CA at 1250 rev/min (Figure 7–53), about [0.9-1.5] $^{\circ}$CA at 2000 rev/min

(Figure 7–54), and about [0.4-2.0] ^{O}CA at 2750 rev/min (Figure 7–55) This leads to ①higher theoretical thermal efficiency, ②higher heat transfer from the fluid to the combustion chamber wall, and ③lower exhaust gas temperature. The observed decrease in exhaust gas temperature was up to 4.7^{O}C at 1250 rev/min (Figure 7–13), up to 6.7^{O}C at 2000 rev/min (Figure 7–14), and up to 10.3^{O}C at 2750 rev/min (Figure 7–15). The lube oil temperature should increase due to the increased engine temperature brought by higher heat transfer from the combustion product to the combustion chamber wall. However, with the setting of the cooling water system of the test bench, the lube oil temperature did not reveal significant changes (Figure 7–16 to Figure 7–18).

The reasonable operation modes will be those providing the highest integrated net HR. It is found that the reasonable modes were, mostly, DL3 at 1250 rev/min and 2750 rev/min whereas DL4 at 2000 rev/min. These modes, accompanied with the strength of the LPG-air premixed charge, the total fuel-air equivalent ratio, and the substitution are shown in Table 7-3. The reasonable substitutions were in the ranges about [34%÷58%], [27%÷40%], and [21%÷40%] at 1250, 2000, and 2750 rev/min, respectively.

@ Although the dual fuel operation provided higher HRR rate compared to the neat diesel, the total energy conversion efficiencies in dual fuel modes were lower. Following possible factors might contribute to the efficiency deterioration:

- Unburnt LPG in the pre chamber: When the ignition sources by the pilot diesel injection were not powerful enough to consume the whole mixture in the pre chamber within the limit time;

- LPG energy loss by blow-by: Part of the LPG occupying the cylinder might leave to crankcase or be absorbed to the oil film.

- The combustion chamber geometry: As explained in Section 5.2.1, the swirl pockets and recesses area on the piston crown are designed to improve diesel combustion by producing twin vortices and limiting the jet-flow in the swirl pocket to reduce heat transfer from the flow to the main chamber wall and enhance the air utilization. However, in HMC dual fuel operation this causes negative effect since the jet-flow is prevented to spread out fast in the main chamber. In addition, the gap between the piston and cylinder

head is small, thus the flame propagation can also not spread out fast and far to consume the LPG in the main chamber.
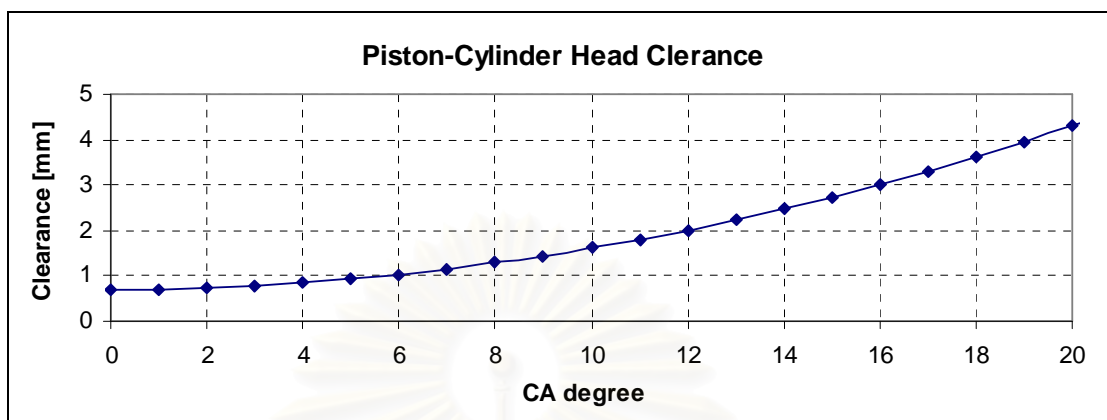
Figure 7–43   Clearance between the top of piston crown and cylinder head.
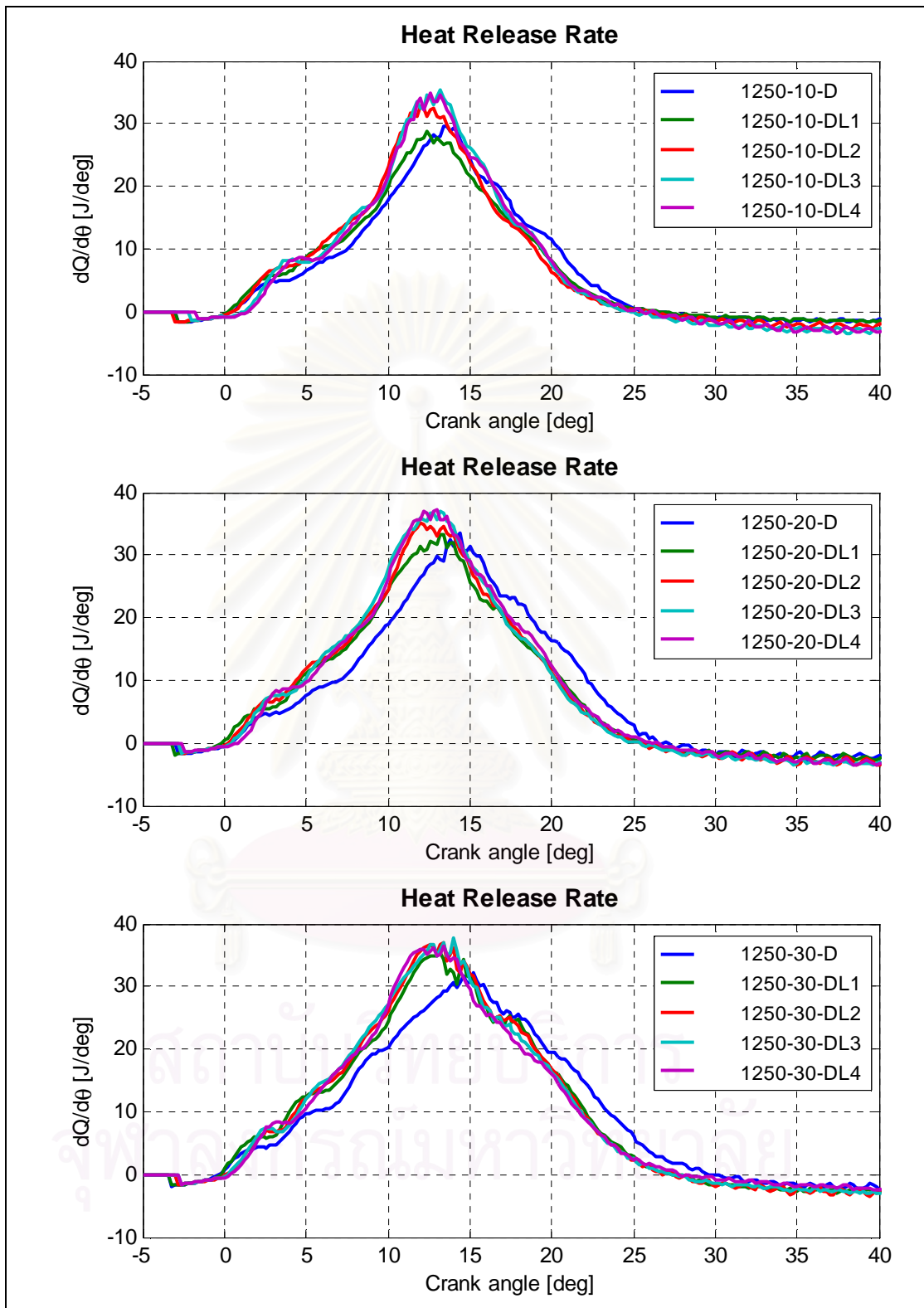
Figure 7–44   Net HRR at 1250 rev/min, 10, 20, and 30 Nm (diesel and LPG-diesel)
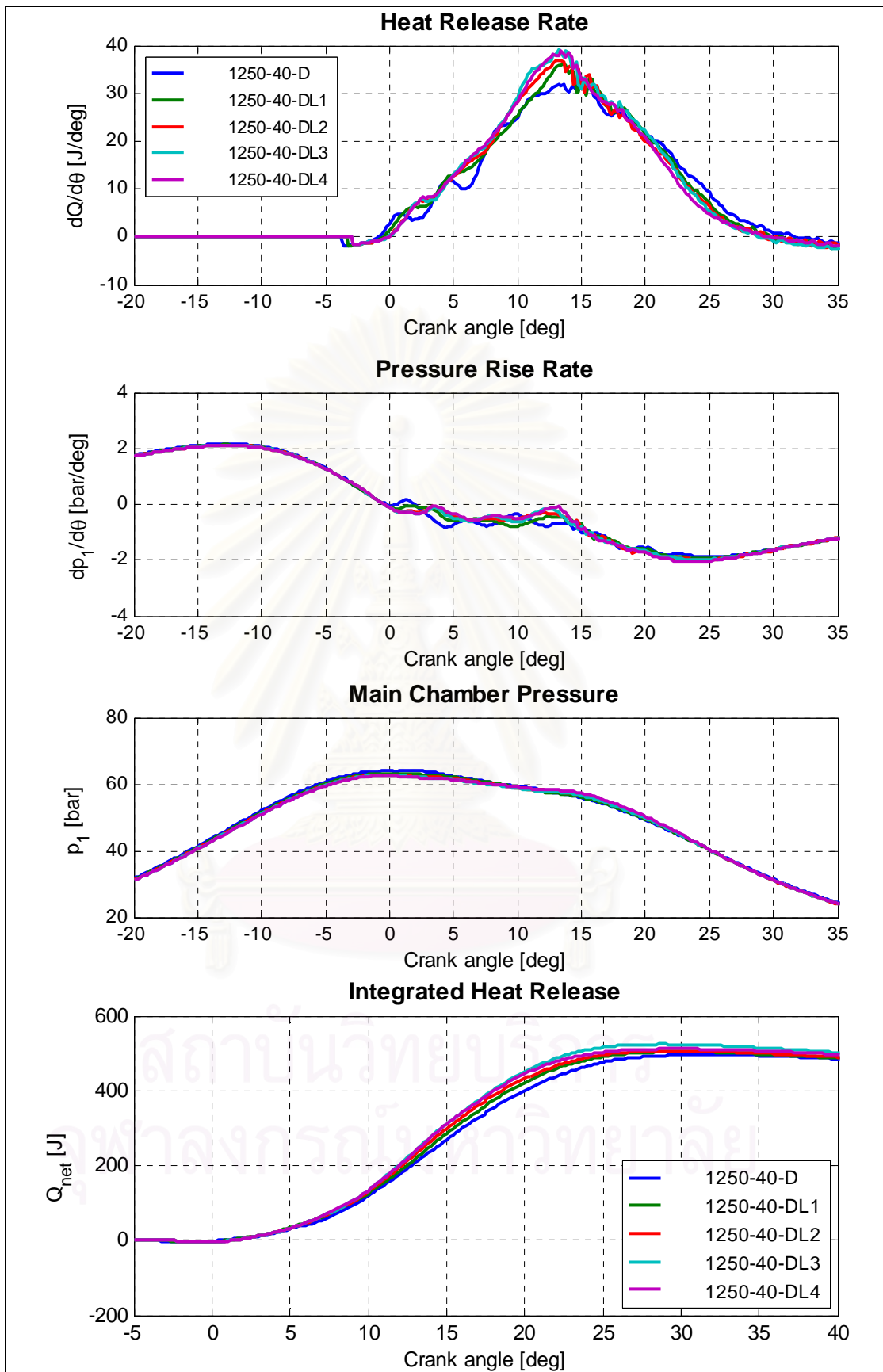
Figure 7–45   Net HRR, main chamber PRR, pressure, and integrated NHR at

1250rev/min, 40 Nm (diesel and LPG-diesel)
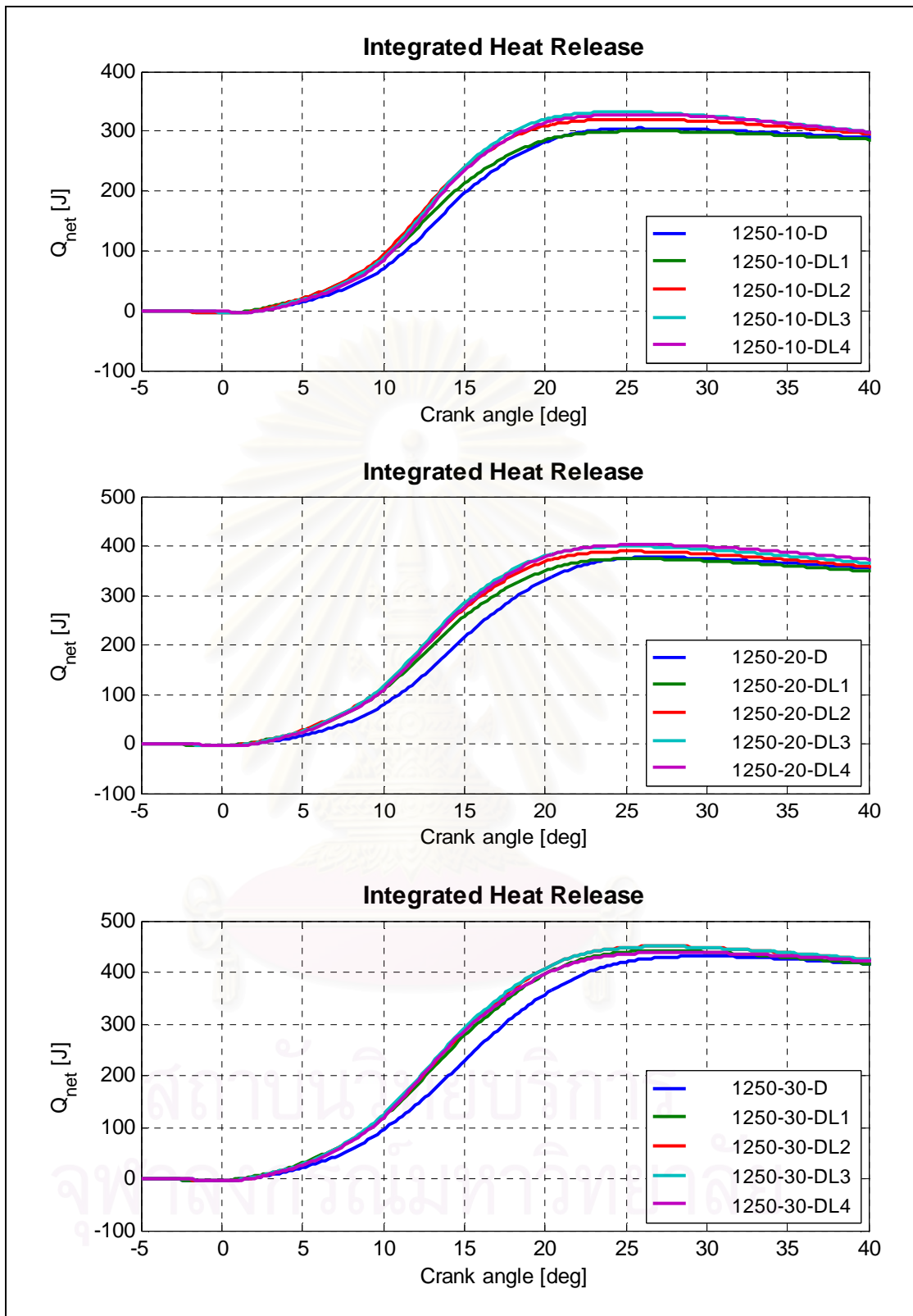
Figure 7–46   NHR at 1250 rev/min, 10, 20, and 30 Nm (diesel and LPG-diesel)
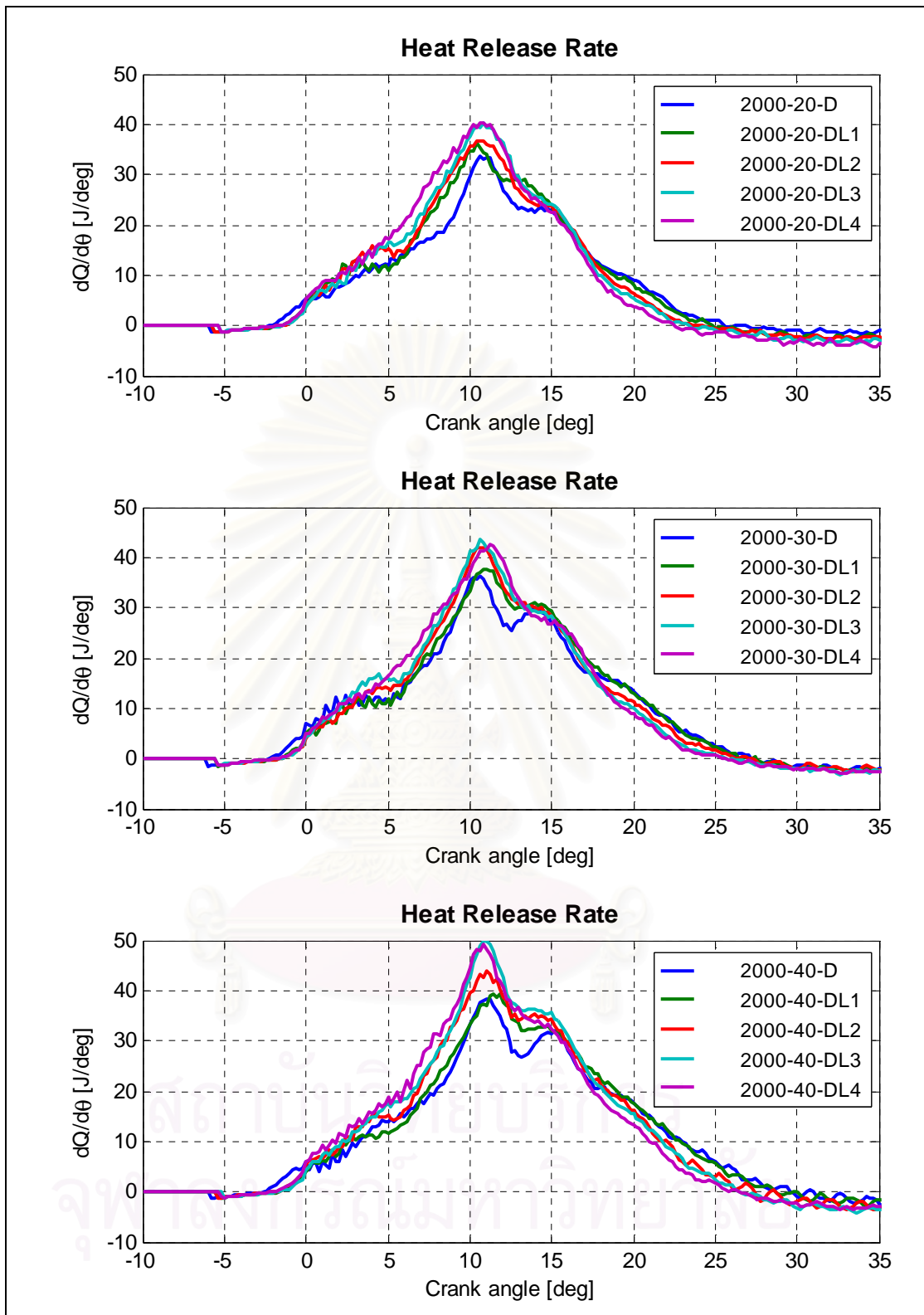
Figure 7–47   Net HRR at 2000 rev/min, 20, 30, and 40 Nm, (diesel and LPG-diesel)
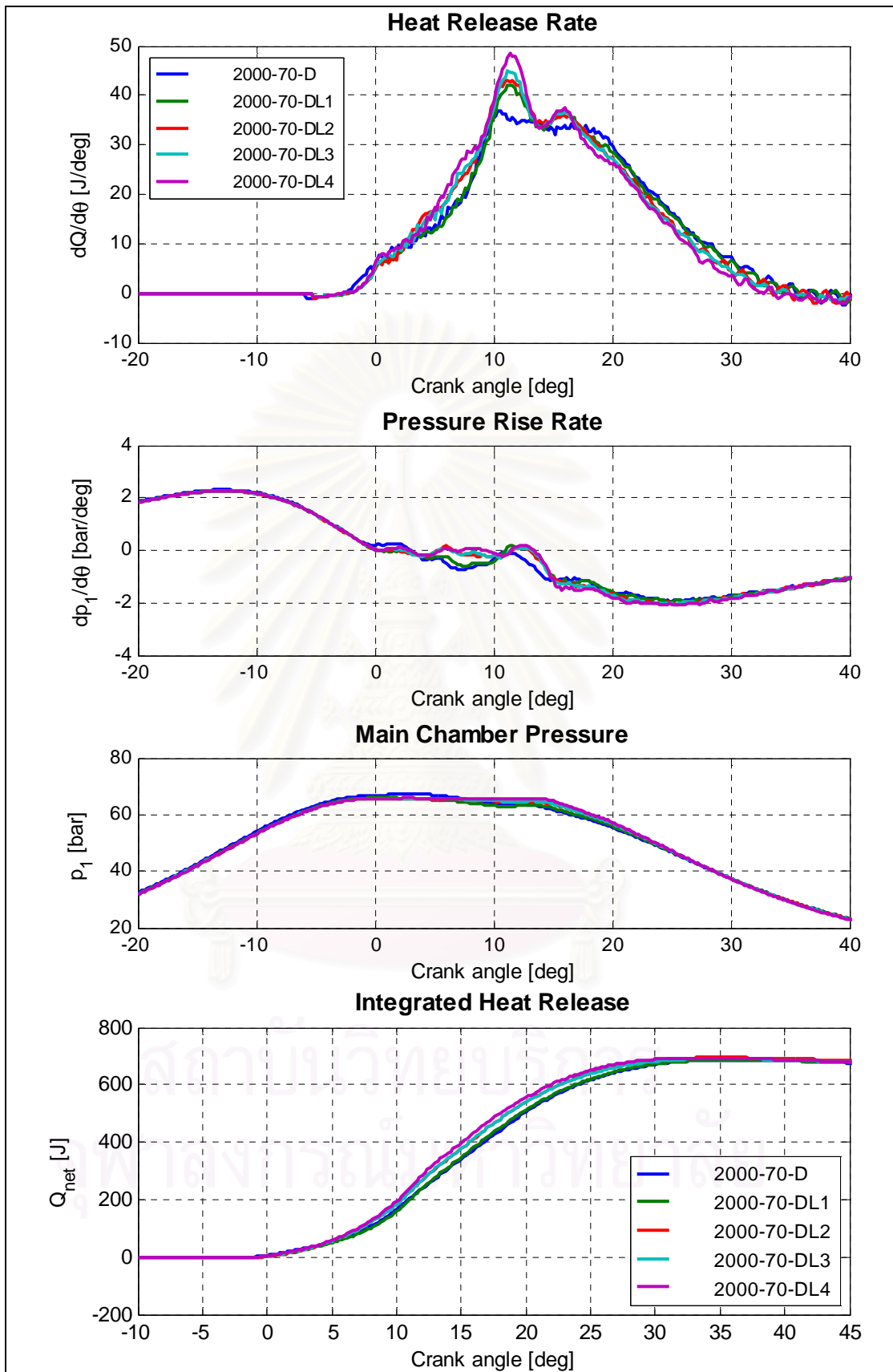
Figure 7–48   Net HRR, main chamber PRR, pressure, and integrated NHR at 2000

rev/min, 70 Nm, (diesel and LPG-diesel)
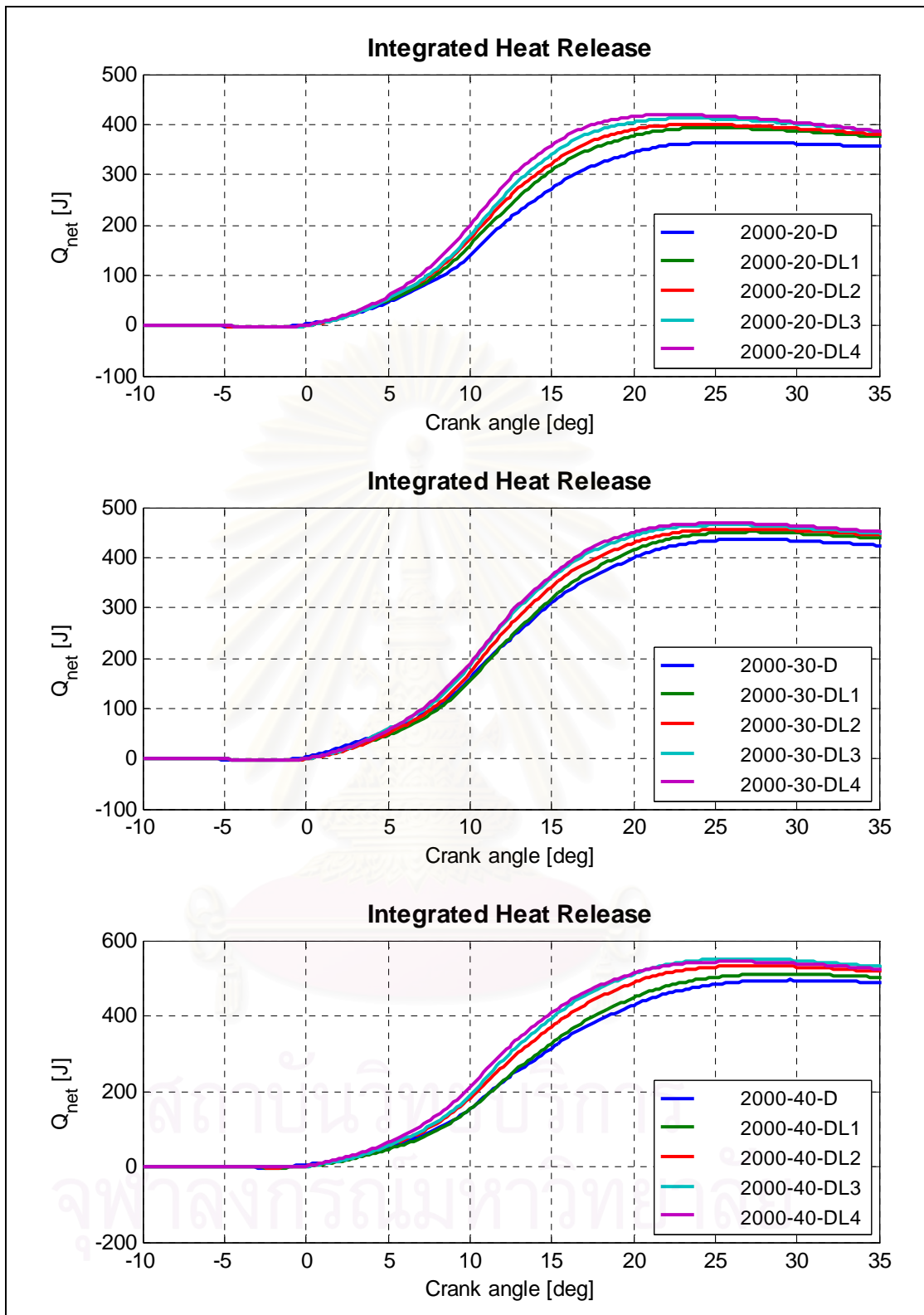
Figure 7–49   NHR at 2000 rev/min, 20, 30, and 40 Nm, (diesel and LPG-diesel)
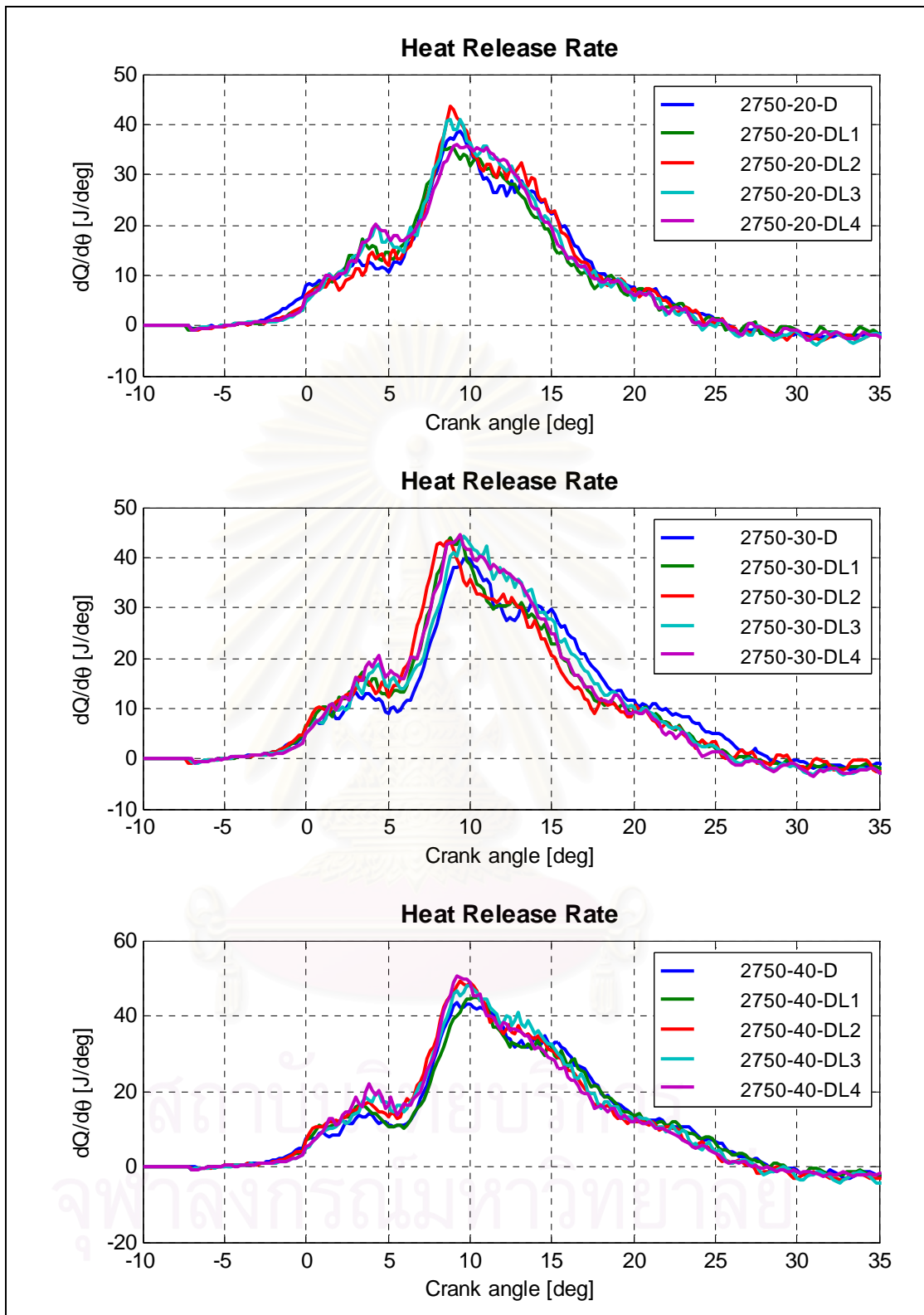
Figure 7–50   Net HRR at 2750 rev/min, 20, 30, and 40 Nm, (diesel and LPG-diesel)
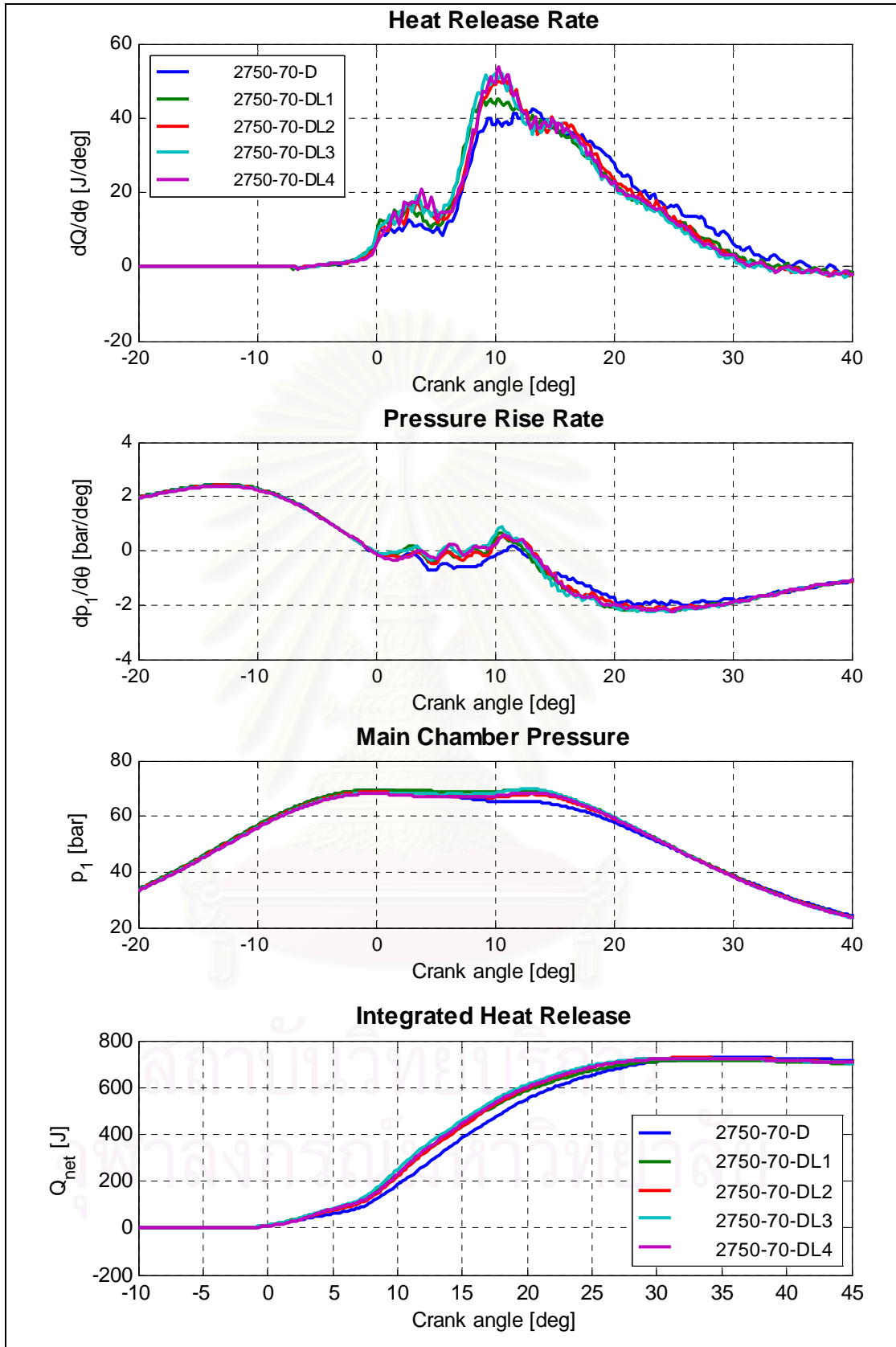
Figure 7–51   Net HRR, main chamber PRR, pressure, and integrated NHR at

2750rev/min, 70 Nm, (diesel and LPG-diesel)
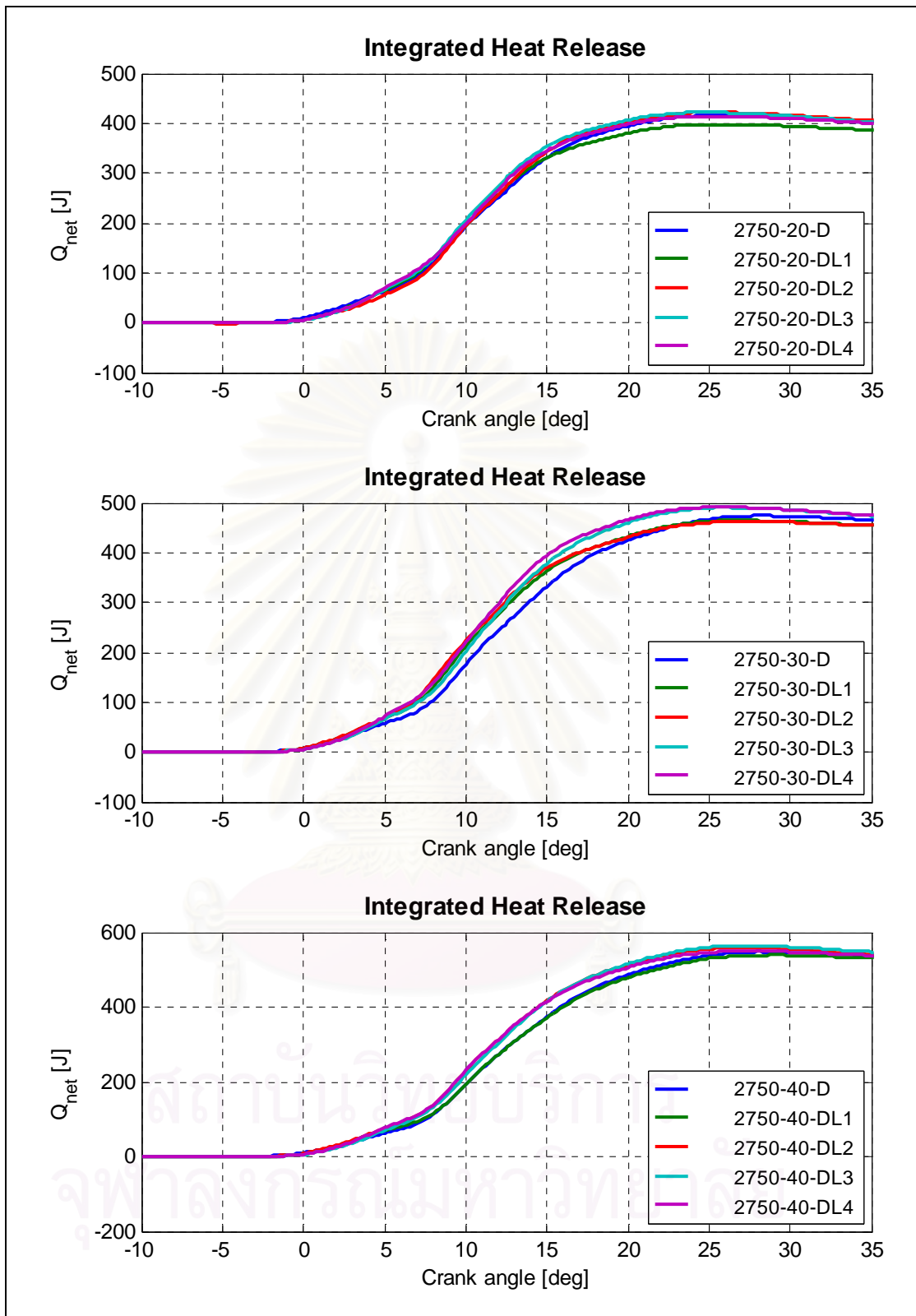
Figure 7–52   NHR at 2750 rev/min, 20, 30, and 40 Nm, (diesel and LPG-diesel)
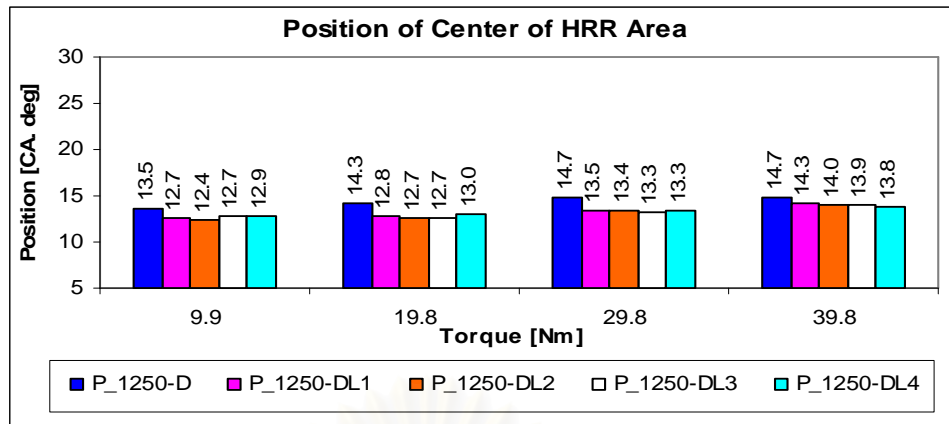
Figure 7–53   Position of the center of HRR area # 1250rev/min, diesel and LPG-diesel
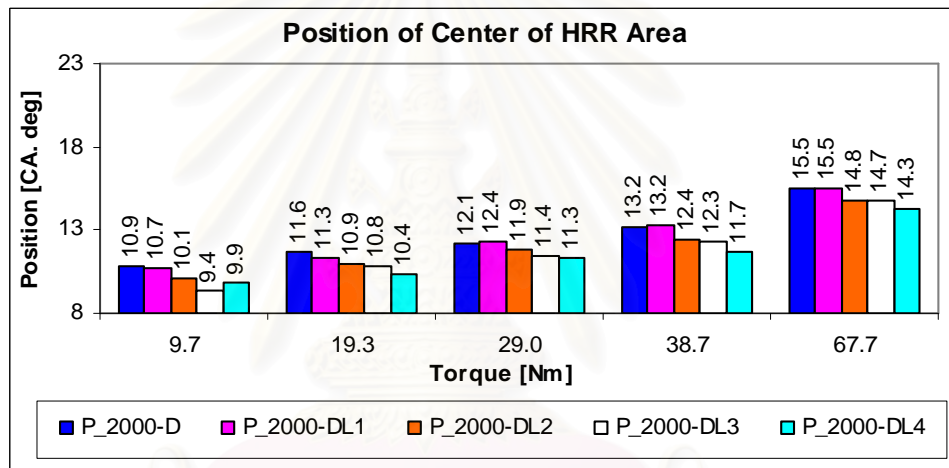
Figure 7–54   Position of the center of HRR area # 2000rev/min, diesel and LPG-diesel
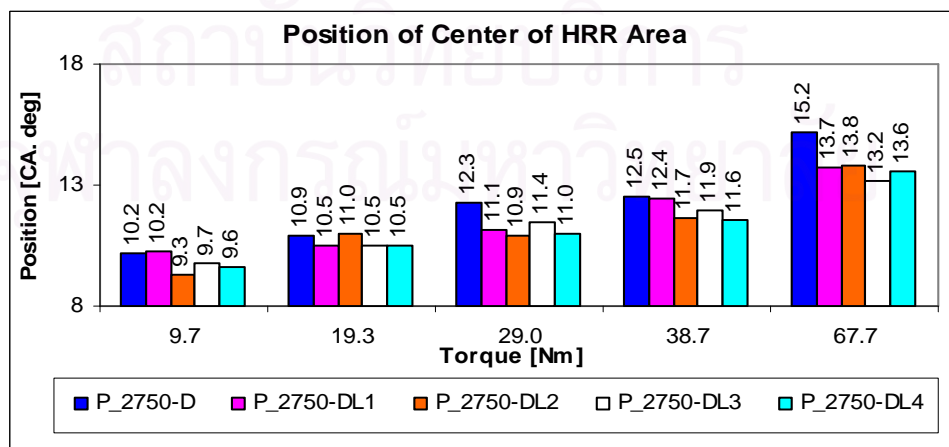
Figure 7–55   Position of the center of HRR area # 2750rev/min, diesel and LPG-diesel

Table 7-3   Modes of LPG-diesel operation that provide highest NHR

| Engine speed	Brake Torque	Operation mode	Fuel-Air equivalent ratio		Substitution
Rev/min	(Nm)		ϕg	ϕt	Sub (%)
1250	40	DL3	0.11544	0.31127	34.0
	30	DL3	0.11544	0.27634	36.8
	20	DL3	0.11558	0.22976	45.9
	10	DL3	0.11556	0.18692	58.0
2000	70	DL4	0.14220	0.45481	27.6
	40	DL4	0.14207	0.35294	31.7
	30	DL4	0.14231	0.31653	35.3
	20	DL4	0.14217	0.27998	40.2
2750	70	DL3	0.11321	0.46243	21.2
	40	DL3	0.11325	0.35841	24.8
	30	DL4	0.13801	0.33638	32.8
	20	DL3	0.11361	0.29298	30.9

@ The peak of pressure and pressure rise rate, cyclic variation:

Since the test engine is an IDI engine, the peaks of cylinder pressure and pressure rise rate pressure in the engine cycle may be the one produced by the combustion process or due to compression and they depend on engine torques. If the peaks of pressure are caused by compression, the peaks in dual fuel modes were lower than that in diesel modes. Conversely, if they are caused by combustion they tend to be higher than that in neat diesel fueling.

In dual fuel modes, if the peaks of PRR are caused by compression they are similar to that in diesel modes and appear approximately around 12°CA bTDC (Figure 7–45). Combustion process maintains the high pressures generated by compression. In these cases, the PRR is negative in the combustion period and may reach a local

maximum value close to that in the compression stroke. Statistical analysis for chamber pressure is shown in Figure 7–56 to Figure 7–60. Following features can be recognized:

- The mean values of maximum pressures in main and pre chamber in neat diesel and dual fuel modes are not much different, within few bars in cases the peaks were produced by combustion.

- At 1250rev/min, the STD and COV of the peak of pressure in both chambers at 1250rev/min were small, within 1% and those of PRR were within 3%.

- At 2000 and 2750rev/min, the COV of peak main chamber pressure was higher with dual fuel and seemed to increase proportionally with LPG ratio, but still within 3%. The COV in PRR in main chamber was comparable for neat diesel and dual fuel, seemed unchanged around approximate 45%.

- The STD and COV of the peaks of prechamber pressure seemed comparable in neat diesel and LPG-diesel modes, within about 2.8%.

- The STD and COV of PRR in prechamber seemed to increase proportionally with LPG ratio. These COV at 1250 rev/min were the lowest, followed by that at 2750 rev/min (within 5%), then those at 2000 rev/min (up to about 12%).

The COV_{IMEP} are presented in Figure 7–61, Figure 7–62, and Figure 7–63 for 1250, 2000, and 2750 rev/min, respectively. The following trends in COV_{IMEP} are addressed:

- The COV_{IMEP} seemed to increase proportionally with LPG ratio at all speeds.

- At 1250 and 2750 rev/min, the maximum of COV increased from about 1.6%, corresponding to neat diesel to about 5%, corresponding to mode L4 of LPG supply.

- At 2000 rev/min, there were dramatically increases of the COV_{IMEP}, from about 1.6%, with neat diesel to about 15%, corresponding to mode L4 of LPG supply.
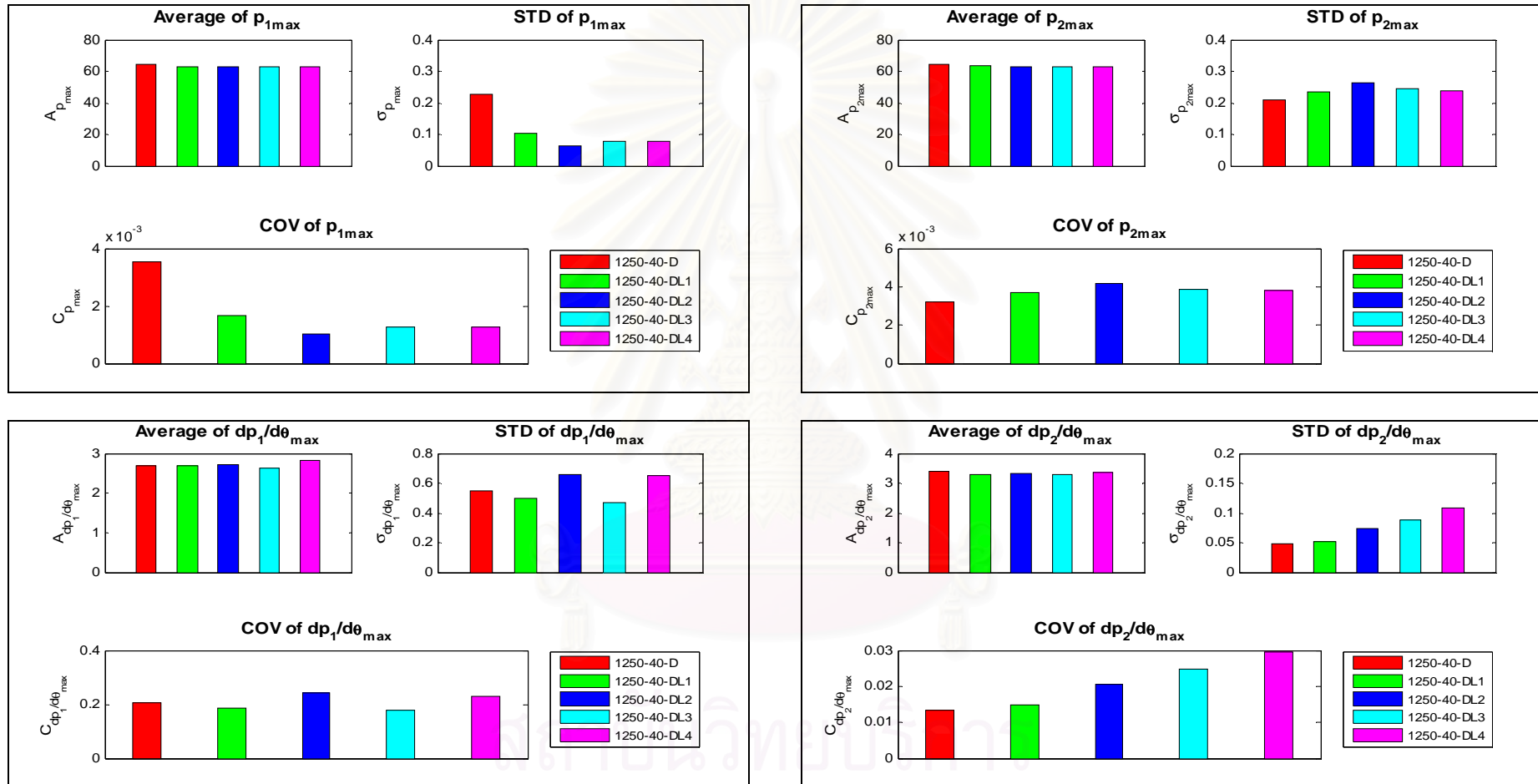
Figure 7–56   Average, STD, and COV of chamber pressure and PRR at 1250rev/min, 40Nm (diesel and LPG-diesel)
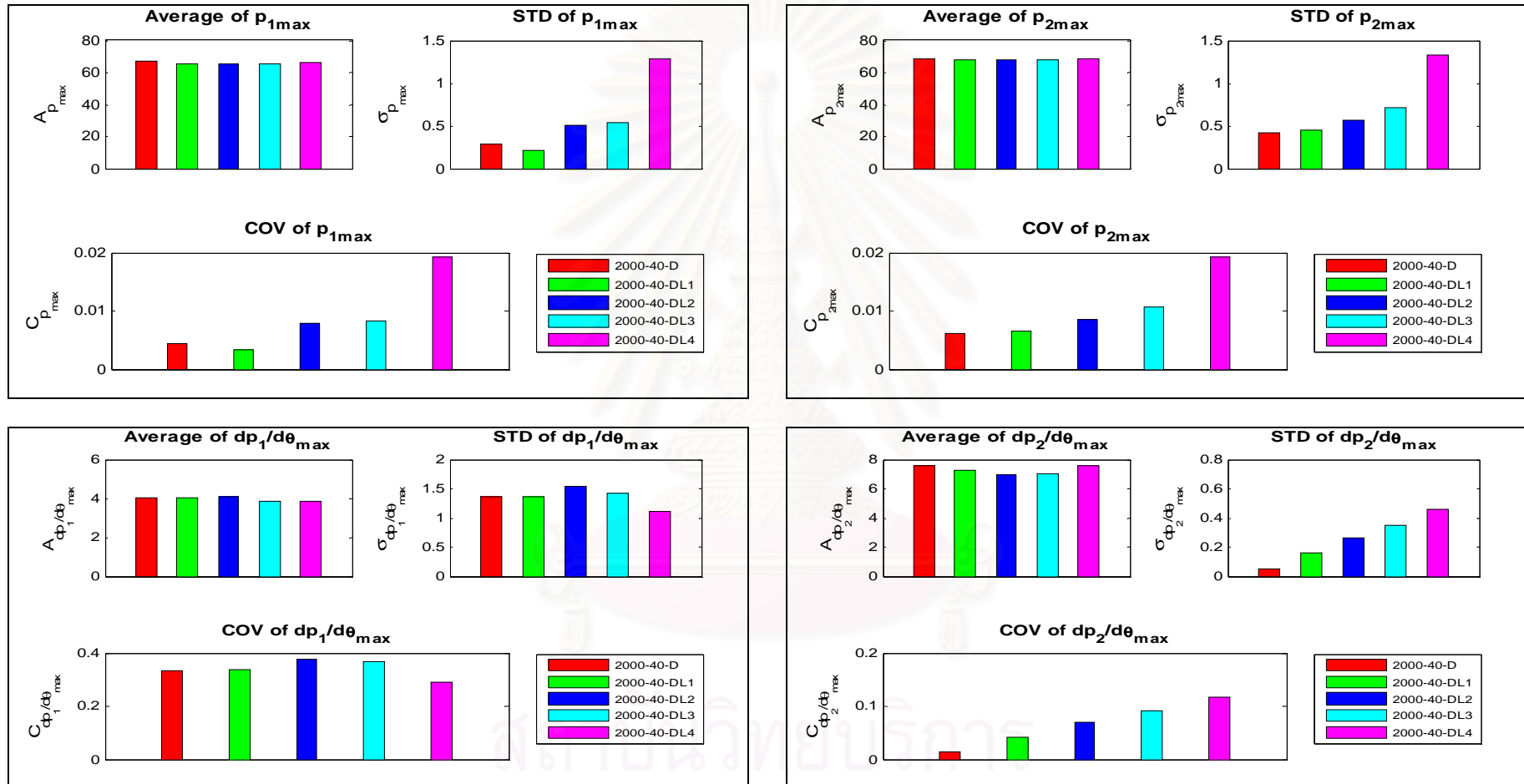
Figure 7–57   Average, STD, and COV of chamber pressure and PRR at 2000rev/min, 40Nm (diesel and LPG-diesel)
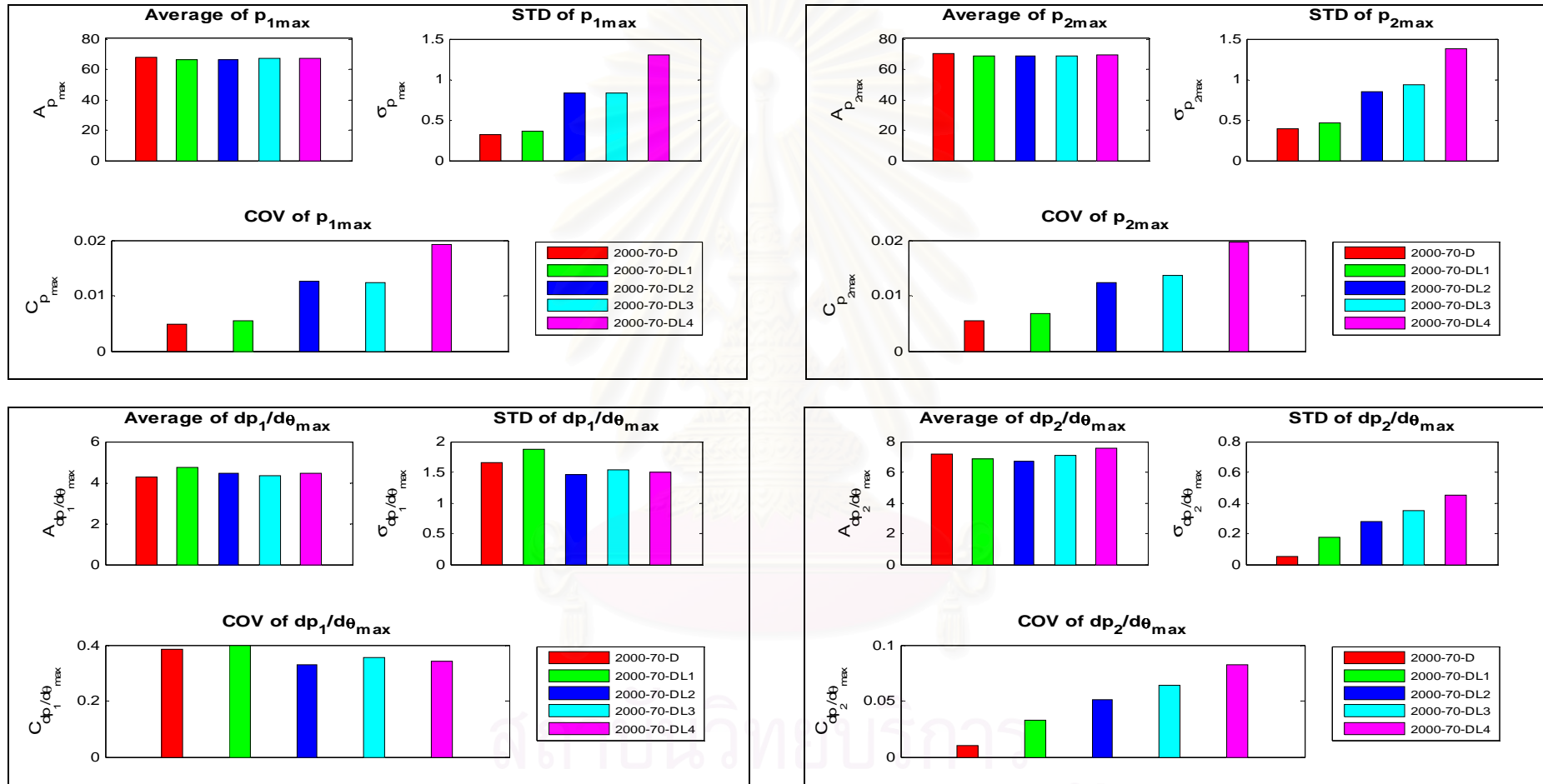
Figure 7–58   Average, STD, and COV of chamber pressure and PRR at 2000rev/min, 70Nm (diesel and LPG-diesel)
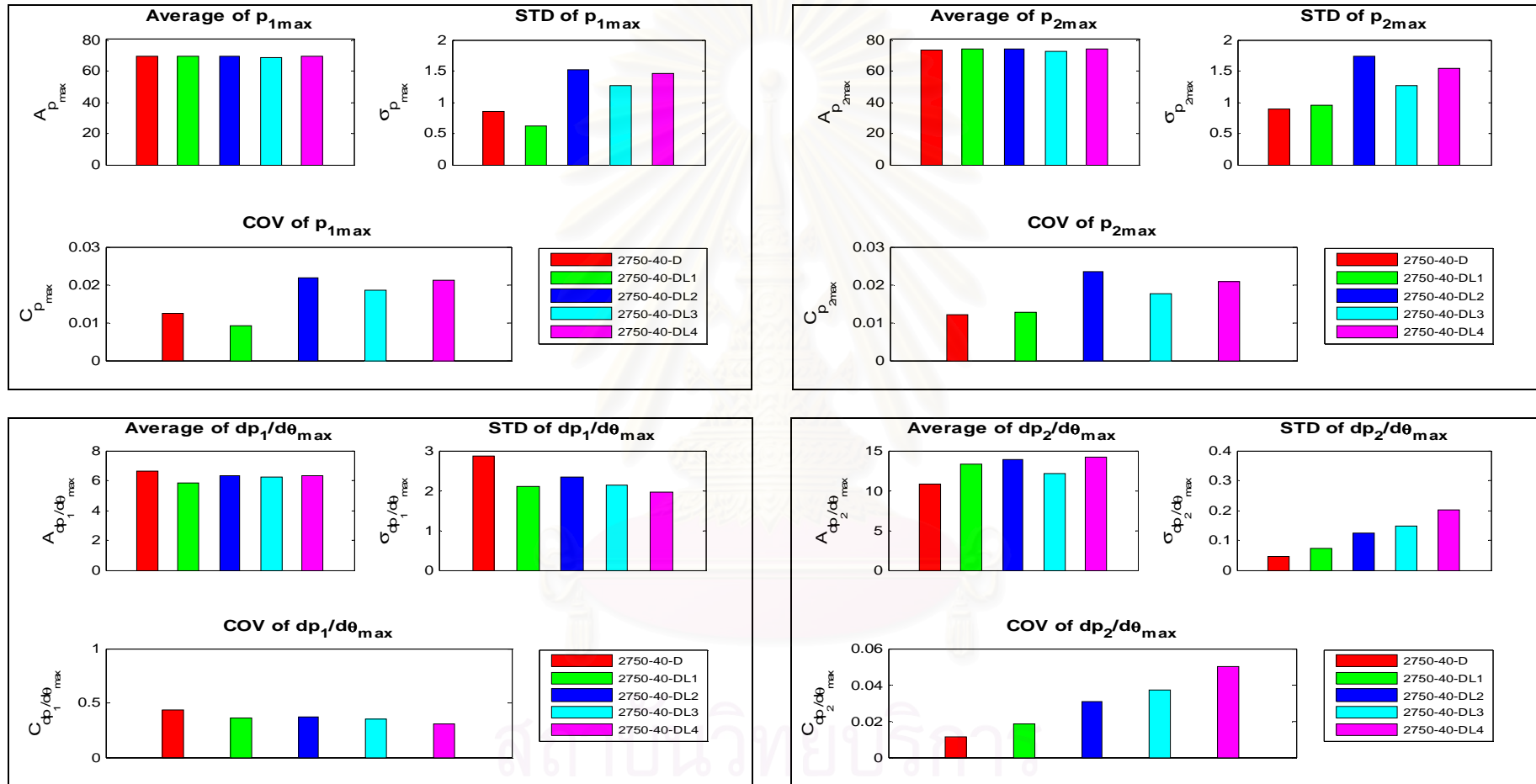
Figure 7–59   Average, STD, and COV of chamber pressure and PRR at 2750rev/min, 40Nm (diesel and LPG-diesel)
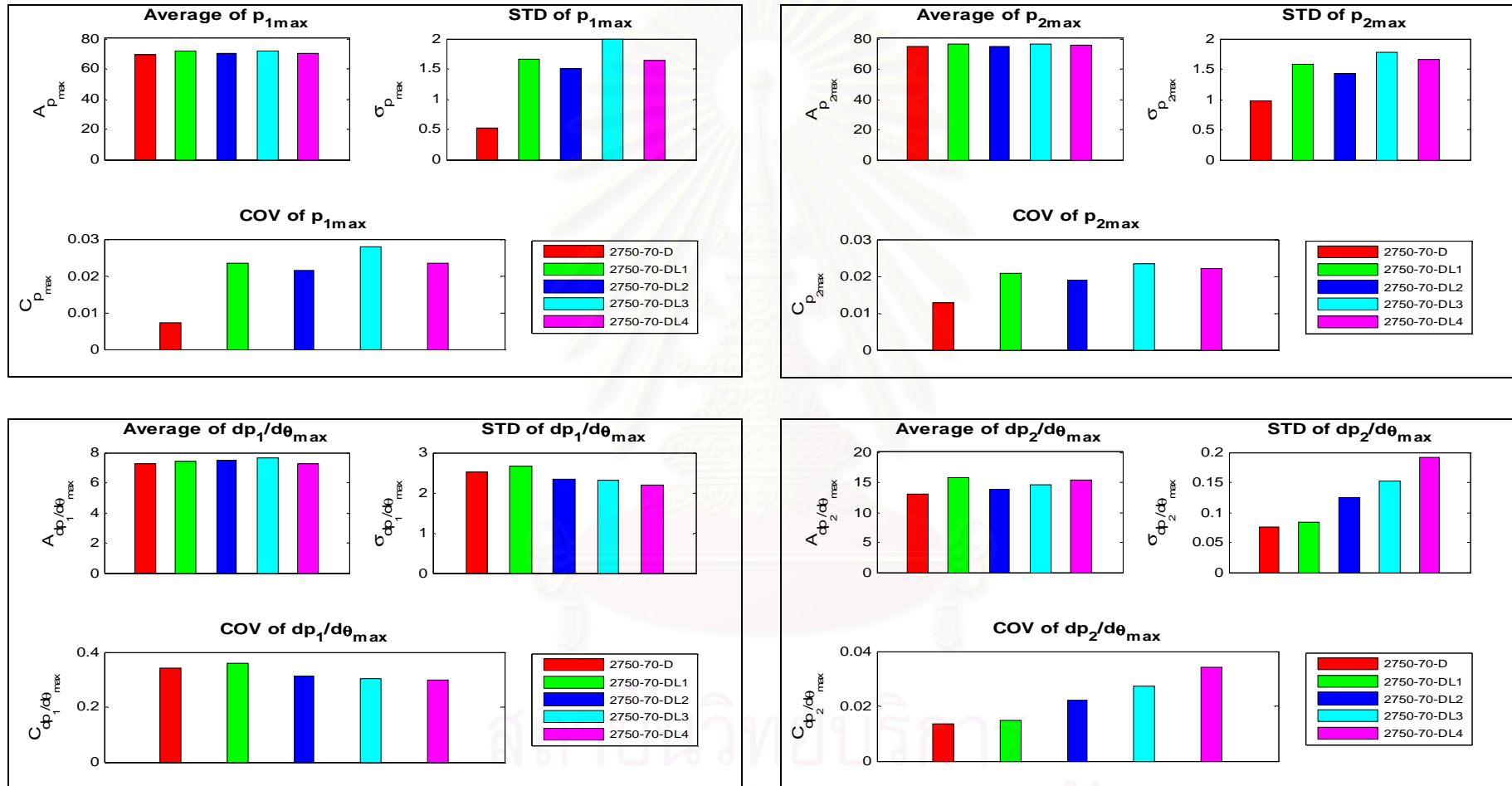
Figure 7–60   Average, STD, and COV of chamber pressure and PRR at 2750rev/min, 70Nm (diesel and LPG-diesel)
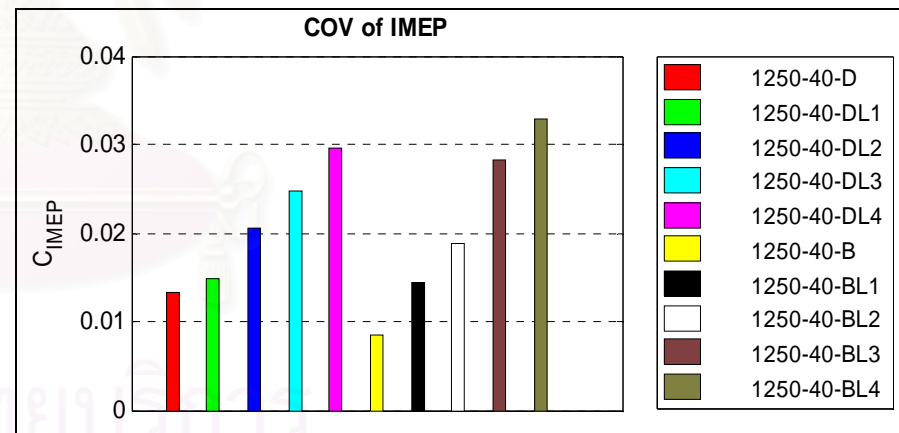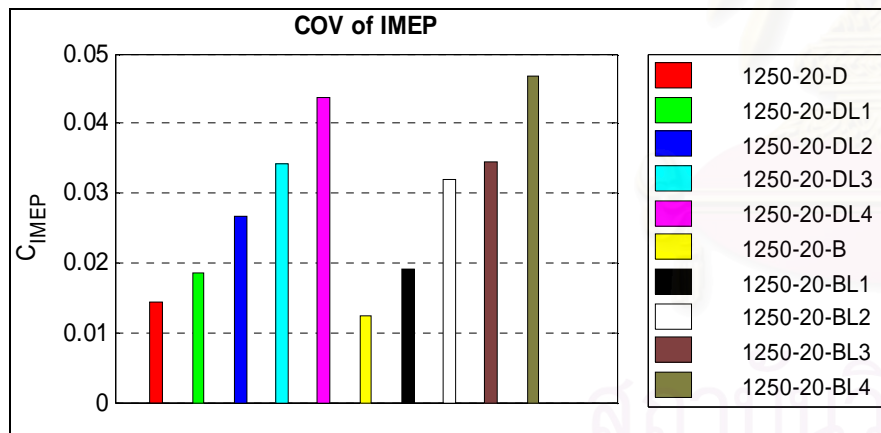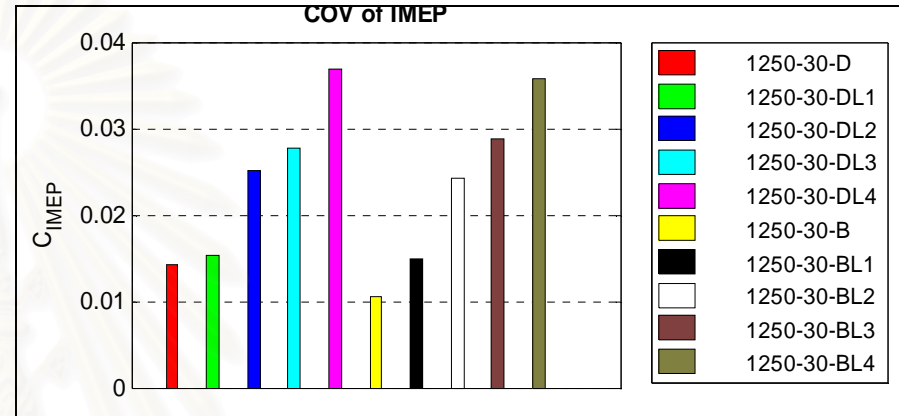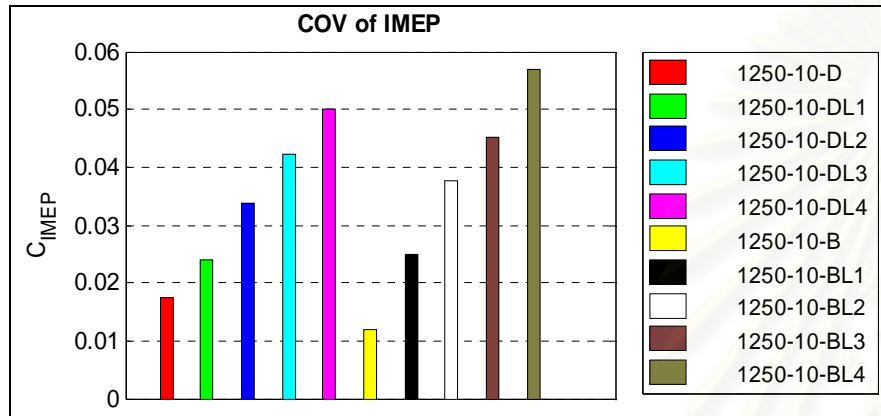
Figure 7–61   COV$_{IMEP}$ at 1250rev/min # Diesel, PME, LPG-diesel, and LPG-PME
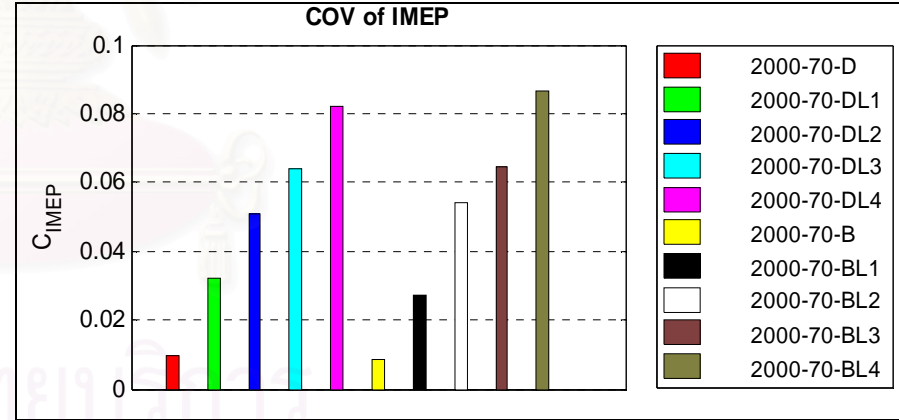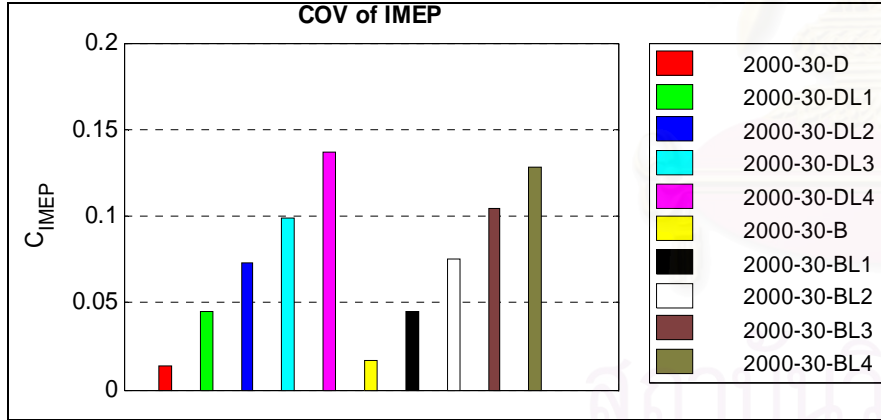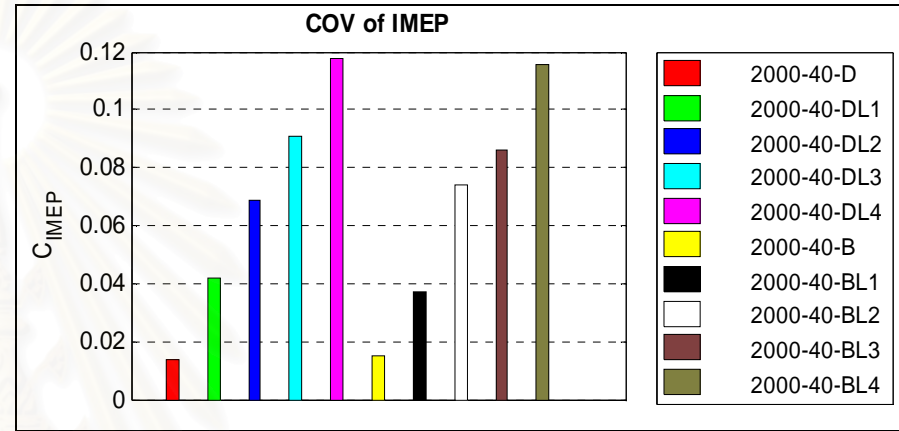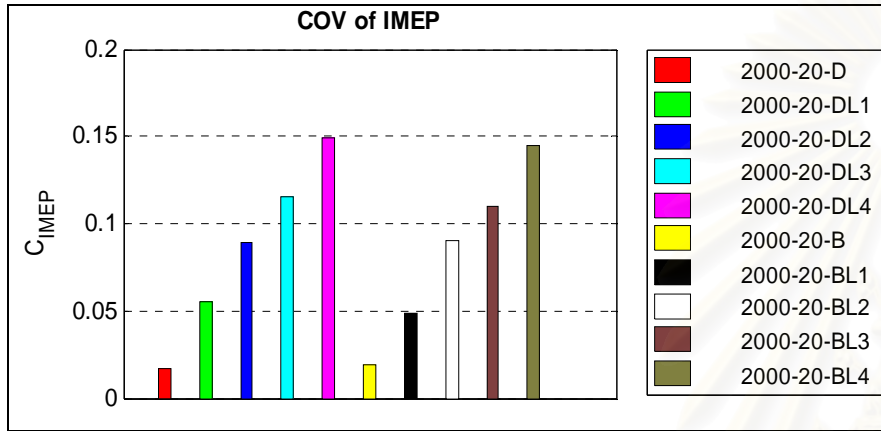
Figure 7–62   COV$_{IMEP}$ at 2000rev/min # Diesel, PME, LPG-diesel, and LPG-PME
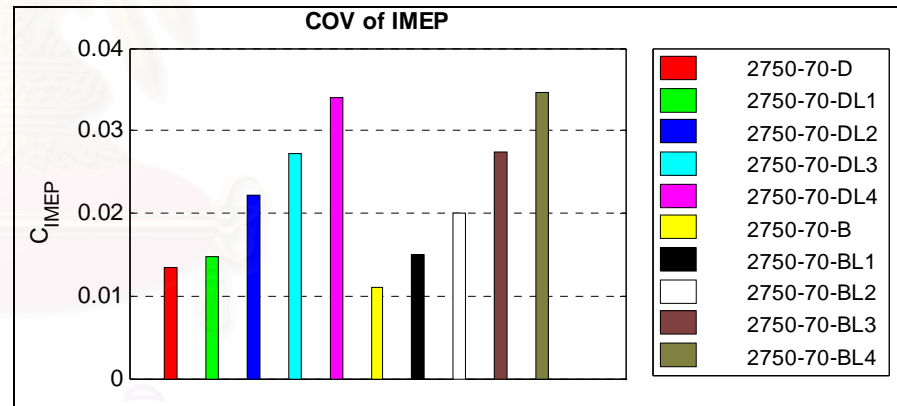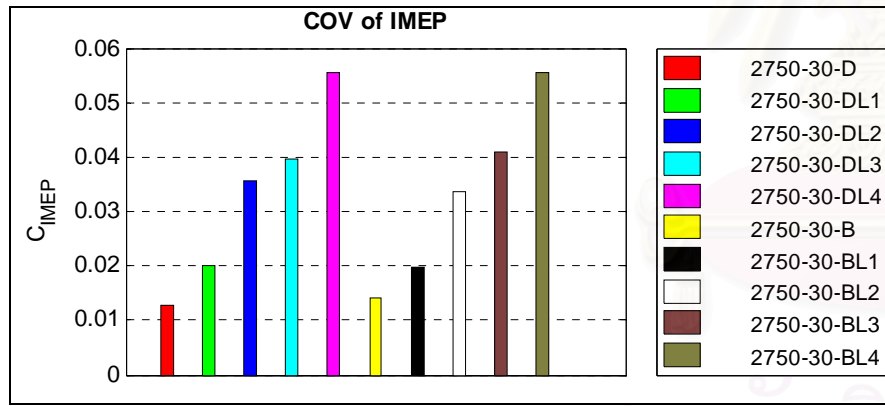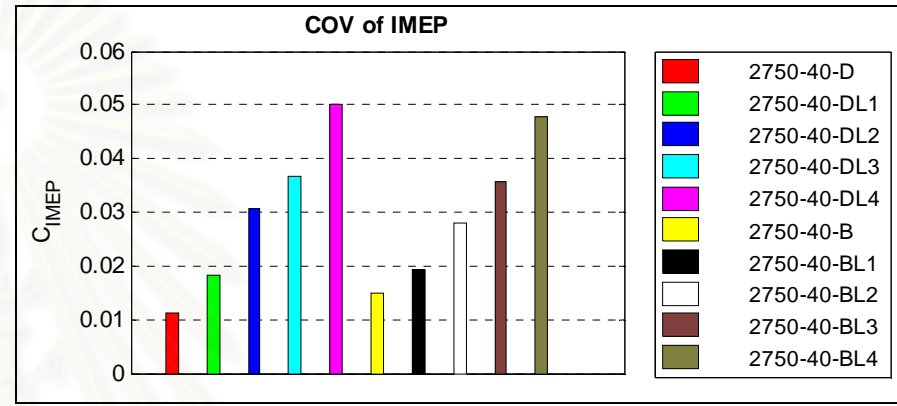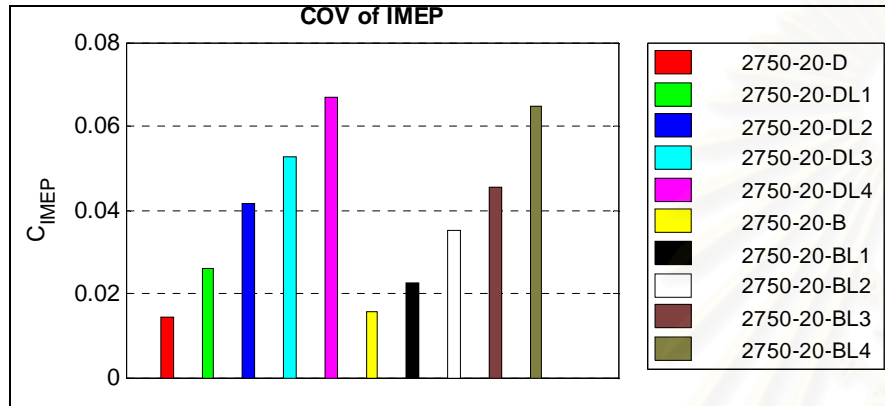
Figure 7–63   COV$_{IMEP}$ at 2750rev/min # Diesel, PME, LPG-diesel, and LPG-PME
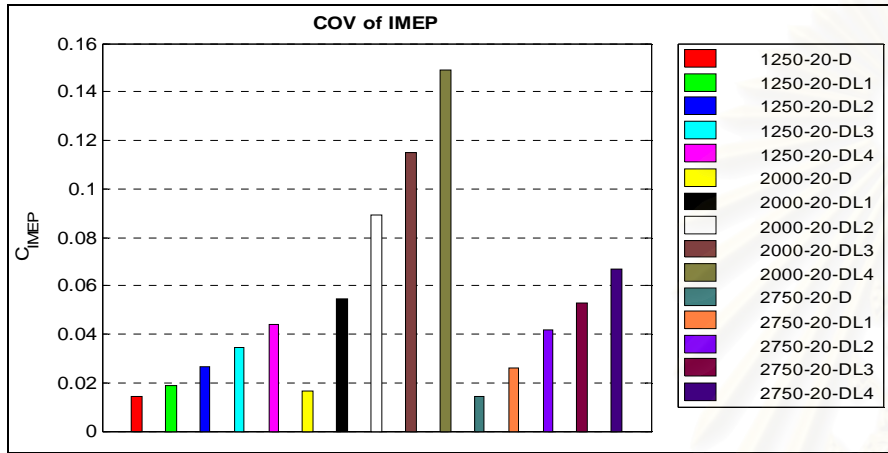
Figure 7–64   COV$_{IMEP}$ at 20Nm, different speeds (Diesel, LPG-diesel)
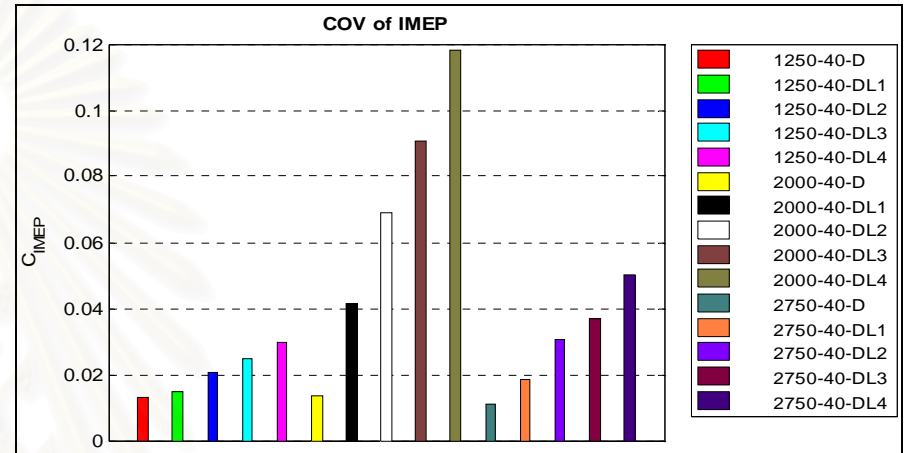
Figure 7–66   COV$_{IMEP}$ at 40Nm, different speeds (Diesel, LPG-diesel)
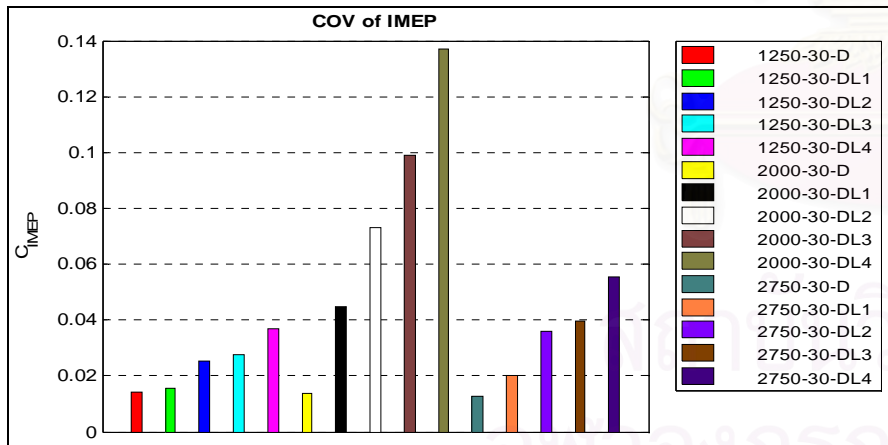
Figure 7–65   COV$_{IMEP}$ at 30Nm, different speeds (Diesel, LPG-diesel)
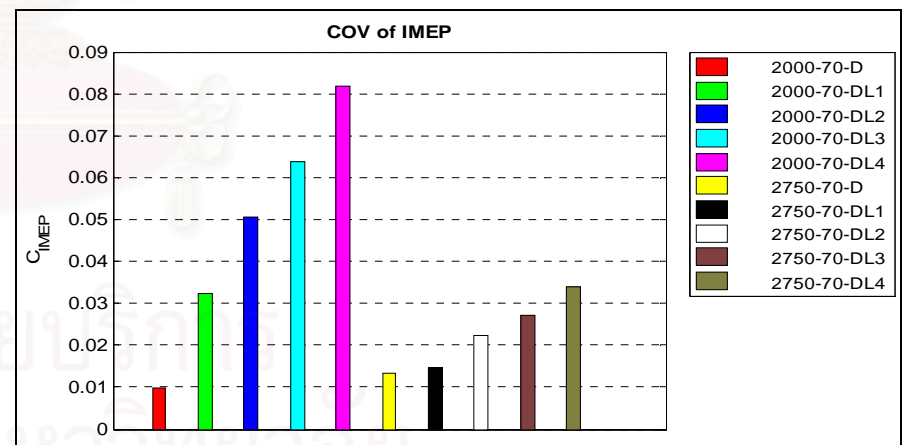
Figure 7–67   COV$_{IMEP}$ at 70Nm, different speeds (Diesel, LPG-diesel)
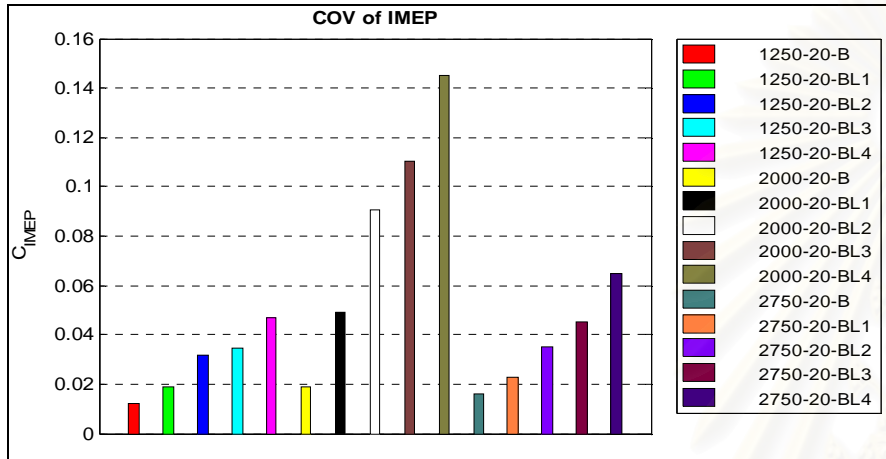
Figure 7–68 COV_{IMEP} at 20Nm, different speeds (PME, LPG-PME)
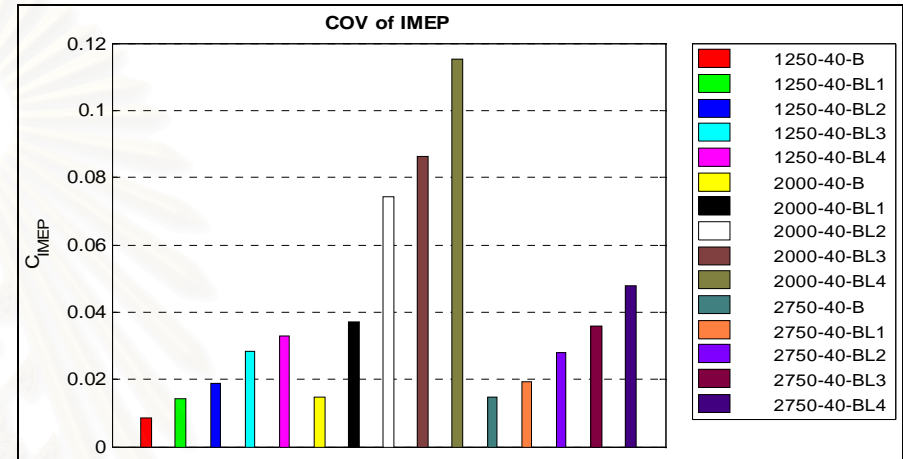
Figure 7–70 COV_{IMEP} at 40Nm, different speeds (PME, LPG-PME)
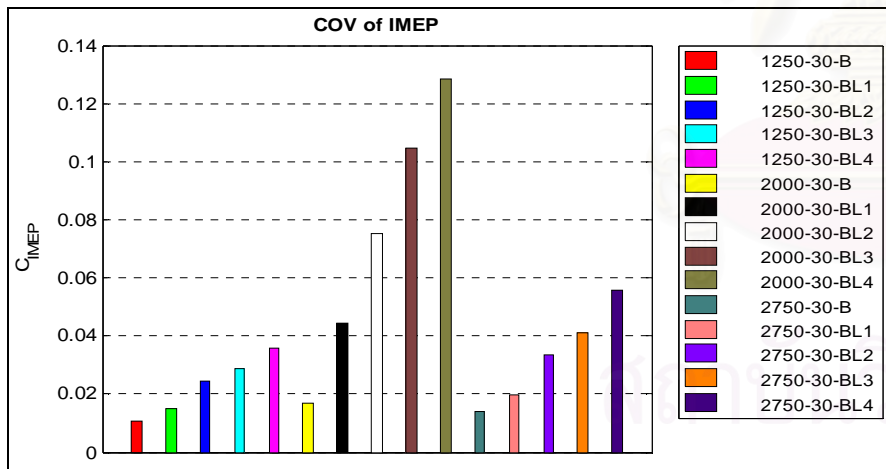
Figure 7–69 COV_{IMEP} at 30Nm, different speeds (PME, LPG-PME)
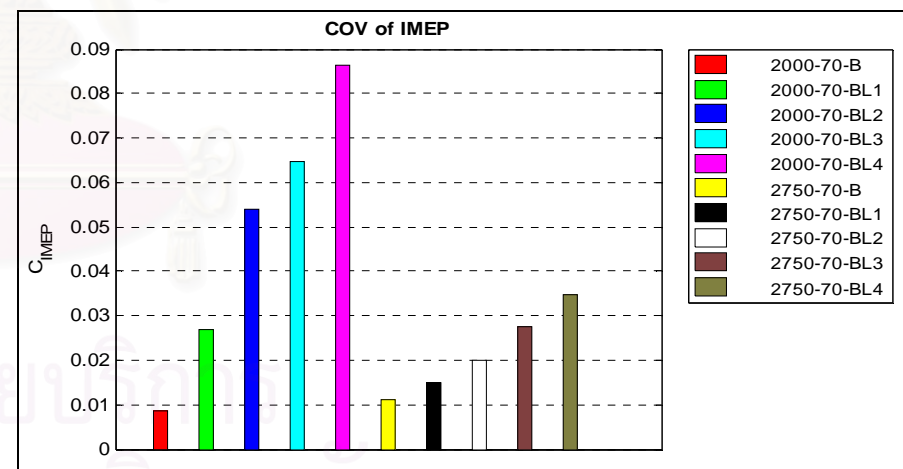
Figure 7–71 COV_{IMEP} at 70Nm, different speeds (PME, LPG-PME)

7.1.3.4. The effect of engine speed on HR characteristic

Comparison in HRR characteristics with respect to the three different speeds is depicted from Figure 7–72 to Figure 7–74 corresponding to engine brake torques of 20, 40, and 70Nm. The time interval corresponding to one degree at 1250, 2000, and 2750 rev/min are 133.3, 83.3, and 60.6 μs, respectively.

Since the operation at the same torque but higher speed requires larger amount of energy, the amount of fuel injection per cycle (in cases presented in each Figure) increased with engine speed. The cooling effect of diesel heating and vaporization caused zigzag which started few degrees aTDC at the left part of the HRR curve. The larger liquid fuel injection mass the more zigzag can be seen. Meanwhile, the injected fuel in the pre chamber was strongly mixed with the air due to its initial momentum and the swirl which is proportional with engine speed. After the zigzag the fuel combusted rapidly, producing sharp increase in the HRR. This period is a part of the mixing-controlled combustion stage which ends approximate 10°CA later. Hence, the rate of change in the HRR before its peaks as well as the peak of HRR depends on the amount of liquid fuel/ engine speed. As observed, these highest values were at 2750 rev/min, followed by that at 2000 and 1250 rev/min.

The values of HRR in the zigzag area tended to be higher at higher speed, higher LPG ratio. This may be due to following reasons. At higher speed, the engine temperature is higher, the effect of blow-by and heat transfer during compression from working fluid to the wall become lesser (higher compression pressure, as seen in Figure 7–38), leading to relatively less cooling effect while a larger amount of liquid fuel continues to burn. In addition, with dual fuel modes the homogeneous mixture in the vicinity of ignition sources burns immediately and contributes to the total HRR.

The rate of change in HRR in rapid-increase period tended to increase with increased engine speed. With all the torques, the HRR curves corresponding to 2750 rev/min increased sharply after the zigzags even they were depressed and became lower at the end of the zigzags compared to that in other two speeds. Whereas significant differences in the peaks of HRR at the same torque and different speeds were observed in diesel operation, the reverse was true in dual fuel modes.
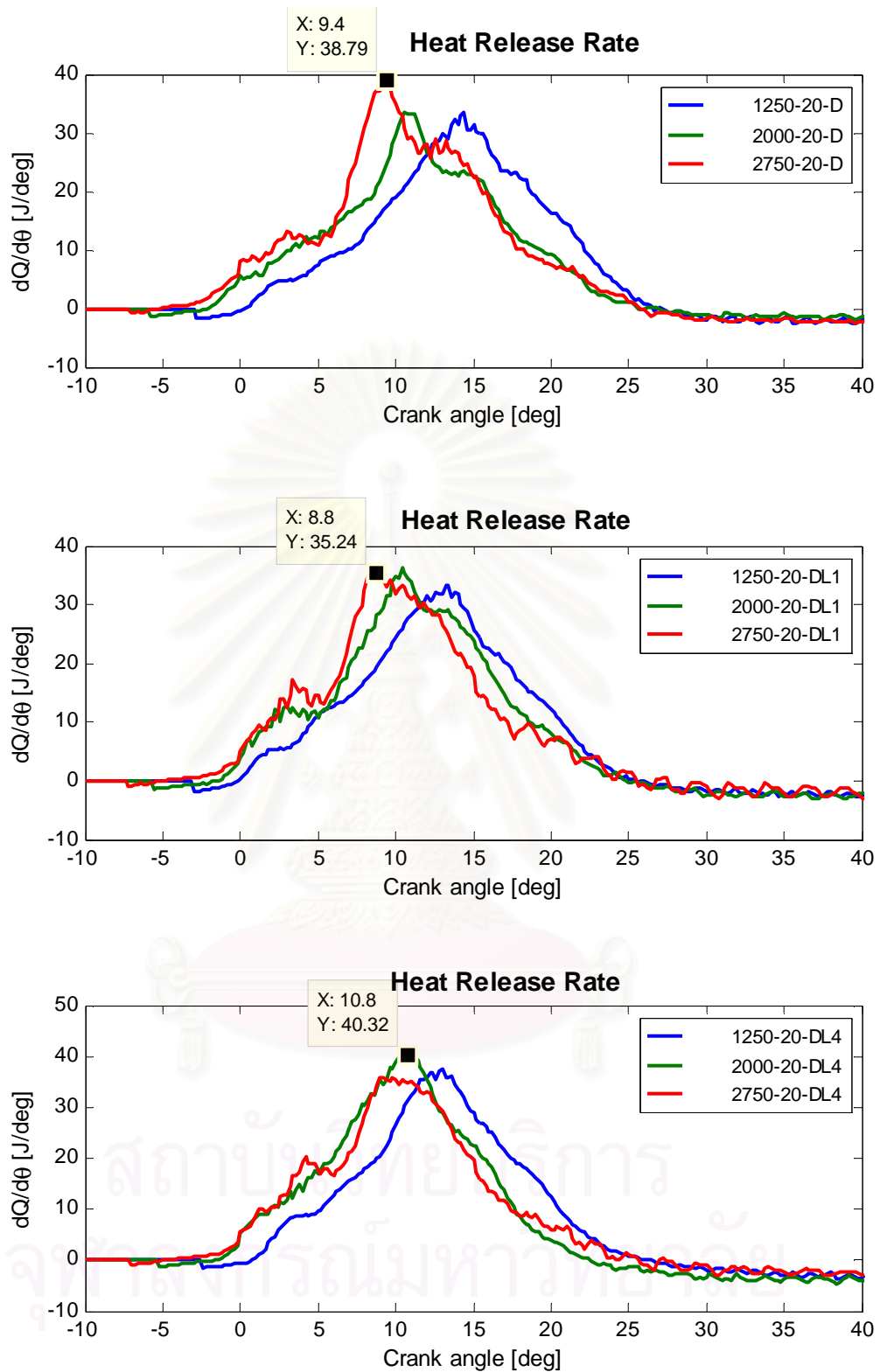
Figure 7–72   Comparison in HRR at 20Nm, different speeds (diesel and LPG-diesel)
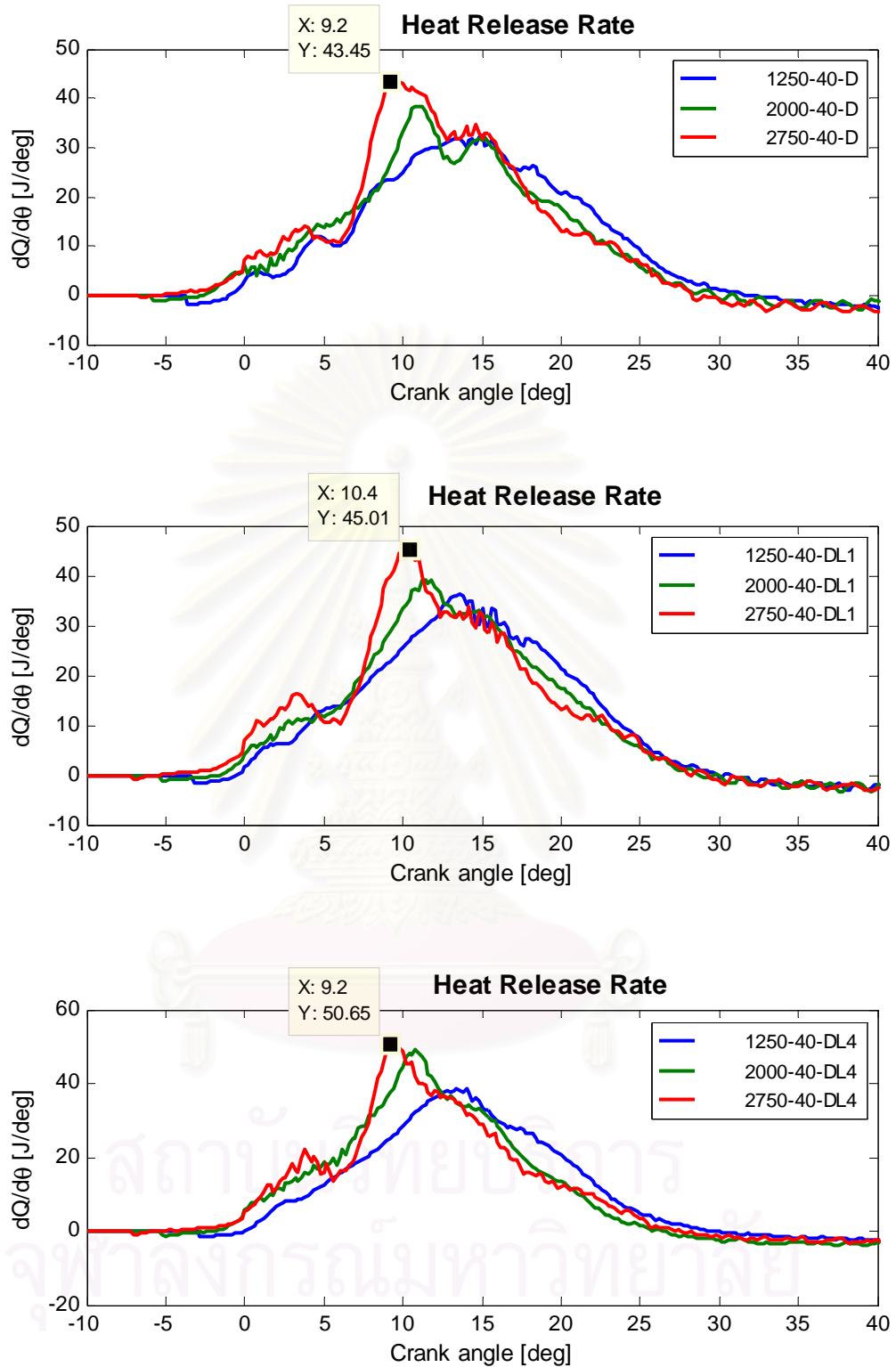
Figure 7–73   Comparison in HRR at 40Nm, different speeds (diesel and LPG-diesel)
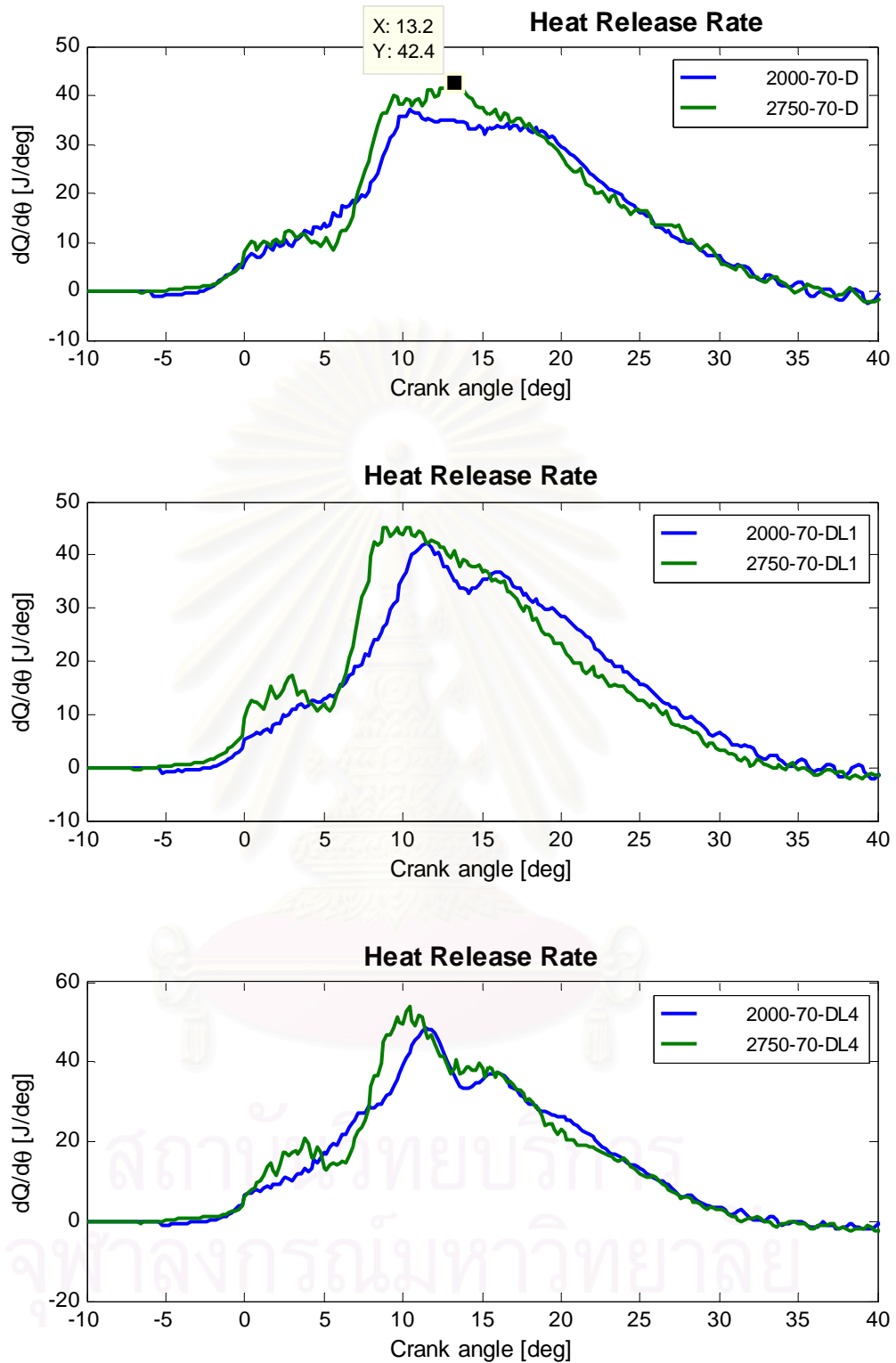
Figure 7–74   Comparison in HRR at 70Nm, different speeds (diesel and LPG-diesel)

7.2.   Effect of the biodiesel on the combustion characteristic of LPG-PME operation

Engine operation with four fixed values of the mixture strength of the LPG-air premixed charge, same as that in LPG-diesel modes at different engine loads and speeds (as described in Section 4.3) had been established and compared to the corresponding LPG-diesel modes.

7.2.1.   Engine performance and energy consumption

The engine could also operate at all planned test points and LPG flow rates without end-gas knocking. The highest biodiesel substitutions at 1250, 2000, and 2750 rev/min were about 60%, 45%, and 38%, respectively. Figure 7–81, Figure 7–82, and Figure 7–83 depict the energy conversion efficiencies in neat diesel modes and energy conversion efficiency fraction corresponding to neat PME and LPG-PME modes at the three engine speeds. The fractions presented here are the ratios between energy conversion efficiencies in the considered modes and that in the corresponding neat diesel modes. There was deterioration trend in the energy conversion efficiency in neat PME as well as LPG-PME operation, similar to that observed with LPG-diesel operation. The relative deterioration was much lower as the engine load increased. At each fixed speed, the deterioration increased as the LPG ratio increased. As revealed, at 1250 rev/min the deterioration was about 8% to 1% in neat PME modes and from 22.5% to 9% as the load increased from 10 to 40Nm in LPG-PME modes. Similarly, the decrease at 2000 rev/min was from 7% to 1% in neat PME modes, and from 13.5% to 6% in LPG-PME modes, as the load increased from 10 to 70Nm. Those at 2750 rev/min were from 4.6% to 4% in neat PME and from 20.4% to 13.4% in LPG-PME modes.

Similar to LPG-diesel the LPG-PME dual fuel resulted in significant decreases in the exhaust gas temperature. The decreases were up to about $5^{O}C$ at 30Nm and 40Nm, 2250 rev/min (Figure 7–87), up to $7.3^{O}C$ at 70Nm, 2000 rev/min (Figure 7–88). At 1250 and 2000 rev/min, the highest decrease appeared at highest torque and mode L4 of LPG supply. At 2750 rev/min (Figure 7–89), the highest decrease appeared in mode L3 of LPG supply, reaching $12^{O}C$ at 70Nm @ mode 2750-70-L3.

The lube oil temperature was almost unchanged: its variation was within $1^{O}C$, similar to that with LPG-diesel fuelling.
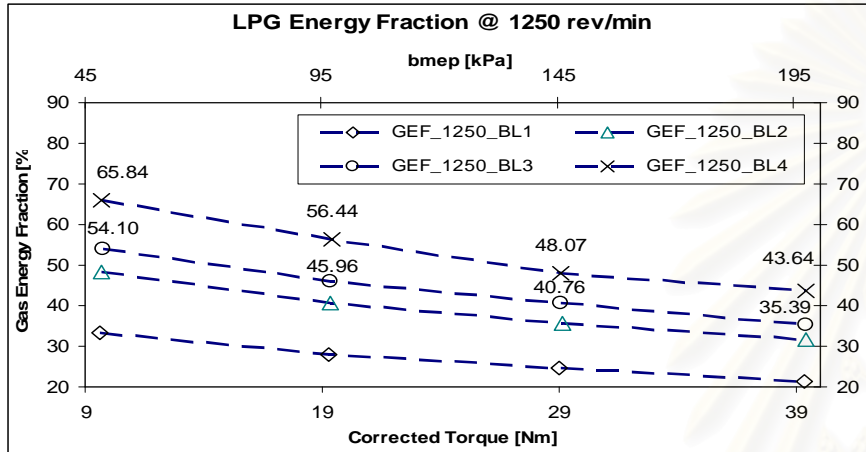
Figure 7–75   LPG energy fraction # 1250 rev/min, LPG-PME modes
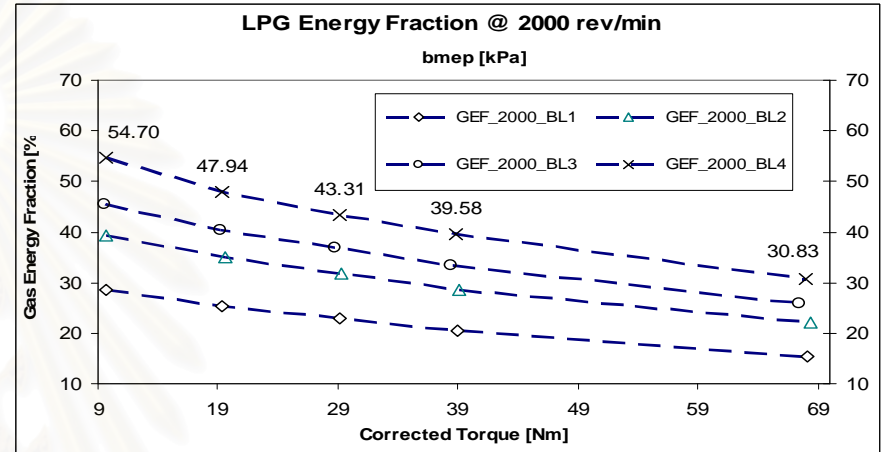
Figure 7–77   LPG energy fraction # 2000 rev/min, LPG-PME modes
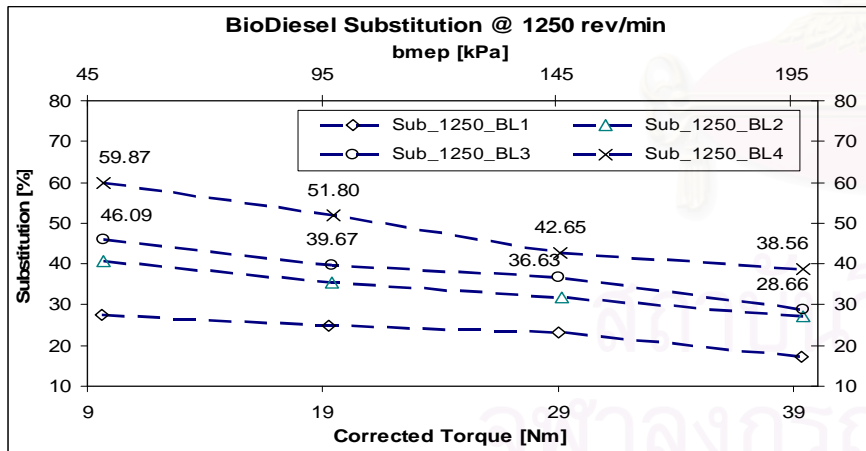
Figure 7–76   Substitution # 1250 rev/min, LPG- PME modes
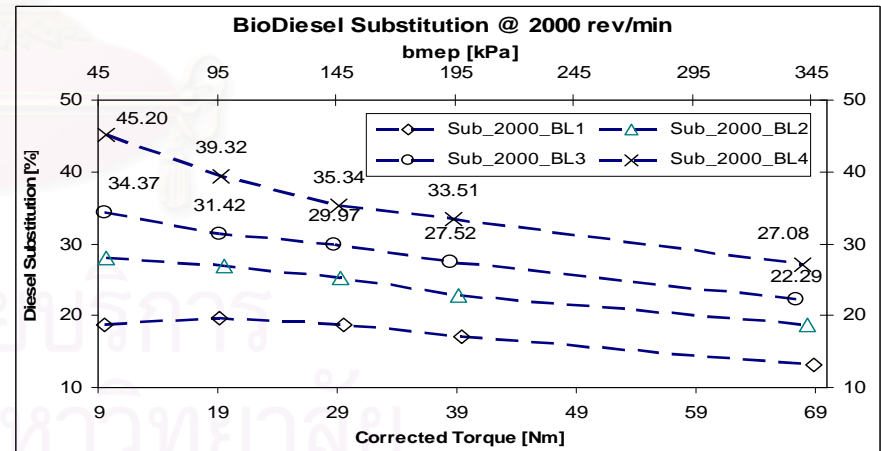
Figure 7–78   Substitution # 2000 rev/min LPG- PME modes
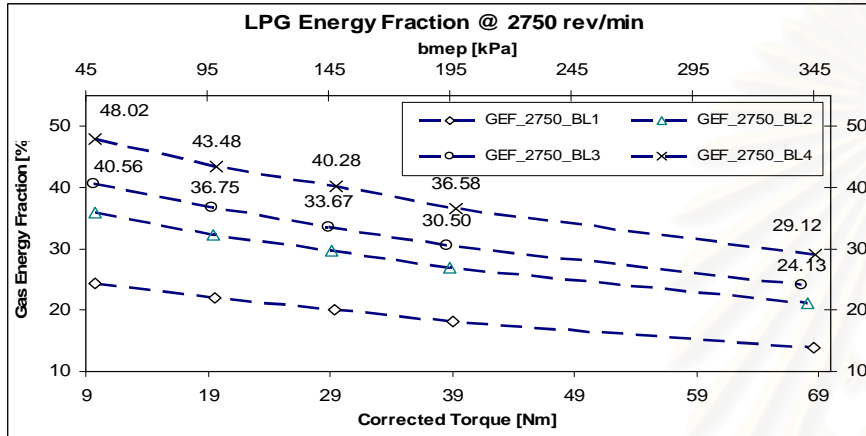
Figure 7–79   LPG energy fraction # 2750 rev/min, LPG-PME modes
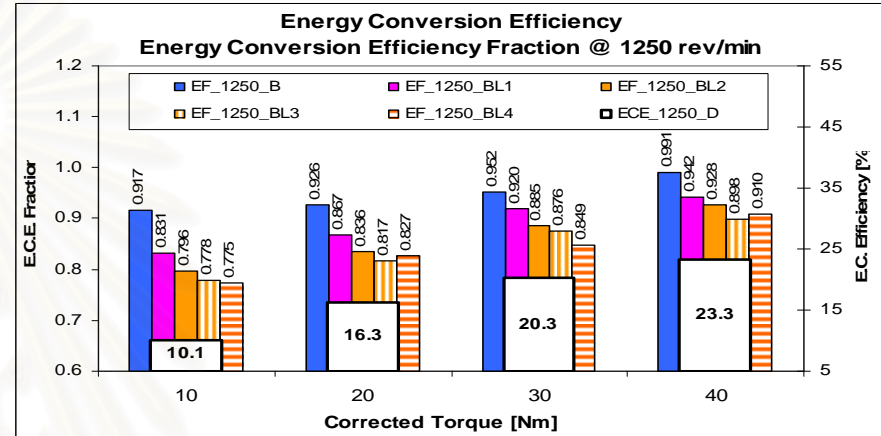
Figure 7–81   ECE # 1250 rev/min, PME & LPG- PME modes
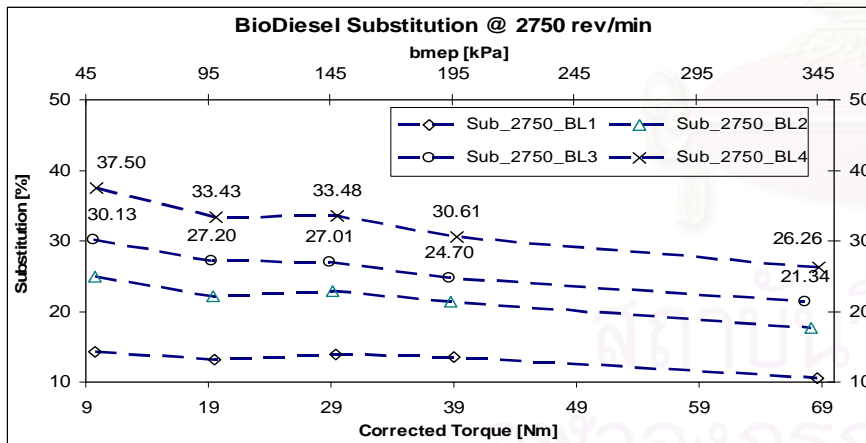
Figure 7–80   Substitution # 2750 rev/min, LPG- PME modes
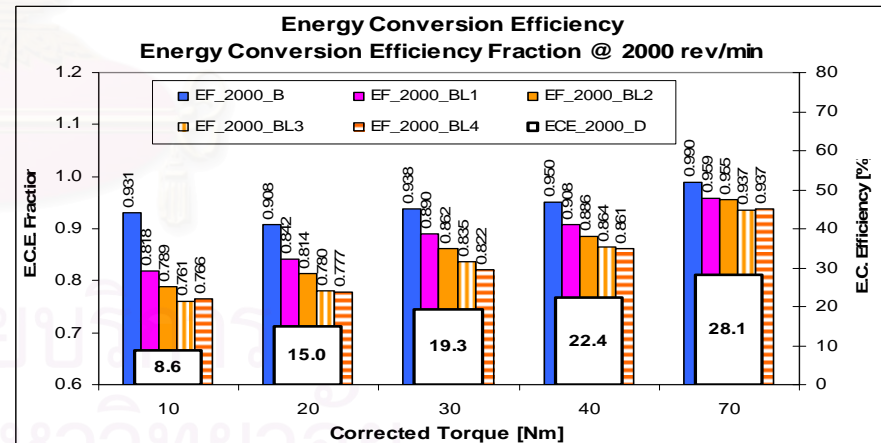
Figure 7–82   ECE # 2000 rev/min, PME & LPG- PME modes
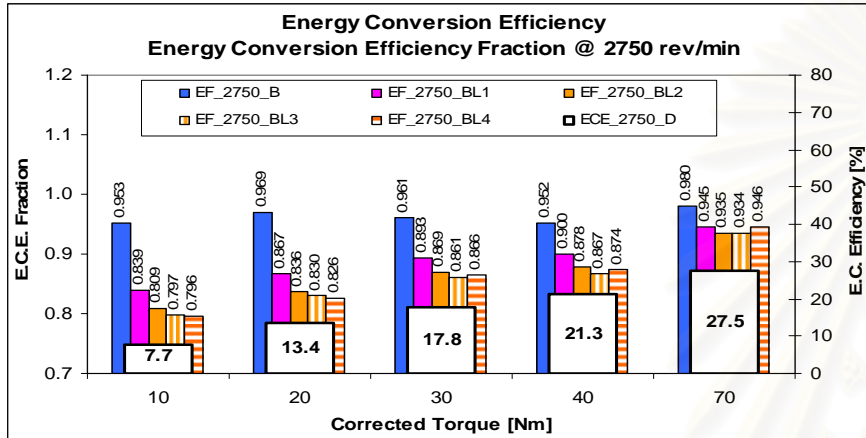
Figure 7–83   ECE # 2750 rev/min, PME & LPG- PME modes
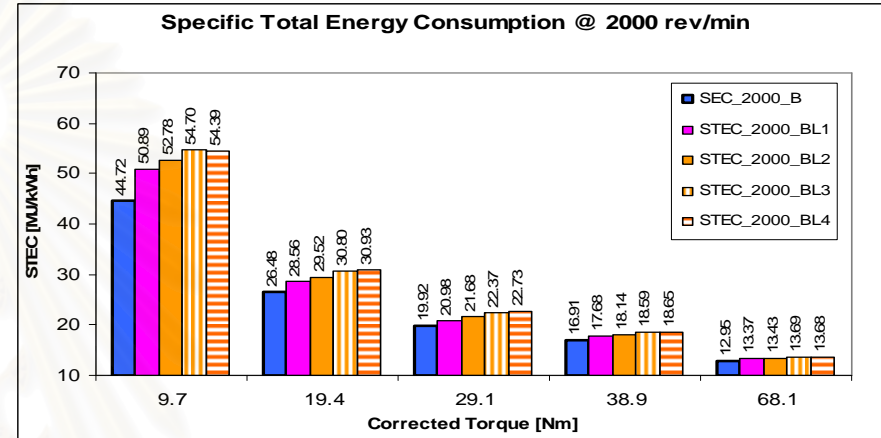
Figure 7–85   STEC # 2000 rev/min, PME & LPG- PME modes
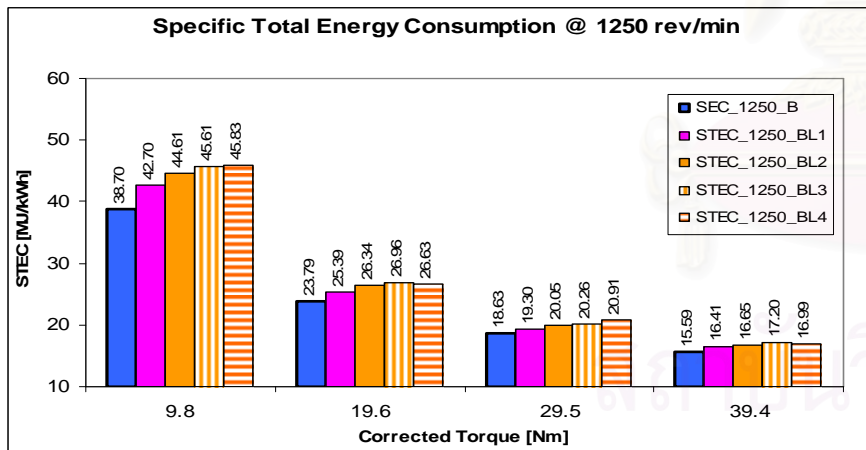
Figure 7–84   STEC # 1250 rev/min, PME & LPG- PME modes
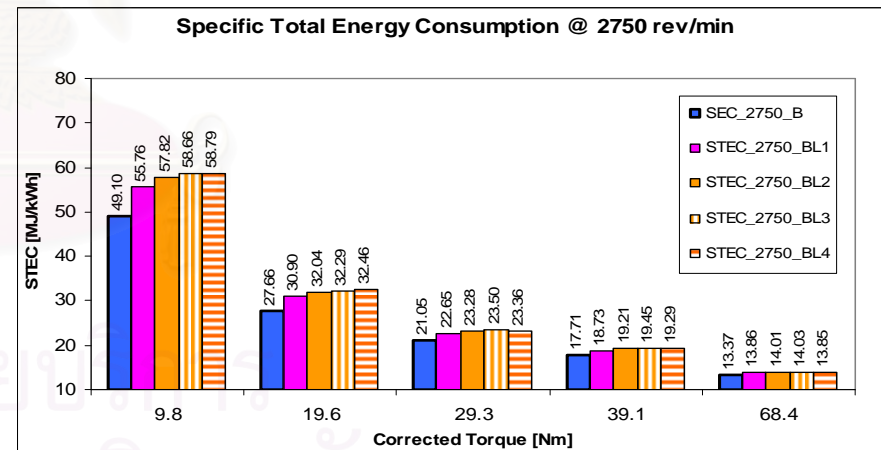
Figure 7–86   STEC # 2750 rev/min, PME & LPG- PME modes
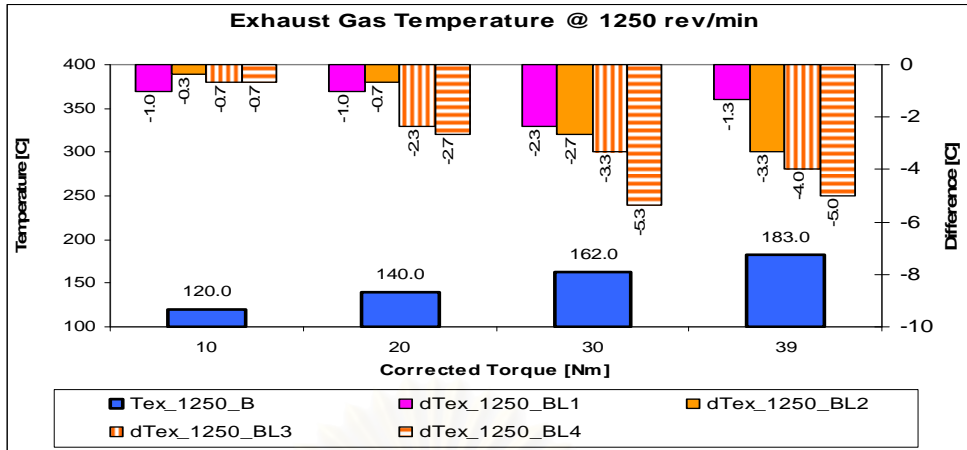
Figure 7–87   Exhaust-gas temperature # 1250 rev/min, PME and LPG-PME
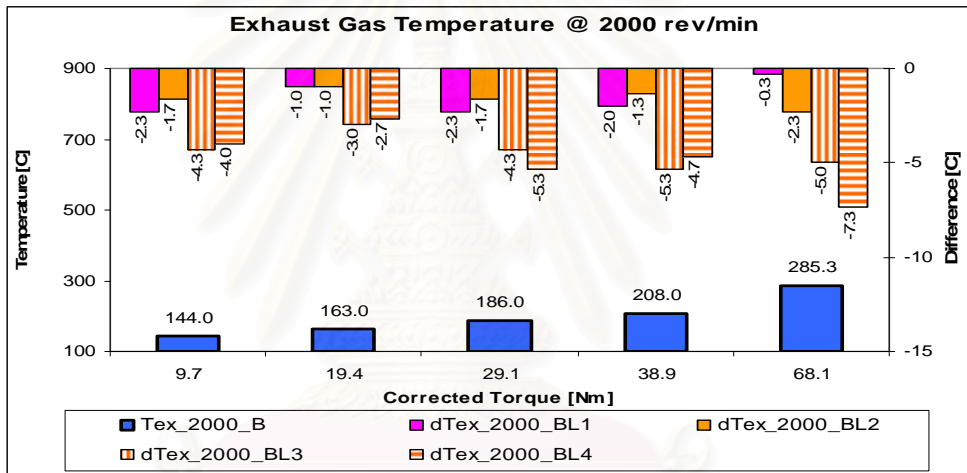
Figure 7–88   Exhaust-gas temperature # 2000 rev/min, PME and LPG- PME
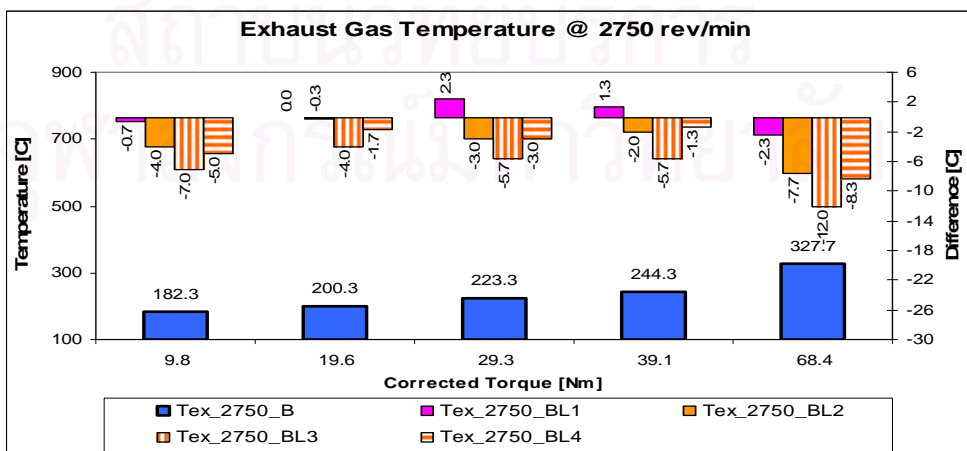
Figure 7–89   Exhaust-gas temperature # 2750 rev/min, PME and LPG- PME
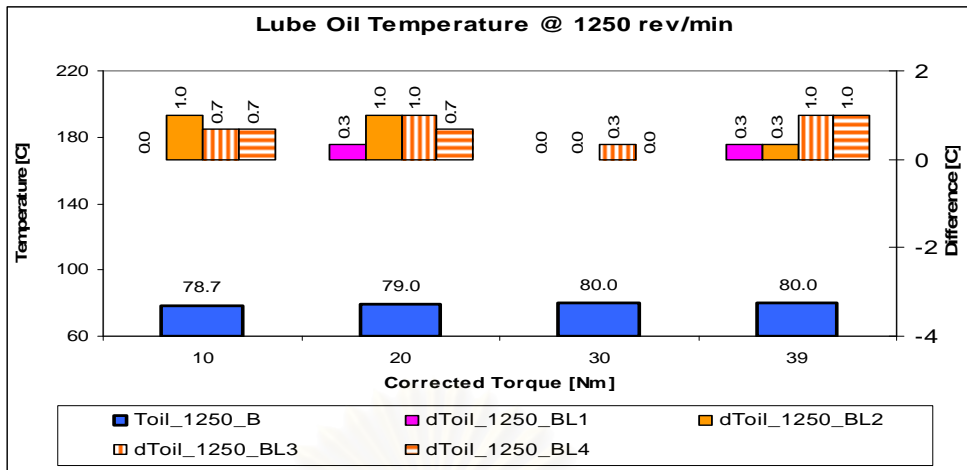
Figure 7–90   Lube-oil temperature # 1250 rev/min, PME and LPG-PME
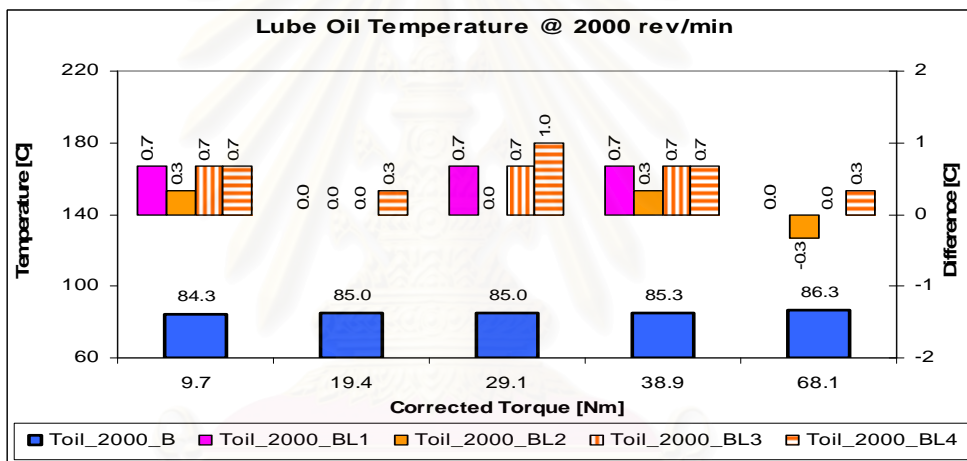
Figure 7–91   Lube-oil temperature # 2000 rev/min, PME and LPG-PME
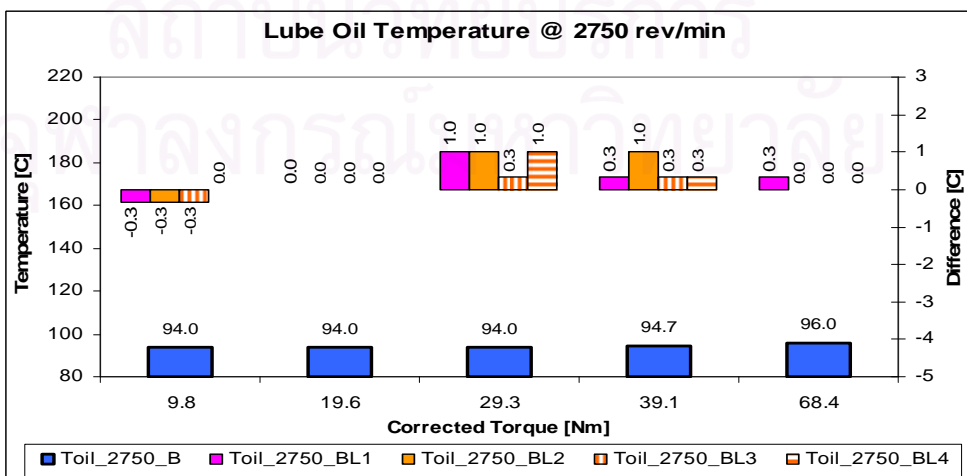
Figure 7–92   Lube-oil temperature # 2750 rev/min, PME and LPG-PME

7.2.2. Behavior of the fuel injection system with the PME

At the same condition of engine speed, torque, and fuel system setting, the injection timing in PME and LPG-PME modes was always earlier that that in diesel and LPG-diesel modes. This is thought due to the resultant effects of the PME properties. It has higher viscosity, higher adiabatic bulk modulus, higher density, and lower heating value compared to the diesel, as seen in Table 3-3 and Table 3-4.

The speed of sound is proportional to the square-root of the adiabatic bulk modulus, and inversely proportional to the square-root of the fuel density. The higher viscosity of the PME tends to reduce the leakage (crevice flow) and effective sectional area of the flow in the fuel system, resulting in higher pressure in the fuel line. The lower heating value of PME causes larger volume of fuel injected per engine cycle, leading to longer injection duration, thus, higher pressure in the fuel line.
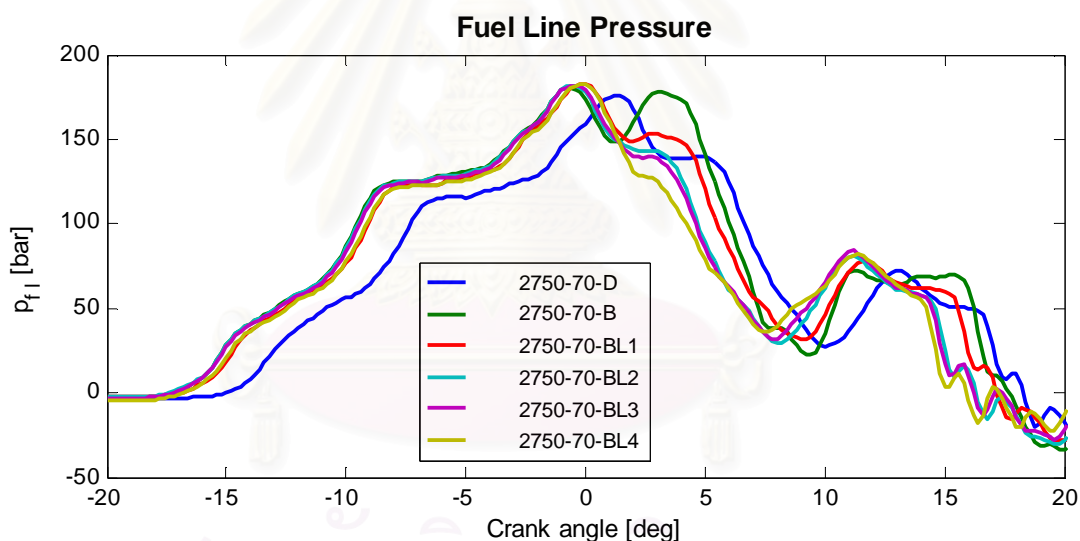
Figure 7–93   Fuel line pressure at 2750 rev/min, 70 Nm (diesel, PME, LPG-PME)

Typical fuel line pressures as the engine ran with the PME are presented in Figure 7–93. All values of the SOI detected by the tool "Combustion Analyzer" are shown in Figure 7–124, and Figure 7–126 for 1250, 2000, and 2750 rev/min, respectively. The advances of injection timing were in the range [0.8-2.4] $^{\circ}$CA, depending on operation mode. The changes of PME injection timing with respect to engine speed, load, and LPG ratio were similar to that in diesel and LPG-diesel fuelling.

7.2.3. Combustion characteristics

7.2.3.1. Spray combustion visualization

Comparison among twelve modes of operation has been made. They include six modes at 1250 rev/min (1250-20-D, 1250-20-DL1, 1250-20-DL4, 1250-20-B, 1250-20-BL1, and 1250-20-BL4) and six modes at 2000 rev/min (2000-20-D, 2000-20-DL1, 2000-20-DL4, 2000-20-B, 2000-20-BL1, and 2000-20-BL4).

The difference between neat diesel and neat PME operation

Firstly, consider the phenomena at 1250 rev/min. The combustion process in the prechamber in these six modes is presented in Figure 7–94 to Figure 7–98. The first and second figures present sequential direct images captured with and without flash. The predicted flame probability distribution, flame temperature distribution, and soot concentration are depicted in Figure 7–96, Figure 7–97, and Figure 7–98, respectively. Fuel line pressure analysis shows that the SOI for these six modes were -2.8, -3.0, -2.4, (Figure 7–39), -4.4, -3.8, and -3.2°CA (Figure 7–124) whereas the first AOS observed in the images with flash were -2.5, -2.5, -2.0,-4.0,-4.5, and -3.0°CA (Figure 7–94).

The PME auto-ignites and burnt few degrees just after its injection without the aid of the glow-plug. The first SOL appeared 2.0°CA after the first AOS (at -2.0°CA as seen in Figure 7–95). The corresponding ignition delay detected from the heat release analysis was 2.4°CA (Figure 7–124). The PME was injected earlier and it combust earlier than the diesel. However, once the diesel auto-ignited its combustion evolution seemed more rapid than the PME. The PME spray (Figure 7–94) revealed longer penetration and smaller angle than the diesel spray.

Observing the images from AOS until 6°CA (Figure 7–95) it is recognized that the PME flame is smaller and less luminous than diesel one. The highest luminosity of the PME flame appeared with at about 8°CA. The flame luminosity then reduced significantly in comparison to diesel flame but the flame seemed to continue longer than the diesel flame. In diesel case, although the EOL of diesel was 28.5°CA (1 degree later than the PME) it can be seen that the flame is of the main chamber. The prediction result of flame probability distribution (Figure 7–96) and the 100% of flame probability distribution (Figure 7–104) provides clear information. Although PME injection starts earlier, the PME combustion seemed less powerful and obstinate than the diesel

combustion; except at 2 and 8$^{\text{o}}$CA, the high probability in the rest images of PME flame revealed smaller size. Towards the end of combustion (from 20$^{\text{o}}$CA), the PME flame was still wider but less strong than the diesel. In addition with smaller but obstinate flame, the PME revealed lower flame temperature as observed in Figure 7–97 and Figure 7–108. The diesel torch combusts vehemently at its top, presenting flare with much more red pixels distributed with wider space at almost the top, from 6 to 10$^{\text{o}}$CA. Conversely, in the PME flame there was merely yellow circle limited by the chamber wall. Except the period from 7.5 to 9.0$^{\text{o}}$CA, the flame temperature (in both ranges above 2300K and above 2600K) in PME mode was lower than that in diesel mode. Images of the soot concentration (Figure 7–98) as well as the soot concentration trace from TDC to 25$^{\text{o}}$CA (Figure 7–111 to Figure 7–115) revealed lower soot concentration in the PME flame. The following factors may contribute to the above addressed features of the PME flame:

a. The higher viscosity may result in larger size of its droplet;

b. The higher density result in longer but narrower spray penetration;

c. The lower heating value requires larger amount of mass injected per cycle (and hence higher energy to heat it);

d. Its inherent lower volatility contribute to the worse vaporization and mixing with the air within available time during combustion process, leading to lower PME flame temperature.

e. The lower adiabatic flame temperature of PME compared to that of diesel.

At 2000 rev/min, the PME combustion process in the prechamber is presented by sequential images in Figure 7–99 to Figure 7–103: The first and second figures are for sequential direct images captured with and without flash whereas the predicted flame probability distribution, flame temperature distribution, and soot concentration are depicted in the three rest figures. The difference between diesel and PME spray and combustion at this speed is similar to that at 1250 rev/min. However, these differences seemed much higher. The illuminated direct images in Figure 7–99 show that the PME spray was longer and narrower than that of diesel. Once the combustion took place, the diesel spray rapidly spread out but the PME spray seemed to penetrate longer and impinge to the chamber wall. Although the PME injection was earlier and it combusted

earlier than the diesel, its combustion evolution was less strong as diesel's combustion. This can be seen with the comparison in direct images (Figure 7–100), flame probability (Figure 7–101 and Figure 7–116) and flame temperature distribution (Figure 7–102, Figure 7–118 and Figure 7–120). The percentage area of 100% flame probability of PME, before about 5°CA was slightly higher than that of diesel and then comparable until 11.5^{O}CA. Beyond this point, the percentage area of 100% flame probability of PME was much lower than that of diesel; about [10%-15%]. The area of flame temperature (both ranges) with PME was also much lower than that of diesel.

The development of the process with dual fuelling

Observing the sequential images at 1250 rev/min with dual fuelling in Figure 7–94, Figure 7–95, and Figure 7–96 it can also be recognized that the flame, in mode 1250-20-BL1, is even initially weaker than that in mode 1250-20-B (before 0°CA), it spreads faster and envelops almost the area, at 6 to 8°CA. In contrast, in mode 1250-20-BL4, the sequential images appear with less luminous and the flame temperature seems lower than that in the two modes 1250-20-B and 1250-20-BL1. In Figure 7–104, it can be seen that whereas the flame probability reached almost the same value as diesel combustion at 7°CA, about just over 30% in mode 1250-20-B and 1250-20-BL1, it had much lower, just about 25% in mode 1250-20-BL4. In mode 1250-20-BL1, the combustion continued with less luminosity and ended with EOL at about 25.5^{O}CA. In mode 1250-20-BL4, although the combustion was shorter the combustion images appeared with lower luminosity than the neat PME. The images of soot concentration revealed the decrease of soot dense in mode 1250-20-BL1, followed by mode 1250-20-BL4. The combustion of all the 3 modes then ended with smaller area of high flame probability distribution than that with diesel mode. The net HRR and the percentage area of flame above 2400K for these three modes are shown in Figure 7–108. In mode 1250-20-BL1, two spikes of high temperature area were generated at 2 and 4°CA; the second rocketed up compared to the values in diesel, PME, and BL4 modes. It is thought due to the benefit of oxygen content in the PME accompanied with the faster combustion of the LPG in the vicinity of the initial PME flame.

Comparison for all modes of operation (the neat liquid and dual fuel modes with the same premixed mixture strength) is depicted from Figure 7–107 to Figure 7–110, and

from Figure 7–116 to Figure 7–120, for 1250 and 2000 rev/min, respectively. These figures reveal that the LPG-PME seemed to result in worse combustion than the LPG-diesel. In summary, at these two speeds and low load (20Nm), all operation modes with neat PME, LPG-PME appeared far to reach the result as good as diesel combustion.

Comparison in the histogram trace (0^OCA to 25^OCA) of the soot concentration is depicted from Figure 7–111 to Figure 7–115 and from Figure 7–121 to Figure 7–123, for 1250 and 2000 rev/min, respectively. It can be seen that the soot concentration with all modes was very low. The "dense-soot-cloud" (level 13) appeared within the range [12.5-17.5] ^{O}CA and the maximum area accounted about 5% at 1250 rev/min and about 7% at 2000 rev/min. Although the concentration with neat PME or dual fuel modes might be higher at some instant, the concentration with diesel mode was always the highest, at the end of combustion period.

CA	1250-20 D	1250-20 DL1	1250-20 DL4		1250-20 B	1250-20 BL1	1250-20 BL4
AOS	-2.5	-2.5	-2.0		-4.0	-4.5	-3.0
-2							
0							
2							
4							
6							
8							
10							
12							
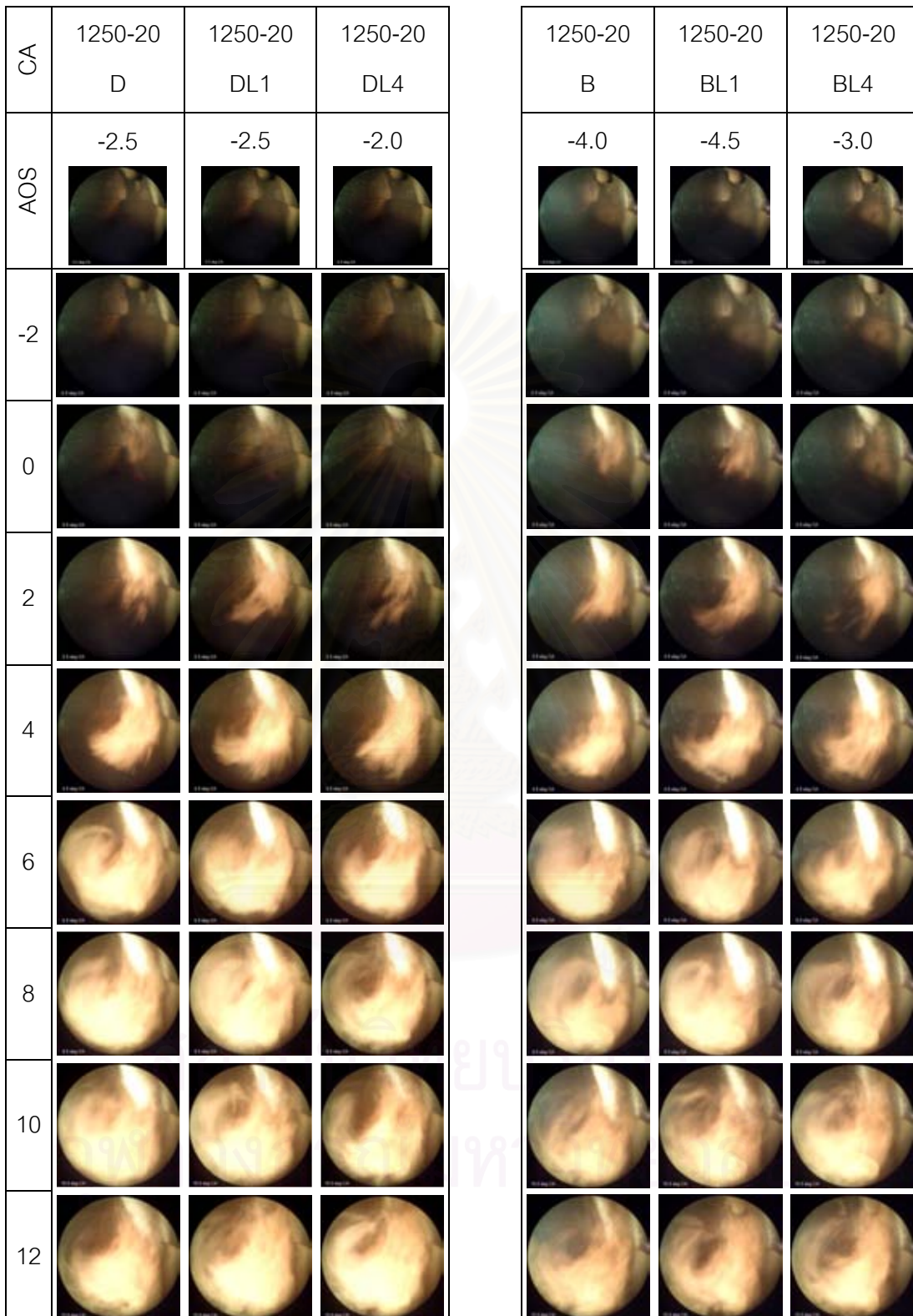
Figure 7–94   Sequential images of combustion process with cool light (modes: 1250-20-D, 1250-20-DL1, 1250-20-DL4, 1250-20-B, 1250-20-BL1, and 1250-20-BL4)

CA	1250-20 D	1250-20 DL1	1250-20 DL4		1250-20 B	1250-20 BL1	1250-20 BL4
SOL	-1.0	-0.5	0.0		-2.0	-1.5	-1.0
0							
2							
4							
6							
8							
10							
12							
14							

Figure 7–95   Sequential images of combustion process (modes 1250-20-D, 1250-20-DL1, 1250-20-DL4, 1250-20-B, 1250-20-BL1, and 1250-20-BL4)

CA	1250-20 D	1250-20 DL1	1250-20 DL4		1250-20 B	1250-20 BL1	1250-20 BL4
16							
18							
20							
22							
EOL	28.5	25.5	23.5		27.5	25.5	21.0

Figure 7-95   Sequential images of combustion process (modes 1250-20-D, 1250-20-DL1, 1250-20-DL4, 1250-20-B, 1250-20-BL1, and 1250-20-BL4) (Contd.)

สถาบันวิทยบริการ
จุฬาลงกรณ์มหาวิทยาลัย
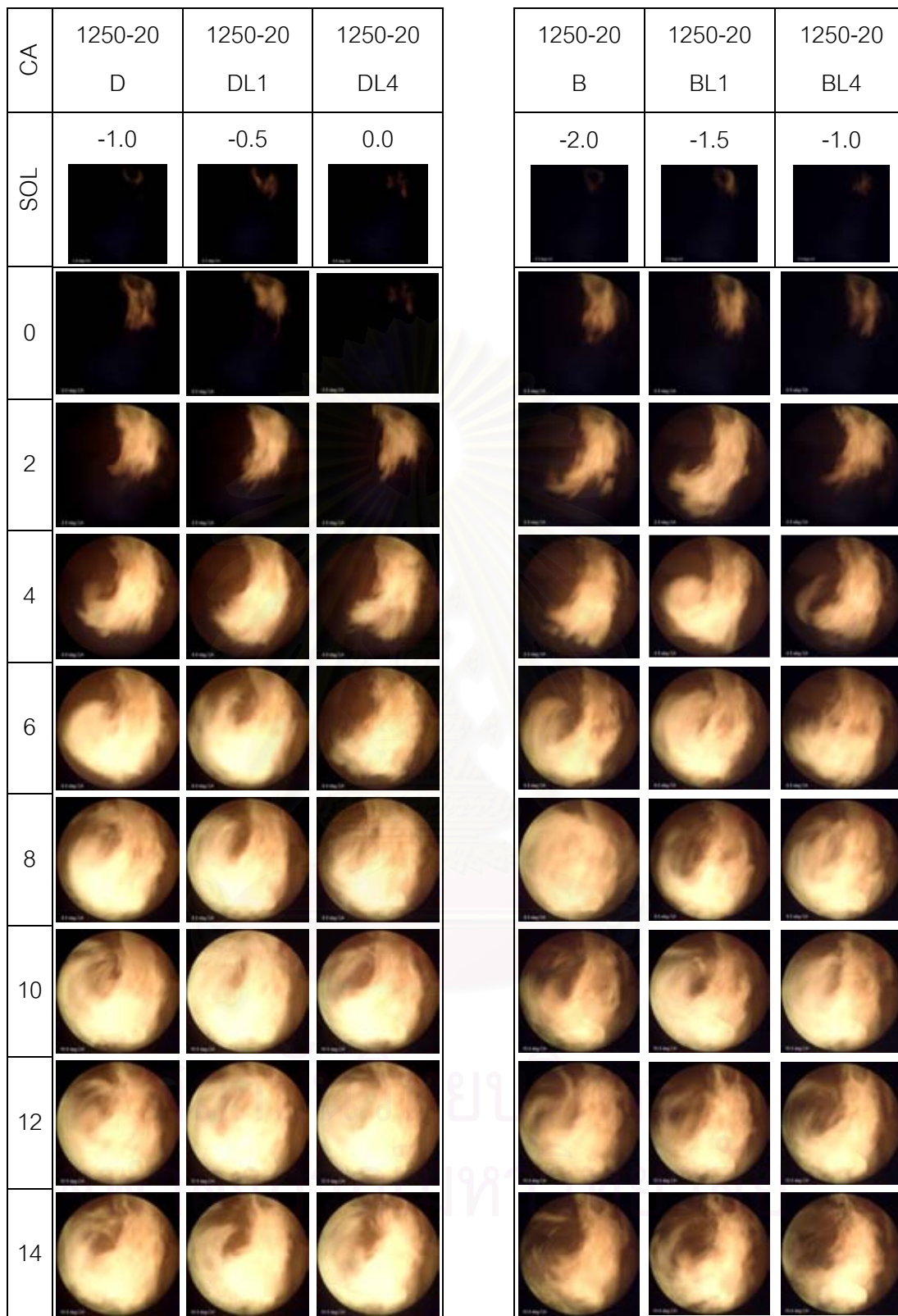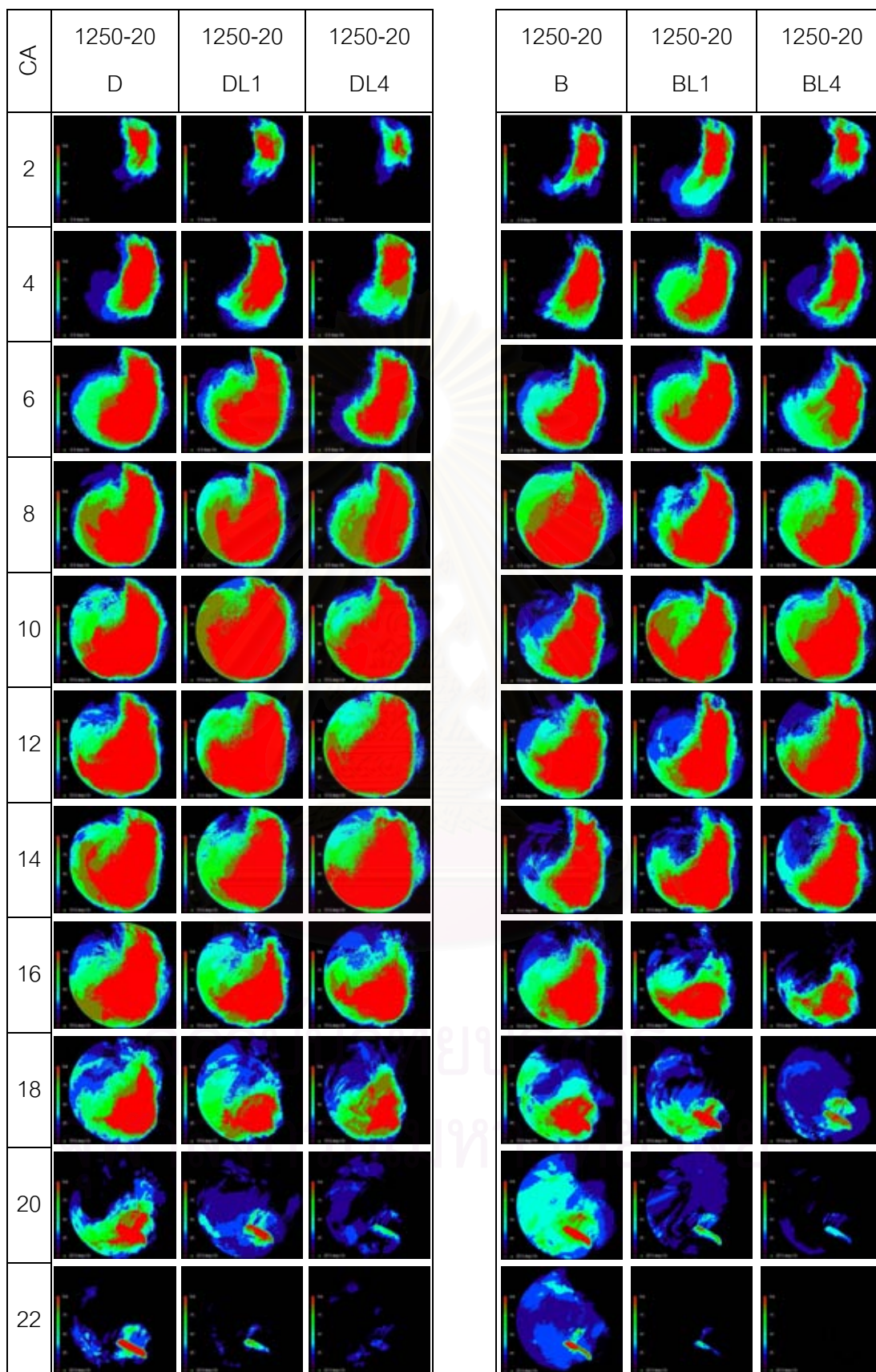
Figure 7–96   Images of flame probability distribution (modes: 1250-20-D, 1250-20-DL1, 1250-20-DL4, 1250-20-B, 1250-20-BL1, and 1250-20-BL4)
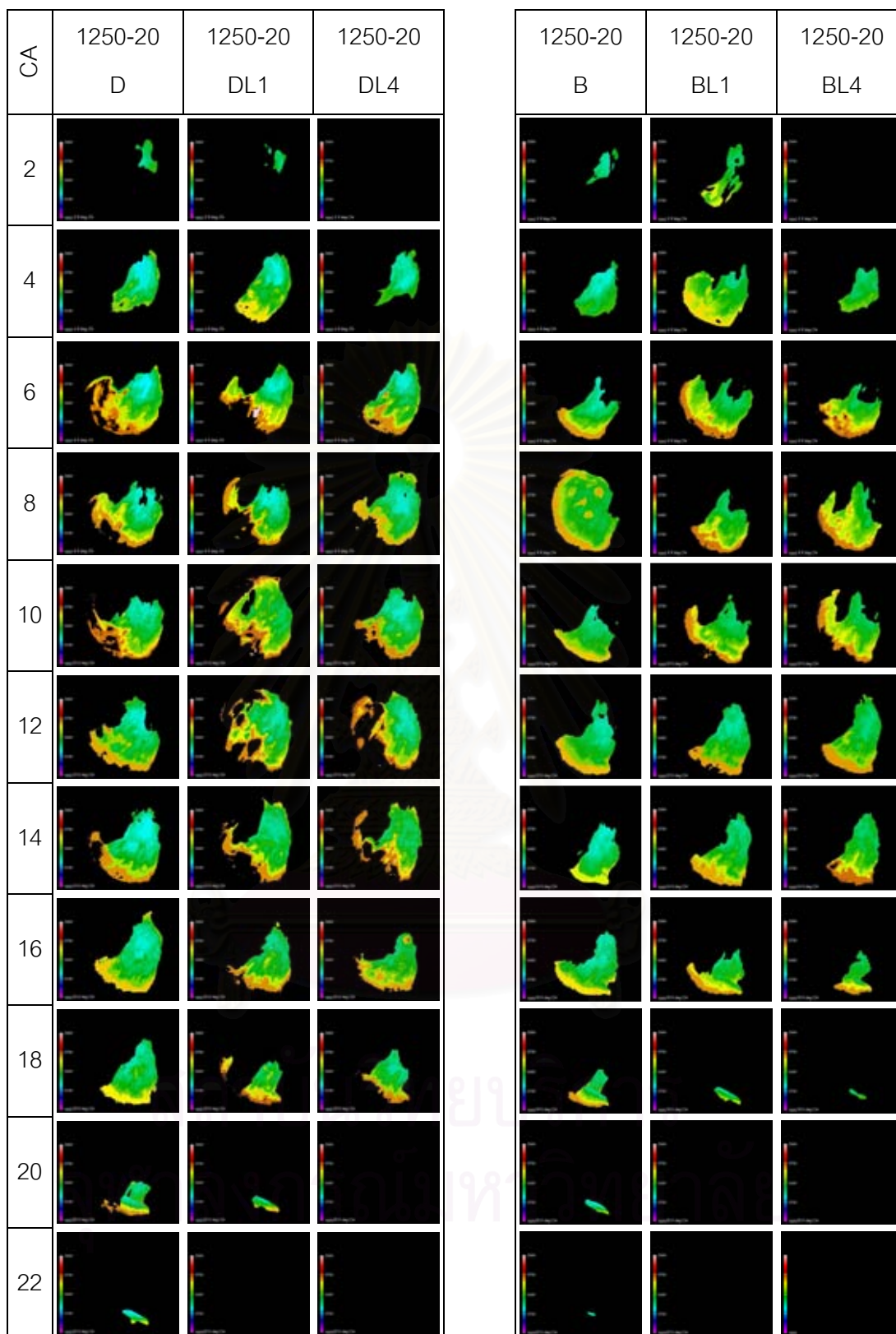
Figure 7–97   Images of flame temperature distribution (modes: 1250-20-D, 1250-20-DL1, 1250-20-DL4, 1250-20-B, 1250-20-BL1, and 1250-20-BL4)

CA	1250-20 D	1250-20 DL1	1250-20 DL4	1250-20 B	1250-20 BL1	1250-20 BL4
2						
4						
6						
8						
10						
12						
14						
16						
18						
20						
22						
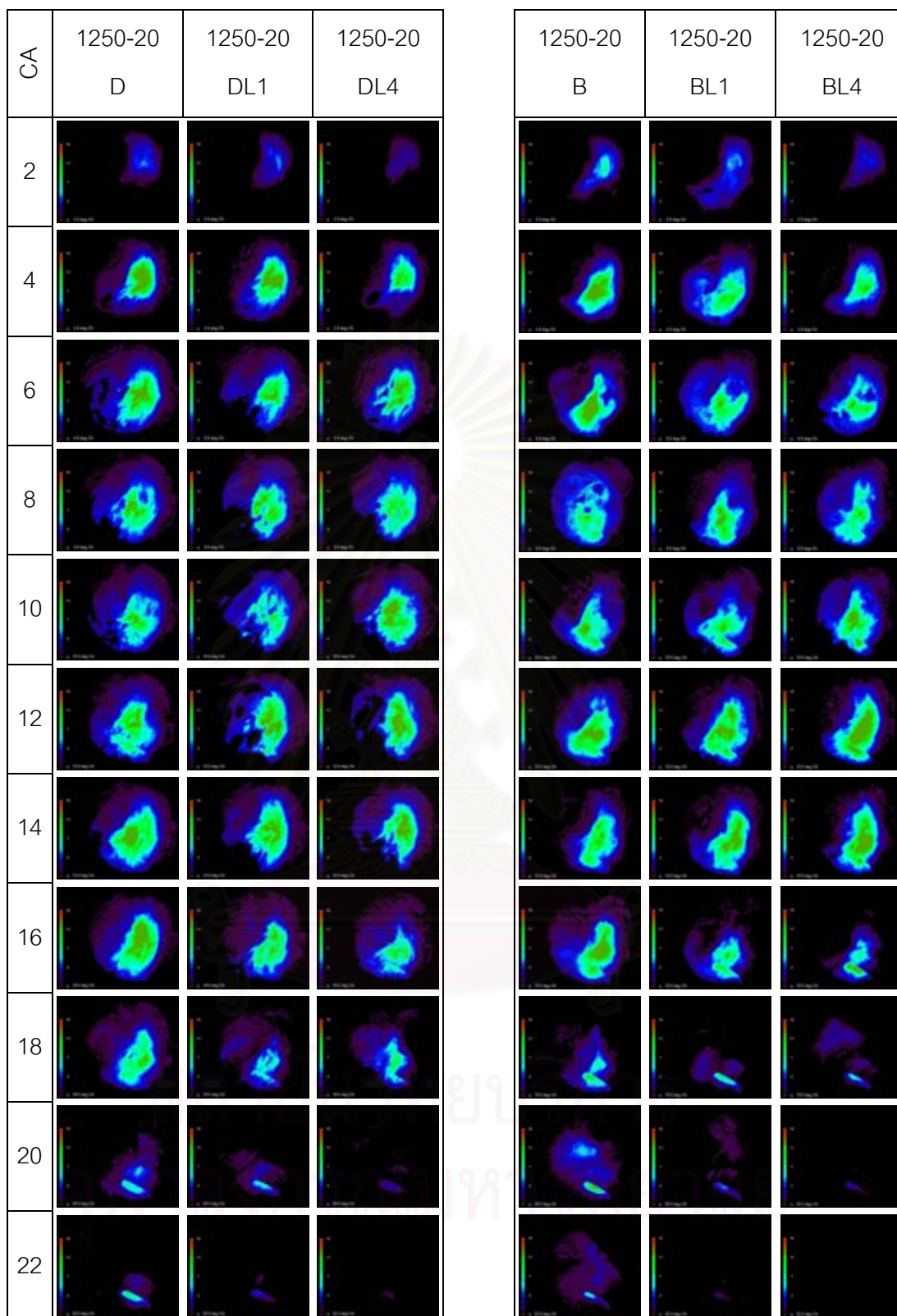
Figure 7–98   Images of soot concentration distribution (modes: 1250-20-D, 1250-20-DL1, 1250-20-DL4, 1250-20-B, 1250-20-BL1, and 1250-20-BL4)

CA	2000-20 D	2000-20 DL1	2000-20 DL4		2000-20 B	2000-20 BL1	2000-20 BL4
AOS	-3.5	-4.0	-4.0		-5.0	-6.0	-6.0
-2							
0							
2							
4							
6							
8							
10							
12							
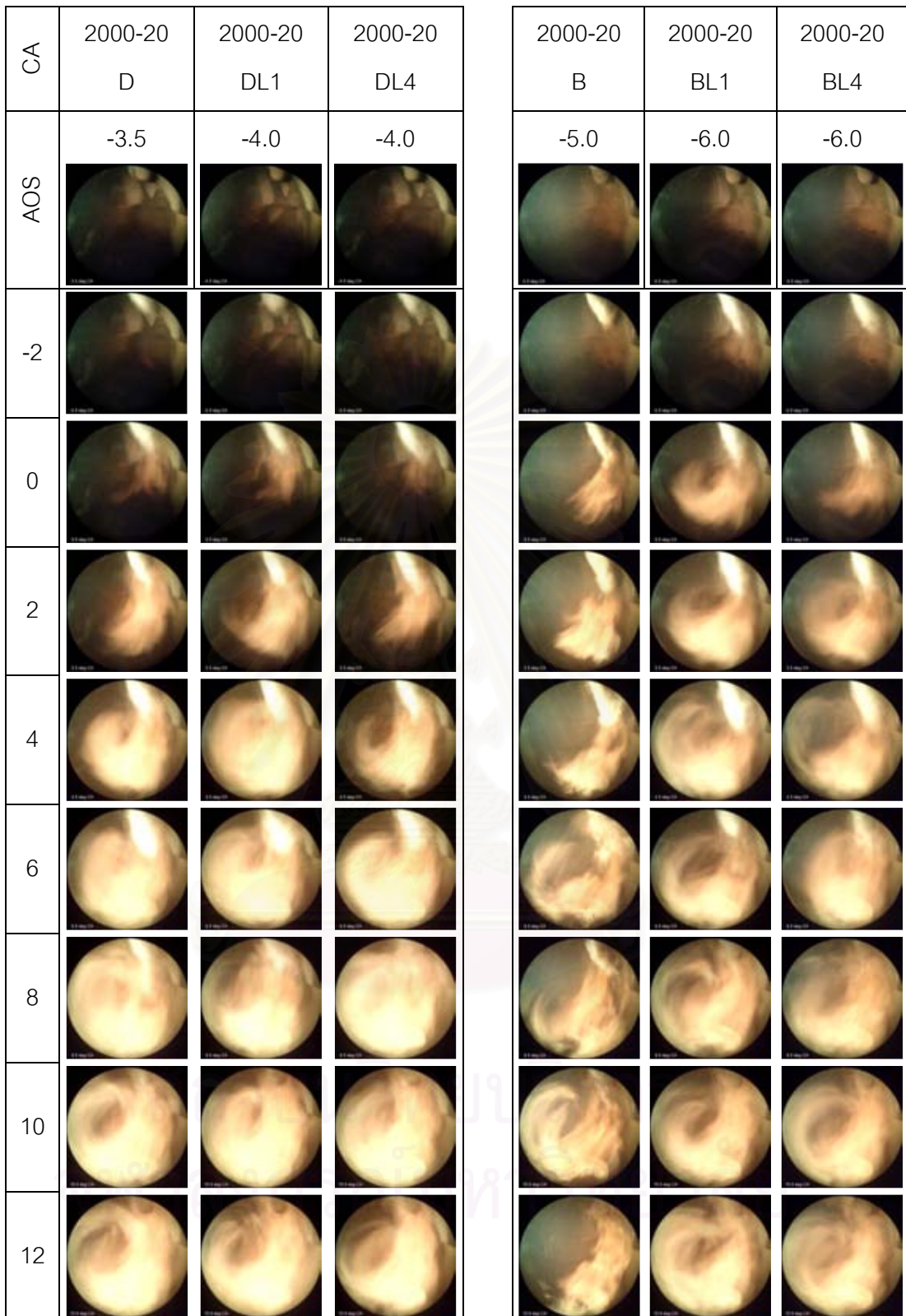
Figure 7–99   Direct images (with flash) of combustion process (modes: 2000-20-D, 2000-20-DL1, 2000-20-DL4, 2000-20-B, 2000-20-BL1, and 2000-20-BL4)

177
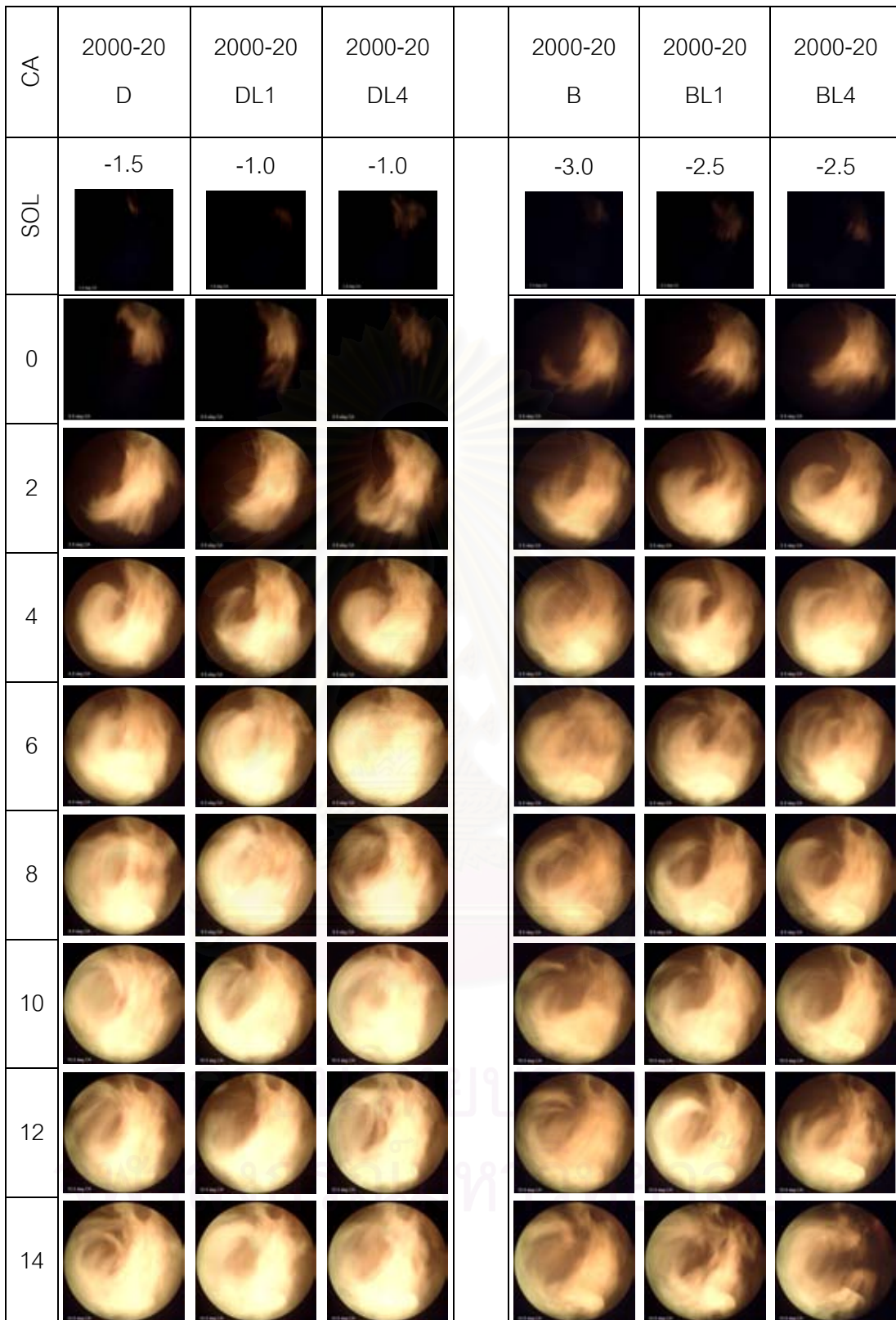
Figure 7–100   Direct images of combustion process (modes: 2000-20-D, 2000-20-DL1, 2000-20-DL4, 2000-20-B, 2000-20-BL1, and 2000-20-BL4)

CA	2000-20 D	2000-20 DL1	2000-20 DL4		2000-20 B	2000-20 BL1	2000-20 BL4
16							
18							
20							
22							
EOL	31.5	24.5	22.0		23.0	21.5	19.0

Figure 7-100   Direct images of combustion process (modes: 2000-20-D, 2000-20-DL1, 2000-20-DL4, 2000-20-B, 2000-20-BL1, and 2000-20-BL4) (Contd.)

Figure 7–101   Images of flame probability distribution (modes: 2000-20-D, 2000-20-DL1, 2000-20-DL4, 2000-20-B, 2000-20-BL1, and 2000-20-BL4)
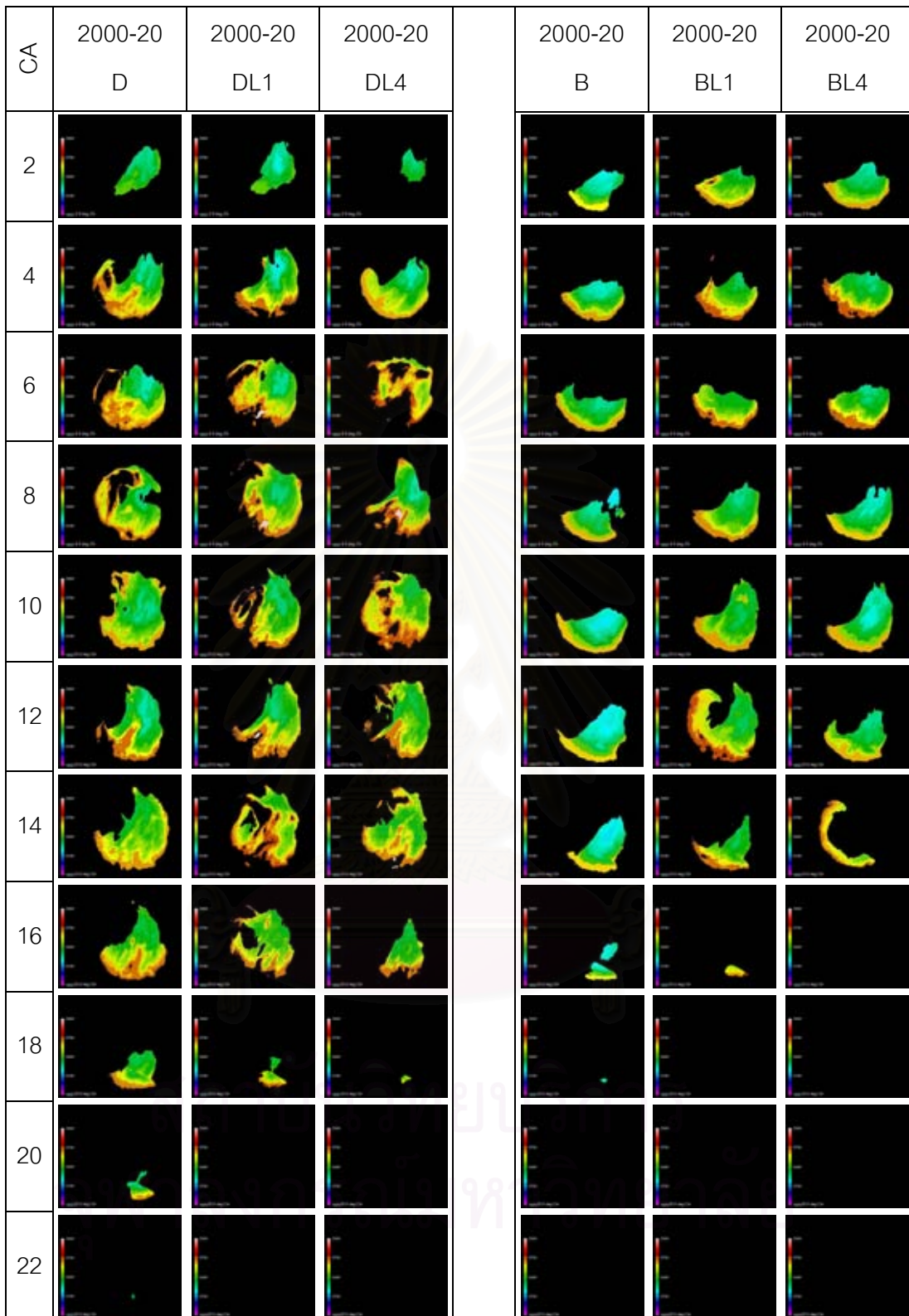
Figure 7–102   Images of flame temperature distribution (modes: 2000-20-D, 2000-20-DL1, 2000-20-DL4, 2000-20-B, 2000-20-BL1, and 2000-20-BL4)

CA	2000-20 D	2000-20 DL1	2000-20 DL4		2000-20 B	2000-20 BL1	2000-20 BL4
2							
4							
6							
8							
10							
12							
14							
16							
18							
20							
22							
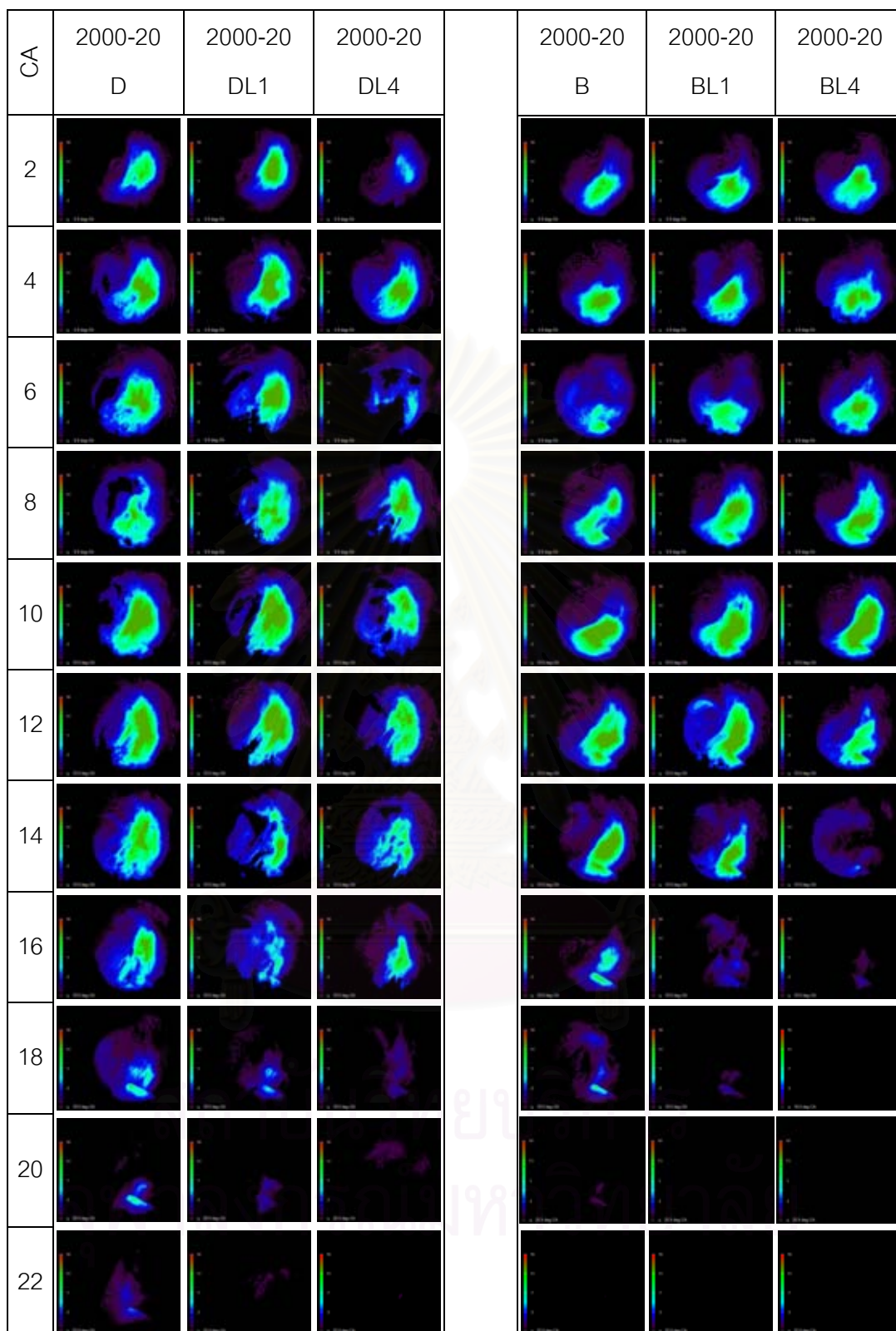
Figure 7–103   Images of soot concentration distribution (modes: 2000-20-D, 2000-20-DL1, 2000-20-DL4, 2000-20-B, 2000-20-BL1, and 2000-20-BL4)
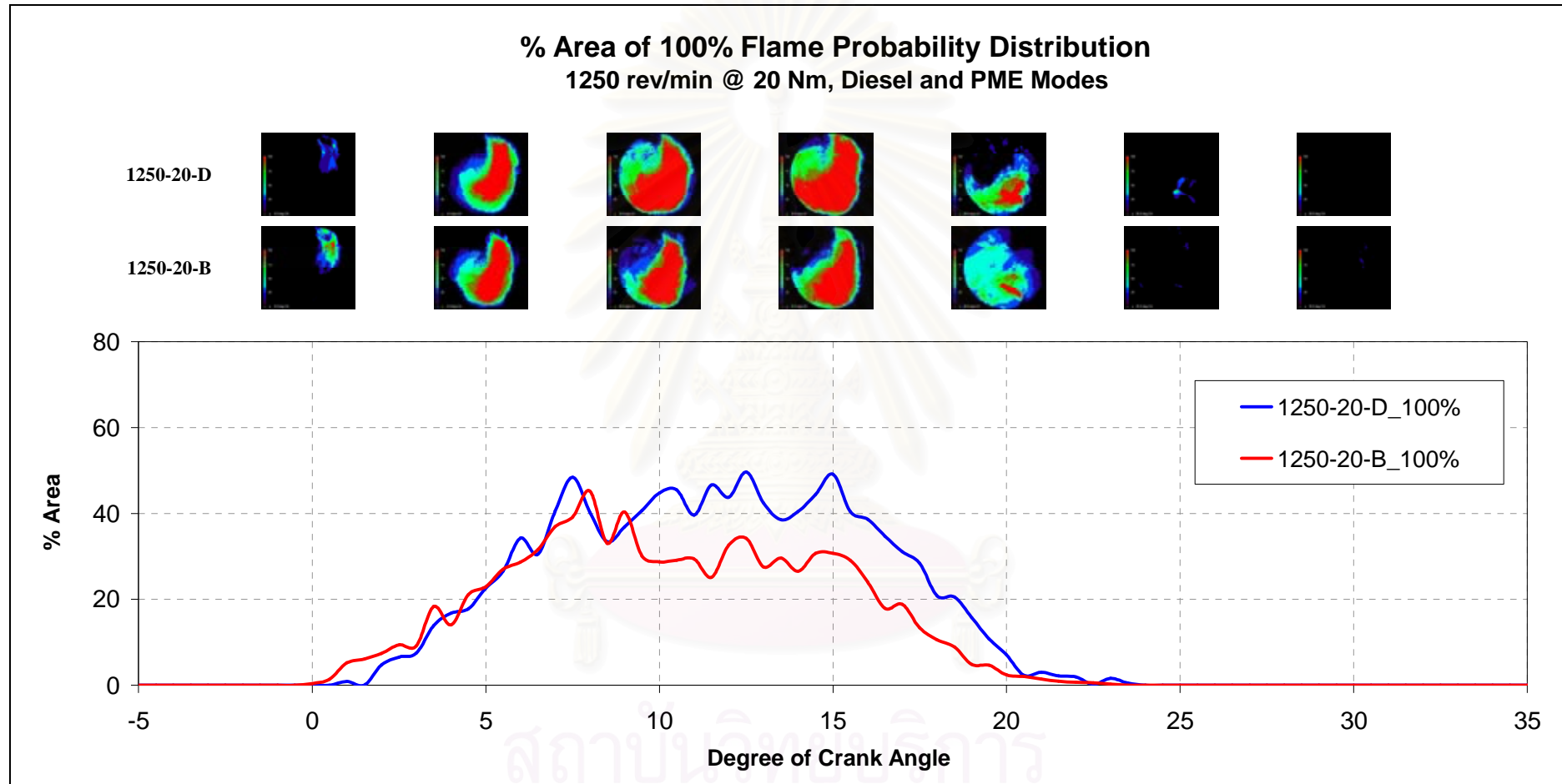
Figure 7–104   Flame probability distribution @ 1250 rev/min, 20 Nm (neat diesel and PME)
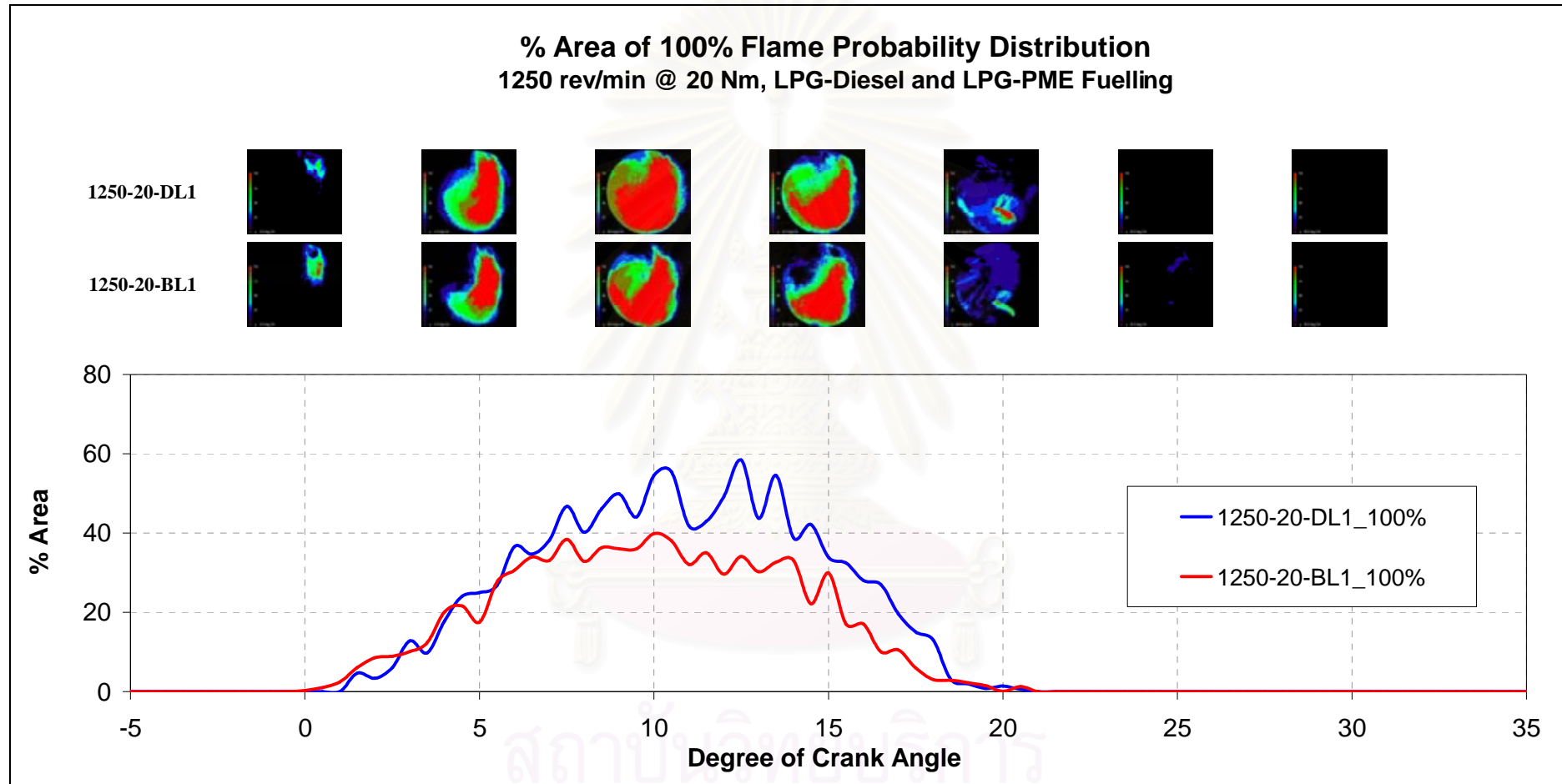
Figure 7–105   Flame probability distribution @ 1250 rev/min, 20 Nm (modes DL1 and BL1)
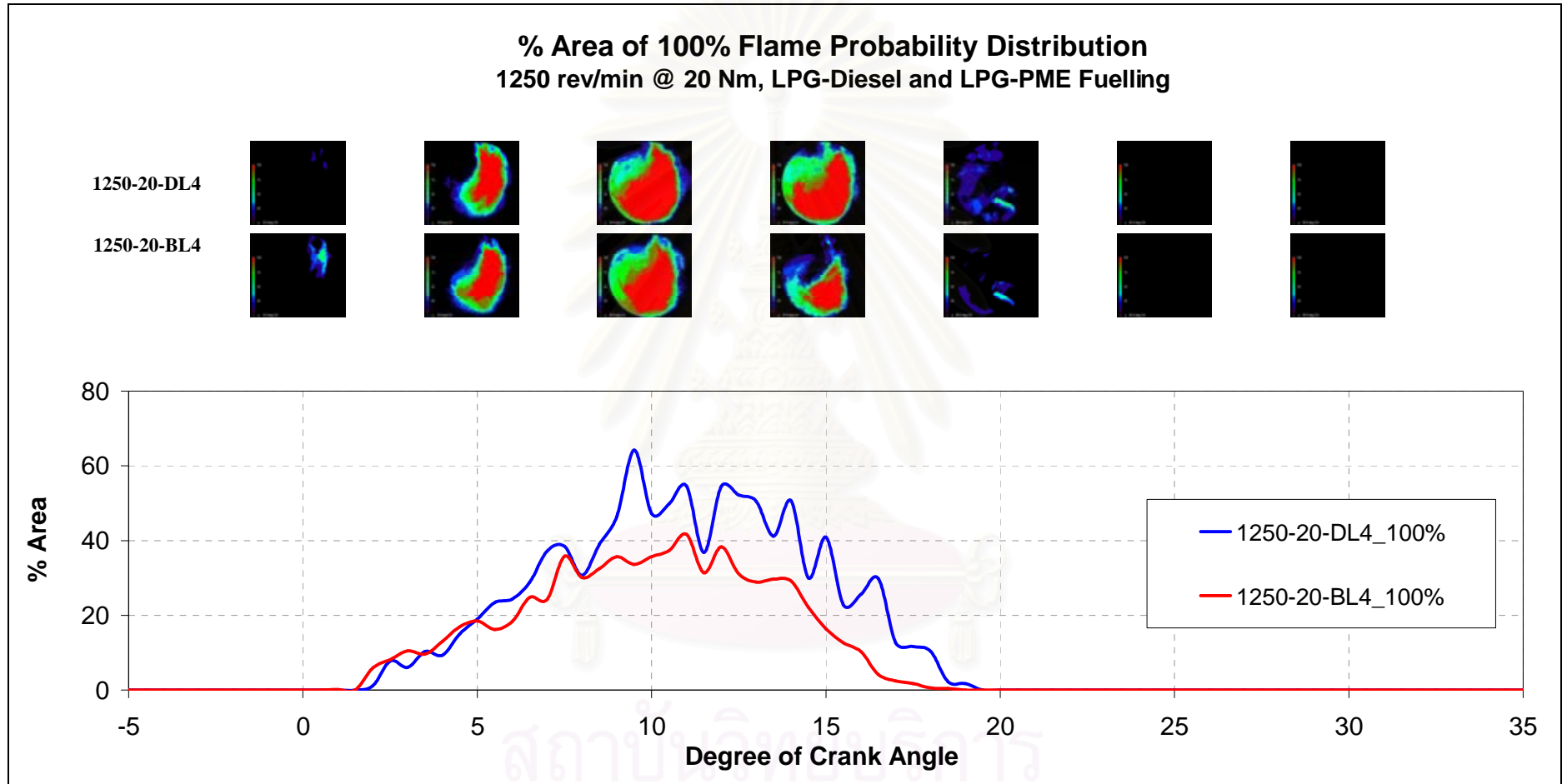
Figure 7–106   Flame probability distribution @ 1250 rev/min, 20 Nm (modes DL4 and BL4)
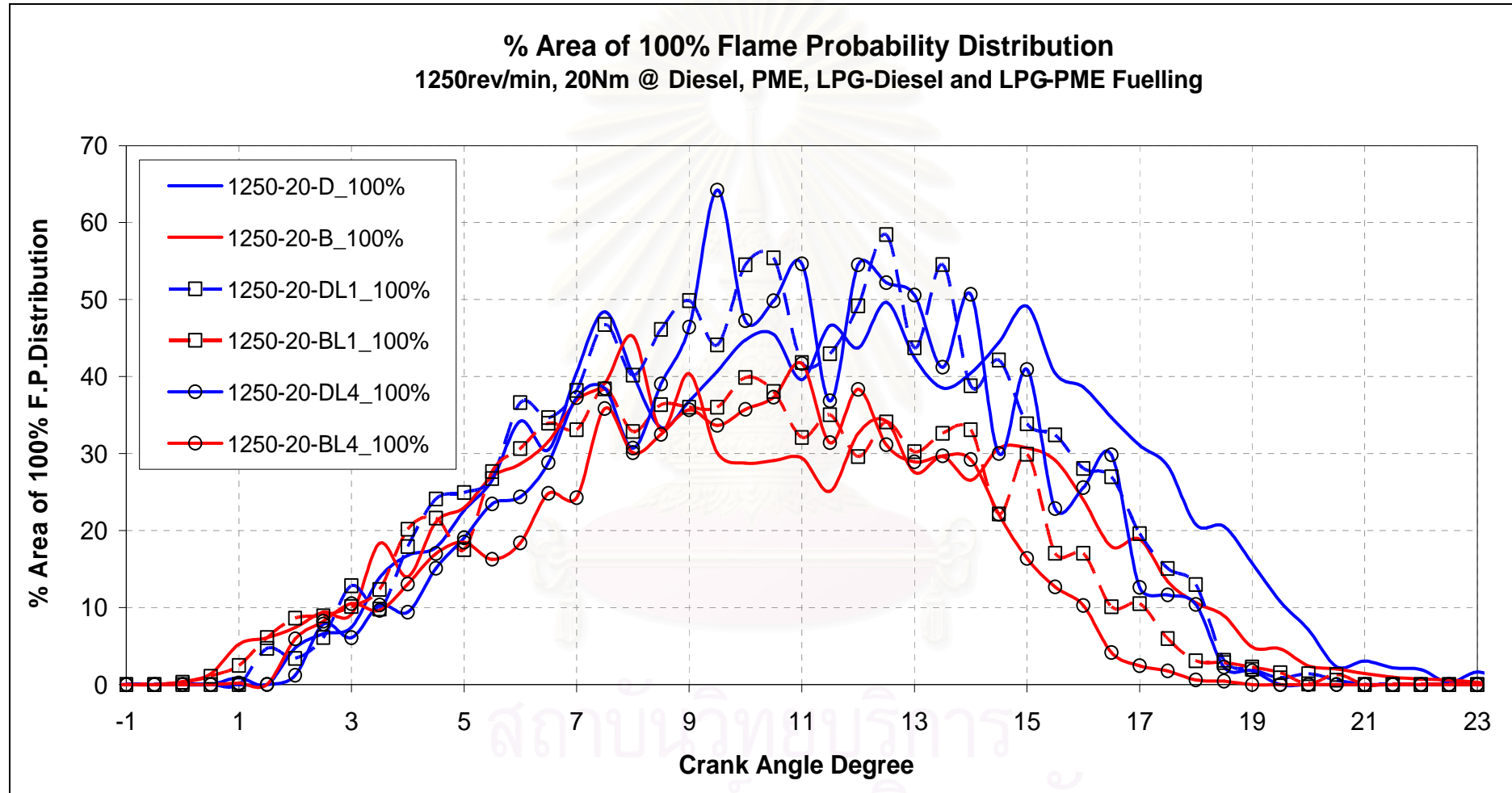
Figure 7–107   Flame probability distribution @ 1250 rev/min, 20 Nm (Diesel, PME, LPG-diesel, and LPG-PME)
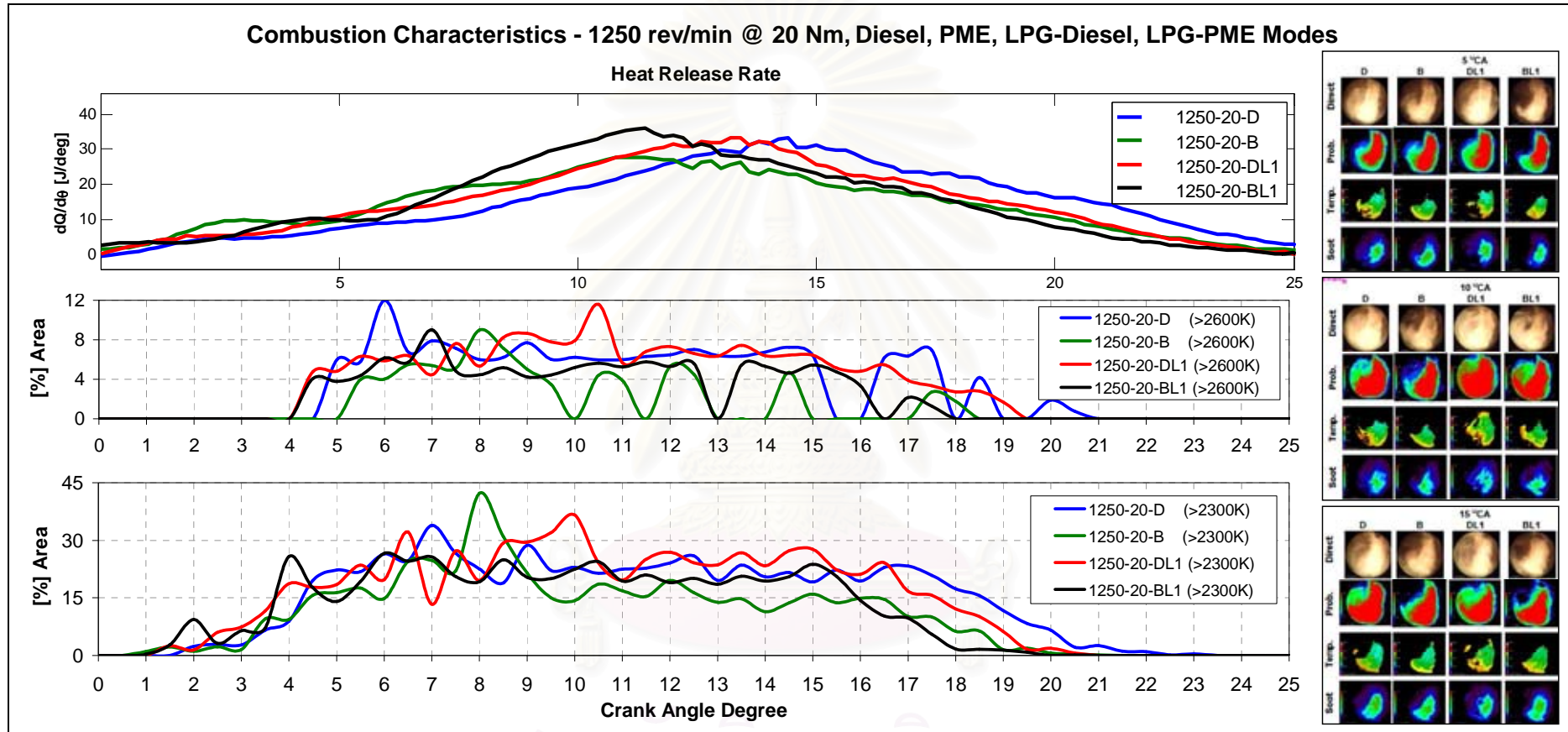
Figure 7–108   HRR and area of flame temperature above 2300 and 2600K @ 1250rev/min, 20Nm, (mode D, DL1, B, and BL1)

 # Image groups are at 5, 10, and 15 ^{O}CA
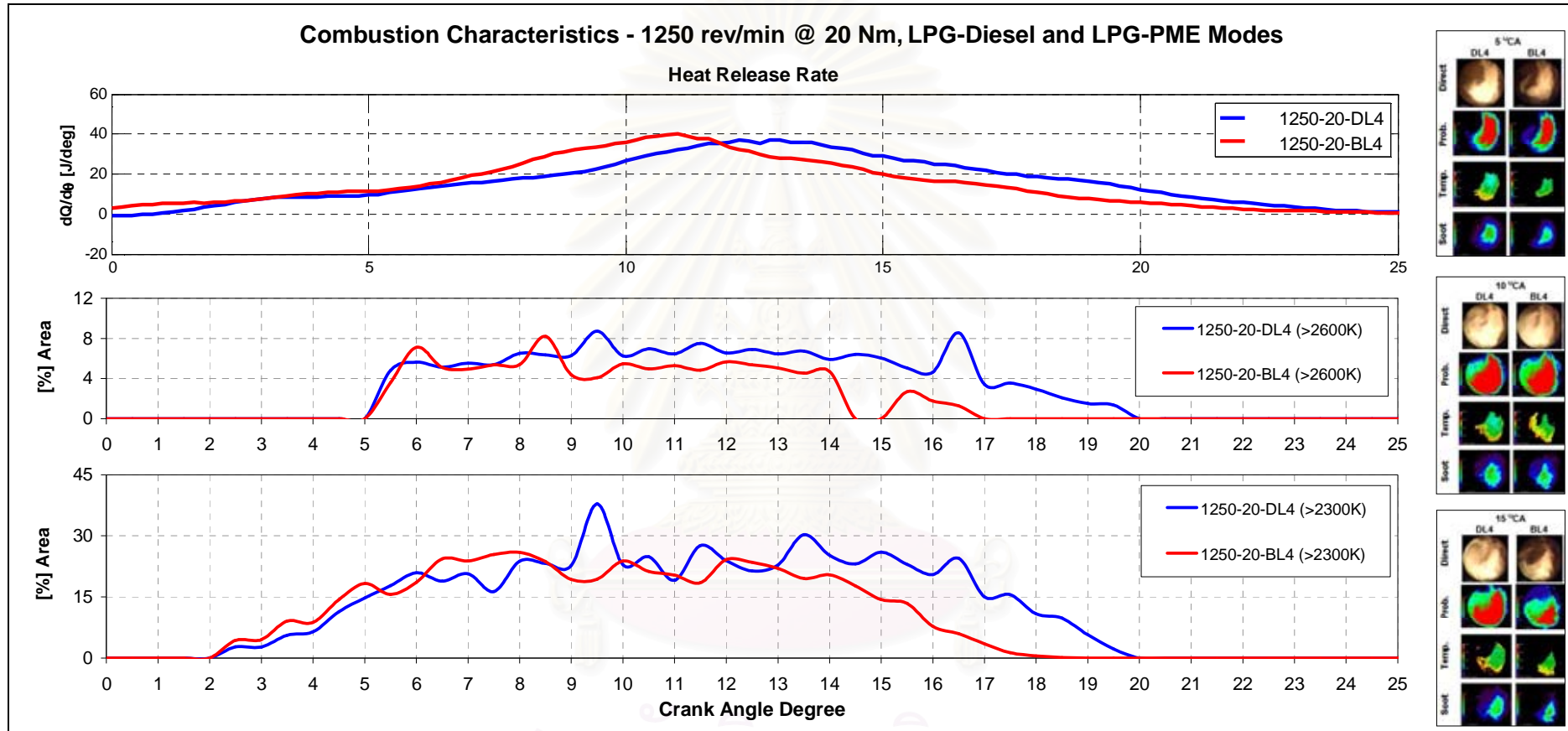
Figure 7–109   HRR and area of flame temperature above 2300 and 2600K @ 1250rev/min, 20Nm (modes DL4 and BL4)

 # Image groups are at 5, 10, and 15 ^{O}CA
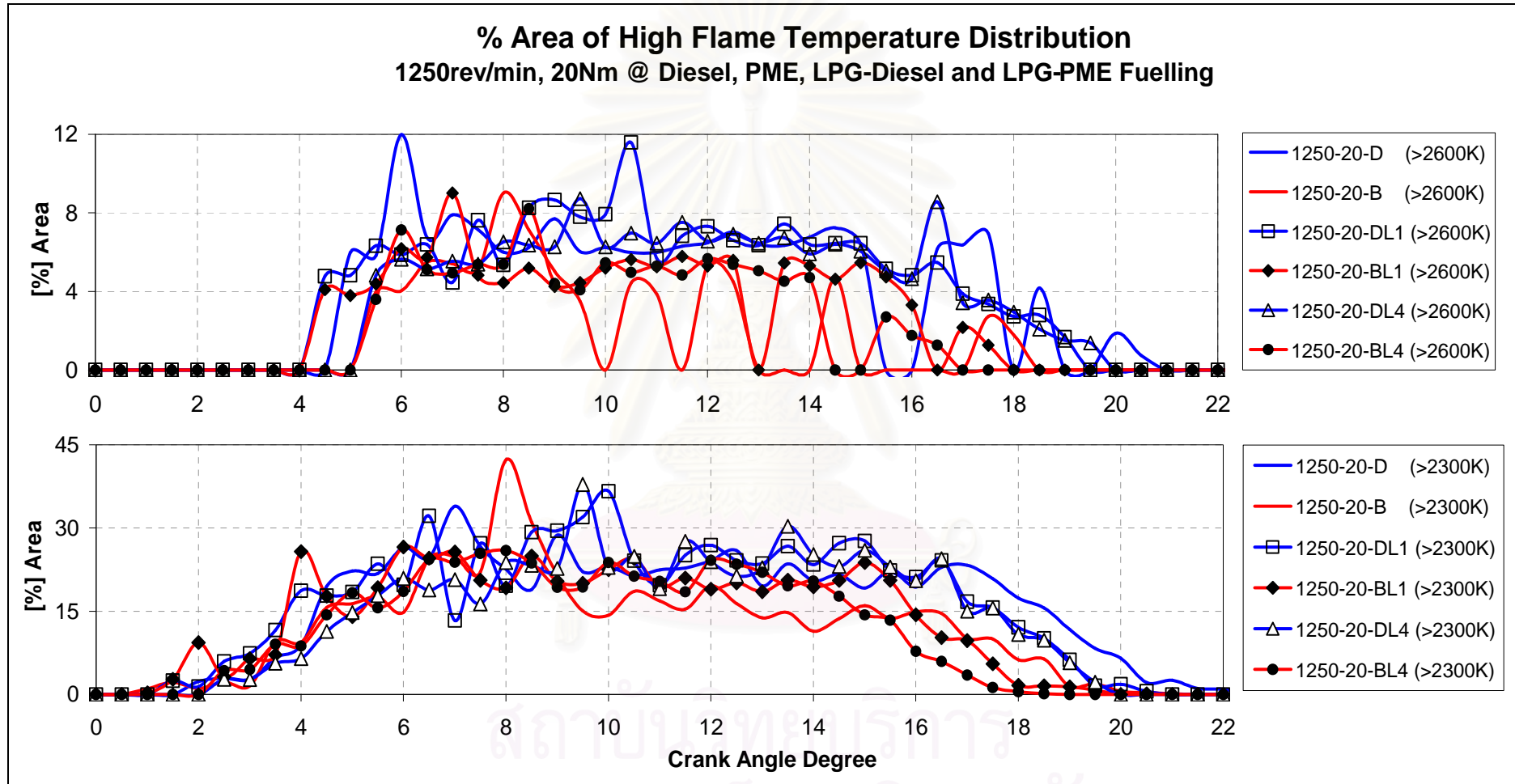
Figure 7–110   HRR and area of flame temperature above 2300 and 2600K @ 1250rev/min, 20Nm (diesel, PME, LPG-diesel, and LPG-PME)
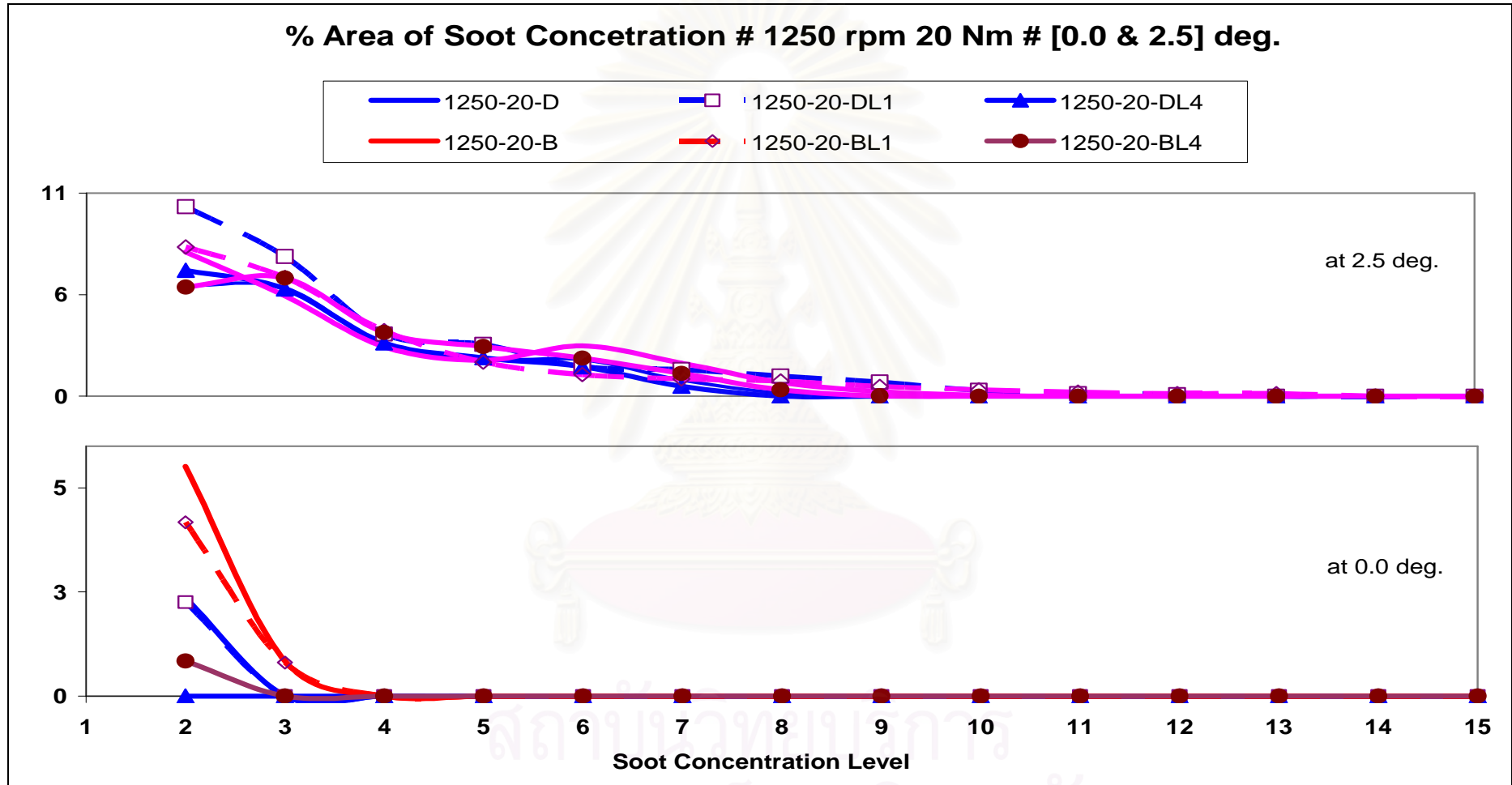
Figure 7–111   Soot concentration at 0 and 2.5 degree @ 1250rev/min, 20Nm (Diesel, PME, LPG-Diesel, and LPG-PME modes)
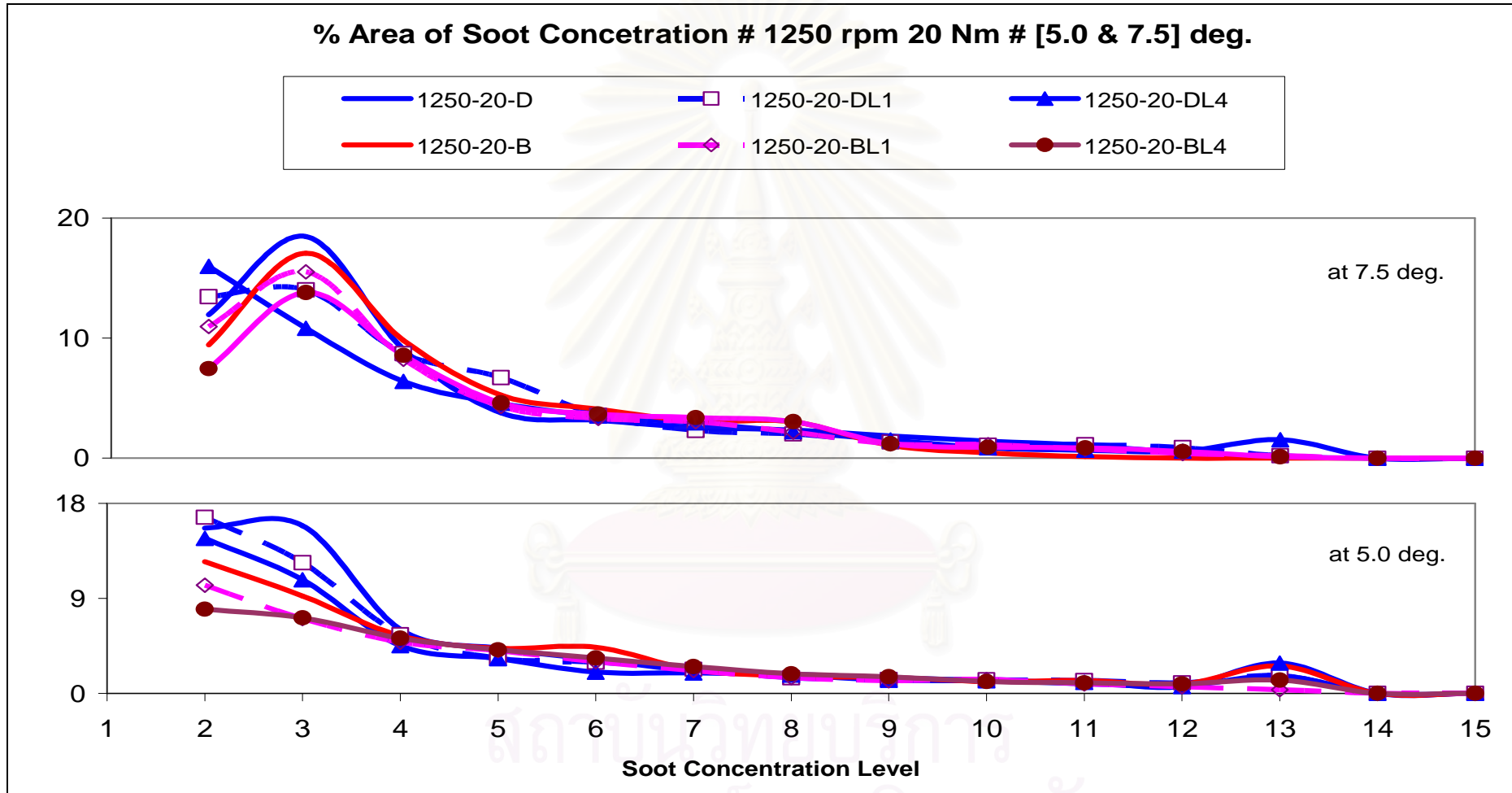
Figure 7–112   Soot concentration at 5.0 and 7.5 degree @ 1250rev/min, 20Nm (Diesel, PME, LPG-Diesel, and LPG-PME modes)
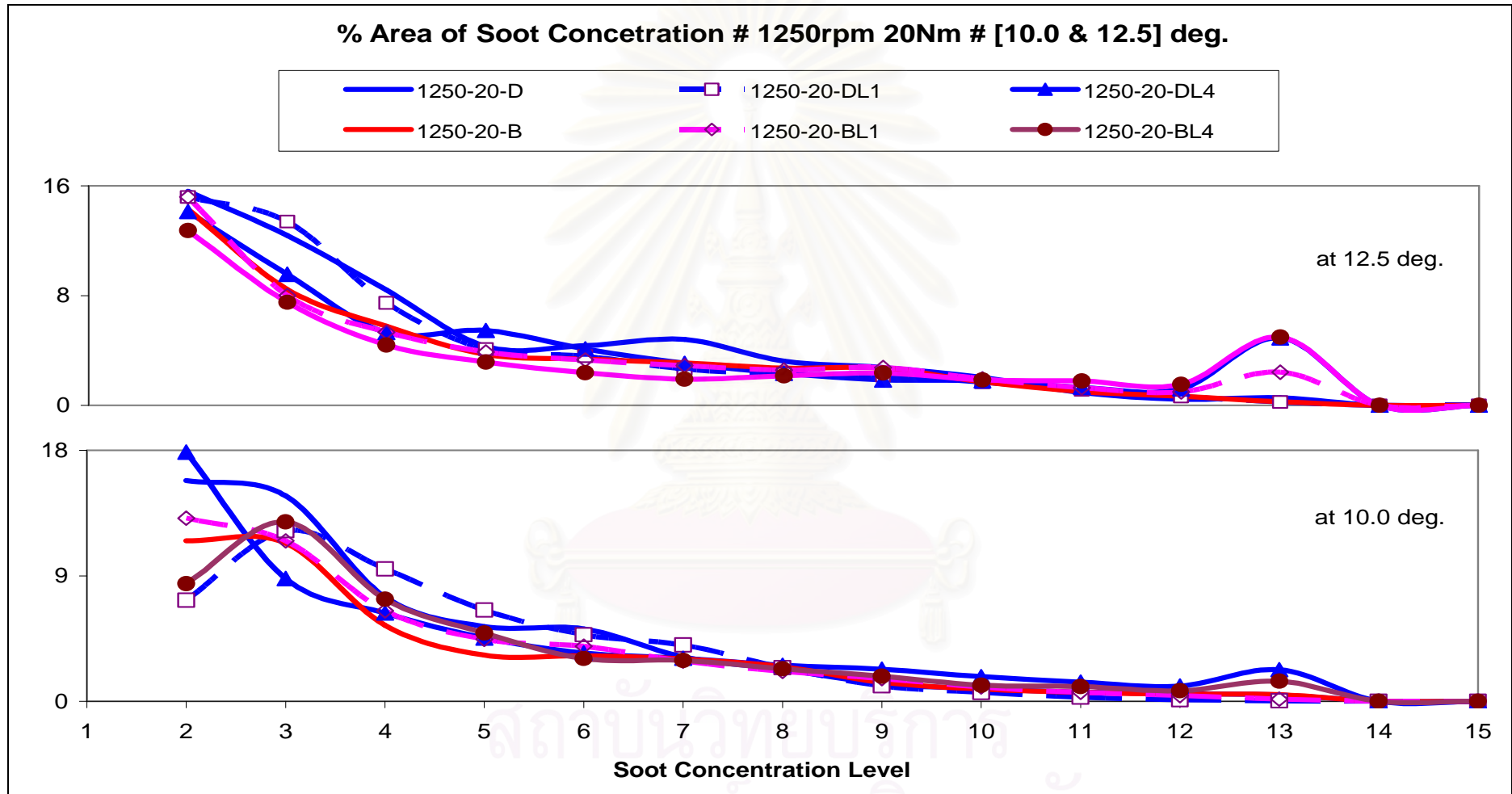
Figure 7–113   Soot concentration at 10 and 12.5 degree @ 1250rev/min, 20Nm (Diesel, PME, LPG-Diesel, and LPG-PME modes)
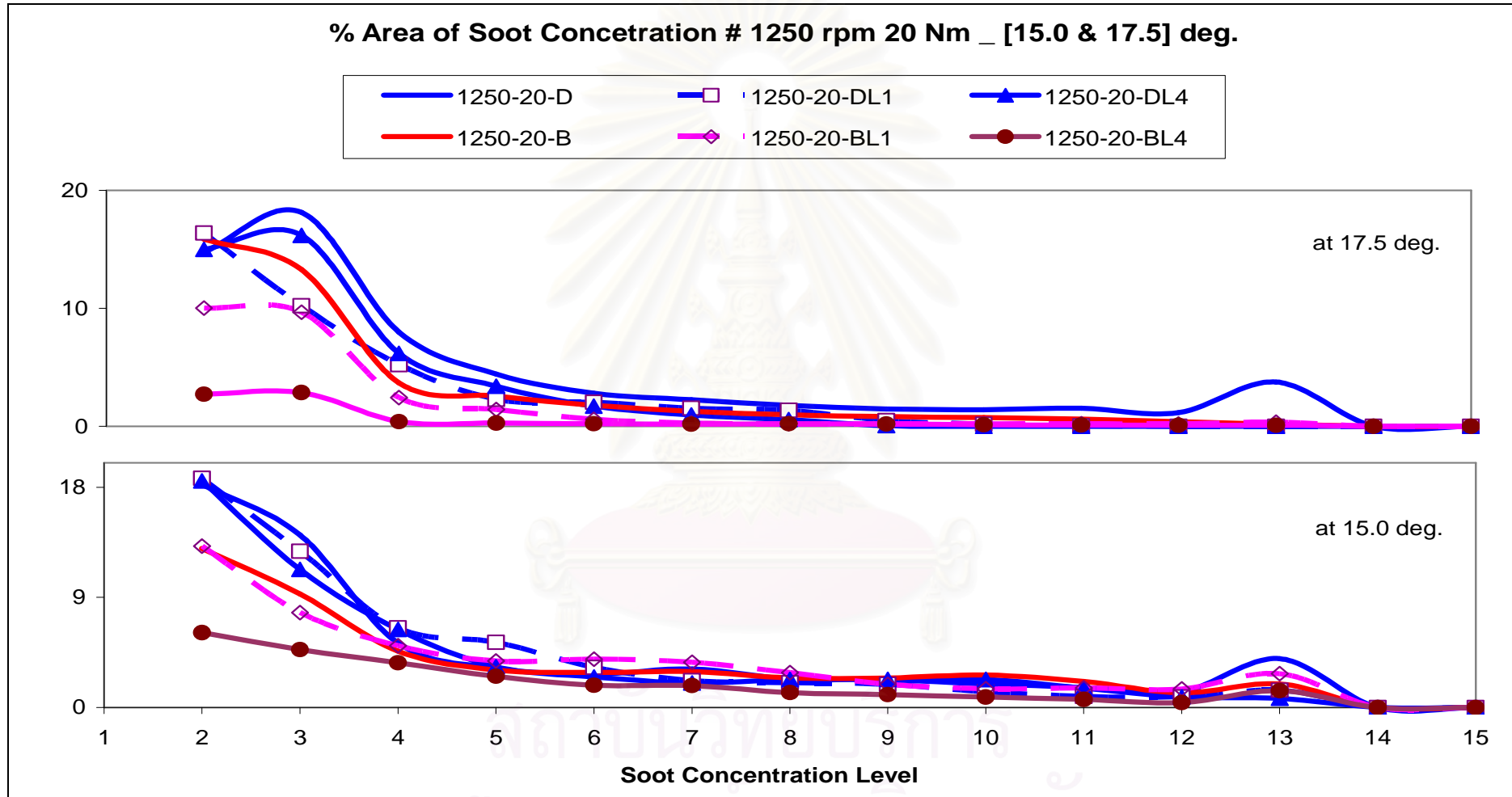
Figure 7–114   Soot concentration at 15 and 17.5 degree @ 1250rev/min, 20Nm (Diesel, PME, LPG-Diesel, and LPG-PME modes)
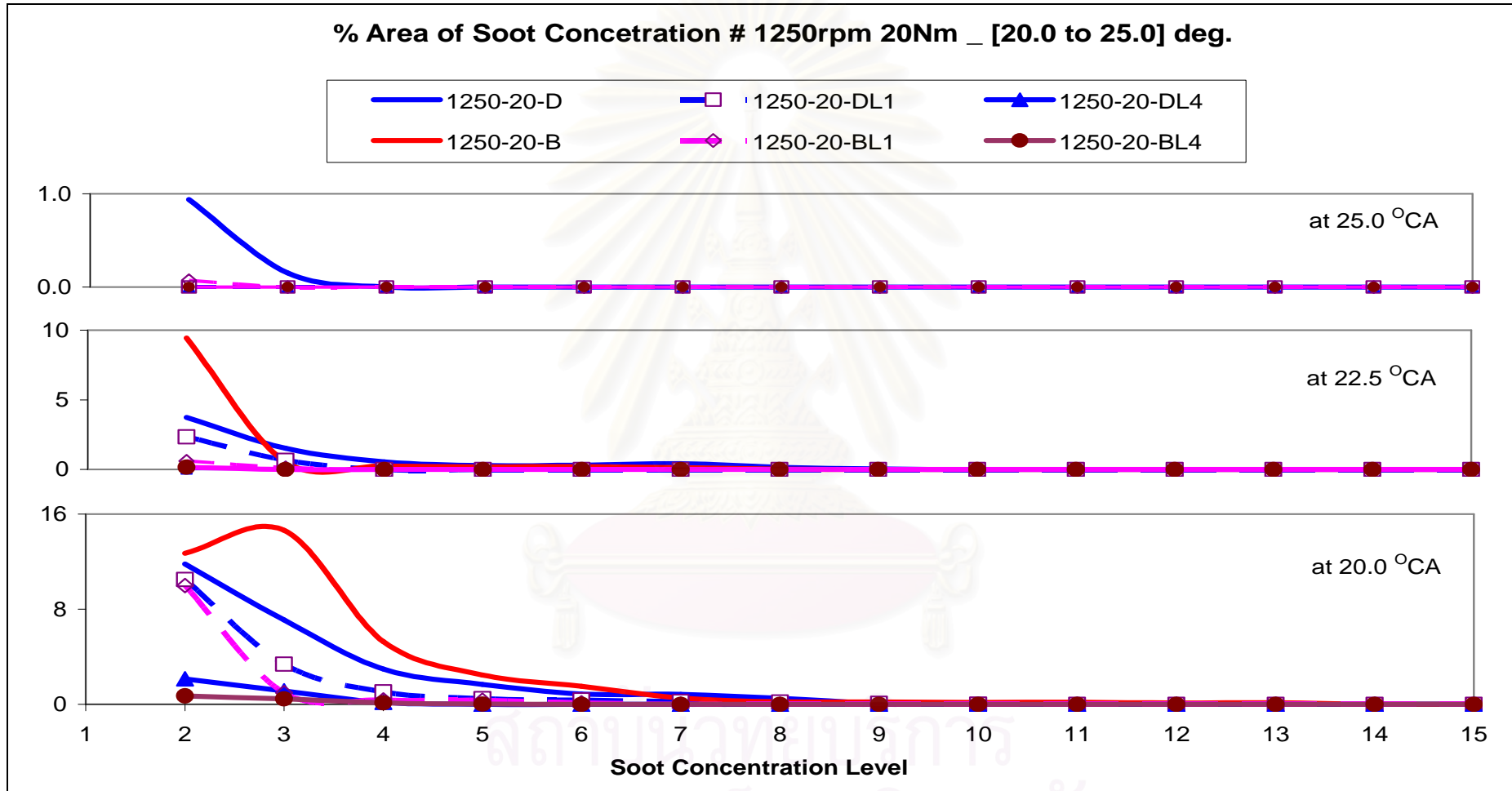
Figure 7–115   Soot concentration at 20, 22.5 and 25 degree @ 1250rev/min, 20Nm (Diesel, PME, LPG-Diesel, and LPG-PME modes)
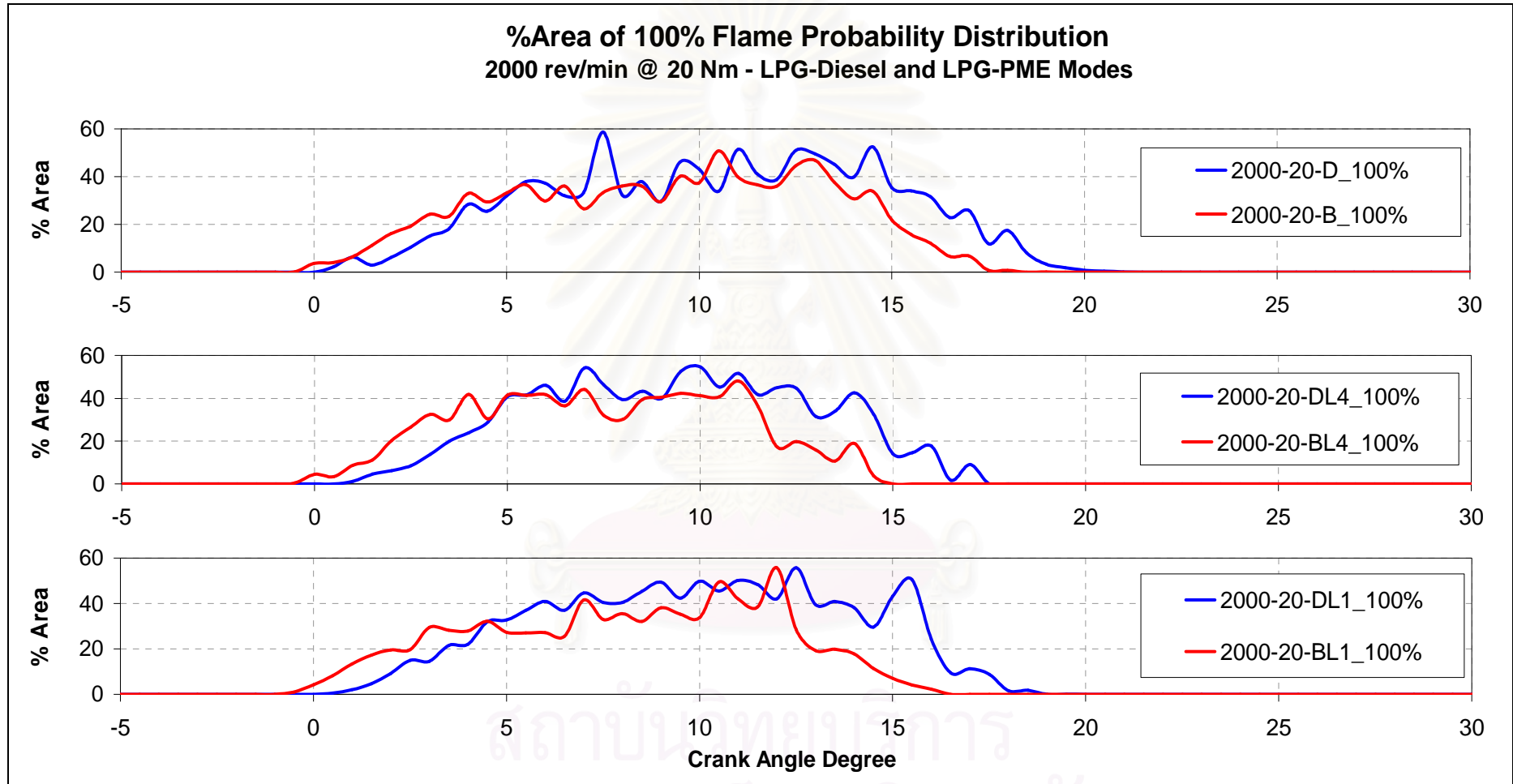
Figure 7–116   Flame probability distribution @ 2000 rev/min, 20 Nm (Diesel, PME, LPG-diesel and LPG-PME)
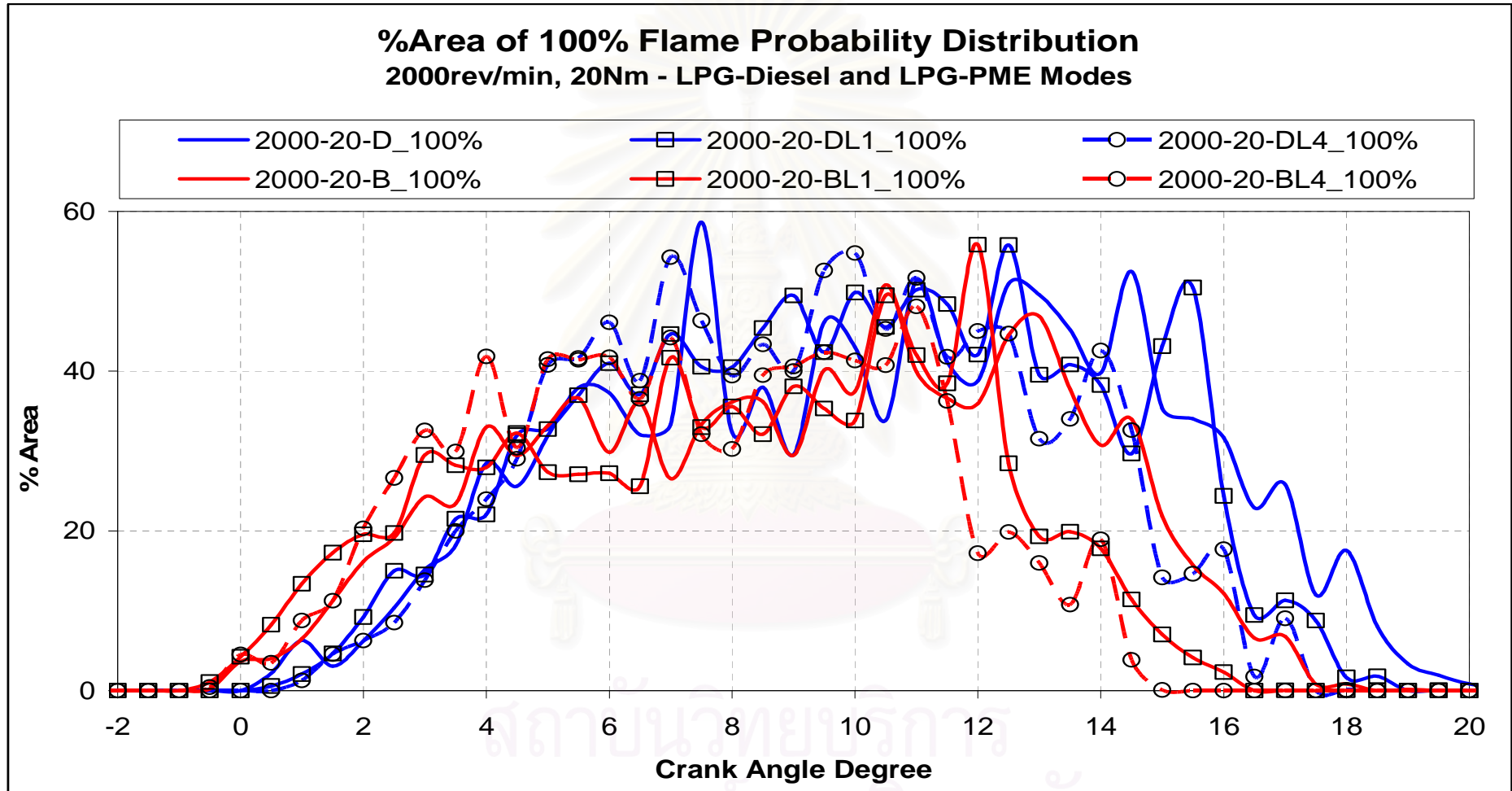
Figure 7–117 Flame probability distribution @ 2000 rev/min, 20 Nm (Diesel, PME, LPG-diesel and LPG-PME)
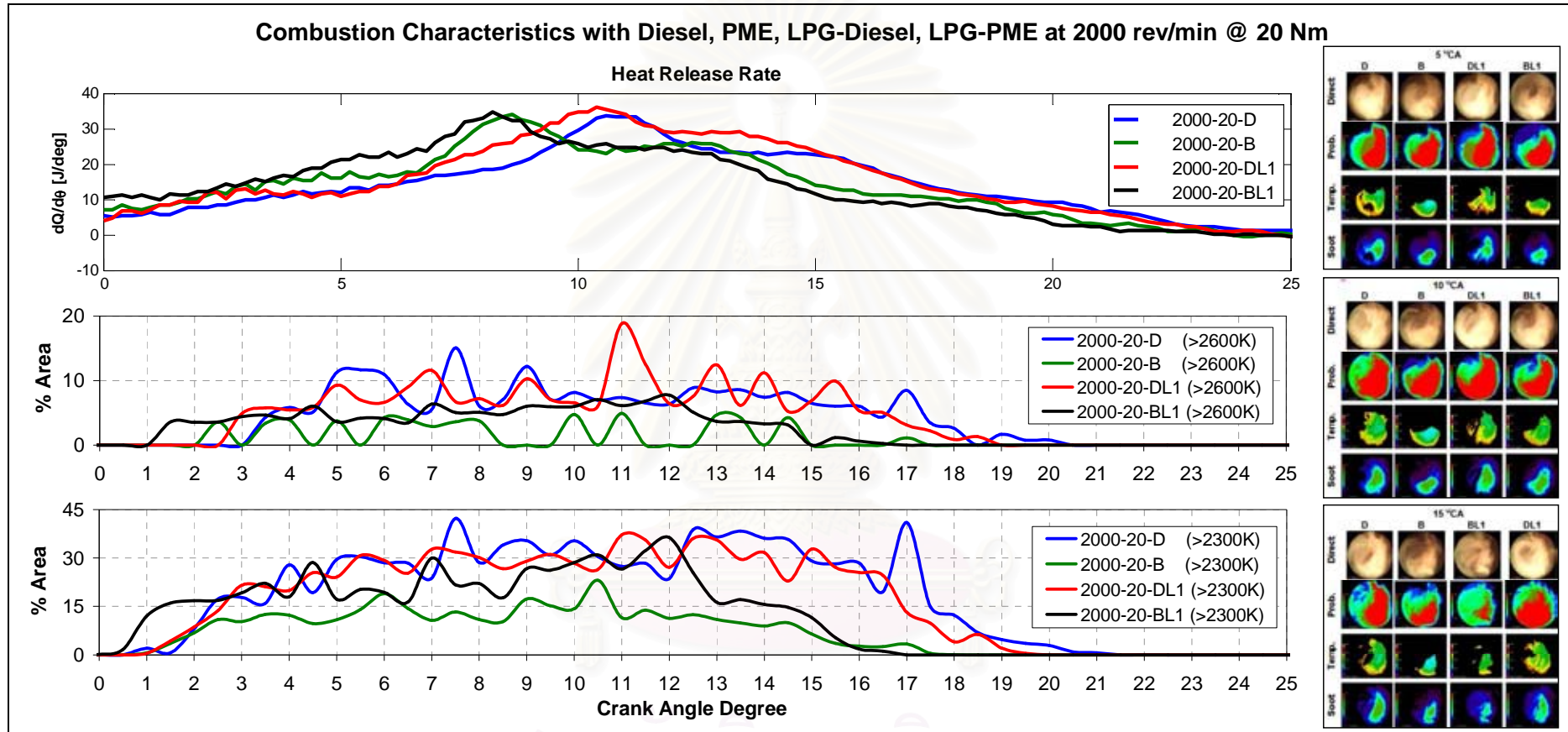
Figure 7–118   HRR and area of flame temperature above 2300 and 2600 @ 2000rev/min, 20Nm (modes D, B, DL1, and BL1)

 # Image groups are at 5, 10, and 15 ^{O}CA
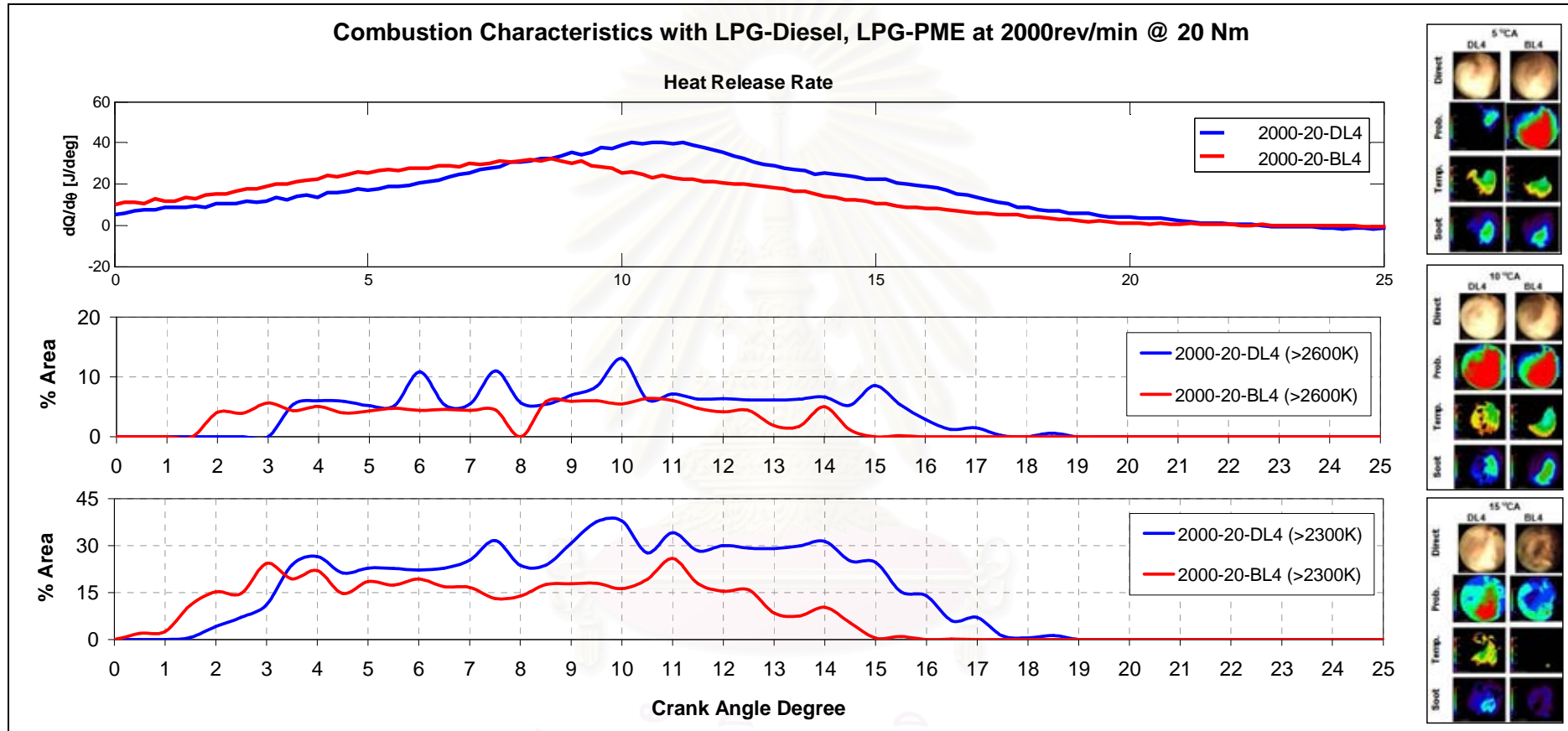
Figure 7–119　HRR and area of flame temperature above 2300 and 2600 @ 2000rev/min, 20Nm (modes DL4 and BL4)

 # Image groups are at 5, 10, and 15 ^{O}CA

% Area of High Flame Temperature Distribution
1250rev/min, 20Nm @ Diesel, PME, LPG-Diesel and LPG-PME Fuelling
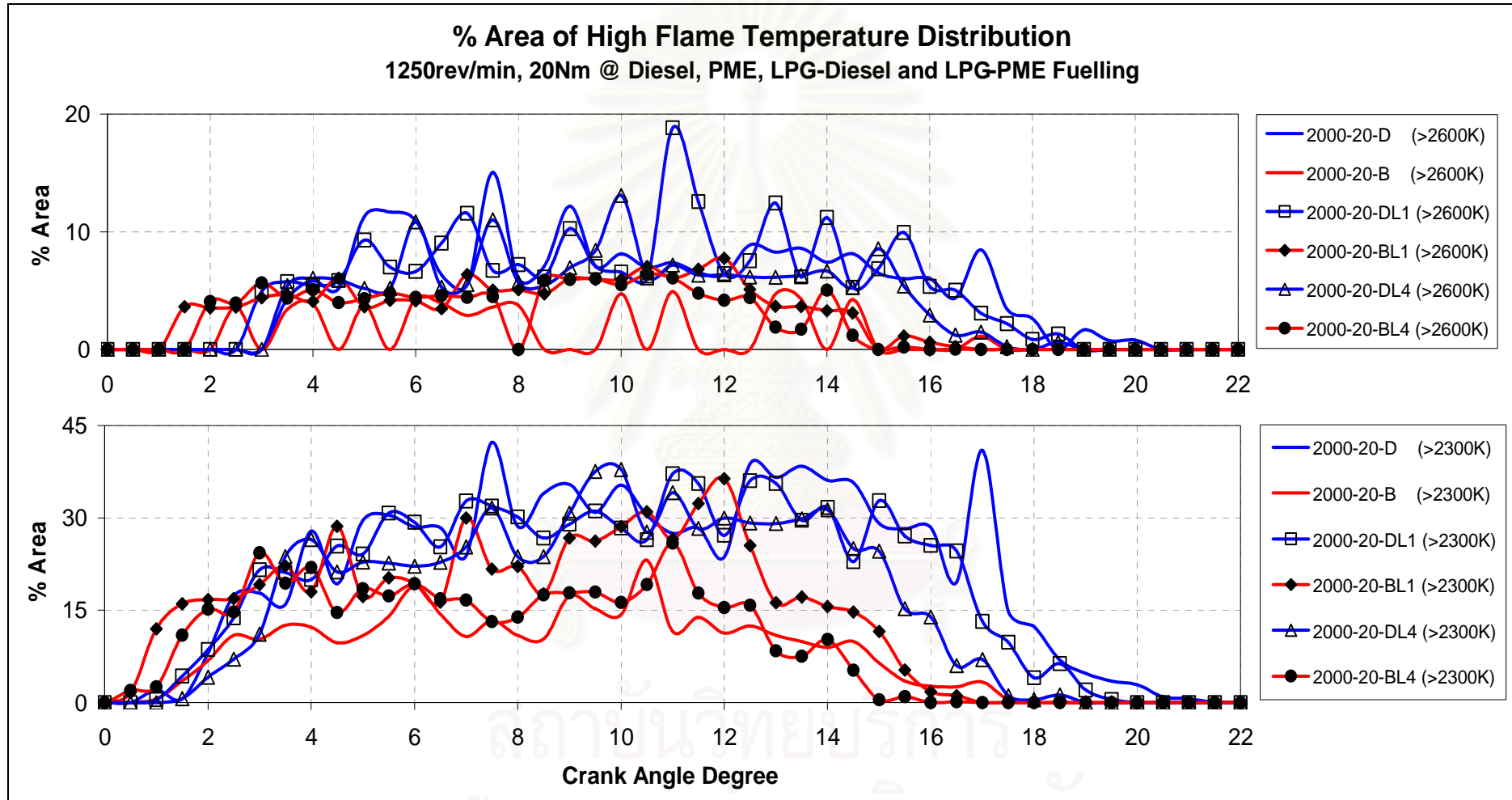
Figure 7–120   HRR and area of flame temperature above 2300 and 2600 @ 2000rev/min, 20Nm (diesel, PME, LPG-diesel, and LPG-PME)
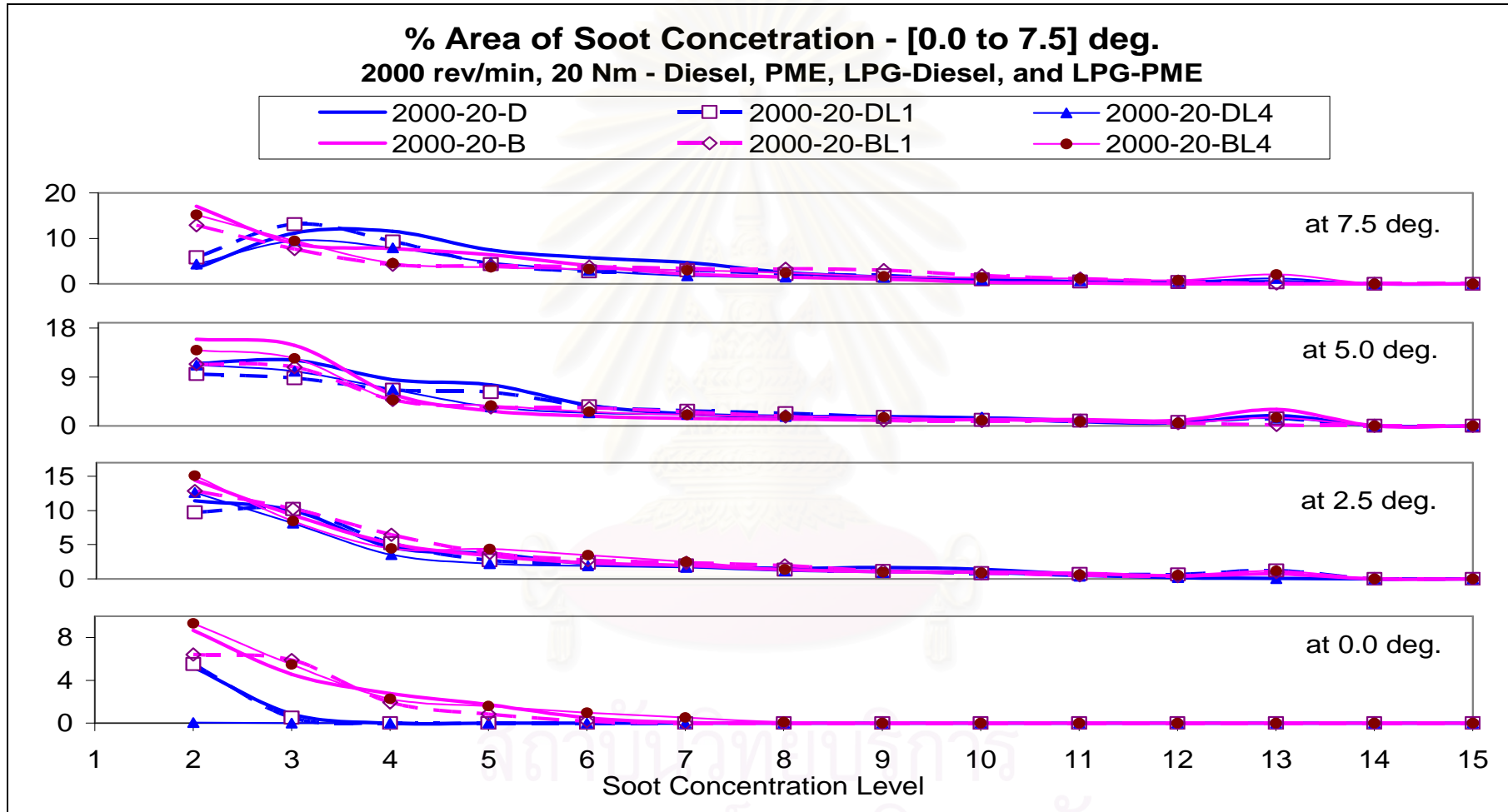
Figure 7–121   Soot concentration trace, 0 to 7.5 degree @ 2000rev/min, 20Nm, (Diesel, PME, LPG-Diesel, and LPG-PME modes)
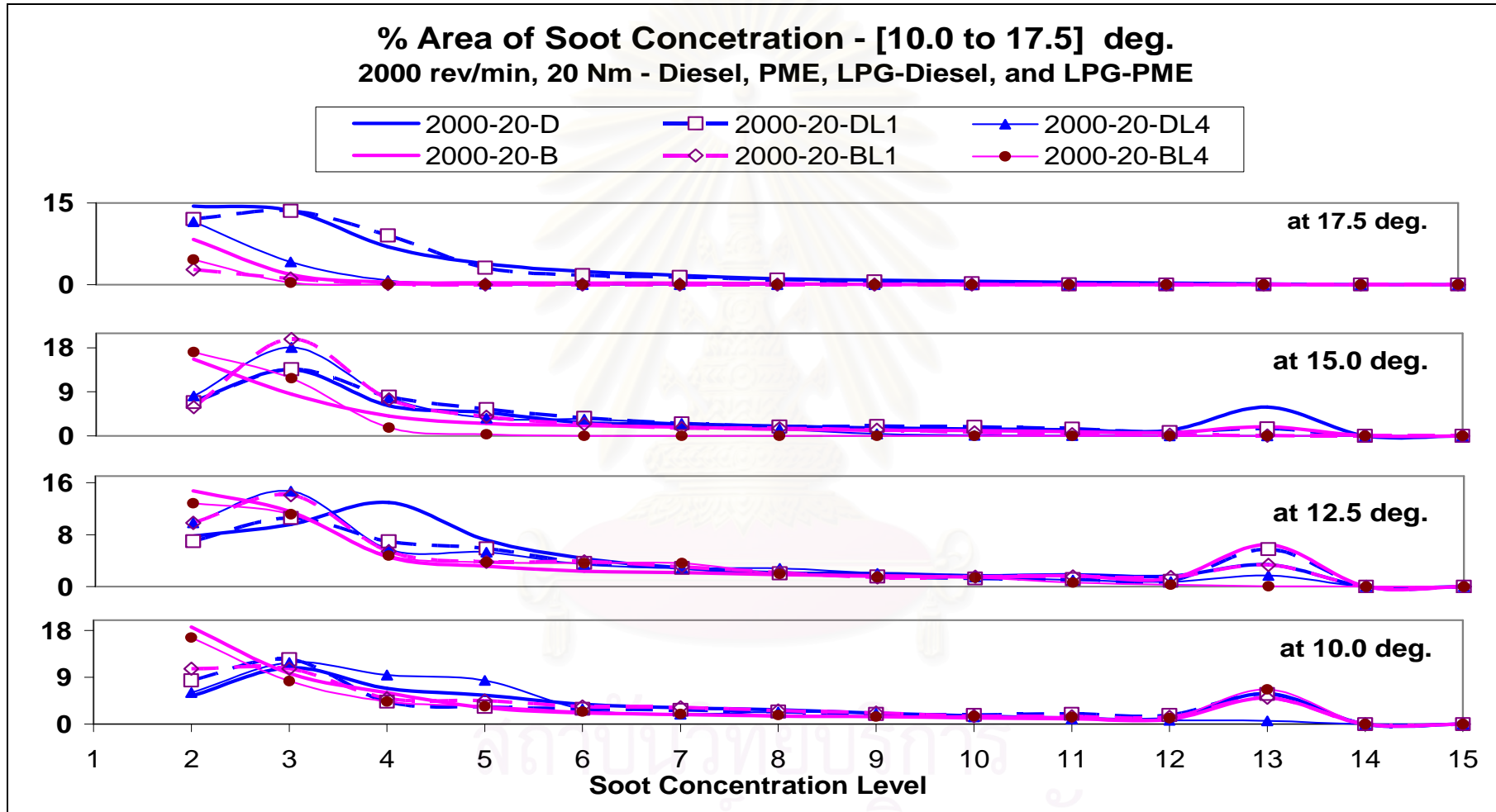
Figure 7–122   Soot concentration trace, 10 to 17.5 degree @ 2000rev/min, 20Nm, (Diesel, PME, LPG-Diesel, and LPG-PME modes)
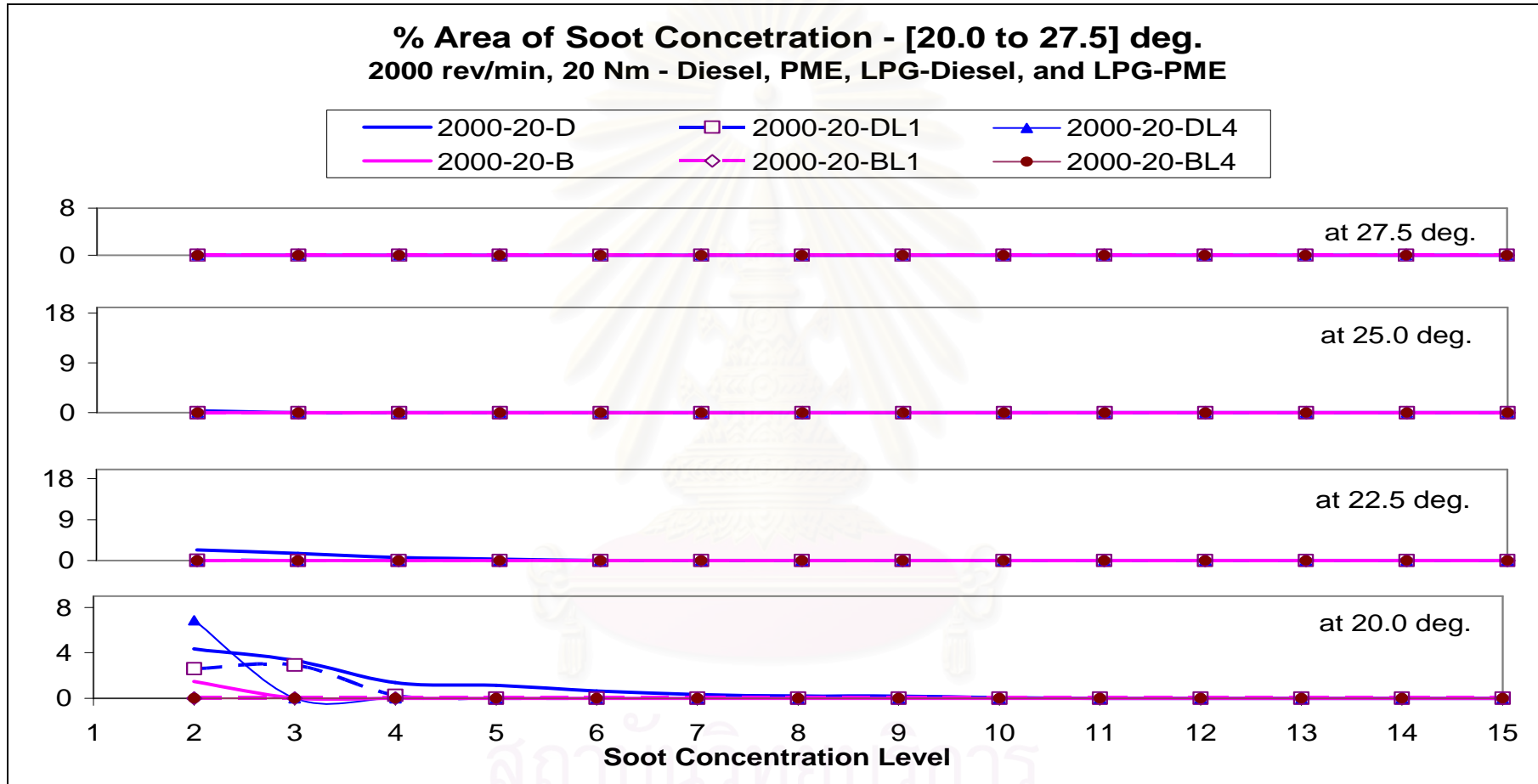
Figure 7–123   Soot concentration trace, 20 to 27.5 degree @ 2000rev/min, 20Nm, (Diesel, PME, LPG-Diesel, and LPG-PME modes)

7.2.3.2. Ignition delay and start of combustion

- The resultant ignition delay with PME and LPG-PME with different LPG ratio is also attributed by the four factors, as analyzed earlier. In addition, it is affected by the oxygen content of the PME. The result of detected ignition delays at different engine speeds, loads, and gas energy fraction are shown in Figure 7–124 to Figure 7–126. At 1250 rev/min, the delay seemed unchanged at lowest load and speed. The highest retardation in the delay was 1.2 degree at 30 Nm, mode BL3. At 2000 rev/min, the LPG ratio seemed to have less effect on the delay, especially at higher load (70Nm). The maximum changes in the delay were about 0.4 degree, at lowest load, mode BL1 and BL2. Almost the same change was observed at 2750 rev/min: the highest change was 0.4 degree at lowest load.

Compared with neat diesel or LPG-diesel modes, the corresponding with neat PME or LPG-PME at 1250 rev/min (Figure 7–39 and Figure 7–124), 2000 rev/min (Figure 7–40 and Figure 7–125), and 2750 rev/min (Figure 7–41 and Figure 7–126) produced shorter ignition delays. These differences reveal the total effect of two factors: the earlier injection of PME has negative effect while the oxygen content in the PME has positive effect on the ignition delay. These shorter delays in cases of neat PME and LPG-PME ascertain that the effect of oxygen content in the PME is dominant over the effect of reduced pressure and temperature brought by the earlier injection.

- The SOC detected by the tool "Combustion Analyzer" is shown in Figure 7–124 to Figure 7–126. The change in SOC was resulted from the change in the SOI and the delay. At low and medium speeds, the SOC in dual fuel mode were later than that in neat PME mode but almost earlier than that in neat diesel or LPG-diesel modes. At 1250 rev/min and constant engine torques, compared to neat PME the retardation was longer with increased LPG; in a range of $[0.6 \div 1.8]^O$CA except mode BL4 (highest LPG ratio). At 2000 rev/min, the SOC were later than that with neat diesel and in the range $[0.4 \div 1.0]^O$CA. However, at this speed when the load increased the retardation became lesser ($[0.4 \div 0.6]^O$CA) as the LPG increased, especially at the same instant in mode 2000-70-

BL4. At 2750 rev/min, the SOC were almost the same (around -8.6, 8.8 ^{O}CA) with different loads and LPG ratio. This might be resulted from two following factors:

- The effect of higher prevailing temperature and pressure. The higher prevailing temperature is due to higher friction, less heat and mass losses while the higher prevailing pressure is due to less mass loss.

- The higher turbulent intensity at high speed.
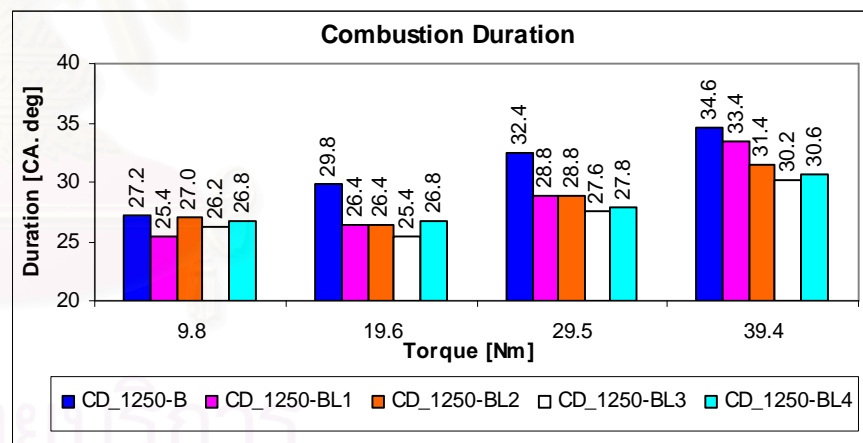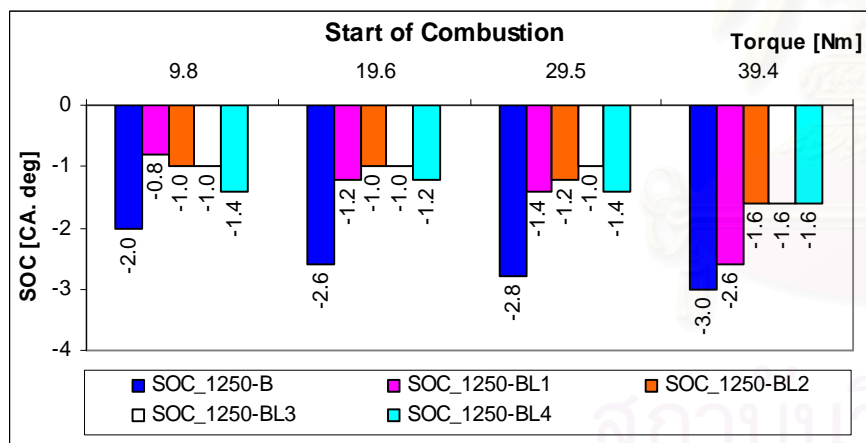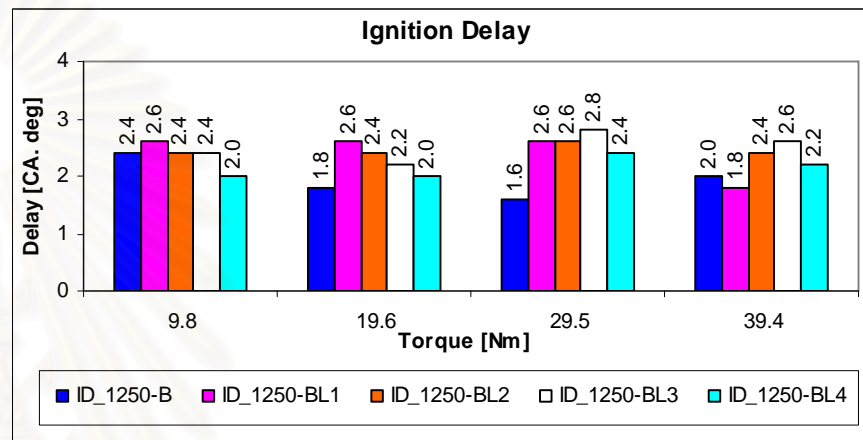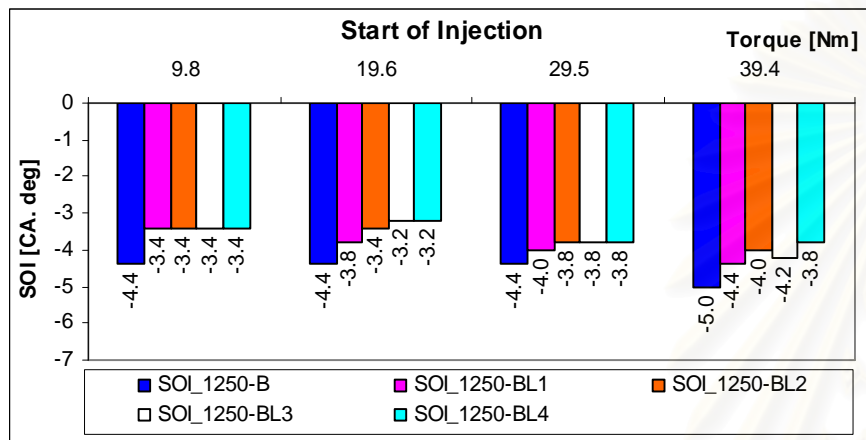
Figure 7−124   SOI, SOC, ignition delay and combustion duration # 1250 rev/min, PME and LPG-PME
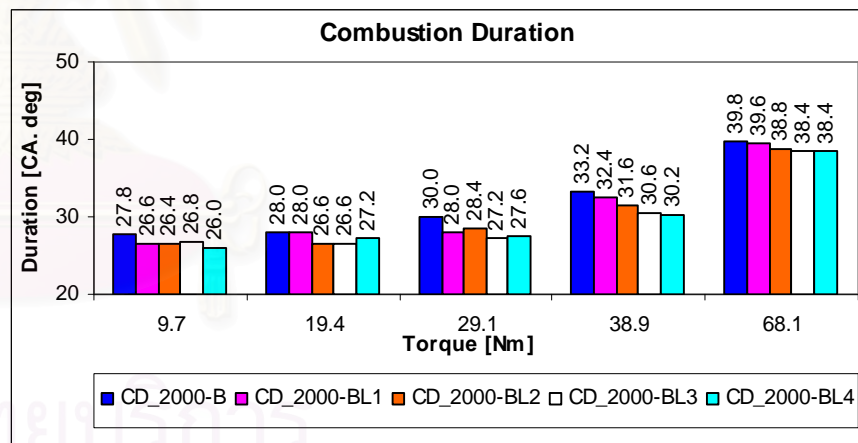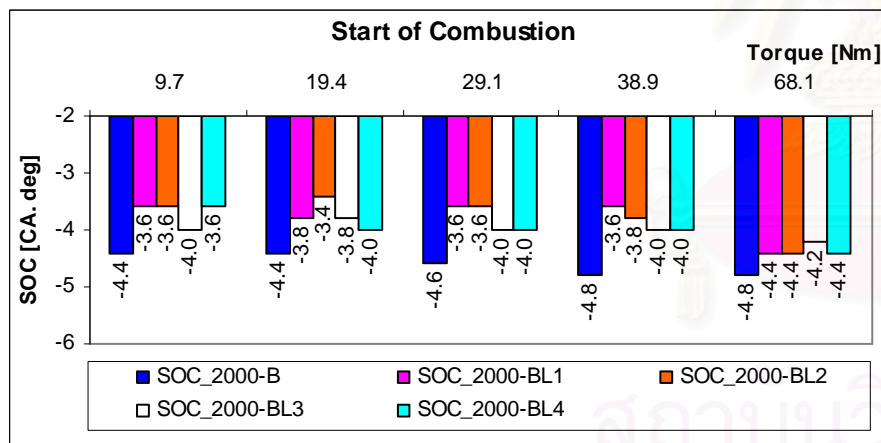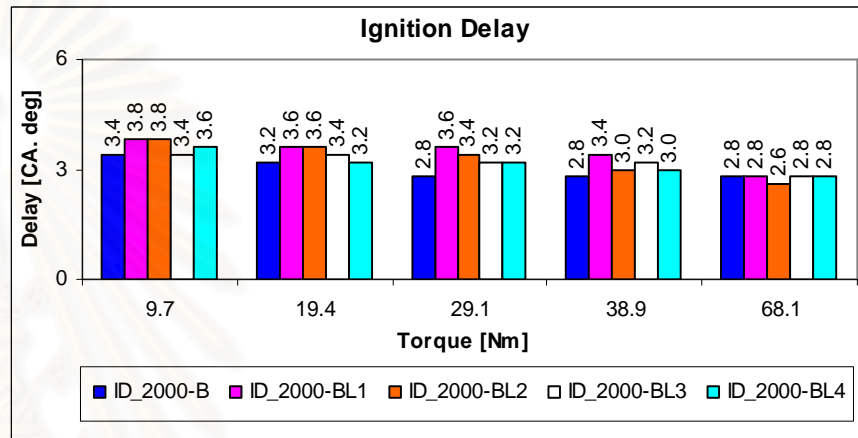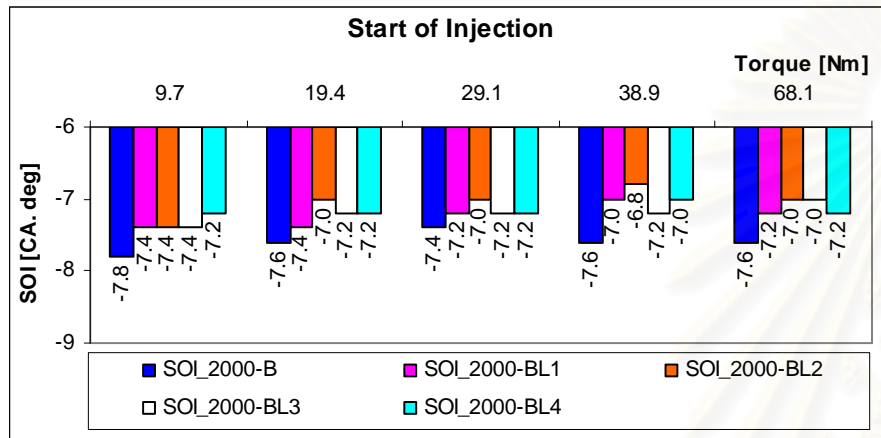
Figure 7–125   SOI, SOC, ignition delay and combustion duration # 2000 rev/min, PME and LPG-PME
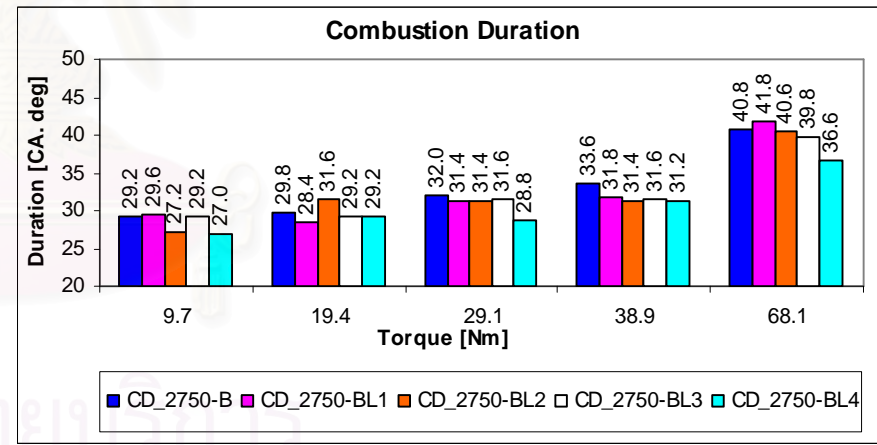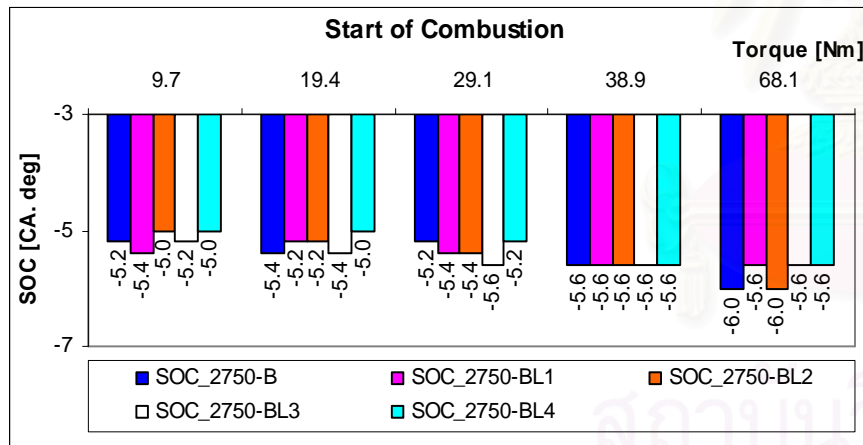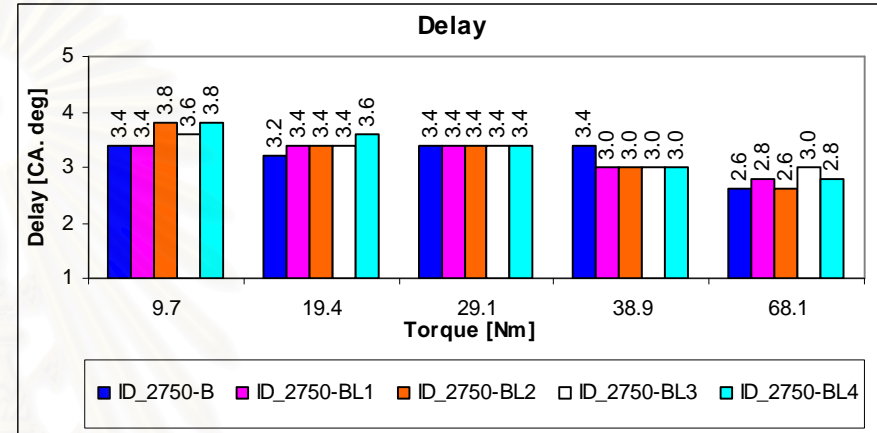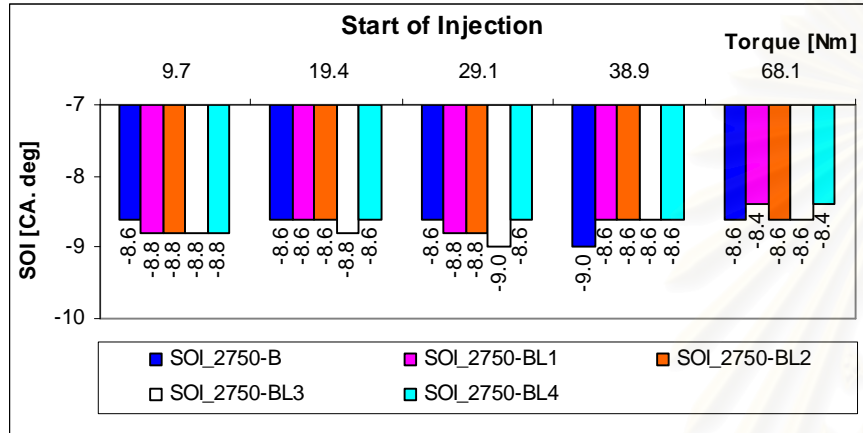
Figure 7–126   SOI, SOC, ignition delay and combustion duration # 2750 rev/min, PME and LPG-PME

7.2.3.3. The heat release rate, peak of pressure, pressure rise rate, and cyclic variation

The net HRR, PRR, and main chamber pressure with neat diesel, LPG-diesel, PME, and LPG-PME modes are presented (Figure 7–127 to Figure 7–133). These parameters for modes D, DL1, and DL4 are presented by the solid-blue, solid-green, and solid-red lines, respectively. Those for neat modes B, BL1, and BL4 are presented by the dash-blue, dash-green, and dash-red lines, respectively. From these figures, these following general features are revealed:

@ The HRR profiles in LPG-PME modes were, also, almost similar to that in neat diesel modes. However, due to earlier injection compared to diesel, the HRR curve moved towards TDC (the left hand side). The movement was about [1÷2] degree at 1250 rev/min (Figure 7–53 and Figure 7–134), [1.8÷2.3] at 2000 rev/min (Figure 7–54 and Figure 7–135), and [1.4÷2.5] at 2750 rev/min (Figure 7–55 and Figure 7–136). This causes two effects: the positive one is theoretically higher thermal efficiency and the negative are higher heat transfer to the chamber wall and higher negative work since part of combustion process takes place as the piston is before TDC. The earlier SOC, hence earlier EOC gives much more time for the product to expanse, leading to lower exhaust gas temperature. Significant decrease in exhaust gas temperature was found and presented in Figure 7–87 to Figure 7–89. The movement in LPG-PME modes was higher compared to neat PME, and appeared proportional to the LPG ratio.

@ The earlier combustion in PME/ LPG-PME modes caused their integrated NHR to become higher than that of diesel/ LPG-diesel modes during the early and main stages but lower at the late stage of combustion. This maintained the high in-cylinder pressure for a period aTDC, or even lifted the pressure up about 10 bars in this period.

@ Since the ignition delays in neat PME or LPG-PME modes were shorter and the combustion started before TDC in LPG-PME modes, part of the HRR curve before the zigzag was higher compared to that in LPG-diesel modes. In the zigzag at 1250 and 2000 rev/min, the HRR with LPG-PME seemed to be depressed and comparable or slightly lower than that in LPG-diesel case. This may be resulted from the higher cooling effect of the PME (because of larger amount of PME injection per cycle compared to diesel injection at the same modes of LPG supply). At 2750 rev/min, the net HRR in the

zigzag zone with LPG-diesel and LPG-PME were comparable since the effect of the enhanced turbulent brought by higher speed was dominant. Just after the zigzag, the net HRR in LPG-diesel cases reduced since the diesel was injected into lower pressure and temperature environment.

@ .At all speeds and loads, whereas the peaks of HRR in neat PME modes were lower than that in neat diesel modes, the peaks in LPG-PME modes might be higher than that in LPG-diesel modes (such as 1250-20-BL1, 2750-20-BL1, 2750-20-BL1 modes). The peaks of HRR in neat PME/ LPG-PME modes occurred approximate [2÷3] degree earlier than the corresponding in neat diesel/ LPG-diesel modes.

@ At all modes of PME/ LPG-PME, although the centers of HRR area were closer to TDC, the late stage of combustion in neat PME/ LPG-PME modes seemed longer than that in neat diesel/ LPG-diesel modes, recognized by the less steep part of HRR curve before its intersection with the abscissa. This might be due to the longer injection duration and lower volatility of the PME compared to the diesel.

@ Similar to LPG-diesel dual modes, although the LPG-PME dual fuel operation provided earlier heat release compared to the neat diesel and LPG-diesel, the total energy conversion efficiencies were lower. The following factors might contribute to this deterioration:

- The incomplete combustion of the LPG in the pre chamber.

- The LPG energy loss by blow-by.

- The combustion chamber geometry.
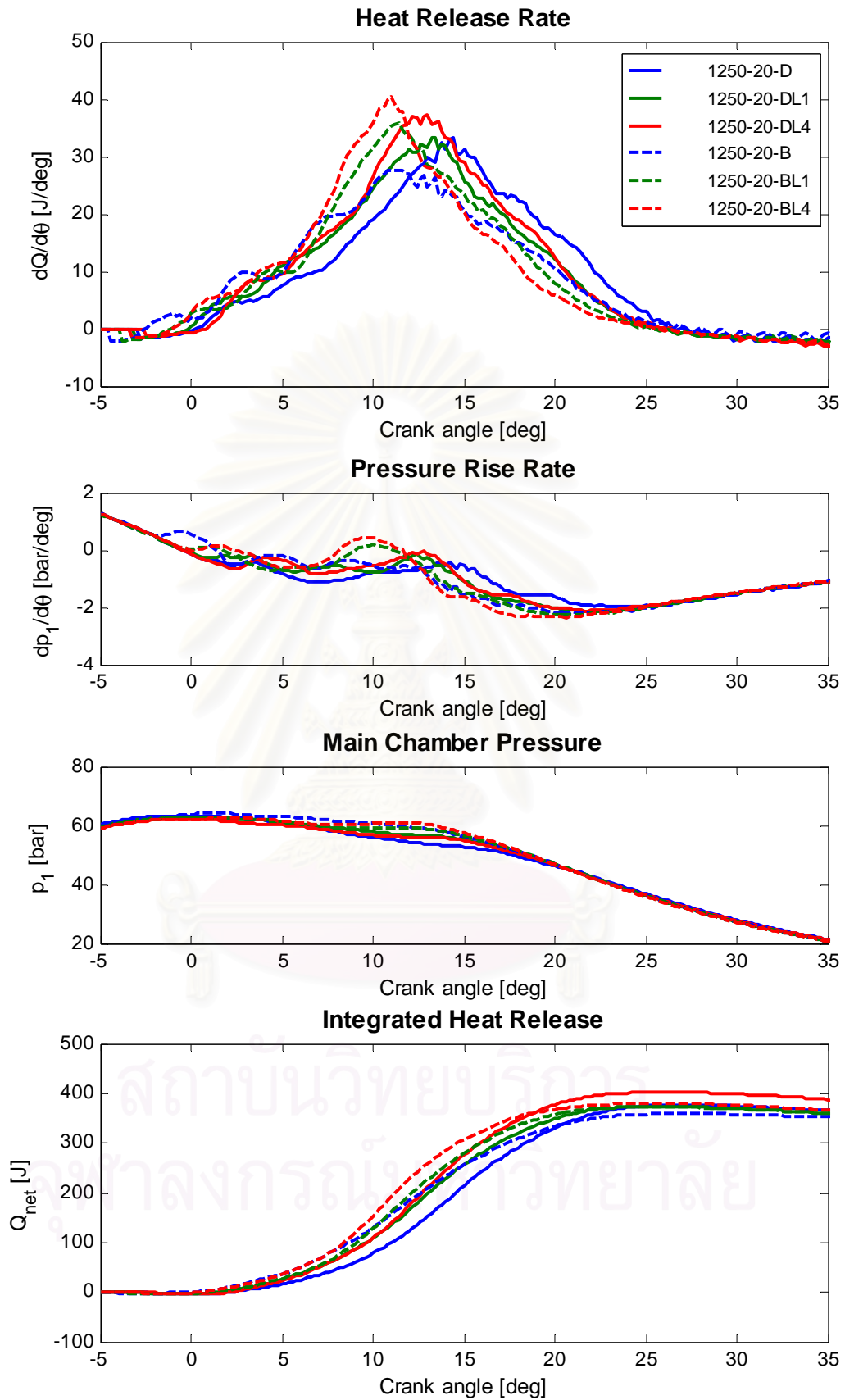
Figure 7–127   Net HRR, chamber PRR, and pressure at 1250 rev/min, 20Nm
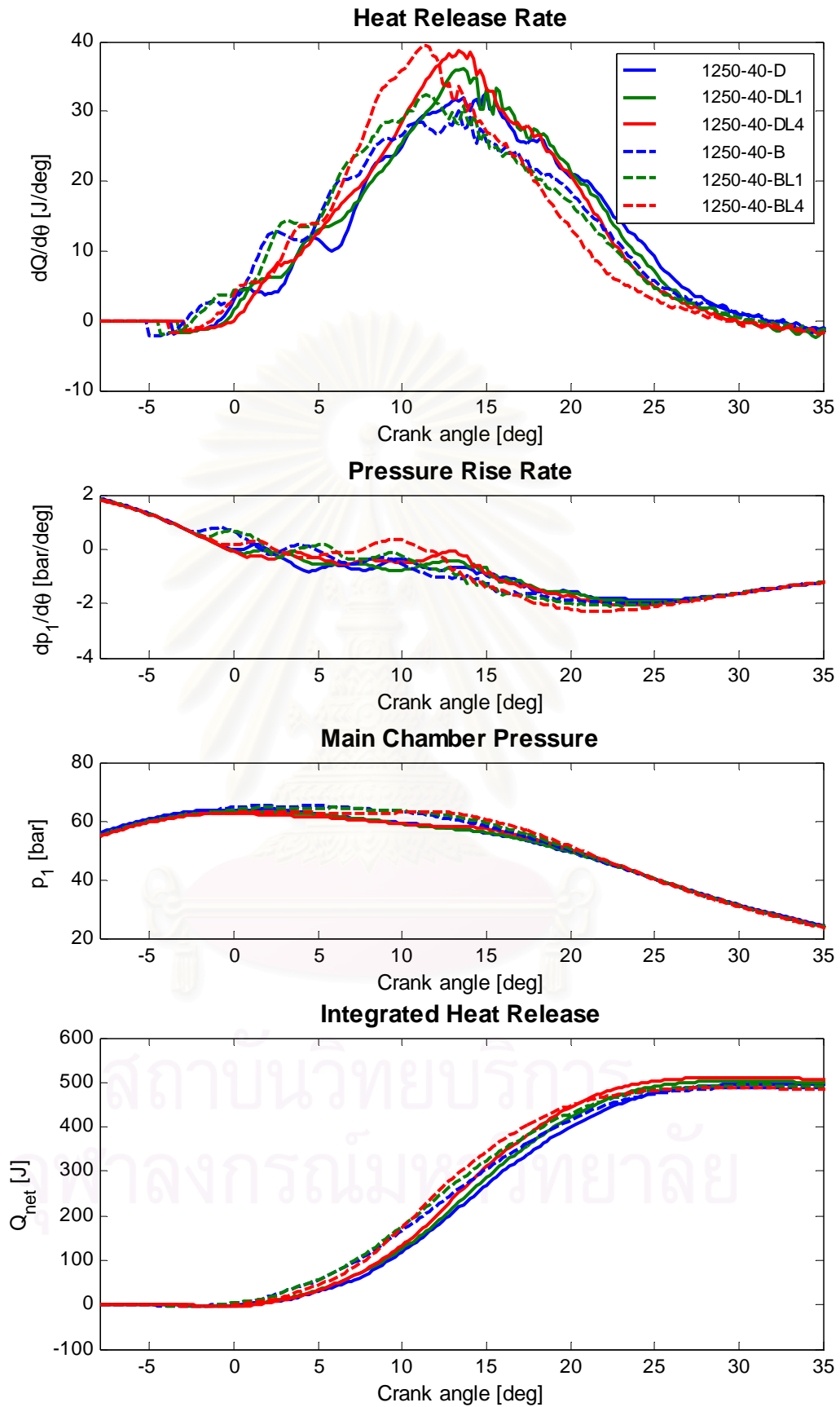
Figure 7–128   Net HRR, chamber PRR and pressure at 1250 rev/min, 40 Nm
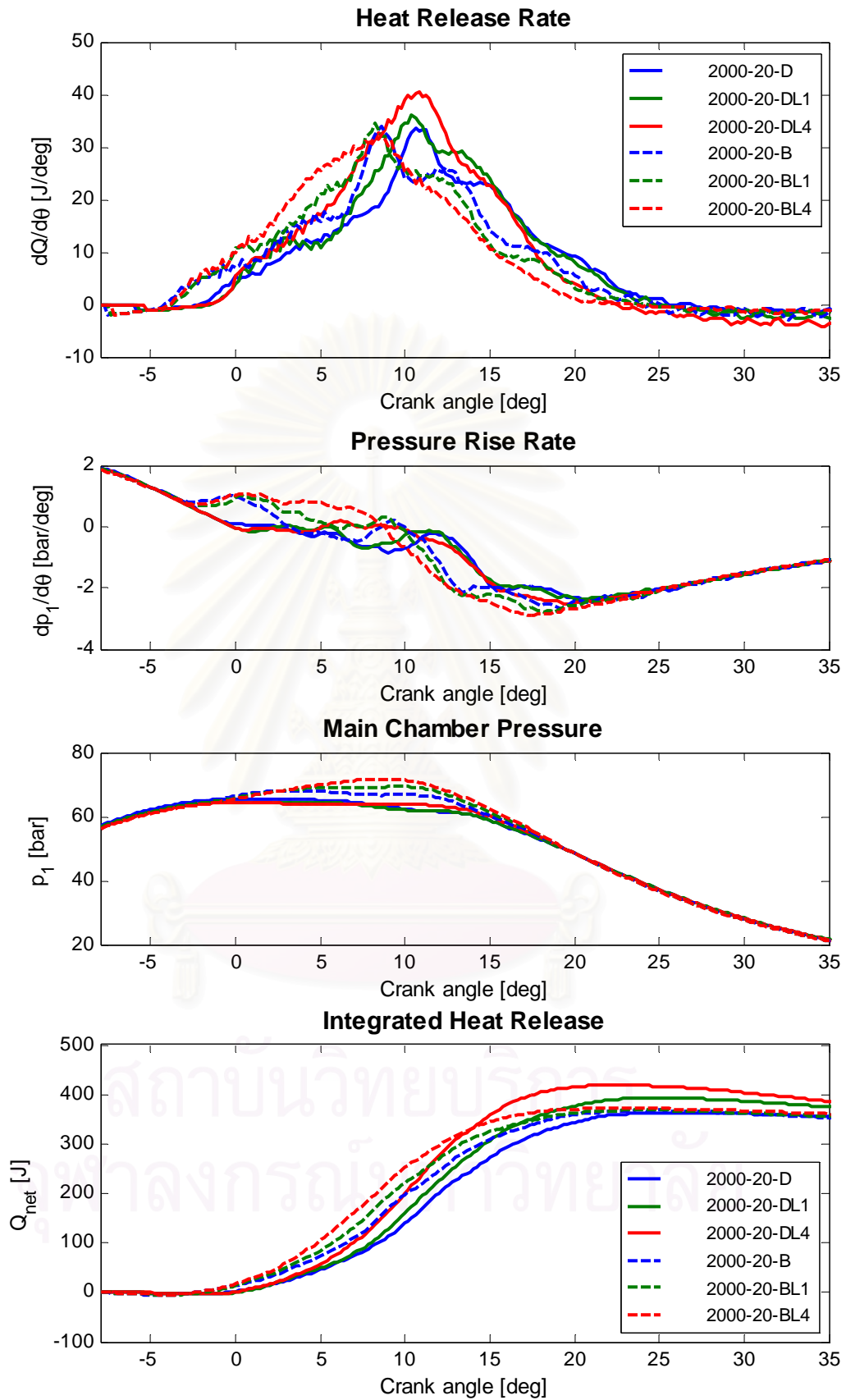
Figure 7–129   Net HRR, chamber PRR and pressure at 2000 rev/min, 20 Nm
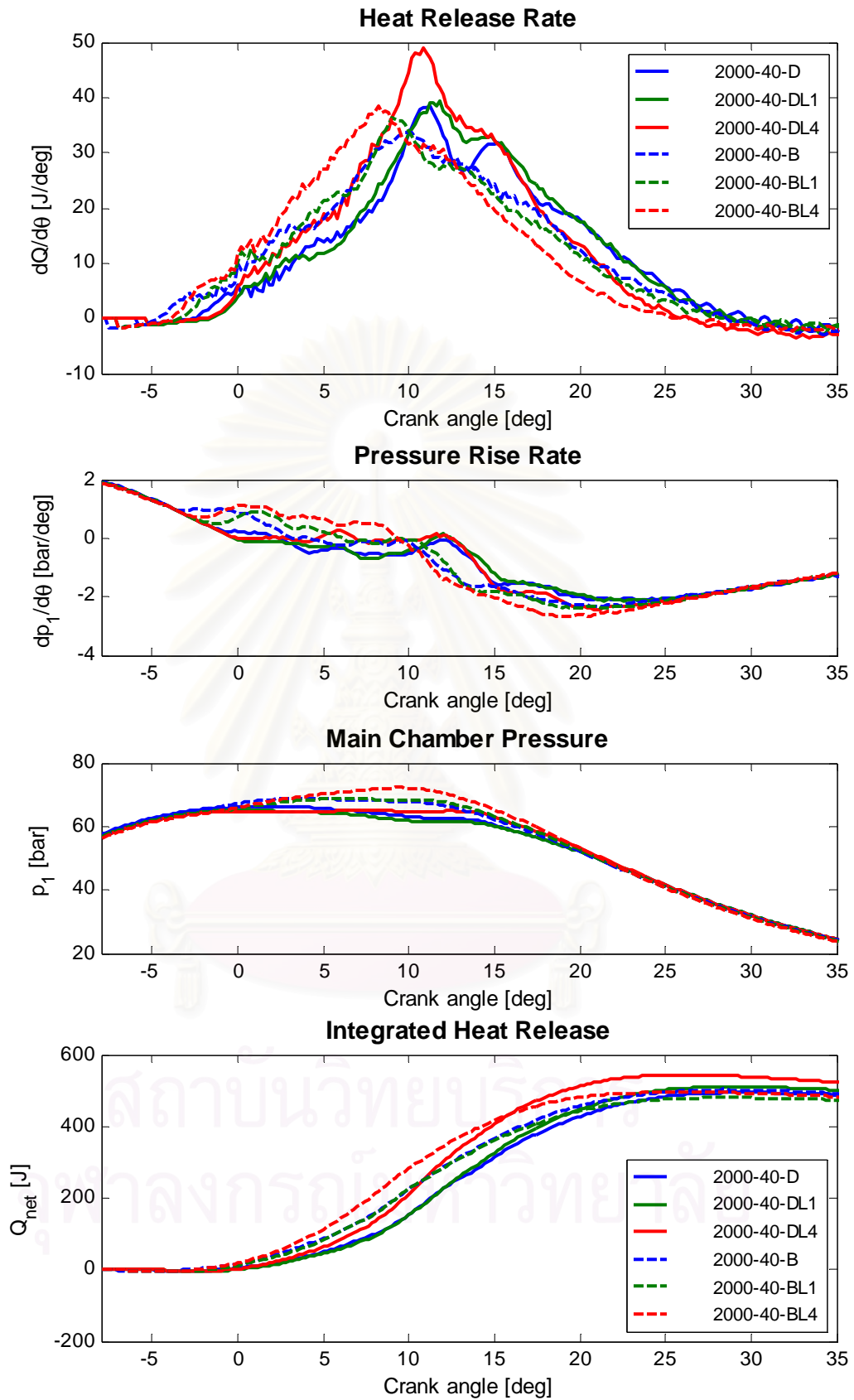
Figure 7–130   Net HRR, chamber PRR and pressure at 2000 rev/min, 70 Nm
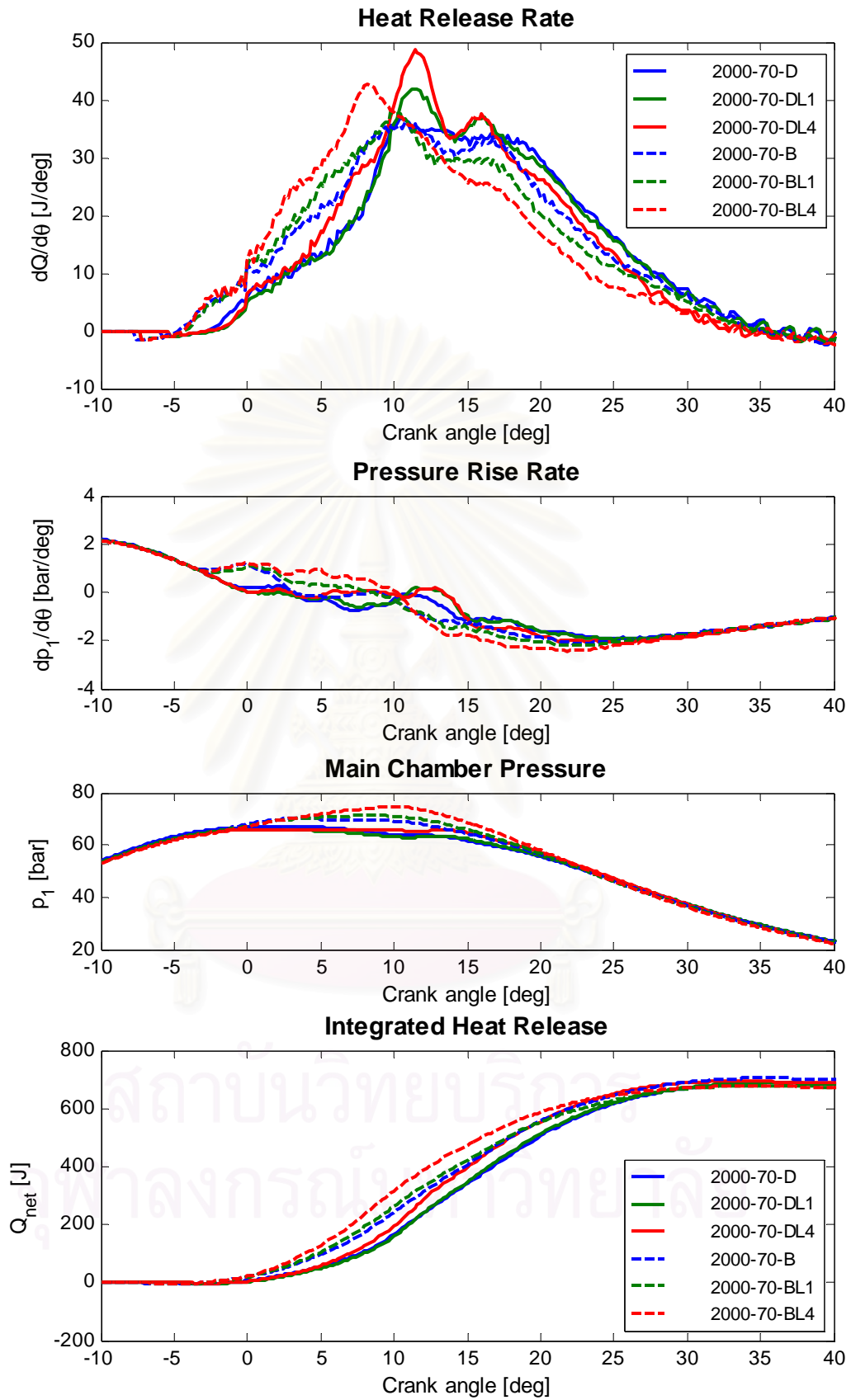
Figure 7–131 Net HRR, chamber PRR and pressure at 2000 rev/min, 70 Nm
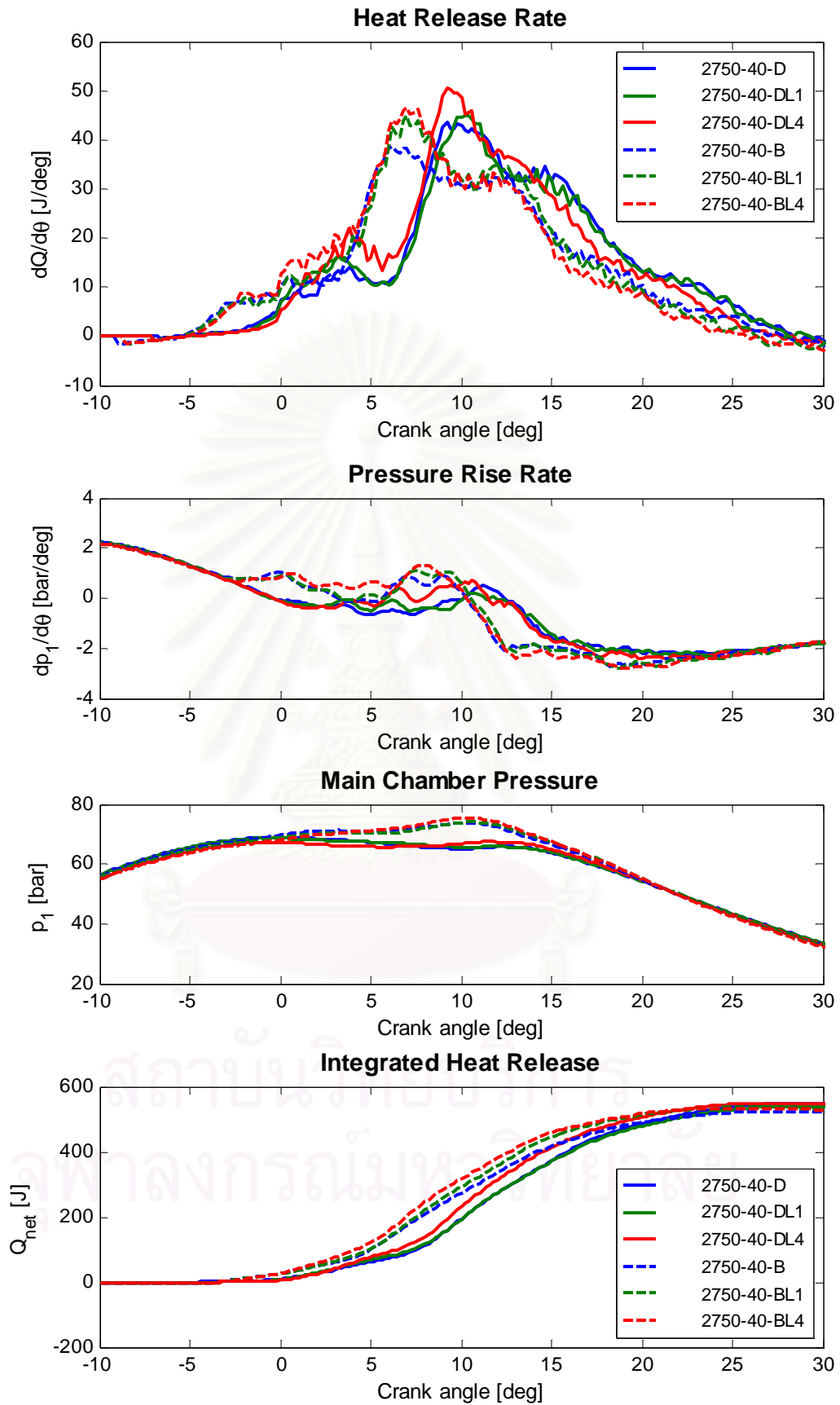
Figure 7–132   Net HRR, chamber PRR and pressure at 2750 rev/min, 20 Nm
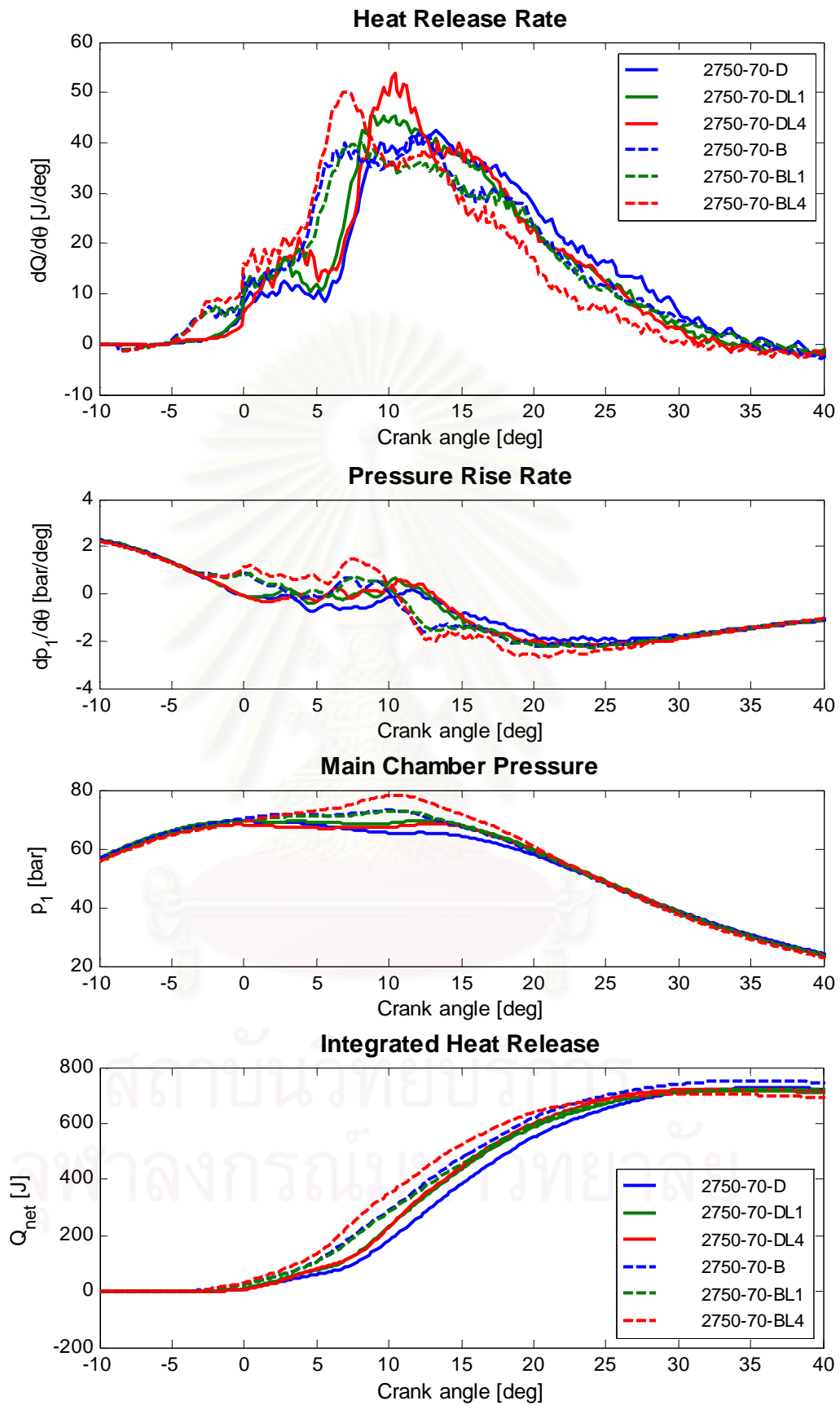
Figure 7–133   Net HRR, chamber PRR and pressure at 2750 rev/min, 70 Nm
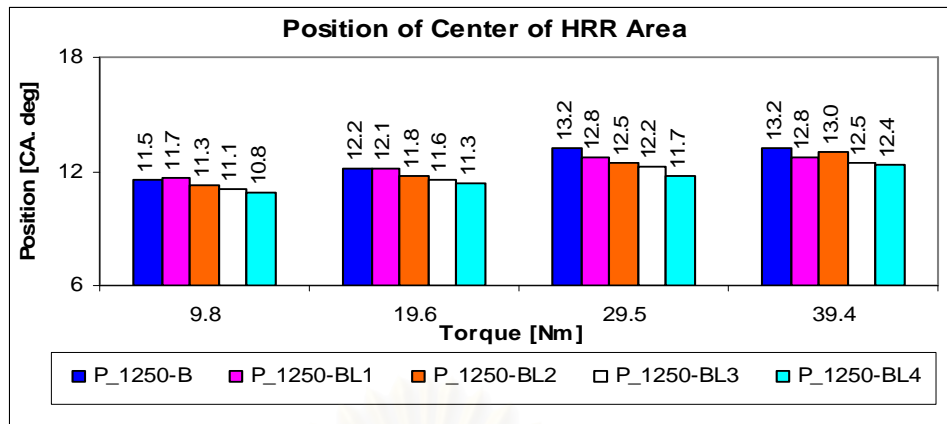
Figure 7–134　Position of the center of HRR area # 1250rev/min, PME and LPG-PME
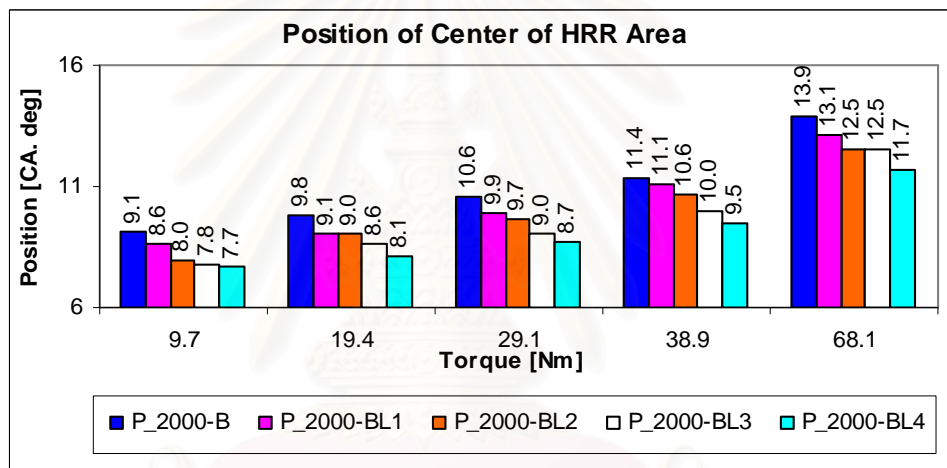
Figure 7–135　Position of the center of HRR area # 2000rev/min, PME and LPG-PME
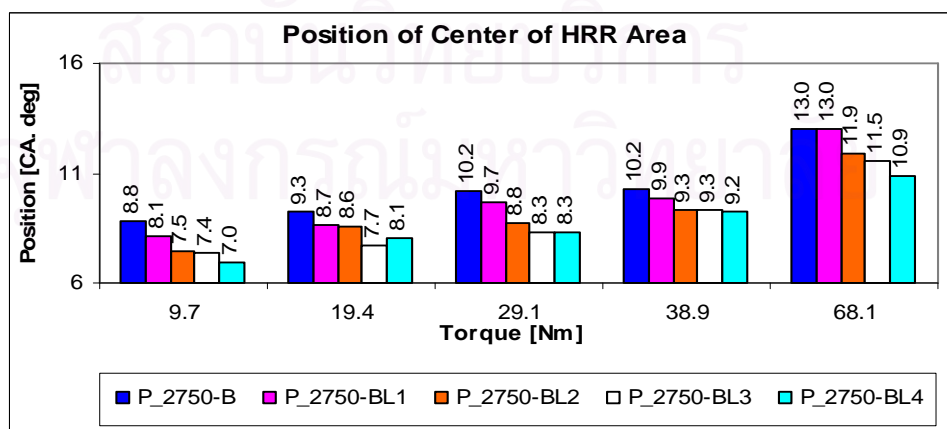
Figure 7–136　Position of the center of HRR area # 2750rev/min, PME and LPG-PME

Similar to LPG-diesel fuelling, the operation modes which provide the highest integrated net heat release will be the reasonable. The predicted NHR results indicate that the reasonable modes were mostly DL4, as shown in Table 7-4. The reasonable substitution was in the ranges of about [34%÷58%], [27%÷40%], and [21%÷40%] at 1250, 2000, and 2750 rev/min, respectively.

Table 7-4   Modes of LPG-PME operation that provide highest net heat release

Engine speed	Brake Torque	Operation mode	Fuel-Air equivalent ratio		Substitution
Rev/min	(Nm)		ϕ_g	ϕ_t	Sub (%)
1250	40	BL4	0.13920	0.31806	38.56
	30	BL4	0.13721	0.28472	42.65
	20	BL4	0.13738	0.24857	51.8
	10	BL4	0.13694	0.20762	59.9
2000	70	BL4	0.14159	0.45769	27.1
	40	BL3	0.11738	0.35106	27.5
	30	BL4	0.14149	0.32574	35.3
	20	BL4	0.14119	0.29372	39.3
2750	70	BL3	0.11309	0.46692	21.3
	40	BL4	0.13954	0.38021	30.6
	30	BL4	0.13977	0.34599	33.5
	20	BL4	0.14001	0.32106	33.4

@ The peaks of pressures and pressure rise rates, and the cyclic variation:

Similar to diesel or LPG-diesel operation, the peaks of pressure and PRR may occur in the compression or combustion process. If the peaks of pressure are caused by compression, the peaks in dual fuel modes were lower than that in PME modes. Conversely, if they are caused by combustion they tend to be higher than that in neat

PME modes. If the peaks of PRR in dual fuel modes are caused by compression they are similar to that in diesel modes and appear approximately 12°CA bTDC. Combustion process maintains the high pressure which is generated by compression. In these cases, the PRR is negative in the combustion period and may reach a local maximum value close to that in compression stroke. Statistical analysis for chamber pressures is shown in Figure 7–137 to Figure 7–141. Following features have been recognized:

- At 1250 rev/min, in neat PME and LPG-PME dual fuel modes, the mean values of maximum pressures in the main and pre-chamber were not much different; within 1.7 bars. However, since the PME was injected earlier and start to burn bTDC the pressure started to increase. In PME-LPG modes, the SOC were later than that in neat PME hence the peaks of pressure in neat PME and mode 1250-40-BL1 were higher than that in diesel/ LPG-diesel modes whereas in the last three modes of LPG-PME the peaks of pressure were comparable to that in diesel/ LPG-diesel modes. The COV in the peak pressures were small; within 2% in main chamber and within 1% in pre chamber. In both chambers, the COV of peak of PRR were small and similar to that in diesel/ LPG-diesel modes; within 3.3%. The COV of peaks of PRR seemed to increase with increased LPG ratio.

- At 2000 rev/min @ 40 Nm, the averages of peaks of pressure in the two chambers were higher than that in diesel/LPG-diesel modes due to earlier SOC (Figure 7–125). The peaks were higher with increased LPG (from just above 69bar to approximate 73 bars, as shown in Figure 7–138. The COV of peak of pressure were comparable to that in diesel/LPG-diesel modes; within 2.5%. The averages of peak of PRR in the prechamber were higher than that in diesel/ LPG-diesel ([9.7÷10.6] compared to [6.8÷7.7] bar/deg) since the combustion start earlier while the total chamber volume decreased. The COV of peaks of the pre-chamber PRR increased with LPG ratio and was comparable to that in diesel/ LPG-diesel modes; within 3%.Similar trends in the peaks of pressure and PRR occurred at higher load (70Nm), 2000 rev/min. The averages of peaks of pressures were higher than that in diesel/ LPG-diesel modes, and increased with increased LPG ratio; within 5 bars

(Figure 7–139). Similar to that in diesel-LPG modes, the COV of peaks of pre-chamber PRR increased sharply with LPG ratio; reaching about 9% with the highest LPG.

- At high speed, 2750 rev/min, the averages of maximum pressures fluctuated when the LPG changed but higher than that in diesel/ LPG-diesel modes. The differences were up to 8 bars at 40 Nm and 70 Nm. The COV of peaks of the both chamber pressures were almost unchanged: around 2.5% and similar to that in corresponding diesel/ LPG-diesel modes. The COV of peaks of PRR, however, still kept the trend; increasing with LPG ratio and being comparable to that in diesel/ LPG-diesel modes; within 4.5%.

The COV_{IMEP} at 1250, 2000, and 2750 rev/min are presented in Figure 7–61 to Figure 7–63, respectively. The following trends in COV_{IMEP} have been addressed:

- The COV_{IMEP} tended to increase proportionally with the LPG ratio at all engine speeds and torques, comparable to that in diesel/ LPG-diesel modes.

- At speed 1250 and 2750 rev/min, the COV_{IMEP} increased from about 1.7% (in neat PME modes) to about 6.5% (in mode L4 of LPG supply).

- At 2000 rev/min, there were dramatically increases in the COV_{IMEP} when the LPG ratio increased. The COV_{IMEP} increased from about [1%÷1.7%] (in neat diesel/PME) to about [8%÷15%] (in mode L4 of LPG supply).

- When the speeds and LPG ratios are fixed, the COV_{IMEP} decreased with increased engine torque since the liquid fuel fraction increased.

- Comparison in COV_{IMEP} with respect to engine speeds is depicted in Figure 7–64 to Figure 7–71. It is observed that at 2000rev/min, the COV_{IMEP} sharply increases; about 3.5 folds compared to that at 1250 and 2750 rev/min. There were moderately higher COV_{IMEP} in LPG-PME modes compared to that in the corresponding LPG-diesel modes; approximate 2% at the highest LPG ratio.
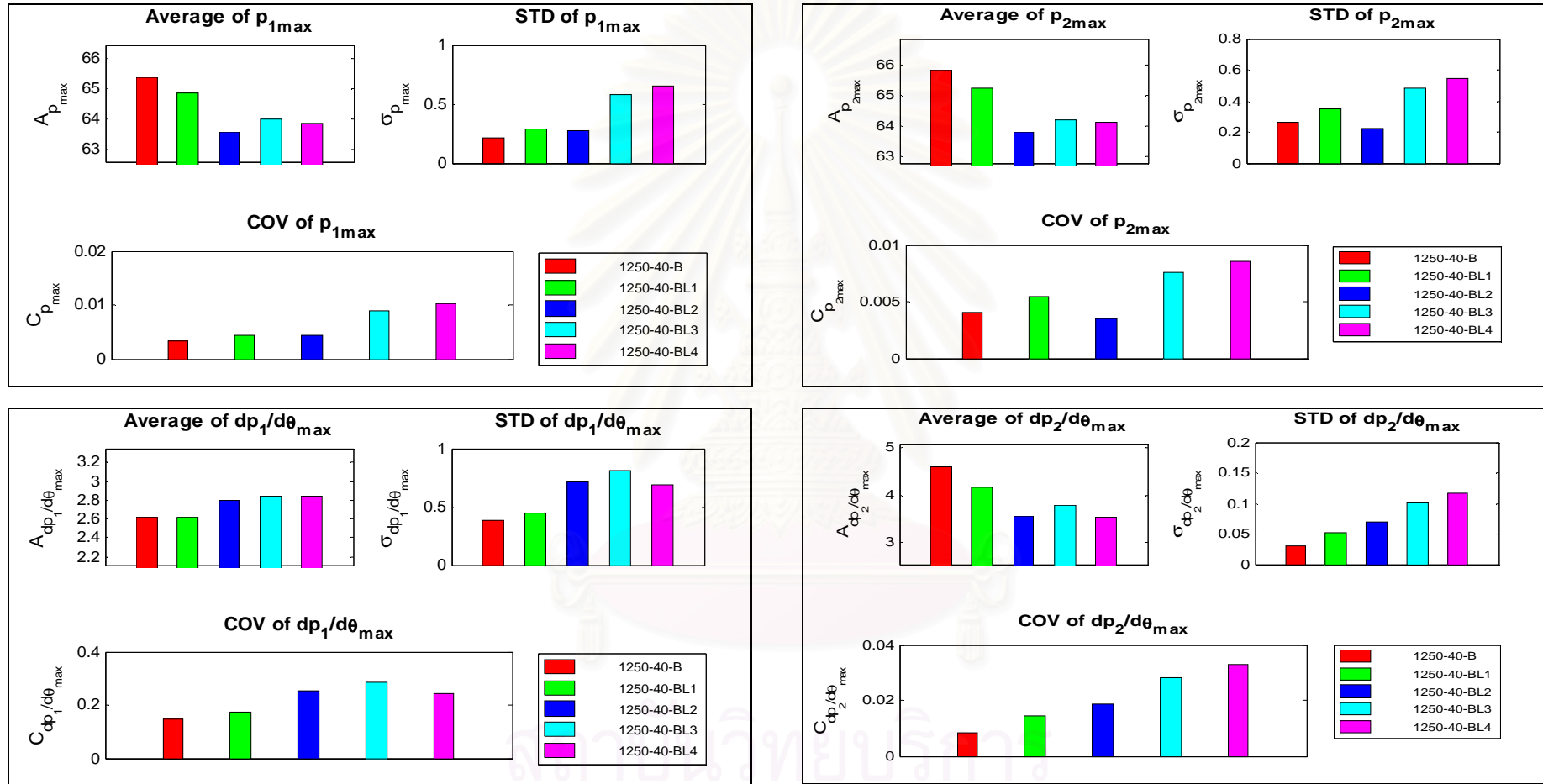
Figure 7–137   Average, STD, and COV of chamber pressure and PRR at 1250rev/min, 40Nm (PME and LPG-PME modes)
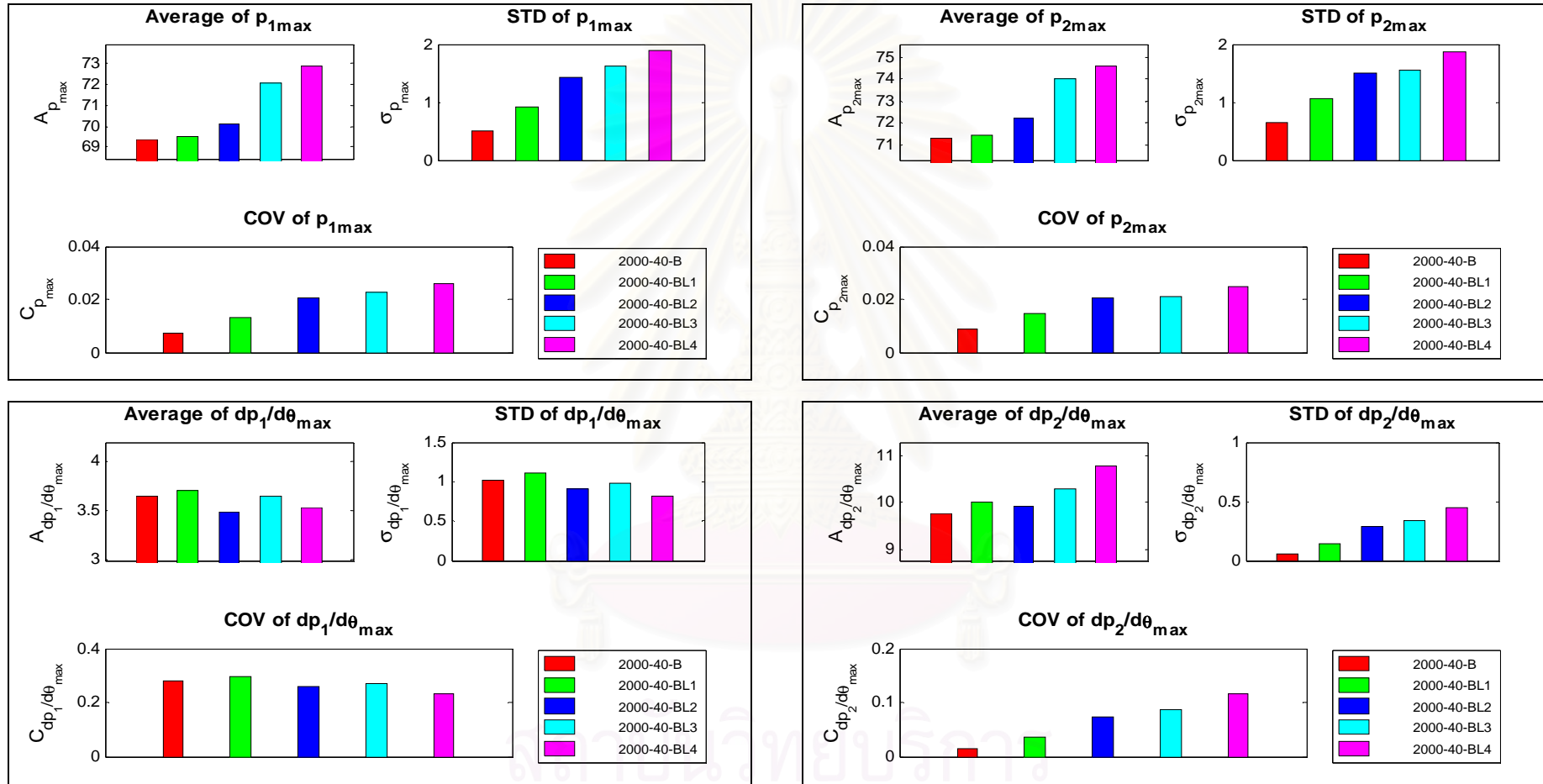
Figure 7–138   Average, STD, and COV of chamber pressure and PRR at 2000rev/min, 40Nm (PME and LPG-PME modes)
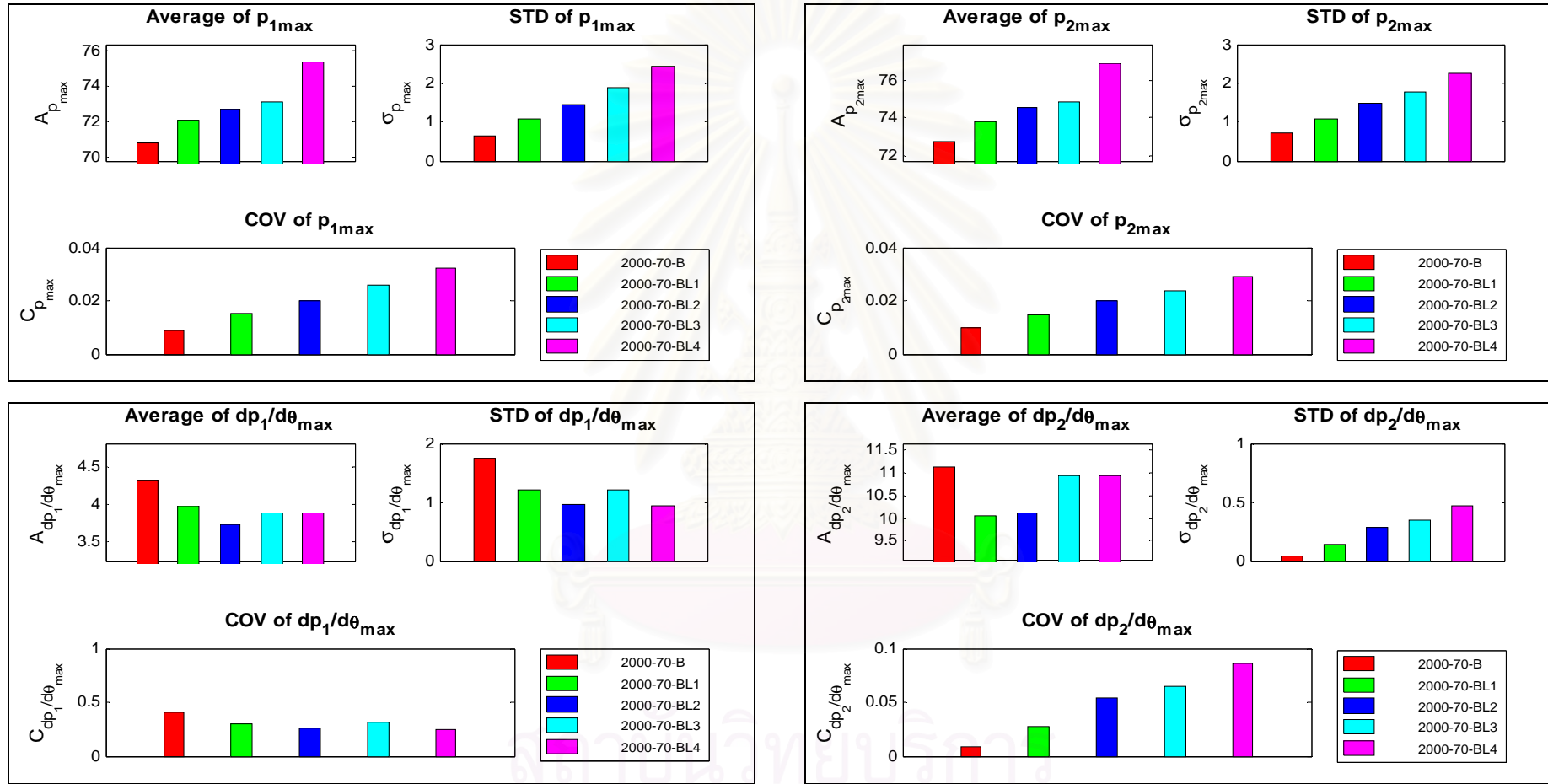
Figure 7–139   Average, STD, and COV of chamber pressure and PRR at 2000rev/min, 70Nm (PME and LPG-PME modes)
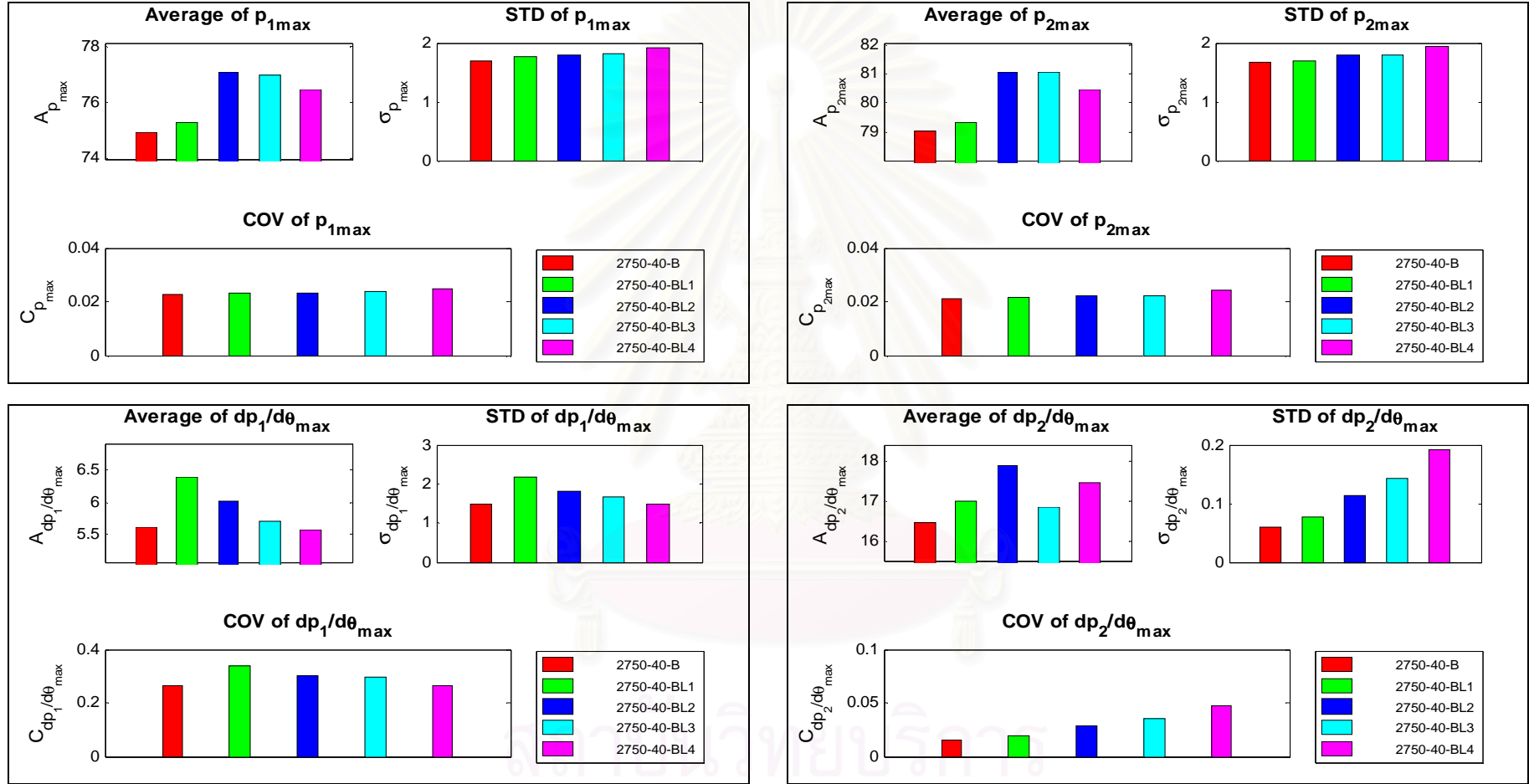
Figure 7–140   Average, STD, and COV of chamber pressure and PRR at 2750rev/min, 40Nm (PME and LPG-PME modes)
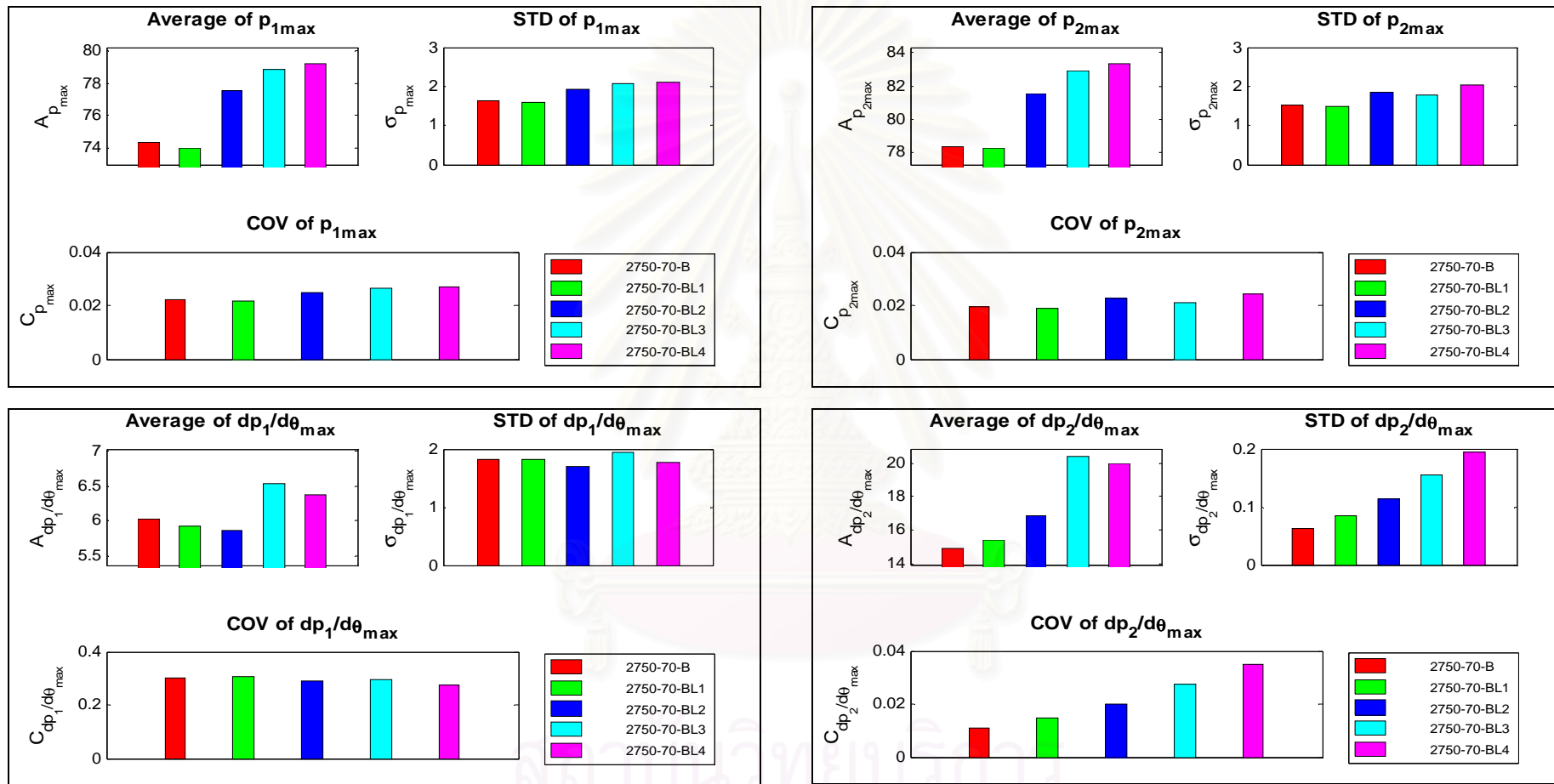
Figure 7–141   Average, STD, and COV of chamber pressure and PRR at 2750rev/min, 70Nm (PME and LPG-PME modes)

7.3. The effect of injection timing

Three values of injection timing were chosen and set for the test engine. The first value (1.22-degree-advanced, designated by i3) was applied for neat diesel, PME, LPG-diesel, and LPG-PME. The second (1.0-degree-retarded, designated by i2) and the third (1.8-degree-retarded, designated by i1) were applied for neat PME/ LPG-PME modes. The total brake energy conversion efficiencies corresponding to these modes of operation are shown in Figure 7–142 and Figure 7–143. The exhaust gas temperatures are shown in Figure 7–144 and Figure 7–145. The oil temperatures are shown in Figure 7–146. The following remarks can be recognized.

In LPG-diesel modes, the advanced injection timing i3 resulted in better total energy conversion efficiencies. These relative increases, in mode DL1 and DL4, were: 4% and 2.6%, 4.7% and 4%, 2.7% and 3.6% at the engine working point (1250@20), (2000@40), and (2750@70), respectively. The operation even was observed to be better (ECE fraction of 1.005) than the diesel baseline at mode 2000-70-DL1-i3.

In LPG-PME modes, the injection timing i3 also resulted in higher total energy conversion efficiencies compared to that with the OEM setting. However, these values were still less than that in the corresponding LPG-diesel modes. In mode BL1, the corresponding relative increases were about 2.7%, 1.0%, 1.0%, and 1.9% at the working point (1250 @ 20), (2000 @ 20) (2000 @ 40), and (2750 @ 70), respectively. Those were about 4% and 0.7% at 1250 rev/min @ 20 and 40Nm, and 1.8%, 1.9%, at 2000 rev/min @ 20 and 40 Nm in mode BL4 of LPG supply. The injection timing i2 seemed not to result significant change in the efficiency in dual fuel whereas the injection timing i1 caused reduction since the combustion took place later, leading to higher energy loss brought by the exhaust gas. With this injection timing (i1), the exhaust gas temperatures in neat PME and LPG-PME modes increased significantly.
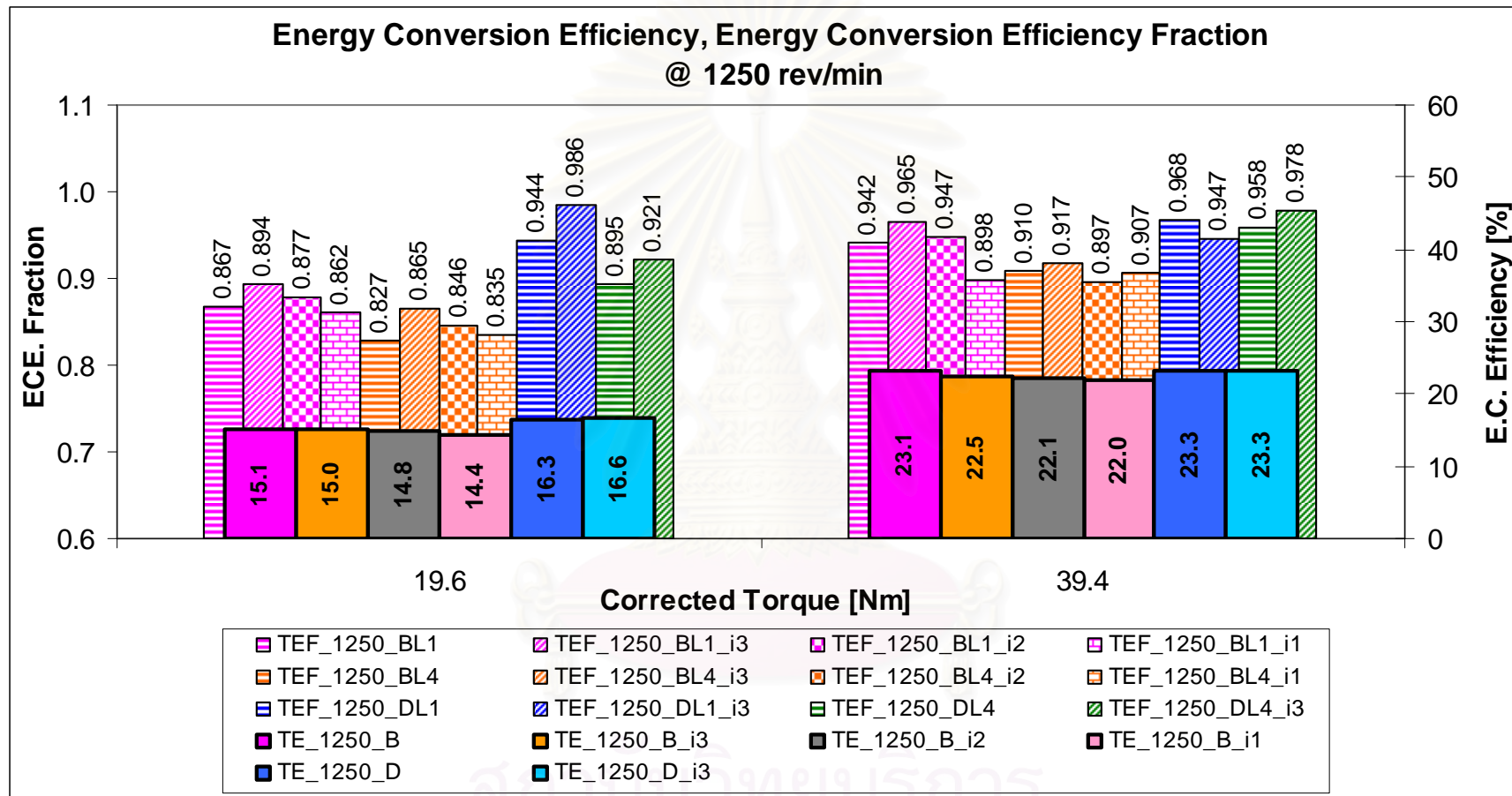
Figure 7–142   ECE and ECE fraction with different modes of operation and injection timing, at 1250 rev/min
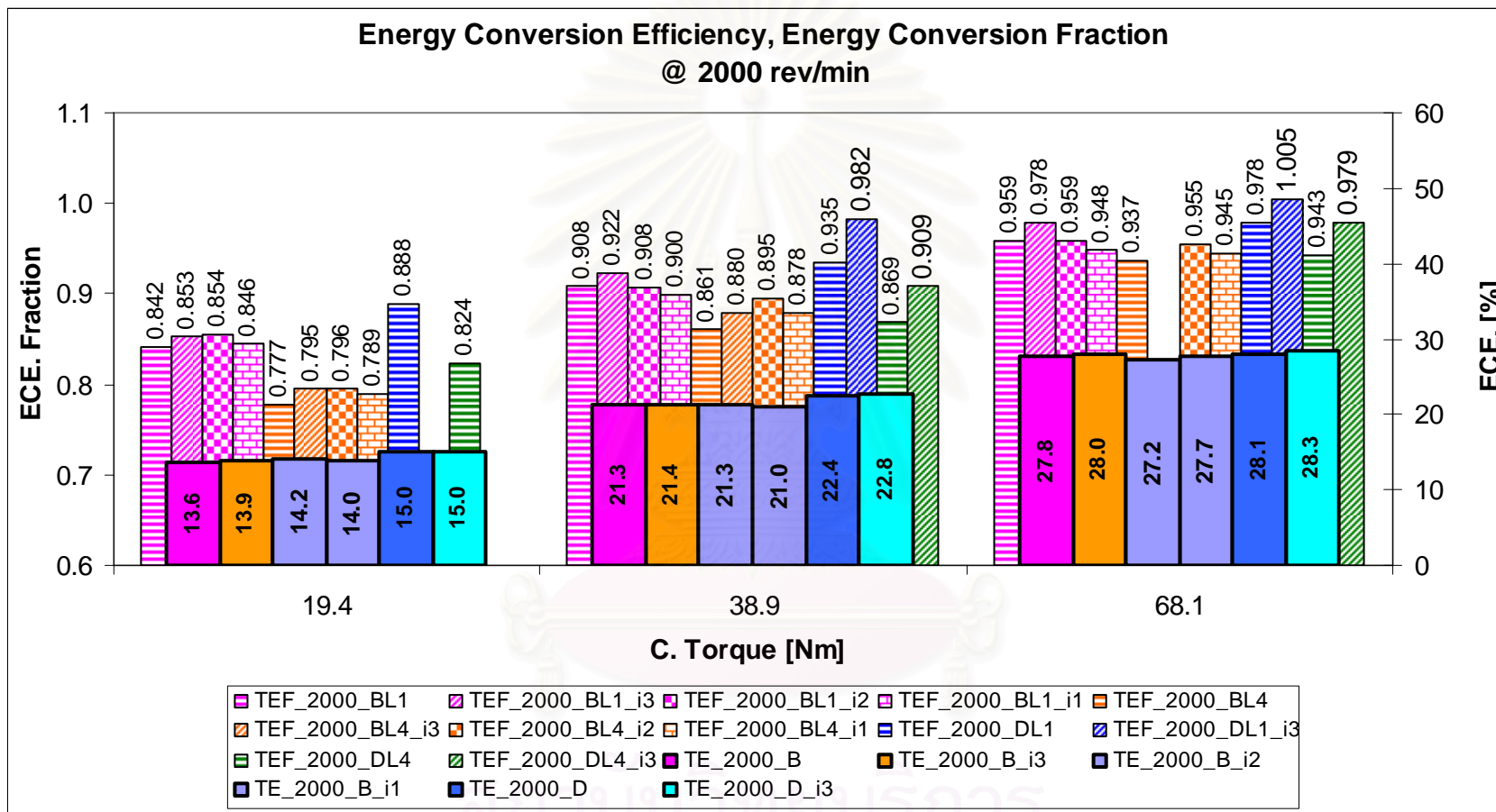
Figure 7–143   ECE and ECE fraction with different modes of operation and injection timing, at 2000 rev/min
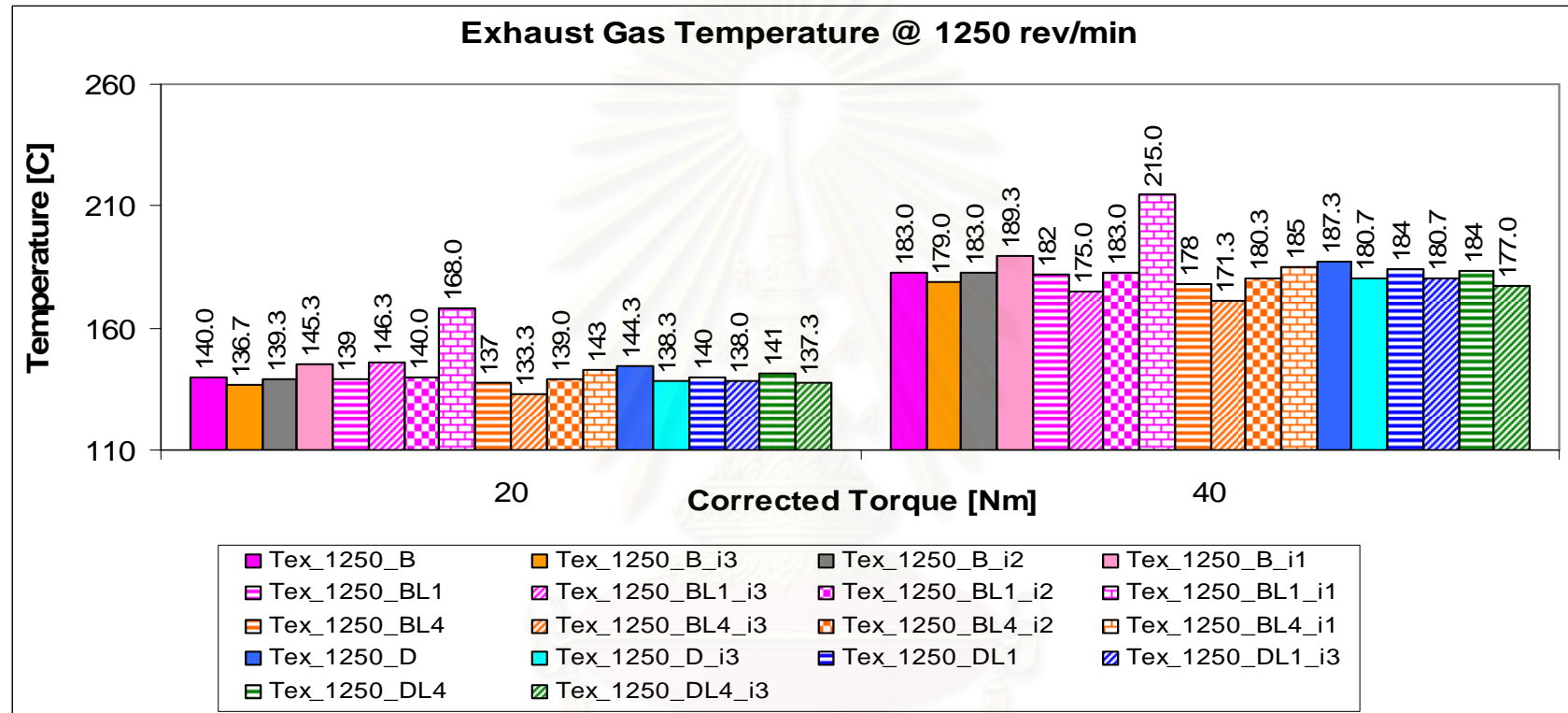
Figure 7–144   Exhaust gas temperature with different modes of operation and injection timing, at 1250 rev/min
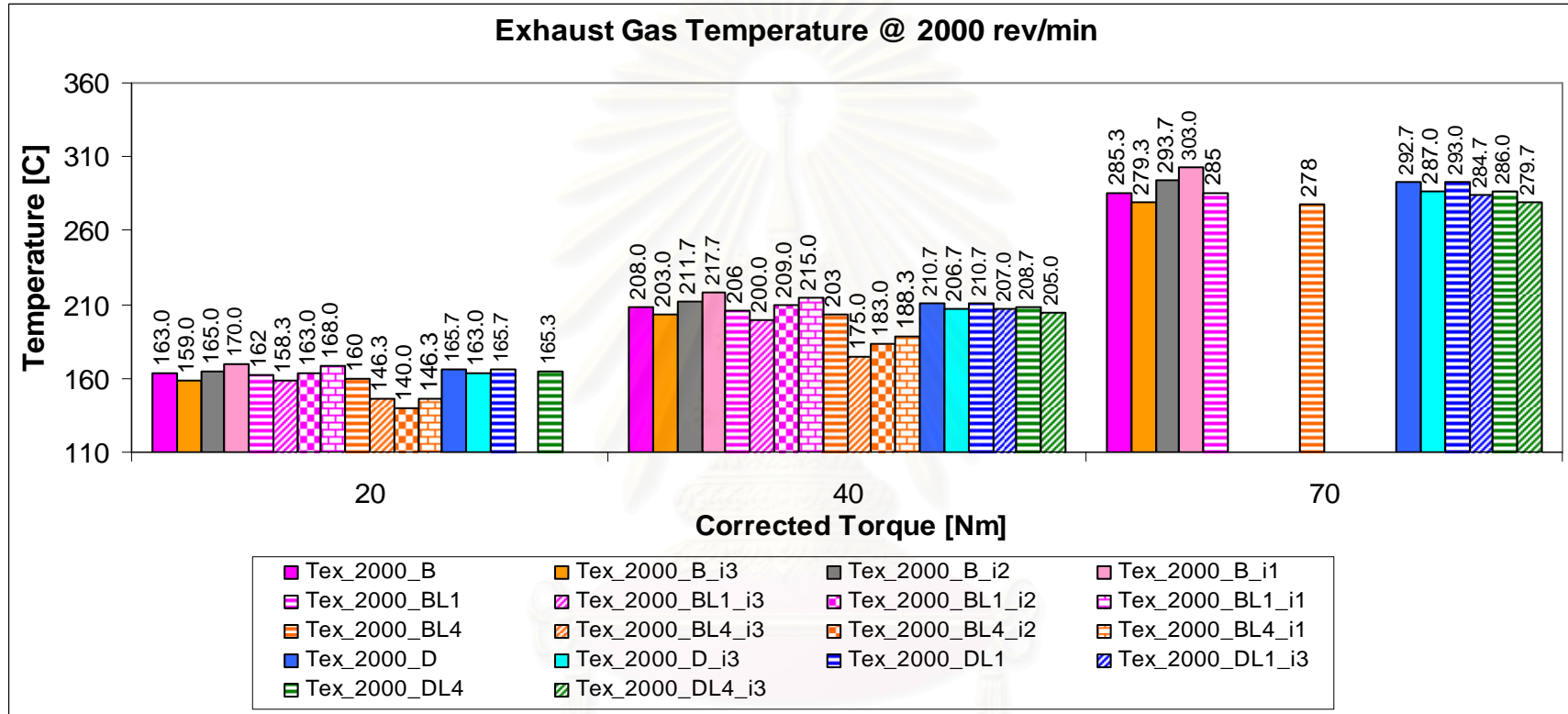
Figure 7–145   Exhaust gas temperature with different modes of operation and injection timing, at 2000 rev/min
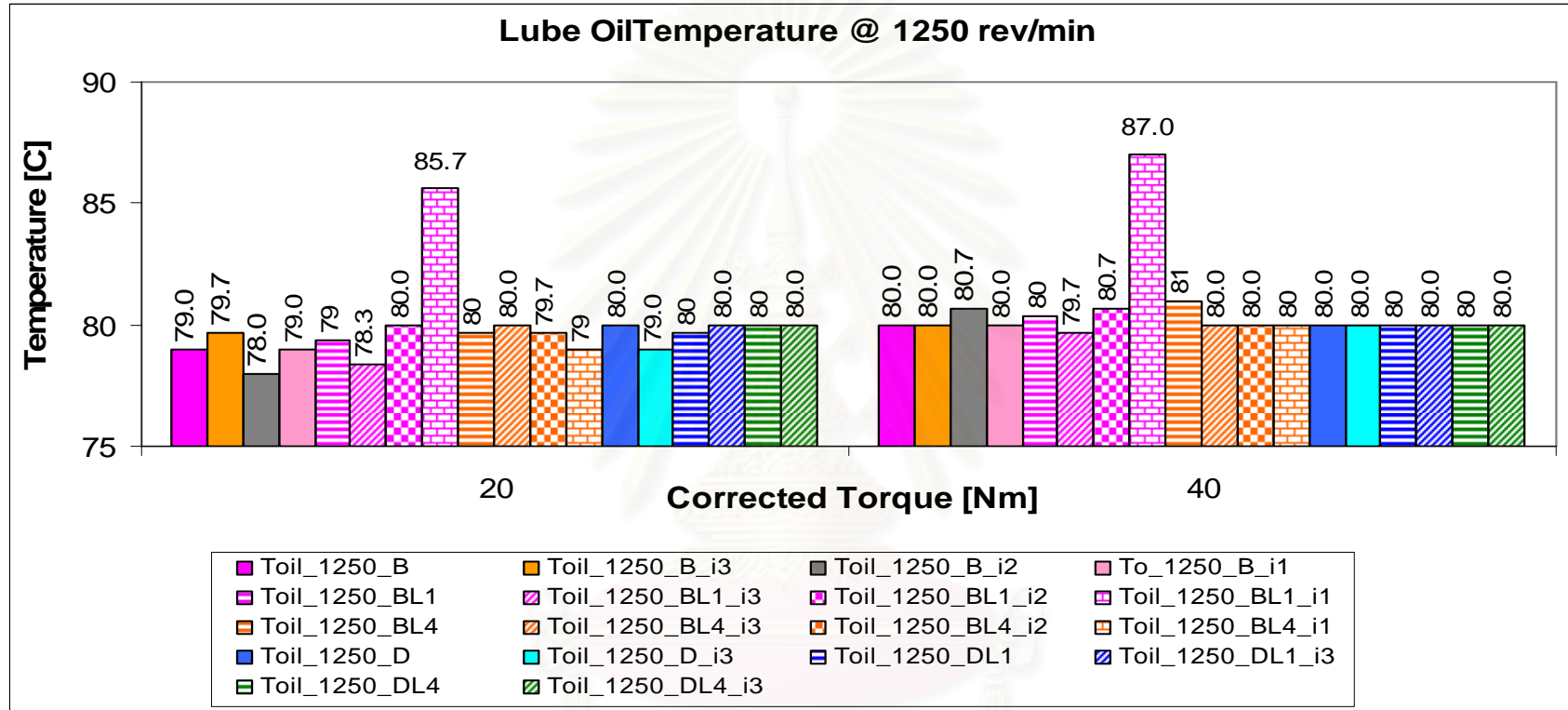
Figure 7–146   Lubricant oil temperature with different modes of operation and injection timing, at 1250 rev/min

CHAPTER 8

CONCLUSION AND RECOMMENDATION

Comparative investigation among the operation with neat diesel, neat PME, LPG-diesel, LPG-PME fuelling at selected high probability operating points followed the ECE15+EUDC test cycle had been made for the test engine, with varied injection timings. The engine ran with the LPG-air premixed charge and under overall lean mixture. The LPG-air premixed charge with 4 steps equivalent ratio in the range [0.064-0.139] was introduced to the engine whereas the total equivalent ratio reached values in the range [0.165-0.476]. The investigation involved measurement and prediction techniques, including fuel consumption measurement, total energy conversion efficiency calculation, heat release analysis, and combustion chamber visualization diagnostics. Following conclusions and recommendation have been drawn:

8.1.   Conclusion on the LPG-diesel operation

The LPG-diesel operation results reveal that the engine was able to operate without knocking at all planned liquid fuel substitution, covering the range approximate 65% at 1250rev/min @ 10Nm to 26% at 2750 rev/min @ 70Nm. There was deterioration in the total energy conversion efficiencies in DF modes compared with the corresponding neat diesel modes. At fixed speed and engine load the deterioration increased as the diesel substitution increased. At fixed speeds and LPG flow rates (fixed premixed LPG-air mixture strength) the deterioration decreased when the engine load increased. The deterioration appeared highest, approximate 17%, at the lowest speed and load (1250rev/min @ 10Nm).

There was not significant difference in the ignition delay in LPG-diesel compared to diesel modes. The delay may decrease although it has been thought to increase. At 1250 rev/min, the delays were the same at 30 and 40 Nm, and the highest difference was $0.4^{O}CA$ at 20 Nm. At 2000 rev/min the highest prolonged delay was $0.6^{O}CA$ at 40Nm (in mode 2000-40-DL1) but also appeared to be advanced $0.6^{O}CA$ at 70Nm (in mode

2000-70-DL4). At 2750 rev/min, the delay appeared to be prolonged at 30, 40, and 70 Nm but advanced at 10Nm, at all modes of LPG supply. The reason for the observed feature in the change of ignition delay might be resulted from the high turbulent intensity in the pre chamber at the time of injection.

The retarded SOC in dual fuel modes had been observed. It was caused mainly by the retarded injection timing resulted from the reduced amount of diesel injection when the LPG increased.

Results from the heat release and visualization analysis indicate that LPG-diesel operation provided faster combustion after ignition of the liquid fuel, shorter combustion duration accompanied with the movement of the center of HRR area towards TDC (even the dual fuel combustion was delayed), leading to theoretically higher thermal efficiency, better energy utilization recognized by the lower exhaust gas temperature. The role of LPG in dual fuel is revealed: it reduces the cooling effect of the liquid fuel at the first half of combustion process and the diffusion combustion of the liquid fuel. The movement of the centers of HRR areas was about [0.6÷1.3], [0.9÷1.5], and [0.4÷2.0] ^{O}CA at 1250, 2000, 2750 rev/min, respectively. The LPG ratios which lead to the highest cumulative net heat release have been considered as the reasonable. These values are corresponding to mode L3 at 1250 rev/min and mode L4 at almost all operating points at 2000 and 2750 rev/min, as listed in Table 7-3.

In LPG-diesel dual fuel modes, the peaks of chamber pressure were higher than that in diesel modes only in cases that they were generated by combustion. In these cases, the highest differences of maximum pressures were within 7 bars. The peaks of PRR which were within 2.7bar/deg might also be generated by compression or combustion. It appeared with positive values around 12°CA bTDC if generated by compression or with negative values at [12÷20] ^{O}CA aTDC if generated by combustion. The STD and COV of the peaks of prechamber pressure seemed comparable in neat diesel and LPG-diesel modes; within about 2.8%. The STD and COV of PRR in prechamber seemed to increase proportionally with the LPG ratio. These COV at 1250 rev/min were the lowest, followed by those at 2750 rev/min (within 5%) and 2000 rev/min (up to about 12%).

The COV_{IMEP} increased and seemed proportionally with the ratio of LPG at all engine speeds and loads. At speed 1250 and 2750 rev/min, the maximum of COV_{IMEP} increased from about 1.6%, corresponding with neat diesel to about 5%, corresponding with mode L4 of LPG supply. At 2000 rev/min, there were dramatically increases of the COV_{IMEP}; increasing from about 1.6%, with neat diesel to about 15%, with mode L4 of LPG supply. The sharp increases of the COV_{IMEP} and COV_{PRR} at 2000 rev/min may be resulted from the effect of resonance in the combustion system, leading to worse combustion in the main chamber.

1.22-degree-advanced injection timing (i3) leaded to better total energy conversion efficiency. The relative increases in the energy conversion efficiencies were seen: 4% and 2.6% at 1250 rev/min @ 20Nm, 4.7% and 4% at 2000 rev/min @ 40Nm, 2.7% and 3.6% at 2750 rev/min @ 70Nm, in mode DL1 and DL4 of LPG supply, respectively. The operation even was observed to be better than the diesel baseline at mode 2000-70-DL1-i3 with the ECE fraction of 1.005.

Although the lubricant oil temperature in DF fuelling is thought higher than that in diesel fueling, a significant change had not been detected, perhaps due to the setting of the cooling water system in the test cell. The decreases in exhaust gas temperature were up to $4.7^{O}C$, $6.7^{O}C$, and $10.3^{O}C$ at 1250, 2000, 2750 rev/min, respectively.

8.2. Conclusion on the LPG-PME operation

The engine could be able to operate with LPG-PME at the planned condition similar as that with LPG-diesel. The substitution appeared lower at low speed and load (about 60%, 42.6%, 38.6% compared to 65.3%, 48%, and 45.5%) but comparable at 2000 rev/in (about 45%, 33.5%, and 27% compared to 46.9%, 31,.6%, and 27.6%) and 2750 rev/min (about 37.5%, 30.6%, and 26.3% compared to 38.3%, 29.2%, and 26.2%). As fuelled with LPG-PME there was also deterioration in the total energy conversion efficiency and the trend was similar to that with LPG-diesel; the deterioration increased with increased LPG ratio or decreased engine loads. The levels of deterioration appeared higher at low speed and load due to the long injection period accompanied with the less turbulent in the pre chamber. The deterioration was higher than that in the corresponding LPG-diesel operation.

The injection timing was earlier when the engine was fuelled with the PME. This is thought due to the higher adiabatic bulk modulus of the PME and the "pump effect" resulted from the higher viscosity, larger volume per cycle of the PME fuel.

The ignition delay in PME/LPG-PME operation was shorter than that in the corresponding diesel/LPG-diesel operation. This is thought due to the total effect of two factors: the earlier injection of PME has negative effect whereas the oxygen content in PME has positive effect on the ignition delay. These shorter delays in case of neat PME and LPG-PME dual fuel ascertain that the effect of oxygen content of the PME on the delay is dominant over the effect of reduced pressure and temperature brought by earlier injection.

At all modes of PME/LPG-PME, although the center of HRR area was closer to TDC, the late stage of combustion in neat PME/ LPG-PME modes seemed to be longer than that in neat diesel/ LPG-diesel modes. This might be resulted from the longer injection duration and lower volatility of the PME compared with the diesel. With LPG-PME dual fuelling, the reasonable LPG ratios were L4 at almost all operating points, as presented in Table 7-4.

The peaks of chamber pressures in PME/LPG-PME modes were not much different with that in diesel/LPG-diesel modes at 1250rev/min but higher (up to 8 bars at 2750 rev/min @70Nm) at higher engine speeds and increased with LPG ratio. The COV_{PRR} was comparable to that in diesel/LPG-diesel modes at 1250 and 2750 rev/min and lower at 2000 rev/min.

Similar trend in the COV_{IMEP} was also observed in LPG-PME operation: to increase with increased LPG ratio at fixed speeds and loads, to decrease with increased engine torques at fixed LPG ratios and speeds, and sharply increase at 2000 rev/min.

Among the varied injection timings, the 1.22-degree-advanced injection timing also resulted in better total energy conversion efficiency. The corresponding relative increases in the energy conversion efficiencies were seen: 2.7% at 1250 rev/min @ 20Nm, about 1% at 2000 rev/min @ 20 and 40Nm, and 1.9% at 2750 rev/min @ 70Nm in mode DL1. Those were about 4%, 0.7% at 20, 40Nm @ 1250rev/min and 1.8%, 1.9% at 20, 40 Nm @ 2000rev/min in mode L4 of LPG supply. The 1-degree-retarded injection

timing (i2) seemed not to result significant change in the efficiency in dual fuel whereas the 1.8-degree-retard injection timing did.

Although the dual fuelling with premixed LPG-air and either diesel or PME pilot injection seemed to provide better combustion recognized by the shorter combustion duration and the movement of the center of HRR area towards TDC, the DF total energy conversion efficiencies were worse than that in the neat liquid fuel. The possible reasons are the energy loss by blow-by and the incomplete combustion in the main chamber because of its geometry which has been optimized for diesel operation.

Based on the observation of phenomena in the prechamber with two color method, it is revealed that the LPG-PME dual fuel seemed to result in worse combustion than the LPG-diesel dual fuel; appearing far to reach the result as good as diesel combustion.

8.3. Conclusion on the agreement of results between heat release analysis and combustion chamber visualization diagnostics:

The heat release model used in this investigation is the traditional model adapted from [3]. The model has been testified reasonable for engine investigation and widely used. The application of the two color method for the prediction of flame temperature and soot concentration is performed with assumption that there is no surface reaction in the soot particles, homogeneous thermal distribution and soot density along the optical penetration depth. This technique is also reasonable for diesel combustion investigation.

In this study, the predicted accumulate net heat release is the total net HR of the two combustion chambers while the visualization has been performed for the prechamber. In addition, the heat release in the combustion process consists of two components; one from liquid fuel combustion and another from LPG combustion. The second component is hardly detected by the two color method since the LPG is naturally in gaseous form. In case of biodiesel, the accuracy of detection of the first component by the two color method also has not been clarified. Therefore, in this study the flame temperature predicted by this method is thought to be underestimated. This can be seen with the analysis results at 2000 rev/min, 20Nm, and LPG-diesel operation: While mode

DL4 was addressed as the reasonable over the other modes by the heat release analysis, it was not agreed by the two color method.

The combination between these two techniques should be applied in the investigation of dual fuelling.

8.4. Contribution of the investigation

The contribution of this study includes:

- The information of combustion characteristics of premixed charge LPG-PME dual fuel which has not been published before.
- The method to determine SOI based on the fuel line pressure.

8.5. Future work

In this study, the reason of high COV_{IMEP} in dual fuel operation regardless liquid fuel type at 2000 rev/min remains unclear. The investigation on exhaust emissions of LPG-PME dual fuel has also not been considered. In addition, the negative effect of the combustion chamber geometry has been mentioned but not quantified. The predicted flame temperature and soot concentration are under-estimated. Further investigation is needed to fill these gaps.

REFERENCES

[1]   Flynn PF, Durrett RP, Hunter GL, Zur Loye AO, Akinyemi OC, Dec JE, and Westbrook CK. Diesel combustion: An integrated view combining laser diagnostics, chemical kinetics, and empirical validation. SAE Paper 1999-01-0509, 1999.

[2]   Dec JE. A conceptual model of DI diesel combustion based on laser-sheet imaging. SAE Paper 970873, 1997.

[3]   Heywood JB. Internal combustion engine fundamentals. New York: McGraw-Hill, 1988.

[4]   Kittelson DB. Engines and nanoparticles: A review. Aerosol Science 1998; 29:575-88.

[5]   Johnson TV. Diesel emission control in review. SAE Paper 2001-01-0184, 2001.

[6]   Bernard C and Rodica B. Diesel engine reference book. Linacre House, Jordan Hill, Oxford OX2 8DP, 225 Wildwood Avenue, Woburn, MA 01801-2041: Butterworth-Heinemann, 1999.

[7]   Aref T and Malcolm LP, "Review of natural gas fuelled locomotive technology (TP 13470E)," Transportation Development Center, Canada, Report 1999.

[8]   Fairbanks Morse Engine Co. Available from: http://www.FairBanksMorse.com, [March 2006].

[9]   Wartsila Co. Available from: http://www.Wartsila.com, [February 2006].

[10]   Duggal VK, Lyford-Pike EJ, Wright JF, Dunn M, Goudie D, and Munshi S, "Development of the high-pressure direct-injected, ultra low NO_X natural gas engine - Final report," 2004.

[11]   Westport Inc. Available from: http://www.westport.com, [February 2006].

[12]   Prakash G, Ramesh A, and Shaik AB. An approach for estimation of ignition delay in a dual fuel engine. SAE Paper 1999-01-0232, 1999.

[13]   Karim GA. Exhaust emission from dual fuel engines at light load. SAE Paper 932822, 1993.

[14]   Karim GA. A review of combustion processes in the dual fuel engine - The gas diesel engine. Progress in Energy and Combustion Science 1980; 6:277-85.

[15]   Poonia MP, Ramesh A, and Gaur RR. Effect of intake air temperature and pilot fuel quantity on the combustion characteristics of a LPG diesel dual fuel engine. SAE Paper 982455, 1998.

[16]   Amagai K, Hashimoto Y, and Arai M. Ignition and combustion characteristics of two-stage injection diesel spray. JSAE Review 1999; 20:407-11.

[17]   Bakenhus M and Reitz RD. Two-Color combustion visualization of single and split Injections in a single-cylinder heavy-duty DI Diesel engine using an endoscope-based imaging system. SAE Paper 1999-01-1112, 1999.

[18]   Hampson GJ and Reitz RD. Two-color imaging of in-cylinder soot concentration and temperature in a heavy-duty DI Diesel engine with comparison to multidimensional modeling for single and split Injections. SAE Paper 980524, 1998.

[19]   Hotta Y, Nakakita K, Inayoshi M, Ogawa T, Sato T, and Yamada M. Combustion improvement for reducing exhaust emissions in IDI diesel engine. JSAE Review 1997; 18:19-31.

[20]   Zambare VV and Winterbone DE. A photographic investigation of multi-stage fuel injection in a single cylinder DI Diesel engine. SAE Paper 1999-01-1501, 1999.

[21]   Arcoumanis C, Bae C, Nagwaney A, and Whitelaw JH. Effect of EGR on combustion development in a 1.9L DI Diesel optical engine. SAE Paper 950850, 1995.

[22]   Ladommatos N, Abdelhalim SM, Zhao H, and Hu Z. Effects of EGR on heat release in Diesel combustion. SAE Paper 980184, 1998.

[23]   Hountalas DT and Papagiannakis RG. Theoretical and experimental investigation of a direct injection dual fuel diesel-NG engine. SAE Paper 2002-01-0868, 2002.

[24]   Papagiannakis RG and Hountalas DT. Experimental investigation concerning the effect of natural gas percentage on performance and emissions of a DI dual fuel diesel engine. Applied Thermal Engineering 2003; 23:353-65.

[25]   Zuo C and Yang M. Operating characteristics and description of a dual fuel engine for Diesel-NG heavy-duty operation. SAE Paper 1999-01-3523, 1999.

[26]   Daisho Y, Yaeo T, Koseki T, Saito T, Kihara R, and Quiros EN. Combustion and exhaust emissions in a direct-injection diesel engine dual-fueled with natural gas. SAE Paper 950465, 1995.

[27]   Ishida M, Amimoto N, Tagai T, and Sakaguchi D. Effect of EGR and preheating on NG combustion assisted with gas-oil in a diesel engine. In: Proceedings of the COMODIA 2001, Japan, 2001.

[28]   Selim MYE. Sensitivity of dual fuel engine combustion and knocking limits to gaseous fuel composition. Energy Conv Mgmt 2004; 45:411-25.

[29]   Kumar MS, Ramesh A, and Nagalingam B. Experimental investigations on a Jatropha oil methanol dual fuel engine. SAE Paper 2001-01-0153, 2001.

[30]   Ishida M, Tagai T, Ueki H, and Sakaguchi D. Ignition and combustion characteristics of methanol mixture in a dual fuel diesel engine. In: Proceedings of the COMODIA, Japan, 2004.

[31]   Selim MYE. Pressure-time characteristics in diesel engine fueled with natural gas. Renewable Energy 2001; 22:473-89.

[32]   Slawomir L. The influence of regulating parameters of dual fuel compression ignition engine fuelled with LPG on its maximum torque, overall efficiency and emission. SAE Paper 2001-01-3264, 2001.

[33]   William PJ, John BN, Van der Lee A, Lovkov O, Koshin VK, and Piatov IS. All electronic dual fuel injection system for the Belarus D-144 diesel engine. SAE Paper 901502, 1990.

[34]   Wong WY, Clark MK, and Stuart RB. Performance and emissions of a NG dual-fueled, indirect injected diesel engine. SAE Paper 911766, 1991.

[35]   Kusaka J, Daisho Y, Kihara R, and Saito T. Combustion and exhaust gas emissions characteristics of a diesel engine dual-fueled with NG. In: Proceedings of the 4th International Symposium COMODIA, Japan, 1998.

[36]   Papagiannakis RG and Hountalas DT. Combustion and exhaust emission characteristics of a dual fuel compression ignition engine operated with

pilot diesel fuel and natural gas. Energy Conversion and Management 2004; 45:2971-87.

[37] Jian D, Xiaohong G, Gesheng L, and Xintang Z. Study on diesel-LPG dual fuel engines. SAE Paper 2001-01-3679, 2001.

[38] Abd Alla GH, Soliman HA, Badr OA, and Abd Rabbo MF. Effect of pilot fuel quantity on the performance of a dual fuel engine. Energy Conversion and Management 2000; 41:559-72.

[39] Abd Alla GH, Soliman HA, Badr OA, and Abd Rabbo MF. Combustion quasi-two zone predictive model for dual fuel engines. Energy Conversion and Management 2001; 42:1477-98.

[40] Abd-Alla GH, Soliman HA, Badr OA, and Abd-Rabbo MF. Effects of diluent admissions and intake air temperature in exhaust gas recirculation on the emissions of an indirect injection dual fuel engine. Energy Conversion and Management 2001; 42:1033-45.

[41] Daisho Y, Takahashi K, Iwashiro Y, Nakayama S, Kihara R, and Saito T. Controlling combustion and exhaust emissions in a direct-injection diesel engine dual-fueled with NG. SAE Paper 952436, 1995.

[42] Lin Z and Su W. A study on the determination of the amount of pilot injection and rich and lean boundaries of the pre-mixed CNG/air mixture for a CNG/diesel dual-fuel engine. SAE Paper 2003-01-0765, 2003.

[43] Sudhir CV, Desai V, Suresh Kumar Y, and Mohanan P. Performance and emission studies on the effect of injection timing and diesel replacement on a 4-S LPG-diesel dual-fuel engine. SAE Paper 2003-01-3087, 2003.

[44] Elliot MA and Davis RE. Dual fuel combustion in diesel engines. Ind. Engng Chem. 1951; 43:2854-63.

[45] Karim GA, Badr O, and Liu B. An examination of the flame spread limits in a dual fuel engine. Applied Thermal Engineering 1999; 19:1071-80.

[46] Liu Z and Karim GA. Knock in dual fuel engines. In: Proceedings of the COMODIA, Japan, 1994.

[47]   Karim GA. An examination of some measures for improving the performance of gas fuelled diesel engines at light load. SAE Transactions 1991; 100:966-76.

[48]   Einang PM, Koren S, Kvamsdal R, Hansen T, and Sarsten A. High-pressure, digitally controlled injection of gaseous fuel in a Diesel engine, with special reference to boil-off from LNG tankers. In: Proceedings of the International Council on Combustion Engines (Conseil International Des Machines a Combustion, CIMAC), 1983.

[49]   Miyake M, Biwa T, Endoh Y, Shimotsu M, Murakami S, and Komoda T. The development of high output, highly efficient gas burning Diesel engine. In: Proceedings of the International Council on Combustion Engines (Conseil International Des Machines a Combustion, CIMAC), 1983.

[50]   Wakenell JF, O'Neal GB, and Baker QA. High pressure late cycle injection of natural gas in a rail medium speed Diesel engine. SAE Paper 872041, 1987.

[51]   Hodgins KB, Hardi G, and Philip GH. Intensifier-injector for natural gas fueling of diesel engines. SAE Paper 921553, 1992.

[52]   Ouelette P and Hill PG. Visualization of natural gas injection for a compression ignition engine. SAE Paper 921555, 1992.

[53]   Hodgins KB, Philip GH, Ouellette P, and Hung P. Directly injected natural gas fueling of diesel engines. SAE Paper 961671, 1996.

[54]   Harrington J, Munshi S, Nedelcu C, Ouellette P, Thompson J, and Whitfield S. Direct injection of natural gas in a heavy-duty diesel engine. SAE Paper 2002-01-1630, 2002.

[55]   Duc PM and Kanit W. Study on biogas premixed charge-diesel dual fuelled engine. Available from: DOI: 10.1016/j.enconman.2007.03.020, [2007].

[56]   Jiang C, Liu T, and Zhong J. A study on compressed biogas and its application to the compression ignition dual-fuel engine. Biomass 1989; 20:53-59.

[57]   Leif G, Pal B, Bengt J, and Per S. Reducing CO_2 emission by substituting biomass for fossil fuels. Energy 1995; 20:1097-113.

[58]   Henham A and Makkar MK. Combustion of simulated biogas in a dual fuel diesel engine. Energy Convers. Mgmt 1998; 39:2001-09.

[59]   Modarres RMR and Karim GA. Examination of the dual-fuel engine performance using low BTU gaseous fuels. In: Proceedings of the 13th International Conference on Thermal Engineering and Thermogrammetry, Budapest, Hungari, 2003.

[60]   Kapur T, Kandpal TC, and Garg HP. Electricity generation from rice husk in Indian rice mills: Potential and financial viability. Biomass and Bioenergy 1996; 10:393-403.

[61]   John GC and Carol RP. Independent power plant using wood waste. Energy Conv Mgmt 1996; 37:1205-09.

[62]   Rejeev MJ and Anil KR. Development of a sugarcane leaf gasifier for electricity generation. Biomass and Bioenergy 1995; 8:91-98.

[63]   Uma R, Kandpal TC, and Kishore VVN. Emission characteristics of an electricity generation system in diesel alone and dual fuel modes. Biomass and Bioenergy 2004; 27:195-203.

[64]   Vyarawalla F, Parikh PP, Dak HC, and Jain BC. Utilisation of biomass for motive power generation - gasifier engine system. Biomass 1984; 5:227-42.

[65]   Parikh PP, Bhave AG, Kapse DV, and Shashikantha. Study of thermal and emission performance of small gasifier dual-fuel engine systems. Biomass 1989; 19:75-97.

[66]   Karim GA, Ito K, Abraham M, and Jensen L. Examination of the role of formaldehyde in the ignition processes of a dual fuel engine. SAE Transactions 1991; 100:975-82.

[67]   Naber JD, Siebers DL, Di Julio SS, and Westbrook CK. Effects of natural gas composition on ignition delay under diesel conditions. Combustion and Flame 1994; 99:192-200.

[68]   Nwafor OMI and Rice G. Combustion characteristics and performance of natural gas in high speed indirect injection diesel engine. Renewable Energy 1994; 5:841-48.

[69] Balasubramanian V, Sridhara K, and Ganesan V. Performance evaluation of a small agricultural engine operated on dual fuel NG system. SAE Paper 951777, 1995.

[70] Mtui PL and Hill PG. Ignition delay and combustion duration with natural gas fueling of diesel engines. SAE Paper 961933, 1996.

[71] Abd Alla GH, Soliman HA, Badr OA, and Abd Rabbo MF. Effect of injection timing on the performance of a dual fuel engine. Energy Conv Mgmt 2002; 43:269-77.

[72] Selim MYE. A study of some combustion characterstics of dual fuel engine using EGR. SAE Paper 2003-01-0766, 2003.

[73] Enoki K, Hayashi S, and Sawa N. Optimum injection timings of gas-oil and methanol in dual fuel CI engine. SAE Paper 932479, 1993.

[74] Department of Energy US. Biodiesel - Handling and use guidelines. Available from: http://www.osti.gov/bridge, [2006].

[75] Knothe G, Gerpen JV, and Krahl J. The biodiesel handbook. Champaign: AOCS Press, 2005.

[76] AVL. Eddy current dynamometer type Alpha 20-500 operating instruction. Graz: AVL List GmbH., 2001.

[77] AVL. Eddy current dynamometer type alpha with BME 300 commissioning instructions. Graz: AVL List GmbH., 2001.

[78] Patrick FD. Measurement and data analysis for engineering and science. New York: McGraw-Hill, 2005.

[79] Regueiro JF. The case for new divided-chamber Diesel combustion systems - Part two: Critical analysis of, and solutions for, swirl-prechamber engines. SAE 2001-01-0274, 2001.

[80] Heisler H. Advanced engine technology. Birlington: Butterworth-Heinemann, 1995.

[81] Krieger RB and Borman GL. The computation of apparent heat release for internal combustion engines. ASME Paper 66-WA/DGP-4, 1966.

[82] Gatowski JA, Balles EN, Chun KM, Nelson FE, Ekchian JA, and Heywood JB. Heat Release Analysis of Engine Pressure Data. SAE Paper 841359, 1984.

[83]   Rakopoulos CD and Hountalas DT. Net and gross heat release rate calculations in a DI Diesel engine using various heat transfer models. ASME 1994; 33:251-62.

[84]   Kouremenos DA, Rakopoulos CD, and Hountalas DT. Theoretical and experimental heat release rate calculations for various types of direct injection Diesel engines. ASME 1994; 33:239-49.

[85]   Bosch RG. Diesel engine management, 4th ed. West Sussex: John Wiley & Sons Ltd., 2005.

[86]   Szybist JP and Boehman AL. Behavior of a Diesel injection system with biodiesel fuel. SAE Paper 2003-01-1039, 2003.

[87]   Choi CY, Bower GR, and Reitz RD. Effect of biodiesel blended fuels and multiple injections on DI Diesel engines. SAE Paper 970218, 1997.

[88]   Zhao H and Ladommatos N. Engine combustion Instrumentation and diagnostics. Warrendale: Society of Automotive Engineers Inc.; 2001.

[89]   AVL. Spectral flame temperature measurement using the two color method. Graz: AVL List GmbH., 2001.

[90]   Lancester DT. Measurement and analysis of engine pressure data. SAE Paper 750026, 1975.

[91]   Chen SK. On-line PC based engine analyzer and simulator. SAE Paper 881256, 1988.

[92]   Chun KM and Heywood JB. Characterisation of knock in a spark ignition engine. SAE Paper 890156, 1989.

[93]   Michael FJB and Gordon Lucas G. The effect of crank angle resolution on cylinder pressure analysis. SAE Paper 910041, 1991.

[94]   Michael FJB, Christopher RP, and John B. Gasoline engine knock analysis using cylinder pressure data. SAE 1998.

[95]   Rocco V. DI Diesel engine in-cylinder pressure data analysis under TDC setting error. SAE Paper 930595v001, 1993.

[96]   Andrew LR. Cylinder pressure based combustion analysis in race engines. Paper 942487, 1994.

[97]   Rohrer R and Chehroudi B. Preliminary heat release analysis in a single-cylinder two-stroke production engine. SAE Paper 932431, 1993.

[98]   Harndorf H, Klosel R, and Volkart A. Optimization of parameters concerning measurement and analysis of cylinder pressure data. In: Proceedings of the MTZ, 1993.

[99]   Zhong L, Henein NA, and Bryzik W. Effect of smoothing the pressure trace on the interpretation of experimental data for combustion in Diesel engines. SAE SAE-2004-01-0931, 2004.
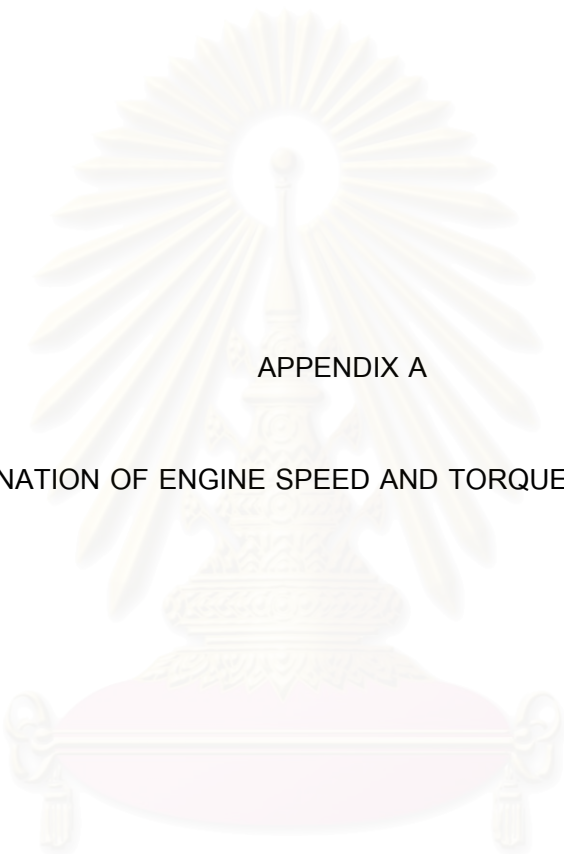
APPENDICES

APPENDIX A

DETERMINATION OF ENGINE SPEED AND TORQUE TEST CONDITION

A.1. The ECE15 + EUDC test cycle

Engine speed and brake torque values chosen for this investigation are those with high frequency of appearance in the ECE15+EUDC test cycle.
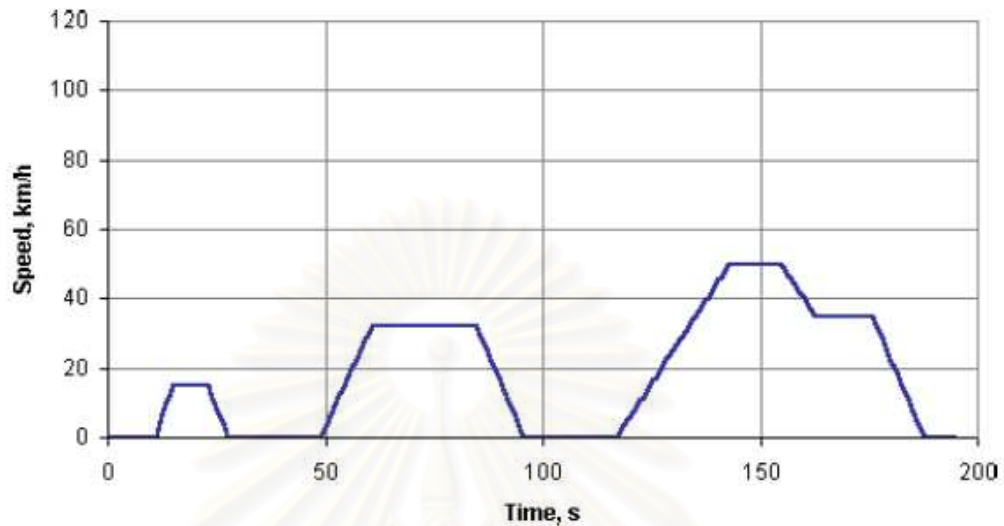
Figure A-1   ECE 15 segment
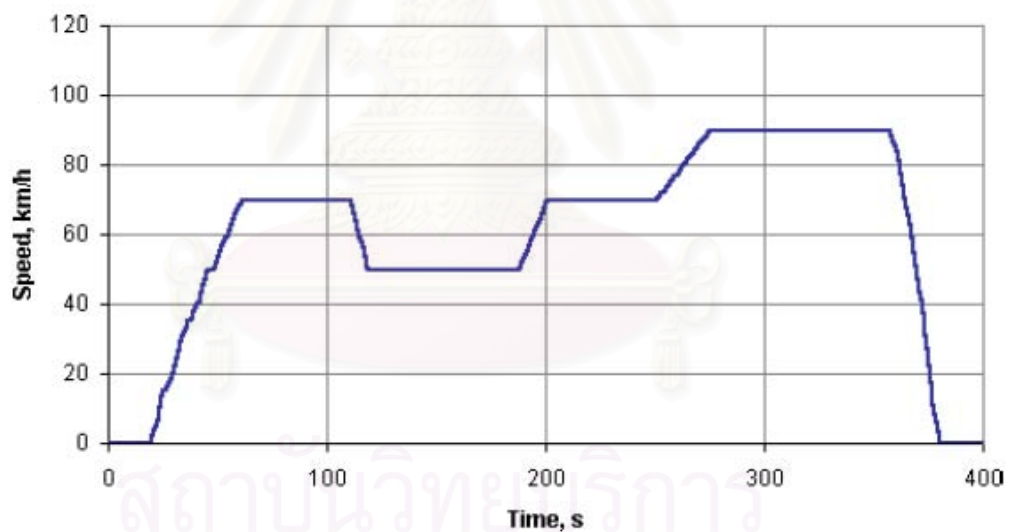
Figure A-2   EUDC segment for low power vehicles

The ECE+EUDC test cycle is performed on a chassis dynamometer. The cycle - also known as the MVEG-A cycle - is used for emission certification of light duty vehicles in Europe [EEC Directive 90/C81/01]. The entire cycle includes four ECE segments, Figure A-1, repeated without interruption, followed by one EUDC (Extra Urban Driving Cycle) segment, Figure A-2. The EUDC segment has been added after the fourth ECE segment to account for more aggressive, high speed driving modes. The alternative

EUDC segment for low-powered vehicle is chosen (maximum speed limited to 90km/h). Time duration is 195 seconds for each ECE15 segment and 400 seconds for the EUDC segment. Total time duration of the test cycle is 780 seconds.

A.2. Determination of engine speed and brake torque

For each certain required vehicle speed in the test cycle, the corresponding engine working speed and brake torque need to be determined.

A.2.1. Vehicle aerodynamics

The vehicle aerodynamic drag is determined by Eq.A-1. The total velocity, V, is the algebraic summation of wind, Vw, and vehicle, Vv velocities.

$$R_D = 0.5\, \rho_{air}\, A\, C_D\, V^2 \qquad\qquad \text{Eq.A-1}$$

$$R_D = 0.5\, \rho_{air}\, \varphi\, W\, H\, C_D\, V^2 \qquad\qquad \text{Eq.A-2}$$

Where,   W – Width of the vehicle

H – Height of the vehicle

φ – Coefficient (φ < 1)

A.2.2. Rolling resistance

Vehicle rolling resistance is generated by the interaction between a vehicle's tires and road, and is calculated as below

$$R_r = R_{rf} + R_{rr} = C_r\, (M_V + M_L)\, g \qquad\qquad \text{Eq.A-3}$$

Where, R_{rf} and R_{rr} are the rolling resistance of the front and rear tires, respectively. The rolling coefficient, C_r is a dimensionless factor expressing the effects of the physical properties of tires and road surface. The rolling coefficient is directly proportional to the level of tire deformation and inversely proportional to the tire radius. Therefore, the coefficient value tends to increase with greater loads, higher speed and lower tire pressure. The rolling coefficient values may vary from 0.013 to 0.3, corresponding with concrete/asphalt and sand road surfaces, respectively.

A.2.3. Grade resistance

Grade resistance, a function of the road slope, is defined as below

$$R_g = M\, g\, \sin\alpha = (M_V + M_L)\, g\, \sin\alpha \qquad\qquad \text{Eq.A-4}$$

A.2.4. Total resistance force

Under steady driving conditions, the vehicle's acceleration is zero, hence the total force opposing the movement of the vehicle consist of the aerodynamic drag, rolling resistance and grade resistance, as show in Eq.A-5. In general, acceleration mode travel, the total resistance force can be defined as Eq.A-6.

$$R_{total}^S = R_D + R_g + R_r \qquad\qquad \text{Eq.A-5}$$

$$R_{total} = \delta_i\,(R_D + R_g + R_r) = \delta_i\,R_{total}^S \qquad\qquad \text{Eq.A-6}$$

Where, δ_i is the torsion mass factor at the ith gear, relative to the unstable rotation of all spin elements in the vehicle. It depends on the gear at which the vehicle travels.

The force resulted from torsion torque transmitted from engine to the driven wheel and the interaction between it and road surface, and acting on the driven wheel by road is termed the tractive force, F_T. It must overcome the total resistance force to maintain the vehicle to travel at a constant speed.

A.2.5. Required engine power

The required engine power, P_e, so as to achieve total vehicle speed of V, is calculated from Eq.A-7.

$$P_e = \frac{R_{total}\,V}{\eta_t} + P_q = \frac{R_{total}\,V}{\eta_t}\,K \qquad\qquad \text{Eq.A-7}$$

Therefore, the corresponding engine speed and torque are as below:

$$T_e = \frac{30\,R_{total}\cdot V}{\pi\,n_e\,\eta_t}\,K \qquad\qquad \text{Eq.A-8}$$

$$n_e = \frac{30\,i_n\,i_{da}\,V}{\pi\,R_W} \qquad\qquad \text{Eq.A-9}$$

where, @ i_n is the gear ratio of the gear box.

@ i_{da} is the gear ratio of driving axle.

@ P_q is the required power for accessory driving (cooling water pump, compressor, dynamo, etc.) Normally, this amount of power is often rated by the proportion of road-load power via a coefficient K (K>1).

A.2.6. Vehicle specification

The test engine is an OEM engine powering light duty trucks; Ford Ranger WL 2.5. Vehicle's parameters used to determine the test conditions are shown in Table A-1.

Table A-1   Specification of Ford Ranger light duty truck

Vehicle model	-	-	Ford Ranger 4x2
Dimension: Width / Height	W / H	m / m	1.695 / 1.625
Weight (with rating load):	$M_V + M_L$	kg	1700
Gear box ratio:	i	-	4.200, 2.215, 1.433, 1.000, 0.825
Final gear:	i_{da}	-	4.444
Radius of wheel:	R_W	m	0.285
Minimum engine speed:	n_{emin}	rev/min	720

A.2.7. Chosen parameter

These related parameters are chosen in their typical range of the light duty truck type, as shown in following table.

Table A-2   Chosen parameters

Parameter	Unit	Range	Chosen value
Density of air, ρ_{air}	kg/m^3		1.184
Drag coefficient, C_D	-		1.0
Rolling resistance, Cr	-		0.015
Transmission efficiency, η_t	-		0.85
Accessory power coefficient, K	-		1.2

A.2.8. Distribution of engine working speeds and torques in the test cycle

Assumption: - During the time of gear change, the engine operates at idle speed and zero brake torque;

- Time duration for gear change at all gear is 2 seconds.

Followed the ECE15+EUDC test cycle, the distribution of engines working speeds and brake torques is shown in Figure A-3 and Table A-4. The numbers in this table represent engine working time (in second) at corresponding engine speeds and brake torques. From this distribution, it is revealed that the engine operates frequently at engine speeds and brake torques as described below.

- The idle condition is the highest distribution.

- At 2000 rev/min, the engine operates mostly at 20 and 40 Nm of brake torque.

- At 2750 rev/min, corresponding brake torques are 10, 30, and 70 Nm.

- At 3500 rev/min, the corresponding brake torque is 100 Nm.
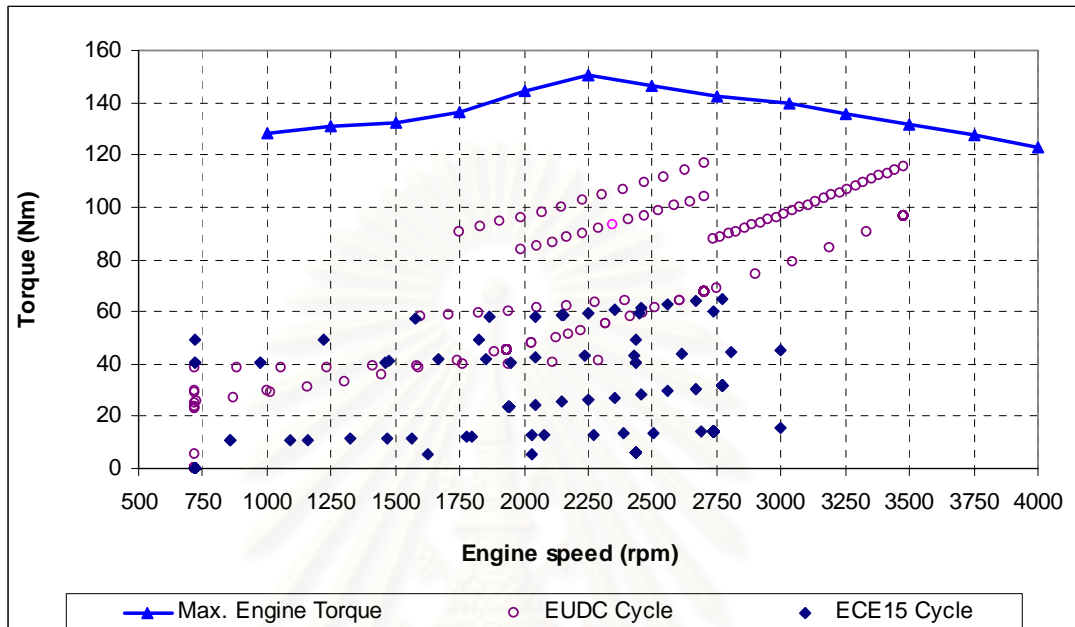
Figure A-3   Engine full load torques, engine brake working torques

A.2.10. Selected engine test speed and torque

From the dynamometer specification, it is clear that the operating point (3500rpm, 100Nm) is out of the dynamometer ability and can not be test.

In order to make comparison with respect to engine speed, additional operating points at 1250 rev/min are to be considered in this investigation. Thus, engine operating points are shown as following table.

Table A-3   Selected test points

Brake torque [Nm] Speed [rpm]	10	20	30	40	70
1250	x	x	x	x	
2000	x	x	x	x	x
2750	x	x	x	x	x

Table A-4 Time period (second) of operating point during ECE15+EUDC test cycle

Speed (rpm)														Torque	
>3875	3626-3875	3376-3625	3126-3375	2876-3125	2626-2875	2376-2625	2126-2375	1876-2125	1626-1875	1376-1625	1126-1375	900-1125	<900	(Nm)	
4000	3750	3500	3250	3000	2750	2500	2250	2000	1750	1500	1250	1000	720	0	Idle
													353	5	<7
						32		4		4			1	10	7-15
				4	100	8	4	8	8	8	8	4	8	20	16-25
							8	56					5	30	26-35
					52	8	4			1	2	2	4	40	36-45
				4	4	16	5	83	10	15	1	9	10	50	46-55
						4	5	6	4		4		4	60	56-65
					12	18	18	2	6	5				70	66-75
				1	103									80	76-85
			1		1			2						90	86-95
			1	3	5	1	4	2	2					100	96-105
		81	3	5	2	3	3	2						110	106-115
		3	5		1	3								120	116-125
		1			1									130	126-135
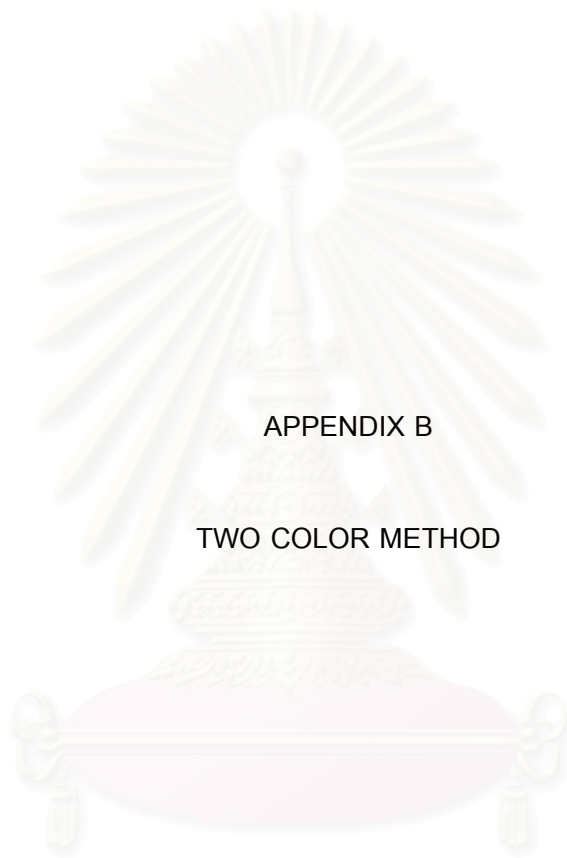
APPENDIX B

TWO COLOR METHOD

B.1. Theory of Two Color Method

B.1.1. Definition of flame temperature

During diesel combustion, both solid soot particles and gaseous combustion products are present. Diesel combustion is dominated by the intense radiation from the soot particles. Since the two-color method utilizes the thermal radiation from soot particles, it directly measures their temperature. The temperature of the combustion gases is not directly measured. However, it can be shown that the temperature difference between the two temperatures is negligible (< 1K) when the ambient gas and soot particles have attained thermal equilibrium, which can be attained in about $10^{-50} \div 10^{-6}$ second within the cylinder. If there is no surface reaction on the soot particles it can also be proven that the soot particles can faithfully follow the surrounding gases temperature as the temperature of the surrounding gases changes with time. Thus, it may be assumed that the soot particle and combustion gas temperatures are approximately the same, and the flame temperature refers to the soot particle temperature.

B.1.2. Principle of the temperature measurement

The thermal radiation at two different wave-lengths is detected and the flame temperature is then determined from their ratio by eliminating an unknown factor. The intensity of radiation from a black body varies with wavelength depends on its temperature, described mathematically by Planck's equation:

$$E_{b,\lambda}(T) = \frac{C_1}{\lambda^5 [e^{(C2/T)} - 1]} \qquad \text{Eq. B-1}$$

where:
$E_{b,\lambda}$ (Wm^{-3}): monochromatic emissive power of a black body at temperature T,

λ (μm): wave length,

T (K): Temperature,

$C_1 = 3.7418 \times 10^{-16}$ (Wm^2): The first Planck's constant,

$C_2 = 1.4388 \times 10^{-2}$ (mK): The second Planck's constant,

The monochromatic emissivity of a non-black body is defined as:

$$\varepsilon_\lambda = \frac{I_\lambda(T)}{I_{b,\lambda}(T)} \qquad \text{Eq. B-2}$$

Where, $I_\lambda(T)$ and $I_{b,\lambda}(T)$ are the monochromatic emissive power of a non-black body and a black body respectively, at the same temperature T and wave length λ. In other words, ε_λ is the fraction of the black body radiation emitted by a surface at wave length λ.

An apparent temperature T_a is introduced and defined as the temperature of a black body emitting the same radiation intensity as a non-black body at temperature T. T_a is also known as the brightness temperature. From this definition of T_a it follows that

$$I_{b,\lambda}(T_a) = I_\lambda(T) \qquad \text{Eq. B-3}$$

Combining the definition for monochromatic emissivity ε_λ with the definition of apparent temperature T gives:

$$\varepsilon_\lambda = \frac{e^{C_2/\lambda T} - 1}{e^{C_2/\lambda T_a} - 1} \qquad \text{Eq. B-4}$$

In practice, ε_λ has been estimated for soot particles by the widely used empirical correlation of Hottel and Broughton,

$$\varepsilon_\lambda = 1 - e^{\left(-KL/\lambda^\alpha\right)} \qquad \text{Eq. B-5}$$

where, K: an absorption coefficient, proportional to the number density of soot particles,

L: the geometric thickness of the flame along the optical axis of the detection system.

The value of α depends on the physical and optical properties of the soot in the flame. Combining two above equations gives

$$KL = -\lambda^\alpha \ln\left[1 - \left(\frac{e^{C_2/\lambda T} - 1}{e^{C_2/\lambda T_a} - 1}\right)\right] \qquad \text{Eq. B-6}$$

The unknown product KL can be eliminated by rewriting the above equation for two specific wavelengths, λ_1 and λ_2:

$$\left[1 - \left(\frac{e^{C_2/\lambda_1 T} - 1}{e^{C_2/\lambda_1 T_{a1}} - 1}\right)\right]^{\lambda_1^{\alpha_1}} = \left[1 - \left(\frac{e^{C_2/\lambda_2 T} - 1}{e^{C_2/\lambda_2 T_{a2}} - 1}\right)\right]^{\lambda_2^{\alpha_2}} \qquad \text{Eq. B-7}$$

The actual flame temperature T is independent of wave length, whilst the apparent temperature T_a and, possibly, the parameter α vary with wave length. The above equation can be solved for the flame temperature T provided the apparent temperature T_{a1} and T_{a2} for the flame are known at the two wavelengths λ_1 and λ_2. These two

apparent flame temperatures can be measured at these two wavelengths using a calibrated two-color optical pyrometer system. In fact, this is the purpose of the two-color system: to provide instantaneous measurements of the apparent temperatures T_{a1} and T_{a2} for the flame at two chosen wavelengths λ_1 and λ_2.

B.1.3. KL factor and soot concentration

As the flame temperature T has been estimated, to combine with Eq.B-6 gives estimation for the KL proportional to the soot concentration. Furthermore, an estimation of soot volumetric density, C_v (the volume of particles in a unit of space), and soot gravimetric density, C_m, (mass of soot per unit volume), can be obtained if some assumptions are made. The volumetric density of particles, C_v, is given by

$$C_V = \frac{1}{6\pi Lm\left(\dfrac{m^2-1}{m^2+2}\right)} \cdot \frac{KL}{\lambda^\alpha} \qquad \text{Eq. B-8}$$

where m is the complex refractive index of the soot particle.

B.2. Implementation

Typical arrangement for the implementation of the two-color method in a diesel engine is shown in Figure B-1.
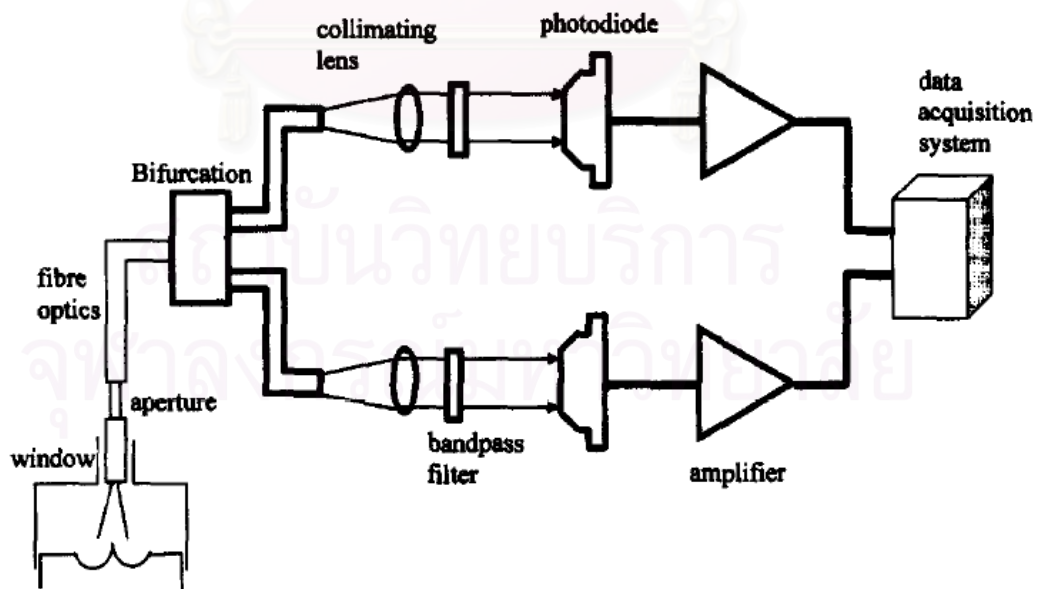
Figure B-1   Schematic layout of a two-color system

A quartz-window allows optical access to the engine combustion chamber. The radiation emitted by a cloud of incandescent soot particles passes through the optical window and the aperture, and then is guided by a fiber-optical bundle to a bifurcation where it is split into two beams. Each beam then passes through a band-pass filter which only allows radiation within a narrow wavelength range (usually 5-20 nm) to go through. The instantaneous signals generated by the photo-diodes are amplified and the resulting voltages at each wave length are then recorded by a data acquisition system. The aperture inserted between the optical window and the receiving fiber limits the field of view of the system to a narrow cone within the combustion chamber. The use of an aperture increases the spatial resolution but the instrument sensitivity is reduced as a result of less radiation reaching the receiving optics. Another important function of the aperture is to reduce the possibility of leaving the field of view unfilled. When only part of the field of view is filled with combustion gas, the brightness temperature of the flame will be underestimated.

B.2.1. Selection of α

The estimation of flame temperature, the KL factor and the volumetric density of soot particles depends on the chosen values of α. They depend on the light wavelength, soot particle size and the refractive index of soot. Fuel type may also have an influence on the value. As the two wave lengths are selected to be in the visible region, its choice is less critical to the estimation of the flame temperature. This is because the flame temperature given by Eq.B-7 is not sensitive to α. This point is clearly shown in Figure B-2, which is calculated for $\alpha = \alpha_1 = \alpha_2$. It is also noted that for wavelengths in the infrared region the influence of the value of α is significant.

Similar effect of α on the estimation of KL is observed. As seen in Figure B-3, the estimation of KL is less sensitive to the value of α if the two wave lengths are chosen in the visible spectrum, whereas the sensitivity is rather large when these two wave lengths are in the infrared region.
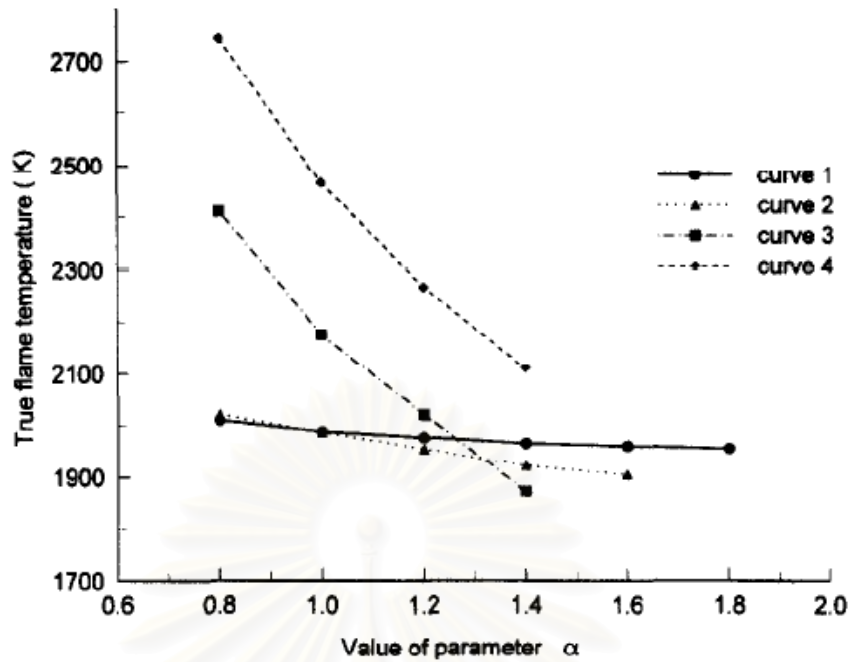
Figure B-2   Effect of the value of the parameter α on the estimated temperature

Wave lengths: Curve 1 & 2: 0.55 and 0.7 μm (visible);

Curve 3 & 4: 2.5 and 4 μm (infra-red)

Apparent temperatures:

Curve 1: 1900 K and 1850 K; Curve 2: 1700 K and 1640 K;

Curve 3: 1400 K and 1050 K; Curve 4: 1600 K and 1200 K
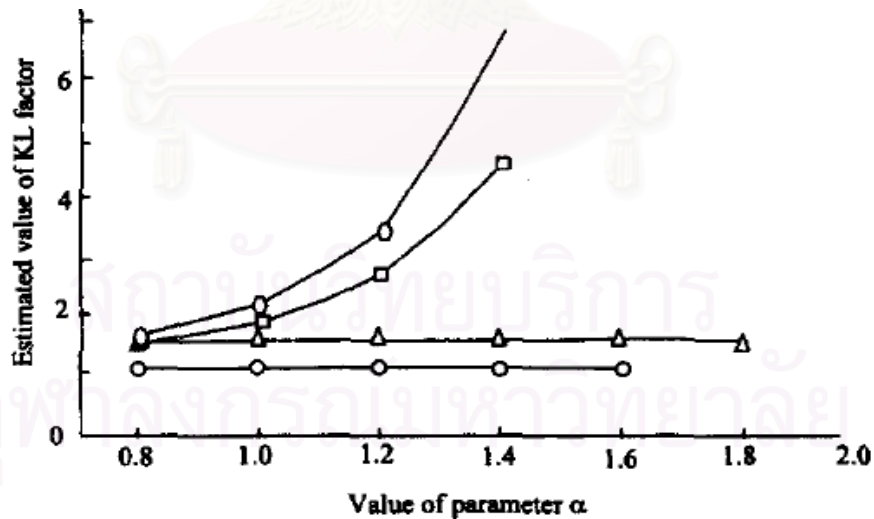
○ Wavelengths: 0.55 and 0.7 μm (visible); Apparent temperatures: 1700K 1640 K

△ Wavelengths: 0.55 and 0.7 μm (visible); Apparent temperatures: 1900K 1850 K

○ Wavelengths: 2.5 and 4 μm (infrared); Apparent temperatures: 1600K 1200 K

□ Wavelengths: 2.5 and 4 μm (infrared); Apparent temperatures: 1400K 1050 K

Figure B-3   Effect of the value of the parameter α on the estimated KL factor
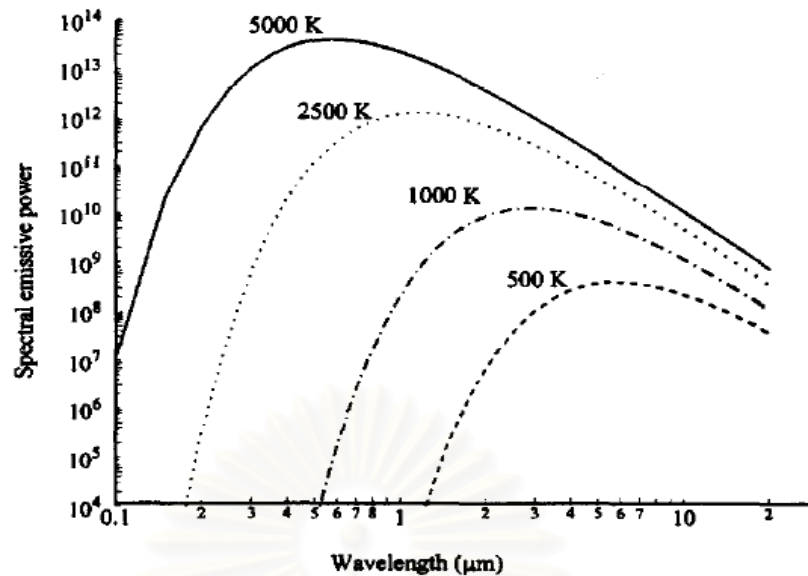
Figure B-4   Spectral radiance of a black body at various temperatures

During combustion, strong band emissions from gaseous species can be present as well as the thermal radiation from soot particles. In the reaction zones of flames, many radicals, such as OH, CH, C_2, HCO, NH and NH_2 may be formed and give appreciable emission in the visible and near ultraviolet regions. In the infrared region, wavelengths must be chosen carefully to avoid radiation or absorption from CO_2, CO, water vapor and fuel vapor. Figure B-5 shows the spectra from various gaseous species in the visible and infra-red region.
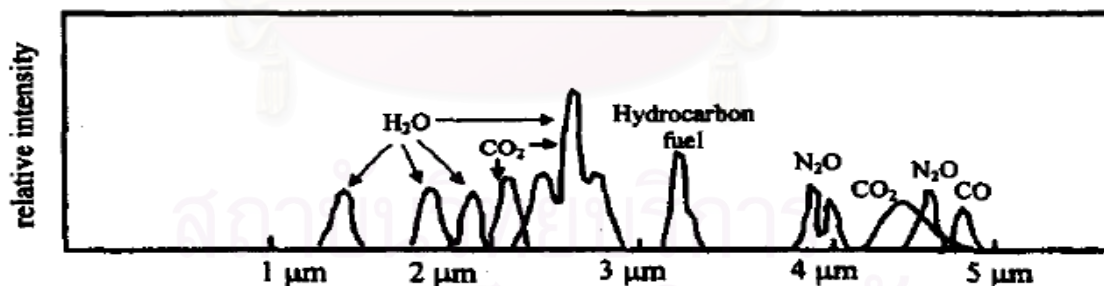
Figure B-5   Emission spectra in the infra-red region for various gas molecules

Photo-diodes with high responsivity in the visible and near infra-red regions are readily available commercially. Also, there are commercially available optical fibers for use as light guides which have a high transmittance in the visible and near infra-red regions. Table B-1 shows a compilation of the wavelengths used by some investigators in the application of the two-color method.

Table B-1   Wave lengths used by investigators in the two color method

Wave length (nm)					Reference
Visible			Infra-red		
λ_1	λ_1	λ_1	λ_1	λ_1	
549	750	-	2300	3980	Matsui et al
529	624	738	-	-	Matsui et al
550	700	850	-	-	Yan and Borman
-	-	-	750	1000	Peterson and Wu
460	640	-	-	-	Kawamura et al
550	650	-	-	-	Shakal and Martin
450	640	-	-	-	Arcoumanis
581	631	-	-	-	Winterbone et al
540	643	-	-	-	Miyamoto et al
600	-	-	-	1000	Bertoli et al
470	650	-	-	-	Shiozaki

B.2.2. Calibration

The method measures apparent temperatures T_{a1} and T_{a2} of the flame at wavelengths α_1 and α_2. These temperatures are then used to obtain the actual flame temperature. Since the two-color system will produce initially only voltages V_{λ_1} and V_{λ_2} corresponding to the radiation from the flame at the two wavelengths, the system must be calibrated so that the two voltages correspond to the apparent flame temperatures. This can be done using a source of black body radiation to generate a calibration relation between voltage-output against black body temperature for each wavelength. Once the calibration relations have been produced for the two wavelengths, the instantaneous voltages can be converted to the apparent temperatures T_{a1} and T_{a2}. The flame temperature, T, and the KL factor can then be obtained from Eq. B-7 and Eq. B-6.

B.2.3. Data acquisition and analysis

The output from a two-color system is normally converted into voltages by the photo-diodes before subsequent calculations are carried out to obtain the flame

temperature and soot loading. A high-speed data acquisition system is used to collect the amplified signal outputs from the photo-diodes on a crank angle basis using the output from a shaft encoder as the clock for data acquisition. Large cycle-by-cycle variation in radiation, however, presents in diesel combustion. The radiation signals could be very irregular because of the motion of soot clouds. The irregularity in radiation signals could also be caused by the random location of ignition and combustion. It has been found that the large cyclic variation of the radiation signals gives a large variation in the results of the KL factors. The flame temperature, though, has been found to be less affected by the cycle-by-cycle variation. Some form of ensemble average, therefore, is required to obtain the temperature and KL measurement from this method.

There are two ways to obtain an ensemble-averaged temperature and KL factor. In the first approach, which Matsui et al used, the voltage outputs corresponding to the radiation intensity at the two wavelengths at each crank angle for 1000 cycles are ensemble-averaged. The averaged voltage outputs for the two wavelengths are then used in the calculation of the flame temperature and KL factor. An alternative approach is to use ensemble averaged temperature and KL factor. In this method, the signal for each cycle is used to calculate the temperature variation at each crank angle degree during a particular engine cycle. Then, the individual cycle temperatures are ensemble-averaged over many cycles. As the flame temperature and KL factor are not linearly related to the radiation intensity, it is expected that these two approaches may not generate the same results. Yan and Borman compared two methods and found that the difference between them is small for the KL factor and temperature through most of the combustion period. The first approach is preferred as it is computationally faster and reduces the influence of noise in temperature calculation.

B.2.4. Accuracy

- Effect of soot deposition on window

Soot accumulated on the optical window, during the tests, reduces its transmissivity and causes error in flame temperature and soot concentration estimation. Matsui et al found that in a direct injection diesel engine a reduction of 14% in transmissivity at $\lambda = 0.55 \mu$m resulted in an error of around 1% in the flame temperature and less than 5% in the estimate of the soot concentration.

- Wall reflections

The radiation detected includes not only the direct radiation from the flame (soot+gaseous species), but also the radiation reflecting from the walls, and the thermal radiation by the wall surfaces. Since the wall-surface temperatures are much lower than the soot particle temperature, their effect can be ignored in the visible region. In infrared region, significant radiation from walls is present and its effect needs to be taken into account. In their work, Matsui et al found that the effect of reflected radiation from an opposite wall on the estimation of temperature is very small (of the order of 2 or 3 K), whilst the error in the determination of the KL factor is at most 10% at very low soot concentrations, falling to 2% at high soot concentrations. When the infrared wave lengths are used, the error in the estimated temperature ranges from 50 to 150 K, whilst the error in the estimated value of the KL factor is up to 50% greater at low soot concentrations than at high soot concentrations.

- Effect of non-uniform temperature and soot

The two-color method only gives a true flame temperature if a spatially uniform temperature exists along the line of sight. Actual, the non-uniformity of temperature and soot concentration will affect the physical meaning of the flame temperature as well as the KL measured by this technique. Yan and Borman showed that the effect of the soot concentration non-uniformity on the measured temperature is less severe than the effect of uneven temperature on the KL factor. If a severe non-uniform distribution of temperature exists, the KL factor will be underestimated.

Generally, the temperature measured by this method is higher than the arithmetic mean temperature because the rate of change of monochromatic intensity with temperature becomes greater with increasing temperature. The flame temperature closer to the window will have a larger effect on the measured temperature than flames further away. The measured temperature will be closer to the maximum flame temperature if the maximum values of temperature and soot concentration are coincident with the line of sight. The non-uniformity of soot concentration has less effect on the measured flame temperature than does the non-uniform temperature on the measured temperature.
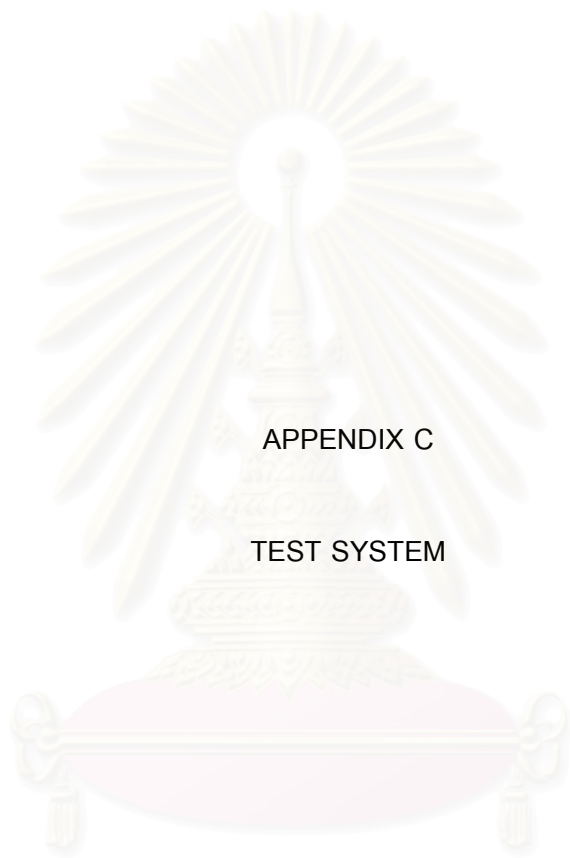
APPENDIX C

TEST SYSTEM

The test system used in this investigation includes ①the engine, ②the dynamometer and control unit, ③the indicating system, and ④the visualization system.

C.1. Test engine:

Test engine is a FORD model WL 2.5L engine used to power light trucks. Its specification is shown in the following table.

Table C-1   Specification of test engine

Parameter	Unit	Value
Brand / Model	-	FORD / WL 2.5L
Engine type	-	4-stroke, 4 cylinder, inline, naturally aspirated, indirect injection
Rated power @ speed	kW @ rpm	60 @ 4100
Maximum torque @ speed	Nm @ rpm	170 @ 2500
Firing order	-	1 - 3 - 4 - 2
Bore / Stroke	mm	93 / 92
Swept volume	cm^3	2499
Combustion system	-	Ricardo Comet MK Vb down-stream glowplug
Chamber volume ratio	%	Pre/Main: 59.3 / 40.7
Compression ratio	-	21.6
- Number of intake valve	-	02 / cylinder
- Inner seat diameter	mm	28
- Number of exhaust valve	-	01 / cylinder
- Inner seat diameter	mm	31
- Fuel pump:	-	- ZEXEL 862 Q910969
- Type	-	- VE axial-piston distributor pump
- Add-on module	-	- Idle-up speed
- Fuel injector type	-	Pintle nozzle (one-nozzle injector)
- Injection pressure	MPa	11.4÷12.1
- Total lube oil quantity	liter	6.7
- Lube oil pressure	kPa	452-529 (at 3000 rpm)

C.2. Dynamometer and control unit

The engine-dynamometer system, Figure C-1, consists of an eddy current dynamometer AVL Alpha 40 (ELB), a power unit AVL LSE 51X and a control and monitoring unit AVL BME 300. The water temperature and water flow of the break cooling system are monitored. The different reactions of events of the maximum speed, torque and power of the break are stored in the database of the system. The BME 300 controls the brake by digital controller. The speed and torque-controller are under lapped with a current-controller.
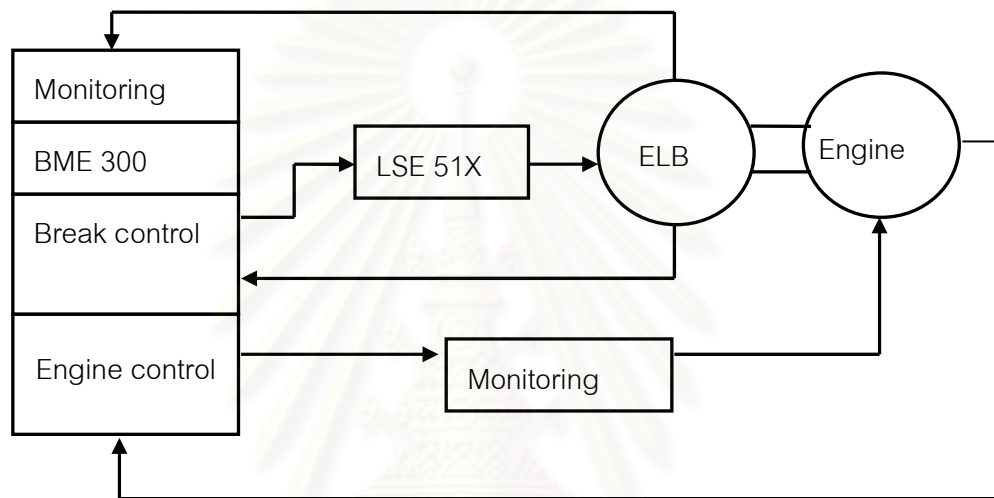
Figure C-1　　　Schematic arrangement of engine-dynamometer-control unit

Dynamometer

The dynamometer Alpha 40 is eddy-current type, produced by AVL List GmbH. Specification of the dynamometer is shown in Table C-2 and Figure C-2.

A regulated torque increase and decrease with high dynamics can be produced by using the controller and power unit LSE 51X. The dynamometer thus becomes controllable working machine that can absorb a freely definable load and keep this load constant. The brake torque is controlled by changing the excitation by means of the power unit LSE 51X. The set point is set at the controller and passed on to the LSE 51X as a corrected output.

The induction caused by the rotation generates eddy currents brakes the test engine. The heat produced by the eddy currents is led off by cooling water which is arranged in such a way that it can not affect the torque measurement. The average specific amount of cooling water required is approximately 28 l/kWh at ambient

temperature of 30^{0}C. The specific minimum amount of cooling water must not fall below 21 l/kWh at ambient temperature of 40^{0}C.

        A load cell is used to measure the actual torque value and a speed pick-up is used to measure the actual speed value. These values are sent to the control unit.

Table C-2   Specification of AVL Alpha 40 dynamometer

Dynamometer type	Eddy Alpha 40 ZG
Nominal torque	75 Nm from 2.060 rpm to 5.100 rpm
Nominal power*	40 kW from 5.100 rpm to 17.000 rpm
Maximum speed	17.000 rpm
Permissible additional mass on the coupling flange at a distance of 50mm	- at maximum speed: 3 kg - at 10.000 rpm: 5 kg
Mass inertia	0.02 kgm²
Direction of rotation	clockwise and counter clockwise
Coolant	Closed cooling water circuit
Temperature monitoring	Temperature limit switch in water outlet pipe
Flow monitoring	Cooling water flow switch in water inlet pipe
Connection box	with EMC cable glands
Load cell type	HBM U2A (accuracy class 0,1)
Total system torque accuracy (typical)	±0.2% F.S.
Digital speed measurement accuracy	±1 rpm / ±1 digit
Color	ultramarine blue RAL 5002
Weight	180 kg
Protection class	IP 54C
Ambient temperature conditions	+5 to +40°C
Ambient humidity conditions	< 95% (dew point must not be reached)

Figure C-2   Output and torque limit of AVL Alpha 40 dynamometer

Dynamometer Monitoring Unit

Dyno Monitoring Unit: BME 300, shown in Figure C-3 was produced by AVL-List GmbH. A BME 300 controls the brake by digital controller. The speed and torque-controller are under lapped with a current-controller.

Figure C-3　　　Dynamometer Monitoring Unit BME

Control

- *Throttle Position Control:* Originally, a pneumatic actuator SMC-SPCP-004 is used to control the throttle position.

- *Cooling Water Temperature Control:* Cooling water system, as shown in Figure C-4 is used to maintain cooling water temperature of the test engine not exceed a predefined value, which can be set from the control unit. Temperature of water at the inlet (outlet cooling water from engine) is sensed and transferred to the control unit. The control unit supplies electricity to a solenoid valve as the temperature reaches the predefined value. Cool water is added to the system, mixing with hot water to reduce temperature. By adjusting a valve on water pipe, the variation range of cooling water can be set. In this investigation, the setting value is 85°C and the cooling water temperature varies in the range from 83°C to 86°C.

Figure C-4　　　Cooling water tank

C.3. Indicating system, DEWETRON Combustion Analyzer CA-5000-SE

This indicating system is manufactured by DEWETRON GmbH., Austria. Its specification is shown in Figure C-5 and the following Table.

Table C-3   Specification of DEWETRON Combustion Analyzer CA-5000-SE system

General specification	
- Resolution:	- 0.1 degree with encoder at up to 8000rpm on 1 channel - 0.2 degree resolution with 4 channels up to 6000 rpm
- Result display	Online mathematics and statistics. Fast online displays (pressure diagram, P/V diagram, …)
- Function	Powerful knocking recognition capability
- Fast stream to disk mode (1 MS/s)	
Input specification	
Max. channels	32 (Internal amplifier slot: 16)
Sampling rate	up to 1 MS/s total
Resolution	12 bit

Input: $\pm$ 10V
     $\pm$ 50V (isolated)
  Charge
	standard
	DAQP-V modules
	DAQP-CHARGE-x modules

Crank or CA input	isolated
Computer system	
Display	17" TFT / resolution 1280x1024 pixels
OS / Processor	Windows XP Professional / Intel 2.8 GHz
Memory / Hard disk	1 GB / 250 GB high speed
DVD drive	DVD-/+RW
Interface	USB, RS232, LPT, Ethernet
System specification	
Dimension / Weight	460 x 351 x 200 mm / approximate 17 kg
Operating temperature	-10 to 50 $^{\circ}$C
Storage temperature	-20 to 70 $^{\circ}$C
Humidity	10 to 80 % non cond., 5 to 95 % relative humidity
Vibration	MIL-STD 810F 514.5, procedure I
Shock	MIL-STD 810F 516.5, procedure I
Power supply	90 to 260 VAC

Figure C-5   DEWETRON Combustion Analyzer CA-5000-SE system

- Dynamic signal amplifier

Figure C-6   DEWETRON amplifier model DAQP-CHARGE-A

Three dynamic signal amplifiers, model DAQP-CHARGE-A, in the system are used to collect pressure history of the fuel line, pre and main chamber. Signal from the three transducers is sent to these charge amplifiers via three BNC cables. The specification of these charge amplifiers is shown in Figure C-6 and Table C-4.

Table C-4   Specification of DEWETRON amplifier model DAQP-CHARGE-A

Supported sensors:	ICP$^{\circledR}$ and charge sensors
Sensor type selection:	Push button or software
Sensor connection:	BNC connector
Input ranges: - ICP$^{\circledR}$ input: - Charge input:	0, 20, 40, 60 dB Charge 0.1, 1, 10, 100, 1000 mV/pC
Gain accuracy:	1 % full scale
Input range fine tuning:	programmable
Range selection:	Push button (fixed) or software (all)
Integration:	Single (velocity), double (displacement)
Range and filter: ICP LED: OVL LED: A, V and D LED:	Active with connected ICP$^{\circledR}$ sensor, inactive for charge input Overload control (output voltage > 5 V) Indicator for acceleration, velocity and displacement output
Constant current source:	3.8 to 5.6 mA, > 26 V
Highpass Filters	0.1 Hz, 1 Hz, 10 Hz (±2 dB @ f0)
Lowpass Filters	100 Hz, 1, 3, 10, 50 kHz (±2 dB @ f0)
Filter selection:	Push button or software
Filter characteristics:	Butterworth; 80 dB / decade (24 dB / octave)
Bandwidth, -3dB	0.1 Hz to 50 kHz (±2 dB @ f0)
Typ. SNR @ max. bandwidth: Gain 0.1 and 1 Gain 10 / Gain 100 Gain 1000 / Gain 10000	 90 dB 87 dB / 73 dB 54 dB / 60 dB @ 10 kHz
Output voltage:	±5 V (±6 V peak voltage) Output
Noise:	< 8 mV (all ranges with 50 kHz filter)
RS-485 interface:	Yes
Power supply voltage:	±9 VDC (±10 %)
Power consumption:	0.6 W to 1.2 W (depending on sensor)

Table C-5   Specification of AVL GU12P pressure transducer

Standard Specifications	Unit	
Measuring Range	bar	0-200
Lifetime		load changes: $> 10^8$
Overload	bar	250
Sensitivity (nominal)	pC/bar	15.94 - Main chamber 15.67- Pre-chamber
Linearity	FSO	< ±0.3%
Natural Frequency	kHz	130
Acceleration Sensitivity	bar/g	< 0.001
Shock Resistance	g	> 2000
Operating Temperature Range	°C	up to 400
Thermal Sensitivity Shift		20...400°C < ±2% 200...300°C < ±0.5%
Insulation Resistance at 20°C (68°F)	Ω	$>10^{13}$
Capacitance	pF	7
Mass (without cable)	grams	5
Mounting Torque	Nm	1.5
Thermodynamic Specifications		
Cyclic Temperature Drift	bar	< ±0.6
Load Change Drift		
Max. Zero-line Gradient dp/dt	mbar/ms	1.5
Permanent Zero-line Deviation	bar	2
IMEP-Stability	%	< 3
Accessories		
Cable and Couplings	-	CI41-1, CI42-1 (metal mesh), CC41, E124-10
Cable-Mounting Tool	-	TC01
Adaptor	-	ZF41, AG03*
Mounting Tool	-	TS01 (TT01, TT02), TA14,TA16

Table C-6   Specification of Kistler 607C1 pressure transducer

Parameter	Unit	
Pressure range	bar	4825
Maximum pressure	bar	8615
Resolution, noise	bar rms	0.07
Sensitivity, nom.	pC/bar	1.75
Resonant frequency, nom.	kHz	250
Insulation resistance	Ω	10^{13} (at room temp.)
Hysteresis	%	2
Linearity	%	± 2
Rise time, 10…90%	μsec	1.5
Temperature sensitivity shift	%/^{0}C	0.02
Capacitance, nom.	pF	6
Environmental Vibration sensitivity, axial	bar/g	0.0014
Vibration sensitivity, transverse	bar/g	0.0007
Vibration limit	g	1000
Shock, 1ms pulse width	g	15000
Temperature range	^{0}C	-195 to 260
Temperature sensitivity shift	% / ^{0}C	0.02
Intermittent gas temperature on diaphragm	^{0}C	1649
Mechanical Weight, approx.	grams	12
Housing case	material	Maraging steel
Sensing element	type	Quartz
Mounting torque: 600E42 seal (Cu) 600A10 seal (SS)	Nm	20 27

C.4. Optical diagnostic system

The AVL VisioScope system has been used for combustion chamber visualization. Figure C-7 shows schematically the AVL optical diagnostic system which includes hardware and software to capture in-cylinder phenomena and the software to analyze the phenomena. This system was produced by AVL List GmbH and consists of following components:

- Crank Angle Encoder, Light Tube, and Pulse Converter;

- Light Unit (Engine Timing Unit, cold light source and Strobe);

- PCO PixelFly CCD Camera;

- Combustion Chamber Endoscopy;

- Standard accessories;

- Set of connecting cables;

- Computer with AVL VisioScope software;
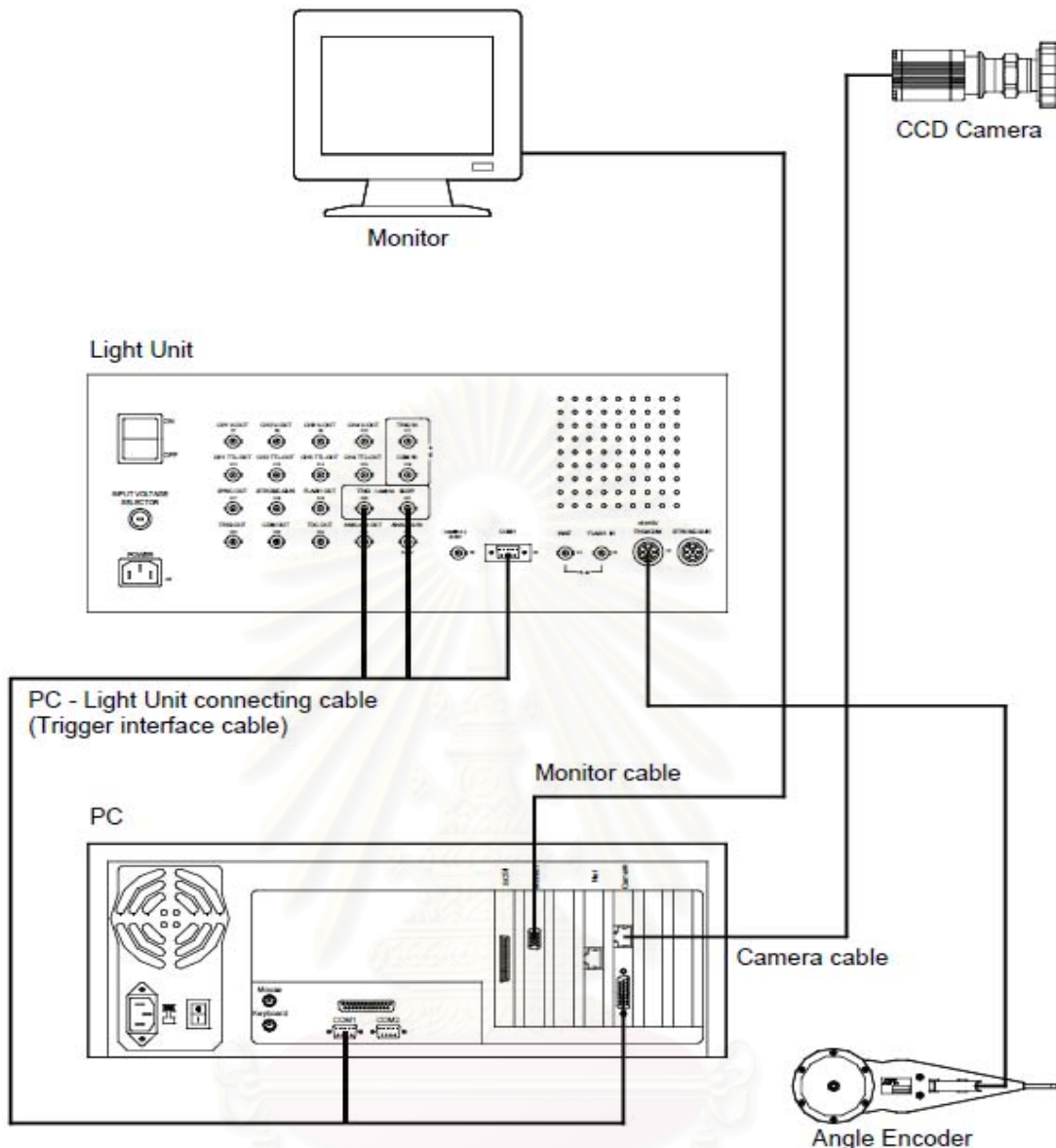
Figure C-7   Diagram of the AVL optical diagnostic system

- *Crank Angle Encoder*

An AVL 364C angle encoder is used to convert the analogue value angle to digital electrical signals, and thus the crankshaft speed and position are determined, providing the ideal interface between the mechanical and electronic systems. This encoder is also used for the indicating system.

The marker disk is mounted centrically on one end of the crank shaft. The optical pick-up is fixed rigidly on the crankcase. The electrical inputs and outputs of the 364C Angle Encoder are designed to enable the connection of all AVL and equivalent digital

indicating systems. The installation of the encoder at the end of test engine crankshaft is shown in Figure C-8. Position and speed of the crankshaft are sensed to AVL optical diagnostic system and DEWETRON indicating system via an AVL 3016 CDM Conditioner.

Figure C-8   Crank Angle Encoder Installation

Table C-7   Technical data of AVL 364C crank angle encoder

| Speed range	$10 \div 15000$ rev/min
Vibration resistance	Max. 100×9.81 m/s^2 (100 g) for 10 million rev. Max. 200 g for brief periods
Permissible temperature	- Ambient: $30 \div 70$ ^{0}C - At the mounting surfaces: $30 \div 100$ ^{0}C
Service life under extreme load	at least 10 million revolutions at maximum permissible vibrations
Mass load on mounted shaft	approx. 530 ... 630 g, depending on mounted position of encoder (min. in horizontal position)

- Light Tube and Pulse Converter
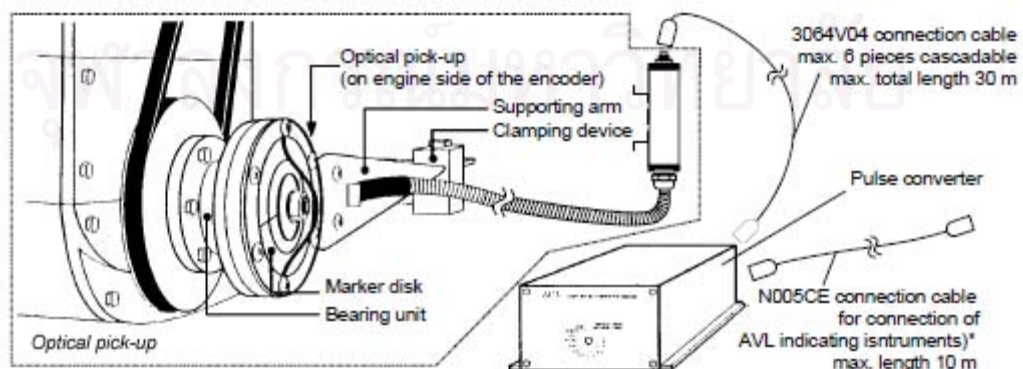
Figure C-9   Connection between Encoder, Light Tube, and Pulse Converter

The light tube transmits infrared light to the angle marks or the trigger mark via the relevant optical fiber. Light is either reflected from the metal mark or reflector or absorbed by the dark metal in between depending on the position of the marker disk. The reflected light signals from the encoder are conditioned in the pulse converter to TTL signals. The trigger pulse is synchronized with the first negative angle mark edge after the trigger signal.

The crank angle output delivers 3600÷36 balanced square-wave pulses per revolution depending on the setting of the RESOLUTION selector. When both signal edges are processed, the resolution is from 0.05÷5deg. CA.

The arrangement between the AVL 364C encoder, the AVL Light Tube, and the AVL 3064A02 Pulse Multiplier is shown in Figure C-9.

-Light Unit and Strobe Gun

Figure C-10   AVL Light Unit

Table C-8   Specification of AVL Light Unit

Power Supply:	100 / 230 V switchable
Strobe	
Frequency:	10 Hz max.
Light yield with fiber optic cable:	40 mJ / flash
Flash duration:	20 μs
Cold light source	
Infinitely variable light output	
High light output due to high quality condenser system	

The AVL Light Unit, shown in Figure C-10, is used to:

⊕ Measure the engine speed for optical diagnostics

⊕ Generate infra-red light and send to the AVL 364C Encoder;

⊕ Pickup the pulse from the AVL Pulse Converter,

⊕ Synchronize the test engine TDC with the indicating system, or another measurement system. This is done with the Strobe Gun.

⊕ Supply cold light to needed space for visualization;

⊕ Communicate with other indicating systems.

-CCD camera

The AVL VisioScope system is supplied with CCD Camera PixelFly VGA Color with resolution of 640✕480 pixel as shown in Figure. This camera and the interface card are manufactured by PCO Computer Optics GmbH.

Figure C-11   CCD camera MO0145

-Combustion Chamber Endoscopy

Combustion Chamber Endoscopy consists of:

- 3 endoscopes with integrated cooling channels (one with 0°, one with 30° and one with 60° viewing angle);

- 1 light guide (one lighting head with 0°, one with 30° and one with 70° lighting angle);

- Combustion chamber window (two of each with 0°, 30° and 70°)

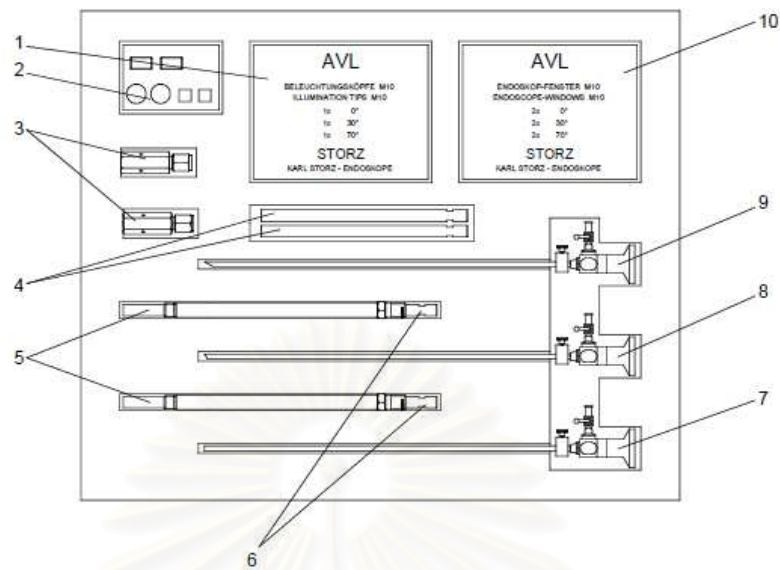- 2 sets of cylinder head adapter parts;

Miscellaneous parts.

Figure C-12   AVL endoscope set

Table C-9   AVL endoscope set

Item	Designation		Material No.
1	Illumination tips		MO0127
	Spare parts	Optical head 0°	MO0125
		Optical head 30°	MO0124
		Optical head 70°	MO0123
2	Accessories container		BO2613
3	Clamping nuts		BO2614
4	Pressure sleeves		YM3302
5	Cylinder head inserts		YM3301
6	Dummies		YM3303
7	Air-cooled endoscope, 0°		MO0116
8	Air-cooled endoscope, 30°		MO0117
9	Air-cooled endoscope, 60°		MO0118
10	Endoscope window set		BO2736
	Spare parts	Endoscope window 0°	BO2737
		Endoscope window 30°	BO2738
		Endoscope window 70°	BO2739

Table C-10   Specification of endoscopes

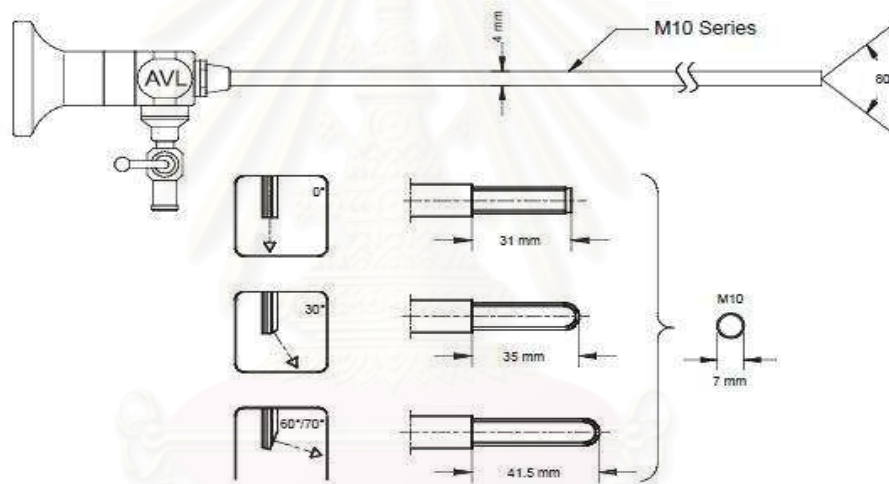| Three different viewing angle:	0° straight ahead
	30° forward view
	60° angled view
Visual field:	80° (wide-angle)
Length of shaft (working length):	330 mm
Tube diameter:	4 mm
Cooling medium:	clean compressed air (~6 bar)
Operating temperature un-cooled:	150 $^{\circ}$C max.

- **Combustion Chamber Windows**

Figure C-13   Endoscope and combustion chamber windows

The combustion chamber windows consist of a steel sleeve as the window mounting and a quartz glass tube with a flat or semi-rounded end. There are three different shaped windows to match the various viewing angles of the endoscopes. They are used to separate the endoscope from the fluid in the combustion chamber.

Figure C-13 shows the AVL endoscope M10 and the set of three combustion chambers windows.

- **Lighting set**

Lighting set is used to supply cold light from the light unit to the combustion chamber. A lighting head made of quartz glass is connected to the AVL fiber optic cable (Light Guide) MO0106 and screwed with the locking nuts to the cylinder head

installation sleeve in the same way as the combustion chamber window. There are three lighting heads with 0°, 30° and 70° lighting angle.

Figure C-14   Lighting Set

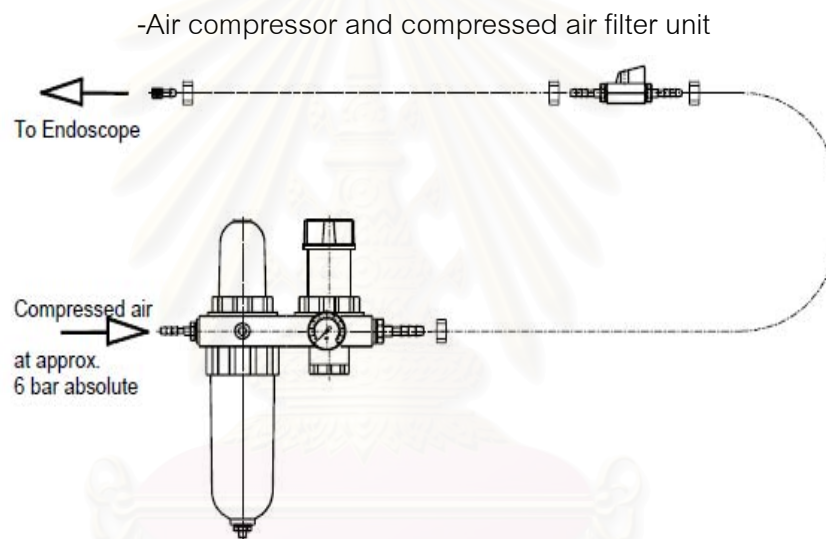-Air compressor and compressed air filter unit

Figure C-15   Oil- and dust-free air supply for endoscope-cooling

This unit supplies clean compressed air at approximate 6 bar and temperature not exceed 20°C to the endoscope; to protect it from overheating which can cause irreparable damage to the equipment. A pressure regulating valve with pressure gauge is integrated in the Filter Unit to adjust the supply pressure. The arrangement is shown in Figure C-15.

-Computer and software

A computer, as described in Table C-11, with the software AVL VisioScope ThermoVision version 1.1 is used to control the optical diagnostic system, to capture and store the captured data for off-line processing, as well as process the data including

functions as fuel spray, flame area distribution, flame temperature, soot concentration (based on two-color method).

Table C-11   Computer configuration for optical diagnostic

CPU:	Intel Pentium III Processor
Operating system:	Microsoft Windows NT 4.0
SCSI controller:	Adaptec AHA2940 Wide SCSI Controller
Hard disk:	Ultra Wide SCSI hard disk
Interface card for camera communication:	PCO
DVD writer:	HP DVD Writer 200i

C.5. Other instruments

- Electronic balances used for fuel measurement:

Table C-12   Specification of balance used for LPG measurement

Brand/model	ZENTECH / JWA60K	Unit
Capacity	60	kg
Division	2	g
Absolute uncertainty	0.6	g

Table C-13   Specification of balance used for liquid fuel measurement

Brand/model	ACU / AWM	Unit
Capacity	30	kg
Division	2	g

Author's Biography

Mr Phan Minh Duc was born in 1969. He graduated from the Department of Mechanical Engineering, Danang University, Vietnam. He has worked for Danang University. He got scholarship for abroad study from the Ministry of Education and Training, Vietnam and started the PhD. Program in the Faculty of Engineering, Chulalongkorn University since November 2003.